

**Preparation, Characterization and Evaluation of Solid Dispersion of  
Abiraterone Acetate for Solubility and Oral Bioavailability  
Enhancement**

**THESIS**

Submitted in partial fulfillment  
of the requirements for the degree of

**DOCTOR OF PHILOSOPHY**

by

**Manisha Vinayak Choudhari**

**ID. No. 2019PHXF0055P**

Under the Supervision of

**Prof. Gautam Singhvi**

and Under the Co-Supervision of

**Prof. Ranendra Narayan Saha**

**&**

**Dr. Sunil Kumar Dubey**



**BITS Pilani**  
Pilani | Dubai | Goa | Hyderabad | Mumbai

**BIRLA INSTITUTE OF TECHNOLOGY AND SCIENCE, PILANI  
2024**

# **BIRLA INSTITUTE OF TECHNOLOGY AND SCIENCE, PILANI**

## **DECLARATION**

I hereby declare that the thesis work entitled **“Preparation, Characterization and Evaluation of Solid Dispersion of Abiraterone Acetate for Solubility and Oral Bioavailability Enhancement”** is an original piece of work carried out under the guidance of Prof. Gautam Singhvi in the Department of Pharmacy, Birla Institute of Technology and Sciences (BITS PILANI), Pilani campus. I have not submitted this thesis for the award of any other degree from any other university/institute.

Manisha Vinayak Choudhari  
2019PHXF0055P  
Research Scholar  
Department of Pharmacy  
BITS Pilani, Pilani campus

Date:

Place: Pilani, Rajasthan, India

# BIRLA INSTITUTE OF TECHNOLOGY AND SCIENCE, PILANI

## CERTIFICATE

This is to certify that the thesis entitled **“Preparation, Characterization and Evaluation of Solid Dispersion of Abiraterone Acetate for Solubility and Oral Bioavailability Enhancement”** submitted by **Manisha Vinayak Choudhari**, ID. No. **2019PHXF0055P** for award of Ph.D. degree of the institute, embodies original work done by him under my supervision.

### **Supervisor**

Prof. Gautam Singhvi  
Associate Professor  
Department of Pharmacy  
BITS-Pilani, Pilani Campus,  
Rajasthan

### **Co-Supervisor**

Prof. Ranendra Narayan Saha  
Chief Scientific Advisor, Biophore Group of Companies,  
Hyderabad  
Former Vice Chancellor (Acting) BITS Pilani  
Former Director, BITS Pilani Dubai  
Shri B K Birla & Smt Sarla Birla Chair Professor (former)  
Senior Professor of Pharmacy (Former)  
BITS-Pilani, Pilani Campus, Rajasthan

### **Co-Supervisor**

Dr. Sunil Kumar Dubey  
General Manager  
R & D Healthcare Division Emami Ltd,  
Belgharia, Kolkata

## Table of Contents

<b>Contents</b>	<b>Page no.</b>
<i>Acknowledgment</i>	<b>ii-iv</b>
<i>Abstract</i>	<b>v-xii</b>
<i>List of tables</i>	<b>xiii-xiv</b>
<i>List of figures</i>	<b>xv-xix</b>
<i>List of abbreviations and symbols</i>	<b>xx-xxii</b>
<b>Chapter 1</b> Introduction	<b>1-40</b>
<b>Chapter 2</b> Drug and Polymer Profile	<b>41-63</b>
<b>Chapter 3</b> Analytical Method Development	<b>64-102</b>
<b>Chapter 4</b> Preformulation Studies	<b>103-114</b>
<b>Chapter 5</b> Formulation of Abiraterone Acetate-HPMCAS based Solid Dispersion	<b>115-149</b>
<b>Chapter 6</b> Formulation of Abiraterone Acetate-HPMC HME based Solid Dispersion	<b>150-187</b>
<b>Chapter 7</b> Pharmacokinetic studies	<b>188-196</b>
<b>Chapter 8</b> Summary and Conclusion	<b>197-201</b>
Appendices	<b>202-207</b>

# Acknowledgment

"Gratitude is the fairest blossom which springs from the soul."

– Henry Ward Beecher

I would like to express my most sincere gratitude and deepest appreciation to Prof. Ranendra Narayan Saha, Scientific Advisor of Biophore Group of Companies, Hyderabad, who was my former supervisor prior to his superannuation and after he continued as my co-supervisor. I would always remain indebted to him for his guidance, constant support, encouragement, and taking me under his wing and encouraging me to think independently and strive for higher standards in research work and professional development.

I am sincerely thankful to Prof. Gautam Singhvi, Associate Professor, Birla Institute of Technology and Sciences Pilani, Pilani Campus, for being my supervisor, for his persistent support insightful guidance, and for always being available to discuss ideas and provide feedback. His mentorship has been an integral part of my academic journey. His expertise and insights were invaluable in shaping the direction and depth of my study. His commitment to excellence and profound knowledge of the field significantly contributed to the quality and rigor of my research.

I express my sincere gratitude to my co-supervisor Dr. Sunil Kumar Dubey, General Manager, Medical Research, R & D Healthcare division, Emami, for his guidance, timely advice, and encouragement throughout my research work. I am particularly thankful for his availability and willingness to provide constructive feedback at every stage of the project. I am deeply grateful for the learning experience and the professional development gained under his mentorship.

I am deeply grateful to Prof. V. Ramgopal Rao, Vice-Chancellor, BITS-Pilani, Prof. Sudhirkumar Barai, Director, BITS Pilani, Pilani Campus, Col. Soumyabrata Chakraborty (Retd), Registrar, BITS Pilani, Pilani Campus.

I am thankful to Prof. Shamik Chakraborty, Associate Dean, AGSRD, BITS Pilani, for providing excellent work facilities and a stimulating research environment. I also wish to extend my heartfelt thanks to Prof. Anil B. Gaikwad, Head, Department of Pharmacy, for their unwavering support and for providing the necessary resources during my research work.

I am profoundly grateful to my Doctoral Advisory Committee (DAC) members, Prof. Anil B Jindal, and Prof. Murali Monohar Pandey, for their thorough review and constructive feedback on my thesis.

I am thankful to all my faculty members of the Department of Pharmacy, Prof. R. Mahesh, Prof. S. Murugesan, Prof. Rajeev Taliyan, Prof. Deepak Chitkara, Prof. Anupama Mittal, Prof. Sandeep Sundriyal, Prof. Richa Shrivastava, and Prof. Pragyanshu Khare. I am thankful to Dr. Sushil Kumar Yadav for supporting animal studies.

I would also like to extend my sincere thanks to my labmates Dr. Vamshi Krishna, Dr. Tejashree Waghule, Dr. Shrividya Gorantla, Dr. Mahipal Reddy, Dr. Rupesh Jain, Ms. Sakshi Priya, Ms. Yashika Tomar, Ms. Vaibhavi Desai, and Ms. Pragati Kumbar for their immense support, giving their precious time, patience in always listening to me and motivation.

I am thankful to Colorcon Inc USA for providing the fellowship. My special thanks to Mr. Shantanu Damle, Technical Director, Colorcon Asia Pvt Ltd, for his guidance and extensive knowledge in the field, which have greatly enhanced the quality of my research work.

All my seniors and colleagues Dr. Kowthavarapu Venkata Krishna, Dr. Saurabh Sharma, Dr. Kishan Italiya, Dr. Nisha Sharma, Dr. Ginson George, Dr. Pracheta Sengupta, Dr. Sudeep Pukale, Dr. Samrat Mazumdar, Dr. Geetika, Dr. Paramita, Dr. Swetha, Dr. Violina, Dr. Swati, Dr. Karan, Dr. Rupesh, Dr. Himanshu, Dr. Rajesh, Dr. Amritansh, Dr. Arihant, Dr. Deepak Kumar, Dr. Kedar Prayag, Dr. Moumita Basak, Dr. Nikita Hinge, Dr. Mahipal, Mr. Imran, Dr. Kavyashree, Mr. N. Sai Bhargav, Ms. Reena, Ms. Sriravali, Ms. Nisha, Mr. Mukesh, Ms. Shreya, Dr. Sharyu, Mr. Amit, Mr. Shubham, Mr. Sai Pradyuth, Mr. Vishwadeep, Mr. Shivanshu, Mr. Jayant, Ms. Shobha, Mr. Abhay, Mr. Shrikant, Mr. Shailesh, Ms. Shikha, Mr. Ala Chandu, Ms. Neha, Mr. Giriprasad, Ms. Sonia, Mr. Muzaffar, Mr. Mukul, Mr. Samarth, Mr. Vagesh, Mr. Utkarsh, Ms. Shivangi, Mr. Animesh, Ms. Pranali, Ms. Shivangi, Mr. Pratik, Ms. Lavanya, Ms. Aarti, Mr. Yash, Ms. Jyotika, Mr. Bhupendra, Ms. Priyanka, Dr. Vivek and Dr. Yogeshvaran deserve special thanks for making the pleasant working environment in the lab, for all the fun and enjoyment, help and sarcasm.

I would also like to extend my sincere thanks to the entire non-teaching staff in the Department of Pharmacy, Mr. Puran, Mr. Lakshman, Mr. Tarachand, Mr. Surendra, Mr. Naveen, Mr. Abhishek,

Mr. Sandeep, Mr. Ram Suthar, Mr. Vishal, Mr. Mukesh, Mr. Vikas for their kind support during this work.

I am also deeply grateful to Dr. Atharva Bhide, and Dr. Ajinath Kale for their steadfast support and boundless encouragement. Their unwavering support and positive reinforcement have made every challenge easier to overcome and every moment exceptionally memorable. Their presence has been a source of strength and motivation throughout this journey.

To all my mentors, colleagues, friends, and family who have supported me along the way, your contributions and encouragement have been invaluable. Thank you for believing in me and for making this journey a truly enriching experience.

I am especially grateful to my beloved parents and my elder sister for their constant inspiration, endless love, and countless blessings. Their unwavering support and encouragement have been my greatest strength throughout this journey.

**Manisha Vinayak Choudhari**

## Abstract

Cancer presents a significant global health crisis, with mortality rates escalating worldwide. One of the leading cancers causing problems in men worldwide is prostate cancer, which has been reported to cause about 0.3 million deaths annually. According to the 2024 statistics from the American Cancer Society, it is estimated that there will be approximately 299,010 new cases of prostate cancer and 35,250 deaths related to cancer in the United States. Among treatments, androgen deprivation therapy (ADT) effectively controls prostate cancer by suppressing serum testosterone levels. However, the disease eventually progresses to a phase known as metastatic castration-resistant prostate cancer (mCRPC), where it advances despite continuous testosterone inhibition and ADT. Abiraterone acetate (ABTA) was approved by the USFDA in 2011 and has been highly successful in prolonging the lives of patients suffering from mCRPC. The conventional marketed formulation of ABTA has achieved significant clinical and commercial success, but delivering orally ABTA remains highly challenging and has its own limitations. It falls under the BCS class IV, characterized by extremely poor aqueous solubility ( $< 0.5 \mu\text{g/mL}$ ) as well as low permeability. Its pH-dependent solubility causes ABTA to precipitate when transitioning from the gastric fluid to the alkaline intestinal region, reducing solubility, hindering drug dissolution, and impeding drug absorption across the intestinal membrane. Due to its characteristics, the oral bioavailability of ABTA in humans is estimated to be less than 10% in a fasted state. As of low bioavailability, patients must consume a high daily dose of ABTA (1000 mg per day) to achieve efficacy, which can result in dose-related side effects, causing patients poor compliance. Moreover, ABTA shows significant inter-individual pharmacokinetic variability and strong food effects, with a 7- and 5-fold increase in  $C_{\text{max}}$  and  $\text{AUC}_{0-\infty}$  for low-fat meals and 17- and 10-fold for high-fat meals. Therefore, the commercial tablet must be taken on an empty stomach (2h before and 1h after a meal) to avoid overexposure.

Furthermore, to overcome the above drawbacks of ABTA, a few approaches have been discussed in the literature. However, this approach reveals the inherent limitation. One such approach involves developing ABT hydrochloride salt to improve gastrointestinal solubility; however, data on solubility and dissolution testing is limited. Another approach is nano-amorphous ABTA formulation, which requires reconstitution with water before oral intake, resulting in a 'powder in a bottle' dosage form that can lead to dosing variability and inaccuracies. These reported strategies



are complex, require sophisticated technology, and limited industry feasibility. To address these drawbacks, there is a critical need to develop new pharmaceutical formulations that improve solubility through adequate dissolution, further contributing to enhanced bioavailability of ABTA, leading to better therapeutic efficacy. Changing the formulation approach to make better delivery may overcome many of the above problems for anticancer and other drugs.

Formulation researchers have made numerous efforts to increase the solubility, dissolution, and absorption of drugs by employing several strategies in which solid dispersion (SD) is the effective approach where API is homogeneously distributed in a highly water-soluble or miscible polymeric matrix. However, there is a risk involved with utilizing an SD since the amorphous API can transform back into a more stable crystalline form. Several strategies are employed in SD formulations to counteract the risk of re-crystallization. Consequently, choosing an appropriate polymer for SDs becomes a crucial step, as it not only enhances the API solubility and the dissolution of the SDs but also prevents undesirable API precipitation. Among all the polymers, cellulose plays an important role in SD, maintaining supersaturation by inhibiting the crystallization; it also can improve dissolution, absorption, and in-vivo performance. Hydroxypropyl methylcellulose acetate succinate (HPMCAS) and hydroxypropyl methylcellulose hot melt extrusion (HPMC HME) serve as carriers in the preparation of SD. They help to maintain the drug in a supersaturated state by inhibiting precipitation, thereby increasing the rate and extent of dissolution in aqueous media. HPMCAS and HPMC HME possess distinctive characteristics, such as amphiphilic and hydrophilic properties, respectively, and unique glass transition temperature, different substitution patterns, good miscibility between the drug and polymer, and providing stability, all of which offer an ideal possibility for designing and preparing the polymeric SD.

The thesis proposed and developed a strategic method for designing a novel ABTA SD using the polymeric carriers with industry feasible and scalable approach. This developed formulation will help in overcoming the limitation of the existing formulations and is expected to achieve enhanced solubility, dissolution, and oral bioavailability and the ability to take with or without food, decreasing dose and the frequency of administration, leading to better patient compliance. To meet the above criteria, the objective of this work was to prepare and evaluate ABTA amorphous solid dispersion (SD) using HPMCAS and HPMC HME through the solvent granulation method and

hot melt extrusion method, respectively. The optimized formulation of the ABTA SD was further evaluated for solubility studies, dissolution studies (in-vitro and biorelevant dissolution), characterization, stability, and in-vivo pharmacokinetic studies.

An analysis is an integral part of any formulation development; the present studies encompass the design of an experimental approach for developing a simple, reliable, and rapid RP-HPLC method for the estimation of ABTA. The chromatographic separation was efficiently conducted on a Hypersil Gold C<sub>18</sub> HPLC column, using the mobile phase composition of acetonitrile: K<sub>2</sub>HPO<sub>4</sub> in the ratio of 80:20 (v/v %) at pH 6.5 with an isocratic elution mode. The linearity was established in the concentration range of 0.5-10 µg/mL with r<sup>2</sup> of 0.9998. Furthermore, the limit of detection and the limit of quantification were found to be 0.0978 µg/mL and 0.3260 µg/mL, respectively. Furthermore, different force degradation studies, including hydrolysis, oxidation, thermal, and photolytic, were performed on ABTA. The degradation of ABTA was shown in both acidic (54.16 ± 0.247 after 24h) and basic conditions (35.06 ± 0.458 after 24h). Furthermore, the developed method was successfully employed to quantify ABTA in bulk powder and, in the presence of polymer, did not show a change in the retention time. This indicated method is selective and specific for ABTA in the presence of different sample matrix. The developed method was found to be sensitive, accurate, precise, robust, and selective compared to the reported chromatographic method.

The bioanalytical method was developed to quantify the abiraterone (ABT) and its prodrug ABTA in rat plasma. Due to rapid hydrolysis, ABTA is quickly converted to ABT, resulting in ABTA levels often falling below the quantification limit in most plasma samples. Consequently, pharmacokinetic studies in both animals and humans typically report only ABT plasma concentrations. For bioanalytical method development, we synthesized ABT from ABTA using a basic hydrolysis method. In this study, a novel, simple, specific, sensitive, and simultaneous RP-HPLC method has been developed and validated for the estimation of ABT and ABTA in rat plasma. The analytical procedure involves the extraction of ABT, ABTA, and itraconazole (used as an internal standard) from rat plasma with a simple protein precipitation method. The chromatographic analysis was performed on a Hypersil gold C18 HPLC column. An isocratic mobile phase consisting of acetonitrile and 10 mM K<sub>2</sub>HPO<sub>4</sub> buffer in a ratio of 34:66 (v/v %). the buffer pH was adjusted to 3.0 using orthophosphoric acid, with a flow rate of 1 mL/min, at the

column temperature of 30°C, and the analytes were detected at wavelength 254nm. The calibration curve of ABT and ABTA was linear over a concentration range of 200-5000 ng/mL and 500-5000 ng/mL with  $r^2=0.9991$  and  $r^2=0.9927$ , respectively. The % RSD of the inter-day and intra-day precision of ABT was 1.96-7.40 and 4.20-14.28, whereas the ABTA was 3.75-7.78 and 6.73-13.77, respectively, in rat plasma. The validated RP-HPLC method was successfully applied to a pharmacokinetic study of ABT and ABTA in rats.

Further, before the preparation of SD, the theoretical Hansen solubility parameters suggested that the solubility parameter ( $\Delta\delta$ ) between the ABTA and HPMCAS was below  $7\text{MPa}^{1/2}$ , demonstrating good miscibility of the two. Various ratios of polymer, drug, and lactose monohydrate (1:1:1, 1:2:1, and 1:3:1) with different grades of HPMCAS were utilized to prepare ABTA SD via the solvent granulation method. In this method, the ABTA and HPMCAS (716 and 912) were dissolved in the acetone and then slowly added to the lactose monohydrate, facilitating the solvent evaporation. Furthermore, in the precipitation inhibition study, the concentration of ABTA in the media remained at elevated levels throughout the 180 min period in the presence of pre-dissolved HPMCAS 716 and 912. Upon inducing supersaturation of ABTA in the absence of polymer, instantaneous and complete precipitation was observed in 10 min; the presence of pre-dissolved HPMCAS 716 and 912 polymers provided a pronounced and stable supersaturation. This study exhibited that the HPMCAS 716 and 912 acted as “Spring and Parachute” to impede crystal nucleation and growth.

The solubility of ABTA in SD using HPMCAS 716 (F2) and 912 (F5) with lactose monohydrate (1:2:1) ratios exhibited higher solubility among all SD. The solubility of SD, i.e., F2 and F5 formulation in distilled water, pH 6.8, pH 1.2, FaSSIF (pH 6.5), and FeSSIF (pH 5.0) were observed to be 26-fold, 52-fold, 1.72-fold, 2.53-fold, 1.33-fold and 21-fold, 38-fold, 1.6-fold, 2.35-fold, and 1.16- fold respectively higher than the free ABTA. The results obtained from the differential scanning calorimetry (DSC), powder X-ray diffraction (PXRD) attenuated total reflectance-Fourier transform infrared spectroscopy (ATR-FTIR), and field emission scanning electron microscopy (FE-SEM) indicated that the crystalline state of ABTA converted to its amorphous state during the development of ABTA SD with HPMCAS. In-vitro and bio-relevant dissolution behavior of ABTA was conducted in the various dissolution media, indicating the higher dissolution of ABTA SD compared to free ABTA. In the in-vitro dissolution study, using

pH 1.2 dissolution media, the dissolution rate of ABTA of F2 and F5 SD formulations were 89.54% and 84.88% in 120 min, respectively, suggesting that drug dissolution increased by 1.58 and 1.50-fold compared to the free ABTA. In pH 6.8 dissolution media, the dissolution rate of ABTA of F2 and F5 SD formulations was 10.22% and 6.33% in 120 min, respectively, suggesting that drug dissolution increased significantly by 8.97 and 5.61-fold compared to the free ABTA. In pH 4.5 dissolution media, the dissolution rate of ABTA of F2 and F5 SD formulations was 90.52% and 82.08% in 120 min, suggesting that drug dissolution increased by 1.41 and 1.28-fold compared to the free ABTA. In biorelevant dissolution studies, the FaSSIF dissolution media, the highest drug is dissolved of 36.50% for F2 and 27.13% for F5, was obtained in 120 min, suggesting that the drug dissolution was increased by 4.13 and 3.07-fold compared to the free ABTA. Furthermore, in FeSSIF dissolution media, the highest drug dissolved of 54.10% in F2 and 50.64% in F5 was obtained in 120 min, suggesting that the drug dissolution was increased by 1.68 and 1.58-fold compared to the free ABTA. However, the F2 formulation exhibited superior drug dissolution compared to the F5 formulation, attributed to the variance in the HPMCAS polymer grades—specifically 716 and 912. A greater dissolution of ABTA was noted with HPMCAS 716 compared to HPMCAS 912, highlighting the significant influence of acetate and succinate substitution. The degree of succinate substitution in HPMCAS directly correlates with dissolution; thus, higher succinate substitution yields increased dissolution. HPMCAS 716, with 14-18% succinate substitution, demonstrated enhanced dissolution relative to HPMCAS 912, which contains 10-14% succinate substitution. The stability investigation revealed that ABTA SD did not transform into a crystalline form, potentially attributed to the superior crystalline inhibition property of HPMCAS.

Pharmacokinetic studies were carried out for free ABTA and ABTA SD formulations (F2 and F5) administered orally by gavage as a single dose of 200 mg/Kg of the ABTA or equivalent to. Blood samples (0.5 mL) were collected from the retro-orbital venous plexus at specific time intervals (0.5h, 1h, 2h, 4h, 6h, 8h, and 12h) post-administration, respectively. The free ABTA showed less  $C_{max}$  and  $AUC_{0-4h}$ , which were  $243.27 \pm 24.40$  ng/mL and  $1102.8 \pm 47.6$  ng/mL, respectively. Comparatively, the  $C_{max}$  of ABTA SD of the F2 and F5 batches were  $466.76 \pm 14.75$  ng/mL and  $306.30 \pm 6.22$  ng/mL, increased 1.92-fold and 1.26-fold when compared to the free ABTA. The  $AUC_{0-12h}$  of F2 and  $AUC_{0-8h}$  F5 batch were  $4299.1 \pm 66.7$  ng/mL.min and  $1910.4 \pm 12.97$  ng/mL.

min, increased by 3.89-fold and 1.73-fold, respectively, when compared to the free ABTA. The bioavailability of ABTA SD in the F2 and F5 batches increased by 3.89-fold and 1.73-fold compared to the free ABTA.

Furthermore, the HPMC HME polymer was used to prepare the ABTA SD formulation using the HME (HAAKE MiniCTW) method to improve the solubility, dissolution, and oral bioavailability of ABTA. This innovative HPMC HME variant offers lower glass transition temperature (117-128°C), enhanced melt flow characteristics, and the continued benefits of being a precipitation inhibitor post-dissolution. This advancement allows for extrusion at reduced processing temperatures, addressing challenges such as high glass transition temperature (160-210°C), high torque, and color changes associated with traditional HPMC during HME. The theoretical solubility parameter between the ABTA and HPMC HME was below  $7\text{MPa}^{1/2}$ , suggesting excellent miscibility according to the Hansen solubility parameter. In the precipitation inhibition study, the ABTA in the absence of polymer, complete precipitation could be observed in the 10 min. The presence of pre-dissolved HPMC HME provided a pronounced and stable supersaturation. This study exhibited that the HPMC HME (15 LV and 100 LV) acted as a “parachute” to impede crystal nucleation and growth.

ABTA SD formulations were prepared using the HME method with two grades of HPMC HME (15 LV and 100 LV) at various extrusion temperatures (120°C, 140°C, and 160°C). The physical state of the ABTA SD was characterized by DSC, ATR-FTR, PXRD, and FE-SEM, confirming that ABTA in SD existed in the amorphous state and exhibited molecular interaction, particularly samples prepared at extrusion temperatures of 140°C and 160°C. However, ABTA SD was prepared at the extrusion temperature of 120°C, and a crystalline peak of ABTA was observed in DSC and PXRD. This crystallinity was due to inadequate mixing of the drug and polymer during the hot-melt extrusion (HME) preparation method. The solubility studies of the ABTA SD formulations notably enhanced the ABTA solubility across all media including (3.01 µg/mL -10.96 µg/mL) pH 1.2 (480.25 µg/mL-574.22 µg/mL), pH 6.8 (3.0 µg/mL -6.52 µg/mL), FaSSIF (8.91 µg/mL -21.68 µg/mL), and FeSSIF (82.45 µg/mL- 128.51 µg/mL) compared to free ABTA.

The ABTA SD formulations exhibited superior dissolution profiles, both rate and extent of dissolution, compared to the free ABTA. For SD formulations, dissolution was found to be

increased and varied from 59.61% to 100.67% depending on the nature and concentration of the polymer and process and temperature used. In the in-vitro dissolution study at pH 1.2, the dissolution rate of ABTA increased with increasing the concentrations of HPMC HME 15LV. Specifically, ABTA/SD/2, ABTA/SD/5, and ABTA/SD/8 prepared at 140°C showed dissolution rates of 73.93%, 90.92%, and 95.54% in 120 min, respectively, representing increases of 1.31-fold, 1.61-fold, and 1.66-fold compared to ABTA bulk powder. In contrast, at pH 4.5, the dissolution rate decreased with higher HPMC HME 15LV concentrations. Here, ABTA/SD/2, ABTA/SD/5, and ABTA/SD/8 showed dissolution rates of 96.44%, 87.34%, and 80.45%, respectively, representing increases of 1.65-fold, 1.50-fold, and 1.38-fold compared to the free ABTA. Furthermore, in the dissolution media with pH 1.2 and pH 4.5, the dissolution rate of ABTA decreased as the concentration of HPMC HME 100LV increased. This is because the higher molecular weight of HPMC HME 100LV raises the viscosity of the dissolution media at an even lower concentration. The dissolution rates of ABTA/SD/10 and ABTA/SD/12 at pH 1.2 were 98.12% and 91.28%, respectively, while at pH 4.5, they were 100% and 96.20% after 120 min. This indicates an increase in dissolution by 1.74-fold, 1.66-fold, 1.72-fold, and 1.65-fold, respectively, compared to the free ABTA. Furthermore, among the various extrusion temperatures tested, 140°C proved to be the most suitable for preparing ABTA SD compared to 120°C and 160°C. This temperature also significantly influenced the dissolution of ABTA. Bio-relevant dissolution behavior of ABTA SD in fast and fed conditions exhibited higher dissolution (2 to 5 times) compared to free ABTA.

Pharmacokinetic studies were carried out after an oral administration of free ABTA and ABTA SD formulations (ABTA/SD/2 and ABTA/SD/10) administered orally by gavage as a single dose of 200 mg/Kg of the ABTA. The  $C_{max}$  of optimized ABTA SD of the ABTA/SD/2 and ABTA/SD/10 batches were  $1014.9 \pm 12.97$  ng/mL and  $1514.6 \pm 185.5$  ng/mL respectively, increased 4.17-fold and 6.22-fold when compared to the free ABTA, whereas the  $AUC_{0-8h}$  of ABTA/SD/2 and  $AUC_{0-12h}$  of ABTA/SD/10 batch were  $3243.1 \pm 517.7$  ng/mL.min and  $7342.7 \pm 1147$  ng/mL. min, increased by 2.95-fold and 6.66-fold increase when compared to the free ABTA. The bioavailability of ABTA SD in the ABTA/SD/2 and ABTA/SD/10 increased by 2.95-fold and 6.66-fold compared to the free ABTA.

The study demonstrated that all ABTA SD formulations prepared with HPMCAS and HPMC HME inhibited precipitation and maintained prolonged supersaturation. This significantly enhanced the solubility, dissolution, and bioavailability of ABTA compared to the bulk powder. Thus, the dissolution and bioavailability studies reflected that the prepared SD of ABTA may improve the therapeutic efficacy of ABTA in prostate cancer. The solvent granulation and hot melt extrusion are both industrially feasible and scalable methods for the preparation of SD, revealing the hope of a better treatment strategy for prostate cancer.

## List of Tables

Table no.	Details	Page no.
Table 1.1	Different solubility enhancement techniques for poorly water-soluble drugs	4-6
Table 1.2	Different applications of HPMCAS and HPMC HME in SD with different preparation method	20-21
Table 2.1	Various properties of the different grades of HPMCAS	51
Table 2.2	Difference between the traditional HPMC and HPMC HME	55
Table 2.3	Various properties of the different grades of HPMC HME	56-57
Table 3.1	Calibration data of the ABTA developed UV-spectrophotometric method	69
Table 3.2	Accuracy data of the proposed UV method for the determination of ABTA	69
Table 3.3	Precision study results for the UV method	70
Table 3.4	Statistical data of the regression equations and validation parameters	70
Table 3.5	Robustness data of the proposed UV method	71
Table 3.6	Design matrix enlisting the selected factor using FFD	73
Table 3.7	Design matrix enlisting the selected factor using CCD	74
Table 3.8	Experimental design CCD for each run and response	80-81
Table 3.9	ANOVA results of CCD	81
Table 3.10	Accuracy results the developed HPLC method	86
Table 3.11	Intra-day repeatability and Inter-day repeatability (% RSD) data of the different C samples of the developed HPLC method of ABTA	87
Table 3.12	Robustness results of the developed RP-HPLC method of ABTA	87-88
Table 3.13	System suitability of ABTA	88
Table 3.14	Forced degradation study of ABTA	89-90
Table 3.15	Extraction efficiency of the ABT and ABTA in different organic solvents	98
Table 3.16	Linear regression data for the calibration curve of ABTA and ABTA in rat plasma (n=6).	99
Table 3.17	Precision (% RSD) and accuracy (% bias) of the ABT in the rat plasma samples at QC concentrations of the calibration ranges	99-100
Table 3.18	Precision (% RSD) and accuracy (% bias) of the ABTA in the rat plasma samples at QC concentrations of the calibration ranges	100



Table 4.1	Solution state stability data of ABTA at different aqueous buffers and biorelevant media	111
Table 5.1	Composition of ABTA PM and SD prepared by solvent evaporation method	120
Table 5.2	Composition of ABTA PM and SD prepared by solvent granulation method	121
Table 5.3	Estimation of Solubility Parameter of ABTA using the Hansen Group Contribution theory	126
Table 5.4	Estimation of Solubility Parameter of HPMCAS using the Hansen Group Contribution theory	126
Table 5.5	Estimated solubility parameter and Flory–Huggins drug-polymer interaction parameter values derived for HPMCAS and ABTA	127
Table 5.6	Solubility studies of the ABTA PM and SD	129
Table 5.7	Solubility studies of the ABTA PM and SD with lactose monohydrate	130
Table 5.8	Dissolution parameters of ABTA and ABTA SD dissolution media	143-144
Table 5.9	The composition of the ABTA SD tablet from ABTA SD	144
Table 5.10	Dissolution parameter of ABTA SD tablet in pH 4.5 dissolution media	145
Table 6.1	Compositions of SD of ABTS prepared by HME method	154-155
Table 6.2	Estimation of Solubility Parameter of HPMC HME using the Hansen Group Contribution theory	158
Table 6.3	Estimated solubility parameter and Flory–Huggin’s drug-polymer interaction parameter values derived for ABTA and HPMC HME	158-159
Table 6.4	Extrusion process temperature with different ratios of ABTA and HPMC HME 15 LV and 100 LV SD formulations	163-164
Table 6.5	Solubility of ABTA SD formulations in different buffer media	173
Table 6.6	Solubility of ABTA SD Formulations Expressed as Fold Changes Compared to free ABTA	174
Table 6.7	Viscosity of HPMC HME 15 LV and 100 LV in different pH media	175
Table 6.8	Dissolution parameters of ABTA and ABTA SD in different dissolution media	183
Table 7.1	Pharmacokinetic parameters of free ABTA and ABTA SD after oral administration of rats (Values represent mean + SEM)	193

## List of Figures

<b>Figure no.</b>	<b>Details</b>	<b>Page no.</b>
Figure 1.1	Description of different BCS classes	3
Figure 1.2	Spring and parachute effect to attain high supersaturation for poorly water-soluble drugs.	11
Figure 1.3	Hot melt extrusion process	16
Figure 2.1	Mechanism of action of ABTA	44
Figure 2.2	Chemical structure of HPMCAS	48
Figure 2.3	Schematic representation of (a) the synthesis of HPMC by reacting with cellulose in the presence of chloromethane and propylene oxide and (b) the formation of HPMCAS by the esterification of HPMC using succinic and acetic anhydride	49
Figure 2.4	SWOT analysis of HPMCAS	52
Figure 2.5	SWOT analysis of HPMC HME	58
Figure 3.1	[A] UV absorption spectra (Concentration; 10 µg/mL) and [B] Overlay of ABTA at different concentrations	68
Figure 3.2	Ishikawa Fishbone diagram to determine the potential factors in the HPLC method development	74
Figure 3.3	Half-normal plots and Pareto charts of various critical analytical attributes (CAA), i.e., Retention time (A and B), Tailing factors (C and D), and theoretical plate (E and F)	80
Figure 3.4	3D response surface and 2D contour plots viewing the influence of CMP, viz., pH (A), Volume of acetonitrile (B), and Flow rate (C) on the retention time as the CAA	83
Figure 3.5	3D response surface and 2D contour plots viewing the influence of CMP, viz., pH (A), Volume of acetonitrile (B), and Flow rate (C) on the tailing factor as the CAA	84
Figure 3.6	3D response surface and 2D contour plots viewing the influence of CMP, viz., pH (A), Volume of acetonitrile (B), and Flow rate (C) on the theoretical plate as the CAA.	84

Figure 3.7	Overlay plot illustrating the optimal analytical design space	85
Figure 3.8	(a) Chromatogram of the blank sample, (b) Chromatogram of ABTA	86
Figure 3.9	Chromatograms of ABT and ABTA (10 µg/mL)	89
Figure 3.10	Chromatogram for the different stress conditions studied under (a) Acidic condition (0.1 N HCl), (b) Basic condition (0.1 N NaOH), (c) Oxidation (30 % H <sub>2</sub> O <sub>2</sub> ), (d) Thermal (Hot air oven) (e) U.V. light (f) Humidity (g) Hydrolytic (h) blank sample	89
Figure 3.11	Chromatograms of ABTA in SD formulations	90
Figure 3.12	ATR-FTIR spectrum of ABTA and ABT	94
Figure 3.13	[A] <sup>1</sup> H NMR spectrum of the ABTA [B] <sup>1</sup> H NMR spectrum of the synthesized ABT	95
Figure 3.14	HR-MS spectrum of the synthesized ABT	96
Figure 3.15	Typical chromatogram of [A] Blank rat Plasma [B] blank rat plasma spiked with ABT, ABTA and ITZ	97
Figure 3.16	Linear regression calibration curve of ABT and ABTA	99
Figure 4.1	UV absorption spectrum of ABTA	108
Figure 4.2	[A] DSC thermogram; [B] ATR-FTIR spectrum; [C] PXRD pattern; [D] TGA thermogram of ABTA	109
Figure 4.3	Solubility of ABTA in various aqueous buffers	110
Figure 4.4	Solubility of ABTA in different organic solvent	110
Figure 4.5	Solution stability study of ABTA at different aqueous buffer and Biorelevant media [A] at room temperature; [B] at freeze condition	111
Figure 4.6	DSC thermogram of ABTA, HPMCAS 716, HPMCAS 912 and Lactose monohydrate	112
Figure 4.7	FTIR spectrum of ABTA, HPMCAS 716, HPMCAS 912 and Lactose monohydrate	113
Figure 5.1	Chemical structure of ABTA and HPMCAS	119
Figure 5.2	SD prepared from the solvent evaporation method	128
Figure 5.3	The solubility profiles of all ABTA-SD formulations and PM in different media	129-130
Figure 5.4	The solubility profiles of all ABTA-SD and PM along with lactose	131

	monohydrate in different media	
Figure 5.5	Precipitation inhibition assay of supersaturated ABTA in FaSSIF pH 6.5 in the presence of pre-dissolved HPMCAS 716 and 912 (mean $\pm$ S.D, n = 3)	133
Figure 5.6	Particle size graph [A] of supersaturated ABTA in FaSSIF pH 6.5 in the presence of pre-dissolved HPMCAS 716 and 912 (mean $\pm$ SD, n = 3); Evolution of particle size during supersaturation condition; [B] in the presence of HPMCAS 716; [C] in the presence of HPMCAS 912; [D] in the absence of HPMCAS 716 and 912	134
Figure 5.7	DSC thermogram of [A] [a] ABTA; [b] HPMCAS 716; [c] HPMCAS 912; [d] Lactose monohydrate; [e] P2; [f] P5; [g] F2; [h] F5; [B] [a] ABTA; [b] HPMCAS 716; [c] HPMCAS 912; (d) ABTA: HPMCAS 716 PM without lactose monohydrate; (e) ABTA: HPMCAS 912 PM without lactose monohydrate; (f) ABTA: HPMCAS 716 SD without lactose monohydrate; (g) ABTA: HPMCAS 912 SD without lactose monohydrate.	135
Figure 5.8	PXRD pattern of [A] [a] ABTA; [b] HPMCAS 716; [c] HPMCAS 912; [d] Lactose monohydrate; [e] PM of ABTA with HPMCAS 716 without lactose monohydrate [f] PM of ABTA with HPMCAS 912 without lactose monohydrate [g] SD of ABTA with HPMCAS 716 without lactose; [h] SD of ABTA with HPMCAS 912 without lactose monohydrate; [B] [a] ABTA ; [b] HPMCAS 716; [c] HPMCAS 912; [d] Lactose monohydrate; [e] P2; [f] P5; [g] F2; [h] F5	136
Figure 5.9	TGA of [a] ABTA; [b] HPMCAS 716; [c] HPMCAS 912; [d] Lactose monohydrate; [e] P2; [f] P5; [g] F2; [h] F5	137
Figure 5.10	ATR-FTIR Spectra of [a] ABTA; [b] HPMCAS 716; [c] HPMCAS 912; [d] Lactose monohydrate; [e] P2; [f] P5; [g] F2; [h] F5	138
Figure 5.11.	FE-SEM images of [a] ABTA; [b] F2; and [c] F5	138
Figure 5.12	In-vitro dissolution profile of ABTA and SD formulation [F2 and F5] in different buffer media [A] pH 1.2; [B] pH 6.8; [C] pH 4.5	140-141
Figure 5.13	Biorelevant dissolution profile of ABTA and SD formulation [F2 and	142

	F5] in different buffer media [A] FaSSIF (pH 6.5); [B] FeSSIF (pH 5.0)	
Figure 5.14	In-vitro dissolution profile of in-house prepared ABTA tablet (F21) and ABTA SD tablet dosage form prepared from SD (F17) and (F18) with pH 4.5	144
Figure 5.15	DSC thermogram [A] and PXRD patterns [B] of (a) ABTA; (b) F2 (0 days); (c) F5 (0 days); (d) F2 (90 days); (e) F5 (90 days)	146
Figure 6.1	Structure of HPMC HME	153
Figure 6.2	Precipitation inhibition assay of supersaturated ABTA in FaSSIF pH 6.5 in the presence of the pre-dissolved HPMC HME 15 LV and 100 LV (mean $\pm$ SD, n=3)	160
Figure 6.3	Particle size graph of supersaturated ABTA in FaSSIF pH 6.5 in the presence of pre-dissolved HPMC HME 15LV and HPMC HME 100LV at different concentrations (mean $\pm$ SD, n = 3)	161
Figure 6.4	Preparation of ABTA SD with hot melt method [A] and with the plasticizers [B]	162
Figure 6.5	Hot melt extrusion (HME) instrument for the preparation of ABTA SD	163
Figure 6.6	DSC thermograms of ABTA SD formulations with HPMC HME (15LV and 100LV)	167
Figure 6.7	PXRD patterns of ABTA SD formulations with HPMC HME (15LV and 100LV)	168
Figure 6.8	ATR-FTIR of ABTA SD formulations with HPMC HME (15LV and 100LV)	169
Figure 6.9	TGA of ABTA SD formulations with HPMC HME (15LV and 100LV)	170
Figure 6.10	FE-SEM of ABTA SD formulations with HPMC HME (15LV and 100LV)	171
Figure 6.11	Solubility studies of free ABTA and ABTA SD formulation at different extrusion temperatures in different media [A] water, pH 6.8 and FaSSIF; [B] FeSSIF and pH 1.2	172-173
Figure 6.12	Viscosity of HPMC HME 15 LV and 100 LV in different pH media [A-B] illustrates the viscosity of HPMC HME 15 LV dispersion (1.33 % and 2.66%) in different pH media; [C-D] illustrates the HPMC HME	175

	100 LV dispersion (1.33 % and 2.66%) in different pH media	
Figure 6.13	In-vitro dissolution profile of ABTA SD formulations extruded at different extrusion temperatures 120°C, 140°C and 160°C and different concentrations of HPMC HME 15LV and 100LV in pH 1.2 dissolution media	178
Figure 6.14	In-vitro dissolution profile of ABTA SD formulations extruded at different extrusion temperatures 120°C, 140°C and 160°C and different concentrations of HPMC HME 15LV and 100 LV in pH 4.5 dissolution media	180
Figure 6.15	Biorelevant Dissolution of ABTA SD in [A] FaSSIF (pH 6.5); [B] FeSSIF (pH 5.0)	181
Figure 6.16	PXRD patterns [A] of (a) ABTA; (b) ABTA/SD/2 (0 days); (c) ABTA/SD/2 (90 days); [B] (a) ABTA; (b) ABTA/SD/10 (0 days); (c) ABTA/SD/10 (90 days); DSC patterns [C] of (a) ABTA; (b) ABTA/SD/2 (0 days); (c) ABTA/SD/2 (90 days);[D] (a) ABTA; (b) ABTA/SD/10 (0 days); (c) ABTA/SD/10 (90 days)	184
Figure 7.1	Plasma Concentration -time profile a of free ABTA and ABTA SD (F2 and F5) after oral administration (Values represent mean + SEM)	193

## **List of all abbreviations and symbols**

API	Active Pharmaceutical Ingredients
BCS	Biopharmaceutical classification system
SD	Solid Dispersion
Tg	Glass transition temperature
PVP	Polyvinyl pyrrolidone
PEG	Polyethylene glycol
HPMC	Hydroxypropyl methylcellulose
HPMCAS	Hydroxy propyl methyl cellulose acetate succinate
EC	Ethylcellulose
PVPVA	Polyvinyl pyrrolidone vinyl acetate
CA	Cellulose acetate
CAP	Cellulose acetate phthalate
GRAS	Generally Recognized As Safe
GI	Gastrointestinal tract
PCL	Poly caprolactone
AUC	Area under curve
HME	Hot melt extrusion
ICH	International council harmonization
RH	Relative humidity
PXRD	Powder X-ray diffraction
DSC	Differential scanning calorimetry
ATR-FTIR	Attenuated total reflectance-fourier transform infrared spectroscopy
HPC	Hydroxypropyl cellulose
Cmax	Maximum plasma concentration
% CV	Coefficient of variation
P-gp	P-glycoprotein
BCRP	breast cancer resistance protein
mCRPC	Metastatic castration resistance prostate cancer
ABTA	Abiraterone acetate

ABT	Abiraterone
FaSSIF	Fasted state simulated intestinal fluid
FeSSIF	Fed state simulated intestinal fluid
FDA	Food drug administration
ADT	Androgen deprivation therapy
TGA	Thermogravimetric analysis
FE-SEM	Field emission scanning electron microscopy
CYP	Cytochrome
CFR	Code of Federal Regulations
DHEA	Dehydroepiandrosterone
DHT	Dihydrotestosterone
EAP	Early Access Program
FDA-IID	Food drug administration-Inactive Ingredient database
USP-NF	United state pharmacopeia- national formulary
JPE	Japanese pharmaceutical excipients
SWOT	Strength weakness opportunities threats
LQC	Lower quality control
MQC	Medium quality control
HQC	High-quality control
% RSD	% relative standard deviation
LOD	Limit of detection
LOQ	Limit of quantification
ATP	Analytical target profile
CAA	Critical analytical attributes
FFD	Fractional factorial design
CMP	Critical material parameters
CPP	Critical process parameters
CCD	Central composite design
QbD	Quality by Design
NMR	Nuclear magnetic resonance
TLC	Thin layer chromatography



CPCSEA	Committee for the purpose of control and supervision of experiments on animal
EDTA	Ethylene diamine tetra acetic acid
IS	Internal standard
TBME	Tetra-butyl methyl ether
ITZ	Itraconazole
LLOQ	Lower limit of quantification
HRMS	High resolution mass spectroscopy
AIC	Akaike information criterion
MSC	Model selection criteria
MDT	Mean dissolution time
DE	Dissolution efficiency
t <sub>1/2</sub>	Half-life
T <sub>max</sub>	Time to peak drug concentration
V <sub>d</sub>	Volume of distribution
CL	Clearance
K <sub>e</sub>	Elimination rate constant
MRT	Mean residence time
mg	Milligram
µg	Microgram
θ	Theta

# **Chapter 1: Introduction**

### 1.0 Background

#### 1.1 Today's challenges in drug development: Focus on anticancer compounds

Cancer stands as a prominent global health challenge and one of the primary contributors to worldwide mortality. According to the 2024 statistics from the American Cancer Society, it is expected that there will be approximately 2,001,140 new cases of cancer and 611,720 deaths related to cancer in the United States, which is about 1,680 deaths per day (1). However, the growing challenges of cancer treatment underscore the need not only for the exploration and manufacturing of novel anticancer drugs but also for the improvements of existing ones (2–5). Present anticancer drugs often face a high attrition rate due to inadequate pharmacokinetics, primarily resulting from their low water solubility (5–7). About 65% of presently approved oral anticancer active pharmaceutical ingredients (API) demonstrate poor water solubility, which impedes their capacity to achieve optimal therapeutic outcomes while minimizing toxicity (8). In the past several decades, significant advancements have been made in developing oral formulations for anticancer API. Currently, oral administration is preferred for cancer treatment due to its convenience, painlessness, safety, and cost-effectiveness (9). Moreover, oral dosage forms provide convenient storage and transportation. Ensuring complete and predictable absorption is essential to oral administration. Achieving this necessitates drug solubility in water for effective absorption in the gastrointestinal tract and subsequent entry into the circulatory system. Nevertheless, the majority of anticancer drugs exhibit poor water solubility, leading to incomplete absorption and low bioavailability, contributing to significant inter and intra-individual variation in API concentration in vivo (10,11).

The poor water-soluble anticancer drugs result in less effective formulations or necessitate the use of excipients/carriers with harmful side effects. Briefly, sorafenib tosylate oral kinase inhibitors used to treat liver and kidney cancers (12) fall under the biopharmaceutical Classification System (BCS) class II due to their low solubility and high permeability. Consequently, sorafenib dissolves slowly in the gut, impacting its absorption and resulting in low bioavailability and significant variability between individuals (13). This poor solubility contributes to either ineffective treatment or potential toxicity (14). Additionally, anticancer medications must first be absorbed and enter the bloodstream to achieve optimal therapeutic effects. Intravenous infusion is often preferred to ensure complete bioavailability, as the entire dose is delivered directly into circulation and rapidly distributed to target sites. Nonetheless intravenous administration presents inconvenience to

patients, necessitating hospital visits for treatment and potentially inducing various side effects during the process. For example, the marketed intravenous formulation of paclitaxel (Taxol<sup>®</sup>) was formulated containing the Cremophor EL and ethanol for the solubilization of paclitaxel. However, the use of Cremophor EL has been accompanied by acute hypersensitivity reaction, myelosuppression, neutropenia, and neurotoxicity in patients, despite the premedication efforts, with approximately 44 % experiencing reactions and around 3% facing potentially life-threatening responses (15). Therefore, the limited water solubility of current anticancer drugs presents impediments not only for the oral formulations but also for the intravenous formulations. Thus, improving the solubility of anticancer API is a major obstacle in the development of better cancer therapies in the pharmaceutical industry (2).

### **1.2 Solubility as a critical hurdle for anticancer compounds**

The inadequate water solubility of the anticancer drugs has often been recognized as a significant barrier to their development and clinical application. The drug is not entirely soluble in 250 mL of aqueous solvent within the pH ranging from 1 to 7.5 at a temperature of 37.5°C at its maximum dose strength; it is categorized as poorly soluble according to the BCS system (16,17). BCS classifies drugs into four groups based on their solubility and permeability, as depicted in Figure 1.1. Both BCS Class II and IV compounds demonstrate limited aqueous solubility. Class II drugs, which account for 30% of the market and 60 to 70% of the pipeline, are an ideal target for solubility augmentation. Class IV exhibits low aqueous solubility, inadequate permeability, inter and intrasubject variability, a substantial positive dietary impact, and unpredictable and poor absorption, making oral administration challenging.

Furthermore, poor solubility in water is a fundamental characteristic of numerous anticancer drugs ascribed to two primary factors. Firstly, during the discovery phase, the physicochemical properties of the drugs are not adequately considered. Secondly, the essential hydrophobic structural properties required for their permeability, activity, and stability result in poor aqueous solubility. A significant constraint in the pipeline for developing anticancer drugs has been the insufficient emphasis on drug disposition and pharmacodynamics (18). The widespread application of the “nanomolar rule” in drug development prioritized the selection of substances with nanomolar potency based on the assumption that they would be safe and effective at low doses. However, this approach overlooked crucial factors, such as the physicochemical properties

of these drugs, significantly affecting their pharmacokinetics, safety, and efficacy. As a result, compounds like combretastatin A-4, which exhibit strong cytotoxicity at nanomolar concentrations, were chosen for development but eventually failed due to poor water solubility. Greater emphasis should be placed on improving the safety and efficacy of poorly water-soluble anticancer APIs to optimize their potential as clinical therapies (19,20).

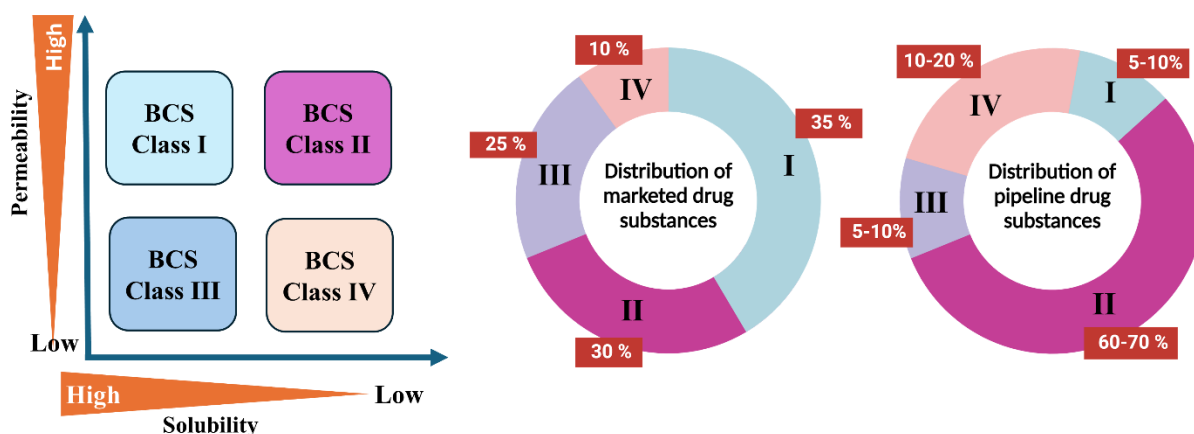


**Figure 1.1.** Description of different BCS classes

The low aqueous solubility of anticancer drugs is attributed to their crystalline structure (21). Conversely, while the amorphous form of certain anticancer drugs exhibits more excellent water solubility, it also tends to be inherently unstable, prompting the preference for synthesizing most anticancer drugs in their crystalline state. For example, bicalutamide utilized in prostate cancer treatment is known for its limited water solubility (22). Numerous studies have evidenced the bicalutamide amorphous form's higher water solubility than its crystalline counterpart. Nonetheless, the instability of the bicalutamide amorphous state often leads to drug recrystallization. Consequently, bicalutamide is predominantly marketed in its less water-soluble crystalline form, underscoring the intrinsic challenge of poor water solubility in numerous anticancer drugs (22,23).

### 1.3 Techniques for overcoming solubility limitations of anticancer compounds

Solubility is a critical physicochemical attribute that influences the bioavailability and therapeutic efficacy of the drug. In the past two decades, with the rise of rapid throughput screening and

combinational screening methods, the dissolution and solubility performance of poorly soluble active pharmaceutical constituents has become a severe concern for formulation development. The requirement of high doses to achieve adequate plasma concentration after oral intake is commonly associated with drugs having low water solubility (24). This obstacle, stemming from their poor aqueous solubility, presents a significant challenge in formulating both novel and generic compounds. Essential for absorption, drugs must be in an aqueous solution at the absorption site. Additionally, the majority of drugs being weakly acidic or weakly basic exacerbates their limited solubility in water (25). To address the challenges various techniques are employed to enhance solubility and dissolution rates within gastrointestinal fluids. These approaches are carefully chosen based on the drug's properties, type of excipients, method of preparation, and intended dosage form.

For enhancement of the solubility of poorly soluble drugs, several formulation approaches have been developed, such as salt formation, use of surfactant, nanosuspension, particle size reduction, complexation reaction, co-crystallization, and solid dispersion, all of which appear to be potentially promising strategies to augment the dissolution profile of hydrophobic entities (17). However, each approach has limitations and advantages, as illustrated in Table 1.1. Hence, identifying the most effective solubility enhancement technique is essential for developing a successful formulation with enhanced oral bioavailability, decreased dose frequency, and increased patient compliance while maintaining a low production cost. The solid dispersion technique holds the most promise for the formulators because of its practicality, economy, ease of preparation, simplicity of optimization, reproducibility, and multiple processing and excipient alternatives.

**Table 1.1** Different solubility enhancement techniques for poorly water-soluble drugs

<b>Solubility Enhancement method</b>	<b>Mechanism</b>	<b>Advantages</b>	<b>Disadvantages</b>	<b>Reference</b>
Particle size reduction	The application of mechanical forces to break down larger drug particles into smaller ones dispersed within a carrier matrix	➤ Reducing the particle size leads to increases in the surface area of the drug particles, which enhances the dissolution rate and bioavailability of the drugs	➤ Reduced particle size increases surface area, exposing it to moisture and oxygen and causing stability issues ➤ Scaling up from lab to commercial scale can	(26)

				cause variability in product performance	
Nano suspension	Prepares ultrafine drug particles suspended in the stabilizing medium	<ul style="list-style-type: none"> <li>➤ Reduction in the particle size, increases the dissolution rate and extent of absorption</li> <li>➤ It has the potential to elevate the amorphous content within particles, altering the crystalline structure and solubility</li> </ul>	<ul style="list-style-type: none"> <li>➤ Complex manufacturing process</li> <li>➤ Physical instability</li> </ul>	(27,28)	
Use of surfactant	Surfactant reduces the interfacial tension between drug particles and the dissolution medium, enhancing wetting, and dispersion	<ul style="list-style-type: none"> <li>➤ Surfactants can stabilize the dispersion of drug particles within the solid dispersion matrix, preventing particle aggregation and maintaining a uniform distribution</li> <li>➤ By facilitating wetting and dispersion, surfactants increase the surface area of drug particles exposed to the dissolution medium, leading to faster dissolution rates</li> </ul>	<ul style="list-style-type: none"> <li>➤ Some of the surfactant shows higher toxicity at higher concentration</li> <li>➤ Surfactants may interact with other formulation components, leading to compatibility issues or changes in the drug stability</li> </ul>	(29)	
Salt formation	Salt formation involves the ionization of the acidic or basic drugs with the counterions, leading to the formation of the salt that is the more soluble in the aqueous media	<ul style="list-style-type: none"> <li>➤ Significant solubility improvement without altering the chemical identity</li> </ul>	<ul style="list-style-type: none"> <li>➤ Limited applicability of certain classes of drugs</li> <li>➤ Some salt forms may exhibit hygroscopic behavior, leading to stability issues in humid conditions</li> </ul>	(30)	
Complexation	Complexation occurs via electrostatic forces, van der Waals forces, or coordination bonding between the drug and ligands. The prepared complex is often more soluble in the aqueous media due to the strong interaction with water molecules	<ul style="list-style-type: none"> <li>➤ Complexation can protect the labile drug molecules against degradation by forming stable adducts</li> <li>➤ Some particular ligands selectively bind to the specific drug molecules, enabling for the targeted drug delivery systems</li> </ul>	<ul style="list-style-type: none"> <li>➤ Not all the complexes remain intact throughout the entire digestive system; some might disintegrate before reaching the target site, which directly affects the bioavailability</li> </ul>	(31)	

Co-crystal	Co-crystals are formed through non-covalent interactions between an active pharmaceutical ingredient (API) and a coformer, leading to the creation of a new crystalline structure with unique properties	<ul style="list-style-type: none"> <li>➤ Co-crystals can improve the stability of drugs, protecting them from degradation, enhancing their shelf life</li> </ul>	<ul style="list-style-type: none"> <li>➤ Finding the specific co-formers for co-crystal formations can be complex and time-consuming due to the trial-and-error approach</li> <li>➤ Some co-crystal formation methods may use hazardous solvents and produce toxic byproducts</li> </ul>	(32)
Hydrotropic system	Hydrotropy is a phenomenon where the addition of a second solute (hydrotrope) increases the aqueous solubility of poorly soluble solutes by forming complexes with them	<ul style="list-style-type: none"> <li>➤ Hydrotropes enhance solubility by modifying the structure of the water molecules around the solutes, facilitating their dissolution</li> </ul>	<ul style="list-style-type: none"> <li>➤ Some hydrotropic agents show toxicity at a specific concentration</li> </ul>	(33)
Amorphous Solid Dispersion (SD)	Amorphous state for the drug lacks the crystal lattice requires no energy to break the crystal lattice,	<ul style="list-style-type: none"> <li>➤ By creating a high surface area for drug dissolution, solid dispersion improves the drug dissolution rate, ensuring faster and more effective drug release</li> <li>➤ Reduced agglomeration</li> <li>➤ Ease of production</li> <li>➤ Wettability improvements</li> <li>➤ Improved bioavailability</li> <li>➤ Flexibility in carrier material selection</li> </ul>	<ul style="list-style-type: none"> <li>➤ Physical instability with changes in crystallinity and decreased dissolution rate over time</li> </ul>	(17)

#### 1.4 Amorphous solid dispersion

In 1961, the solid dispersion (SD) concept was introduced by Sekiguchi and Obi in 1961(34). Subsequently, in 1971, Chiou and Riegelman coined the term, defining it as the incorporation of one or more active ingredients within an inert carrier in solid form, achieved through techniques including melting, solvent, and melting-solvent approaches (35). The careful selection of suitable carriers is crucial for preparing effective and stable SD. The selection of optimal carriers in SD is crucial as they serve numerous properties. Primarily, the carrier is projected to enhance the solubility and dissolution of poorly water-soluble drugs. This can be accomplished in various ways, such as reducing particle size, improving wettability and the amorphous state of the drug,



or a combination of these mechanisms. Secondly, carriers play a crucial role in imparting physical stability to the formulated dispersion, primarily when the dispersion exists in an amorphous state. This stability is achieved through factors such as the carrier's high glass transition temperature ( $T_g$ ), thorough mixing with the drug, molecular dispersion of the drug within the carrier, intermolecular interactions, or a combination of these mechanisms (36–38). In 1960, for the preparation of SD, water-soluble crystalline carriers such as sugars and urea were highly used. This particular SD falls within the class of eutectics. It exhibits remarkable thermodynamic stability owing to its crystalline structure and demonstrates a slower drug release compared to amorphous forms (36,39). However, the constraints associated with crystalline carriers have spurred the exploration of SD using carriers capable of stabilizing drug molecules in the amorphous state.

Since 1961, a wealth of literature has focused on SD technology, as evidenced by approximately 5457 records in the Scopus® database relating to "Solid Dispersion" OR "Solid Dispersions" as of March 2020. Extensive research has been conducted on a wide variety of polymeric carriers such as polyvinylpyrrolidone (PVP), polyethylene glycol (PEG), as well as natural polymers including cellulose derivatives such as hydroxypropyl methylcellulose (HPMC), hydroxypropyl methylcellulose acetate succinate (HPMCAS), and ethyl cellulose (EC). The fascinating physicochemical and thermodynamic properties of these polymeric carriers make them well-suited for formulating SDs (40).

### **1.5 Classification of Polymeric Carriers**

In SD technology, polymeric carriers are utilized, which are classified on the basis of several factors, such as their origin, physical form, ionization potential, and relative hydrophilicity (36,37,39,41). The physical state of the polymeric carrier stands out as a crucial criterion for classification due to its direct impact on the properties of the resulting dispersion. Polymeric carriers are typically categorized into disordered amorphous states and ordered crystalline states. It is broadly acknowledged that crystalline polymeric carriers tend to exhibit constrained drug solubility (42,43). SD with amorphous polymeric carriers enhance solubility and dissolution rates due to the high-energy amorphous phase of the API but often faces stability issues at room temperature due to potential drug recrystallization. Various polymeric carriers, including PVP, HPMC and polyvinylpyrrolidone vinyl acetate (PVP VA), extensively utilized in the SD method,

fall under the classification of amorphous polymeric carriers.

Polymeric carriers are classified into hydrophilic, hydrophobic, and amphiphilic categories based on their differing levels of hydrophilicity. The use of hydrophobic polymeric carriers in SD technology, aimed at enhancing aqueous solubility, may appear counterintuitive. Nonetheless, hydrophobic polymers create highly effective single-phase systems with less soluble drugs and inherently more lipophilic (BCS-II & IV). The drug, when intimately mixed or molecularly dissolved within the polymeric carrier, typically stabilizes in the amorphous state, making it relatively more physically stable compared to hydrophilic counterparts (44,45). Although the carriers are hydrophobic, the increased solubility and dissolution in these dispersions are due to the drug's amorphous state. This state eliminates the need for extra energy to break the crystal lattice, enhancing solubilization (46). Additionally, the hydrophobic carrier prevents drug aggregation in solution, maintaining supersaturation relative to crystalline solubility (47). Examples of hydrophobic polymeric carriers include ethyl cellulose (EC), cellulose acetate (CA), cellulose acetate phthalate (CAP), and Eudragits.

Hydrophilic polymeric carriers are one of the most extensively used polymers to prepare SD formulations. Hydrophilic polymeric carriers emerge as an optimal option for SD since they are hydrophilic, which results in minimal solubility with typically hydrophobic drugs (BCS-II & IV). Due to this, molecularly dissolve a drug, substantial amounts of polymers are required (43,48,49). The deliquescent nature and limited drug loading in high proportions of the hydrophilic polymers exacerbate the phase separation problem, resulting in the SD being physically unstable. Mechanistically, as the hydrophilic carrier dissolves, it releases the drug molecule, forming a supersaturated solution of the drug (40,50). Polymeric surfactants such as di-block and tri-block copolymers exhibit amphiphilic characteristics, which facilitate micellar solubilization and improved wettability, stabilizing a drug in a disordered amorphous state. Amphiphilic polymers, including block copolymers like Soluplus® and various grades of poloxamers, fall under this category. Moreover, polymeric carriers are categorized according to their propensity for ionization. Typically, these polymers exhibit solubility and dissolution properties dependent on pH (51,52).

### **1.6 Criteria for selecting polymeric carriers**

The selection of polymeric carriers for SD preparation can be notably impacted by three factors: safety, kinetic, and thermodynamic aspects. It is conventionally recognized that any excipients used in pharmaceutical formulations should exhibit chemical and pharmacological inertness. Similarly, this requirement extends to polymeric carriers employed in SD preparation, preferably holding a Generally Recognized As Safe (GRAS) status (39,43,53). From the kinetic point of view, the polymer should be able to hinder drug precipitation into its crystalline forms within the gastrointestinal (GI) tract. This is especially pertinent for weakly basic drugs, which tend to precipitate in the intestine due to the prevalence of their unionized states (54,55). Moreover, if the polymer exhibits surfactant properties, the drug's partitioning in micelles could enhance solubility. This solubility enhancement may complement the benefits derived from the high-energy amorphous state (56,57). Hydrophilic and amorphous polymers tend to exhibit deliquescence. In scenarios of low load SD, where the polymer content is typically high, maintaining physical stability becomes challenging due to the potential de-vitrification of the amorphous state and subsequent phase separation (58,59). Moreover, thermodynamic considerations are crucial for the stability of dispersions in an amorphous state. The polymer must possess a high  $T_g$  to ensure the stability of the prepared dispersion at room temperature, thereby reducing the likelihood of Johri-Goldestain (JG) relaxations (60,61). For example, if the goal of the formulation scientist is to create an SD, the chosen polymer must demonstrate strong glass-forming capabilities across various compounds. The polymer's high phase-solubility with the drug is a prerequisite for achieving a homogeneous amorphous system. Additionally, having a high likelihood of adhesive intermolecular interactions, facilitated by hydrogen bond acceptor and donor properties, is desirable for forming stable and uniform amorphous dispersions. From a manufacturing standpoint, the polymer's solubility in organic solvents and its phase-solubility assist in preparing SD by the solvent and melt methods, respectively (54,62).

### **1.7 Understanding polymeric carrier mechanisms in SD**

#### **1.7.1 Inhibition of drug precipitation**

The significant challenge of low aqueous solubility in drug development often leads to poor and inconsistent bioavailability due to limited absorption in the small intestine. Various approaches have been developed to enhance the solubility and rate of dissolution to increase the free drug concentration at the absorption site. A supersaturating drug delivery system is one method to increase the free drug concentration. It is a thermodynamically unstable system, and there is a

tendency to precipitate again the supersaturate drug. In that case, a precipitation inhibitor plays a vital role in inhibiting the precipitation and maintaining the supersaturated state for a prolonged period in the intestine, which increases the absorption of the drug and improves the bioavailability of a poorly water-soluble drug. The supersaturation and precipitation phenomenon can be described by the “spring and parachute effect,” shown in Figure 1.2 (63) which states that, Curve A illustrates the crystalline drug having high stability with low solubility. Curve B illustrates that the API is unstable and quickly falls down in the aqueous media without attaining supersaturation. Curve C illustrates that the API achieves supersaturation, which acts as a “spring” before falling down in the aqueous media, owing to the increases in the nucleation/ precipitation and crystal growth of the API. Curve D illustrates that the amorphous API maintains the supersaturation state for a more extended period due to the presence of precipitation inhibitors, which act as a parachute effect

The polymer that can prevent precipitation is commonly known as a precipitation inhibitor. They maintain the supersaturation by inhibiting the drug molecular aggregation to minimize the risk of precipitation. Recent investigations have provided initial insights into various theories and mechanisms of precipitation inhibitors as follows: the primary mechanisms by which the cellulosic polymers prevent recrystallization, such as reducing drug molecular mobility by increasing the viscosity of the medium and reducing nucleation rate. Additionally, they prevent crystal growth by affecting the diffusion coefficient and altering molecular integration in the crystal lattice by changing the level of solvation in the crystal-medium interface. Generally, the solubility/dissolution of the drug is based on the ability of the polymers to stabilize the drug in an amorphous state, thus enhancing the drug concentration in the dissolution media and preventing crystallization. Common precipitation inhibitors include HPMC, PVP, and HPMCAS (64,65). HPMCAS is one of the most effective precipitation inhibitors among all precipitation inhibitors (63). Reports indicated that HPMCAS had been employed to maintain the supersaturated state of compounds such as nifedipine, ziprasidone, griseofulvin, phenytoin, and sildenafil citrate. Curatolo et al. (64) and Friesen et al.(66) both found that enhanced inhibition resulted from HPMCAS possessing two key attributes: firstly, partial ionization beyond pH 5, facilitating the stable nanosized amorphous drug-polymer aggregates and secondly, the inclusion of hydrophobic domains that offers binding sites for the drug molecules (65).

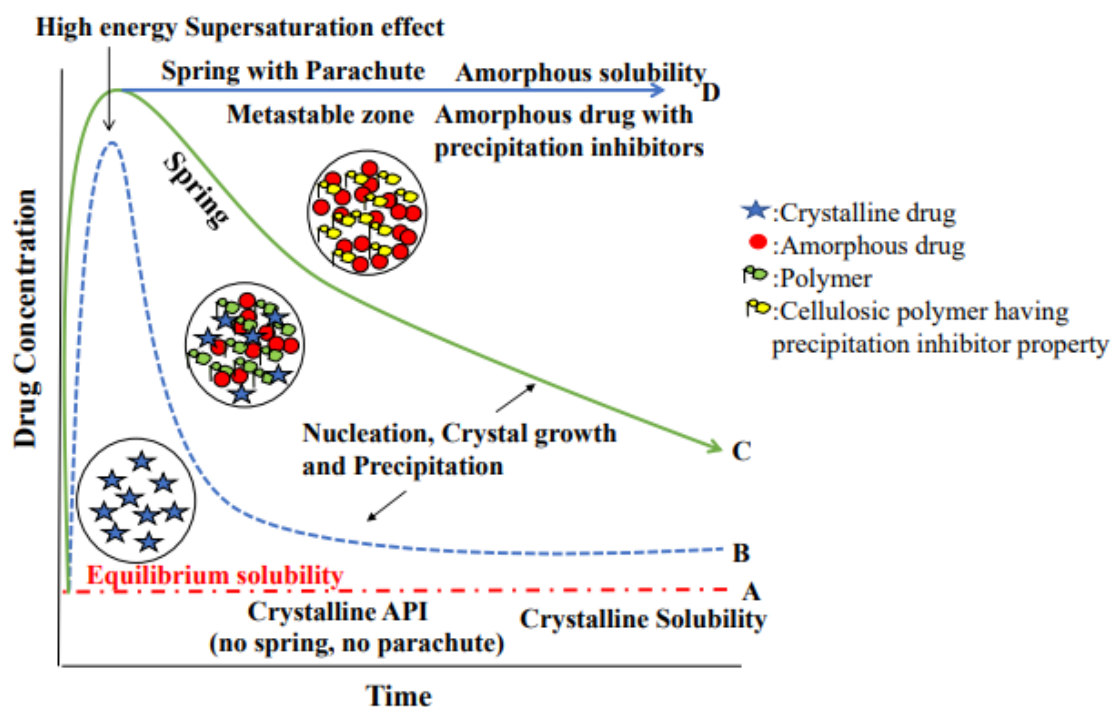


**Figure 1.2.** Spring and parachute effect to attain high supersaturation for poorly water-soluble drugs

### 1.7.2 Antiplasticization effect

The process of a substance becoming rigid or losing its plasticity, known as antiplasticization, was described in thermodynamics as causing an increase in the materials  $T_g$  (67). This increase in  $T_g$  results in higher free energy, promoting the transformation of the amorphous drug into its crystalline form. Combining materials with different  $T_g$  values results in an intermediate  $T_g$  for the mixture. When a low- $T_g$  amorphous drug is mixed with a high- $T_g$  polymer, the polymer is plasticized, and the drug's  $T_g$  increases due to antiplasticization (68). Sathigari et al. found that this anti-plasticizing effect stabilized amorphous efavirenz with Plasdone S-630 by increasing viscosity and reducing drug diffusion. However, experimental  $T_g$  values sometimes differed from theoretical predictions due to suboptimal mixing and non-additive volume effects (69).

### 1.7.3 Intermolecular interaction between the drug and polymer

Paudel et al. found that weak forces like electrostatic, ionic, hydrophobic interactions facilitate bonding among the drug and polymer molecules, stabilizing amorphous SD systems. The strength

of these interactions depends on component miscibility and drug-to-polymer ratio. Infrared and Raman spectroscopy can identify these interactions, significantly affecting SD formulations (70,71).

### **1.7.4 Molecular mobility suppression of amorphous API in SD**

The stability of amorphous drugs in SD is improved by restricted molecular mobility, as polymers can limit the movement of these drugs. Mechanistic assessments of reduced crystallization tendency are crucial for evaluating stability. Techniques like solid-state NMR, DSC, and dielectric spectroscopy are used to measure molecular mobility. Strong drug-polymer interactions, such as ionic or hydrogen bonds, reduce drug mobility, delaying and slowing crystallization. Additionally, a noteworthy study revealed that increased polymer content enhances stability by extending the drug's relaxation period, thus restricting molecular mobility (72,73).

## **1.8 Different methods for the preparation of SD**

### **1.8.1 Melting method**

The melting method, developed by Sekiguchi and Obi in 1961, involves heating a drug and a hydrophilic carrier blend above their eutectic point, then rapidly cooling and solidifying the mixture. This simple, cost-effective technique has been used to formulate SD of drugs like paclitaxel (74), albendazole (75), sulfathiazole (34), fenofibrate (76), and furosemide (77). For instance, an SD of paclitaxel with poloxamer 188 and PEG enhanced drug release from poly( $\epsilon$ -caprolactone) films, achieving over 90% release within 1 hour at a 1:3 drug-to-poloxamer ratio (78).

### **1.8.2 Solvent evaporation method**

The solvent evaporation method is widely used in the pharmaceutical sector to enhance the solubility of poorly water-soluble drugs, particularly for heat-sensitive components. This technique involves dissolving the drug and carrier in a volatile solvent, followed by solvent evaporation with continuous agitation, producing an SD. The resulting SD is then subjected to crushed and sieved. Introduced by Tachibana and Nakamura in 1965 (79), this method was first applied to  $\beta$ -carotene and PVP in chloroform. It prevents drug decomposition due to low-temperature evaporation. This approach has significantly increased the solubility and dissolution of anticancer drugs like paclitaxel and docetaxel, with docetaxel's emulsified SD showing 34.2-

and 12.7-fold improvements, respectively, in solubility and dissolution at 2h (80).

### **1.8.3 Spray drying**

Spray drying is a procedure that is commercially accessible, continuous, scalable, and characterized by a very brief exposure feed to mild temperatures in comparison to any heat-based techniques. Due to limited interaction between the liquid particles and the heated air stream, the decomposition of active constituents is minimal. Various processes are involved in the spray drying process, starting from introducing the feed comprising of the drug, polymer, and other additives through a preheated spray nozzle into a drying chamber (containing a hot air stream) and causing atomization of the feed. This atomization causes the enlargement of the surface area of the droplets, thus facilitating the evaporation of the solvent, leaving the solid particulates separated by using a cyclone. The feed injection rate, inlet temperature, and atomization are essential spray drying process parameters. It is essential to optimize these variables to obtain a uniform amorphous dispersion. Moreover, spray drying has been broadly exhibited for preparing SD to enhance the solubility and bioavailability of poorly water-soluble drugs (21). For example, Herbrink et al. prepared the nilotinib SD using spray drying to improve the solubility. Soluplus was chosen as the optimal carrier following in vitro dissolution investigations. With a drug-to-Soluplus ratio of 1:7, the solubility of nilotinib was enhanced by 630-fold compared to the pure drug (81).

### **1.8.4 Freeze drying**

Freeze drying, often referred to as lyophilization, is a widely utilized approach for preparing SD, especially in the context of thermosensitive drugs. This technique includes atomizing a feed liquid containing poorly water-soluble or insoluble APIs and excipients. This atomization process occurs directly into a cryogenic liquid at room temperature, creating a frozen micronized powder. Subsequently, this powder is subjected to a drying process. In contrast to conventional techniques, freeze drying presents numerous benefits, including the generation of amorphous structures that increase the solubility of drugs and the production of powders with large surface areas. One significant advantage of freeze drying is in its ability to be used for thermolabile drug and carrier materials, effectively addressing the issue of stability encountered during the process of SD production. Although freeze-drying has numerous benefits, it is essential to acknowledge its inherent limitations. This includes the significant expenses involved in the preparation process, the vast amount of time required to eliminate any residual solvent, the difficulty in selecting a solvent

that is compatible with both the drug and carrier molecules due to variations in freezing temperatures, the necessity of maintaining the sample temperature below the  $T_g$  of the frozen concentration fraction for an extended duration, and the need for an adequate vapor pressure of the solvent during the lyophilization process (82). Freeze drying offers advantages such as amorphous structure formation and increased stability of sensitive materials during storage. In a study involving the anticancer drug exemestane, a phospholipid/sodium deoxycholate SD loaded with exemestane was prepared to enhance the drug's solubility and oral bioavailability (83). Compared to the pure drug, the solubility and dissolution rate of exemestane from the SD were elevated. Additionally, the absorptive transport of the SD exhibited a 4.6-fold increase compared to the conventional drug. Moreover, the area under the curve ( $AUC_{0-72h}$ ) of the drug in the SD was 2.3-fold higher than that of the drug administered alone (84).

### 1.8.5 Hot melt extrusion method

Hot-melt extrusion (HME) has emerged as a highly effective technology within the pharmaceutical industry, demonstrating its reliability across a wide range of applications and in drug delivery systems. The principal use of HME is the improvement of solubility and bioavailability when producing SDs. The HME process combines drug and carrier molecules in a solid mixture (21). This mixture is then subjected to specific temperature and pressure conditions, causing it to melt into a uniform or non-uniform melt phase. The resulting melt phase is subsequently extruded through an orifice to produce extrudates. Melt extrusion is commonly recognized as sustainable technology because it relies solely on temperature and pressure as processing parameters, eliminating the need for organic solvents to produce SD(85). Consequently, this approach effectively mitigates concerns related to residual solvent content. The HME equipment possesses a versatile design that allows for the customization of processes to attain specific objectives and adapt to different raw materials. This is achieved through the adjustment of modular design components, particularly the screws and barrels. According to reports, melt extrusion involving miscible components leads to the production of an amorphous solid solution. On the contrary, when an immiscible component is extruded, it results in the dispersion of an amorphous drug within a crystalline excipient. This method has proven beneficial for preparing SD in a single procedural stage. An extruder comprises a conveyor system for transporting materials and a die system for shaping the materials into the desired form. The hot melt extruder can be categorized into the following zones shown in Figure 1. 3 (A) a feed zone where input materials are introduced,



either as a physical mixture of the drug and polymer or separately; (B) a melting zone consisting only of conveying elements. The temperature in this zone should be maintained based on the melting point of the physical mixture of the drug and polymer (C). The mixing zone is particularly crucial as it ensures the homogeneous mixing of the molten substances. The screw configuration within this zone is comprised solely of the kneading element. The arrangement of the kneading components determines the characteristics and consistency of the solid dosage product. Additionally, a discharge zone is responsible for facilitating the flow of the molten material and ensuring the consistent passage of the mixture via a die, resulting in the formation of extrudates (86,87).

Compared to traditional manufacturing methods, HME offers significant advantages due to its straightforwardness and one-step production procedure, distinguishing HME from other conventional granulation processes, such as wet granulation, high shear granulator, dry granulation by roller compaction, and fluid bed processor. Using an environmentally friendly technology that obviates the need for organic solvents contributes to the long-term cost-effectiveness of this method. The HME technique can be combined with additive manufacturing to create patient-specific dosage forms, thereby expanding its potential applications in the pharmaceutical sector. This approach enables the large-scale production of batches ranging from a few kilograms to several tons, adhering to industrial and good manufacturing practices. Agarwal et al.'s study showcased the HME technique's superiority over spray drying in terms of physical stability assessment of SD at a temperature of 50°C and relative humidity of 51%. The results revealed the presence of birefringent crystals in the spray-dried SD after 3 months, whereas the HME SD remained amorphous, indicating a higher level of physical stability (88).

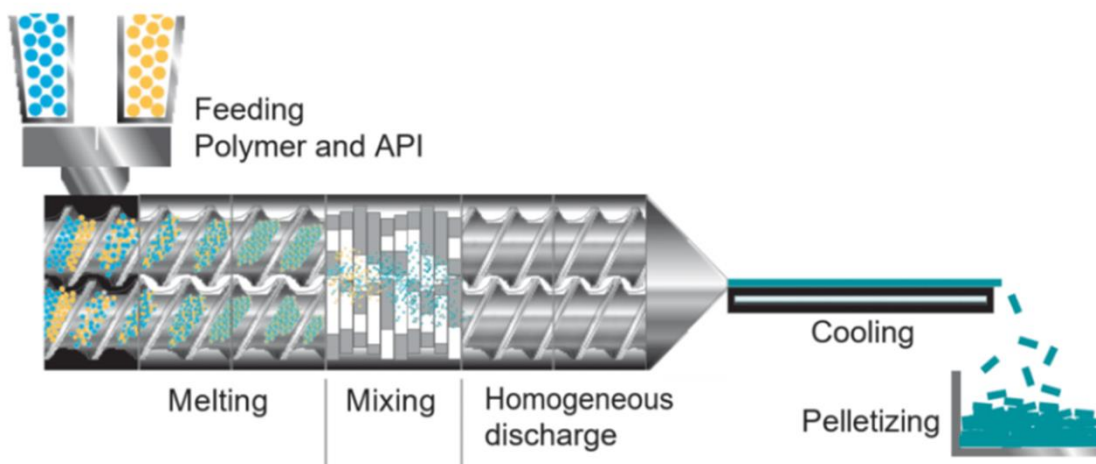


**Figure 1.3.** Hot melt extrusion process (87)

One constraint to consider is that the procedure necessitates the maintenance of elevated processing temperatures, which must be kept below the degradation threshold of the constituents within the formulation. Thus, the inclusion of some plasticizers aids in the reduction of the melt viscosity by decreasing the glass transition temperature ( $T_g$ ) of the mixture, enabling the process to be carried out at lower temperatures. Vitamin E (tocopherol), D-alpha tocopheryl PEG 1000 succinate, poloxamers, Tween®, Myrj®, and low molecular weight PEGs are some of the plasticizers that have demonstrated the capacity to enhance process performance. Material flow qualities are also important in maintaining a steady input rate from the hopper. For materials with limited fluidity, flow aids such as spray-dried mannitol, maltodextrin, and colloidal silica can be utilized. It has progressed from a lab scale to commercial size in recent decades, with products such as Kaletra®, Novir®, Onmel™, Noxafil®, Gris-PEG™, and Viekirax® (Europe)/Viekira on the market (89,90).

### 1.8.6 Co-precipitation method

This method involves initially dissolving the carrier in a solvent to create a solution, followed by adding the drug to the solution with stirring to achieve a uniform mixture. Subsequently, water is slowly added to the homogeneous mixture to trigger precipitation. Finally, the precipitate is filtered and subjected to drying. In a study conducted by Sonali et al., a silymarin SD was formulated using HPMC E15LV as the carrier through different techniques, including kneading, spray-drying, and

co-precipitation. The co-precipitation method yielded a silymarin SD that demonstrated significantly enhanced dissolution ( $p < 0.05$ ) compared to the other two methods. Additionally, the solubility of silymarin from the SD prepared via co-precipitation increased by 2.5-fold compared to that of the pure drug (91).

### 1.9 Stability of SD

The stability of SD is a critical challenge compared to crystalline solids due to their shorter molecular arrangements, which, although enhancing solubility and drug exposure in vivo, often result in physical and chemical instability (92,93). Factors contributing to this instability include inadequate prediction technologies, insufficient understanding of physicochemical properties, and limited manufacturing knowledge. To mitigate these risks, various strategies are employed, such as assessing stability under ICH-guided stress conditions (94) and monitoring changes via techniques like PXRD, DSC, ATR-FTIR, solubility, and dissolution tests (95). SD are inherently metastable and prone to spontaneous conversion to more stable crystalline forms. This transformation is influenced by the drug's interaction with polymers, which reduce molecular mobility (96). Processing and storage conditions, particularly temperature and relative humidity (RH), significantly impact the thermodynamic and kinetic aspects of this process (97).

Thermodynamic stability, molecular mobility, temperature, and moisture are different factors that affect the stability of SD. Thermodynamic stability is influenced by higher supercooling rates, which increase the kinetic barrier to crystallization and reduce molecular mobility (98). Molecular mobility impacts kinetic stability, with reduced mobility minimizing drug re-crystallization (99,100). Temperature affects crystallization, with storage recommendations suggesting temperatures well below the glass transition temperature ( $T_g$ ) or using the Kauzmann temperature ( $T_k$ ) to halt molecular mobility (101,102,103). Moisture absorption in amorphous forms acts as a plasticizer, reducing  $T_g$  and accelerating crystallization, while hydrogen bonding among water, polymer, and API further impacts stability. Techniques like differential scanning calorimetry and spectroscopy analyze these interactions (104,105,106).

### 1.10 Addressing challenges of poorly soluble compounds through SDs

SDs can address the challenges associated with the poorly-water soluble anticancer drug as follows:

### 1.10.1 Improving the oral bioavailability

When compared to free drug, SD formulations can significantly improve the oral bioavailability of low water-soluble anticancer drugs. By enhancing the apparent aqueous solubility in gastrointestinal fluids, SDs enhance the dissolution rate of these drugs (2). For instance, Piao et al. developed an SD with paclitaxel, porous silicon dioxide, and HPMCAS, achieving a sevenfold increase in solubility and bioavailability in rats (107). Similarly, SDs with ceritinib and various polymers like HPMC, HPC, PVPVA, and PVP have also shown enhanced dissolution and bioavailability (108).

### 1.10.2 Minimizing the pharmacokinetic variability

Pharmacokinetic variability significantly impacts the therapeutic effectiveness of anticancer drugs with narrow therapeutic windows. High variability can cause plasma drug concentrations to exceed toxic levels or fall below the minimum effective concentration, leading to toxicity or suboptimal therapy. SD formulations can minimize this variability for poorly water-soluble anticancer drugs. The gastrointestinal pH varies widely due to factors like health conditions, age, food intake, and concurrent medications (109). For example, a docetaxel SD reduced intersubject variability in cancer patients, with % CV for AUC<sub>0-24</sub> decreasing from 85% to 43% and for C<sub>max</sub> from 84% to 51%, compared to a docetaxel premix solution (110). SDs address pharmacokinetic variability by improving solubility, reducing food interactions, decreasing efflux, and mitigating pre-systemic metabolism (111).

### 1.10.3 Enhancing Pharmacokinetic Linearity

Pharmacokinetics of drugs can be either linear or nonlinear. Linear pharmacokinetics means the relationship between the dose and the area under the curve (AUC) is directly proportional; doubling the dose doubles the AUC (109,112). Absorption, distribution, metabolism, and elimination can affect this linearity. SD formulations enhance the pharmacokinetic linearity of poorly water-soluble anticancer drugs compared to conventional formulations. These drugs may show a linear increase in AUC at lower doses but plateau at higher doses due to limited solubility in gastrointestinal fluids. SDs, with higher apparent aqueous solubility, maintain proportional AUCs even at higher doses.

Elacridar, an inhibitor of P-glycoprotein (P-gp) and breast cancer resistance protein (BCRP), is a

promising absorption enhancer for anticancer drugs but is hindered by poor solubility and nonlinear pharmacokinetics (113,114). Sawicki et al. developed binary and ternary SDs of elacridar hydrochloride using polymers like PVP and PVPVA and surfactants like sodium dodecyl sulfate, significantly improving elacridar dissolution compared to physical mixtures. The SD with PVP and sodium dodecyl sulfate achieved complete dissolution and thermodynamic stability. Tablets containing elacridar SD were tested in a clinical trial with doses from 25 mg to 1000 mg, revealing a linear increase in C<sub>max</sub> and AUC across this range. This SD approach provided a predictable, linear pharmacokinetic profile for elacridar, supporting its use in future anticancer drug trials (115).

### 1.10.4 Reducing toxicity

The incidence of toxicities in anticancer medications with narrow therapeutic windows is significantly influenced by the pharmacokinetics of poorly water-soluble drugs. Variability in drug pharmacokinetics can cause plasma-drug concentrations to intermittently exceed safe levels, leading to potentially life-threatening toxicity (116). SD formulations can help reduce this toxicity risk for poorly water-soluble anticancer drugs. For instance, the high interpatient variability in the pharmacokinetics of sorafenib (Nexavar®) ranges from 36% to 91%, increasing the risk of toxicity or subtherapeutic outcomes. Truong et al. developed an SD of sorafenib using Soluplus® and SLS, enhancing its bioavailability and showing the potential to reduce pharmacokinetic variability and associated toxicity (117). Additionally, SD formulations can reduce the dose and pill burden, improving patient compliance (2).

### 1.11 Exploring the role of HPMCAS and HPMC HME as polymeric carriers in SD

Among all the polymeric carriers, HPMCAS and HPMC HME stand out due to their remarkable application in the pharmaceutical dosage form. Recent publications have highlighted the exceptional capabilities of HPMCAS and HPMC HME in preventing the crystallization of API and enhancing the solubility, dissolution rate, and oral bioavailability of poorly water-soluble drugs (118,119).

Numerous publications indicate that each grade of HPMCAS is unique and a suitable polymer to enhance the solubility of the poorly aqueous-soluble drug (119). Winslow et al. prepared an SD of rifapentine-containing cellulose derivatives (HPMCAS) prepared by film casting and cryogenic

grinding. These developed formulations observed the improvement in apparent solubility and maintenance of supersaturated solutions at intestinal pH. It was demonstrated that HPMCAS provided a nearly fourfold rise in total AUC compared to rifapentine alone (120). Shah et al. conducted a study to improve the solubility of vermafunib by changing it into an SD by applying the solvent-controlled precipitation method. The dispersion comprising vermafunib and HPMCAS, in which the drug is molecularly dispersed in the polymeric matrix, improves the solubility of the poorly soluble drug. Vermafunib SD showed almost 30 times higher solubility than the solubility of the pure API (121). Additionally, Curatolo et al. conducted a case study evaluating 41 polymeric carriers to assess their effectiveness in maintaining the supersaturation for nine poorly soluble drugs. Among all these carriers, HPMCAS emerged as the most effective carrier for inhibiting precipitation (64). Xie et al. examined the influence of several polymers on celecoxib crystallization in an amorphous condition. Here, polyvinyl pyrrolidone (PVP) was observed to be minimally effective, with nucleation beginning in 60 min. In contrast, HPMCAS and HPMC delayed/prevented crystallization, where no nucleation was seen during the 6 h of experimentation. Cellulosic polymers were more effective in impeding the crystallization of lipophilic molecules due to their amphiphilic nature (122). Table 1.2 shows the different applications of polymeric carriers HPMCAS and HPMC HME in SD with different preparation methods.

**Table 1.2.** Different applications of HPMCAS and HPMC HME in SD with different preparation methods

<b>Drug</b>	<b>Polymer</b>	<b>Method of preparation</b>	<b>Observation</b>
Fenofibrate	HPMCAS and HPMC	Spray-dried method	Bedi et al. reported the study with fenofibrate SD using HPMCAS, comparing it with regular HPMC using spray drying. The results indicated that HPMCAS provided superior performance over conventional HPMC polymer (123).
Griseofulvin, Nifedipine, Phenytoin	HPMCAS	Spray-dried method	This study concluded that, after conducting tests on 41 materials. It was evident that HPMCAS proved to be the most effective in maintaining drug supersaturation. Drug/HPMCAS spray dried dispersion was more effective in prolonging the supersaturation of the drug

			compared to the other polymer (124).
Nifedipine	HPMCAS	Solvent evaporation method	The solvent evaporation process formulated Nifedipine SD to determine the recrystallization inhibition for all three types of HPMCAS substitution, solubilizing the drug and polymer in methanol. Initial dissolution was higher than the pure drug in all cases, and the HPMCAS with the highest acetyl and lowest succinyl substitution (Type-LF) showed recrystallization behavior (125).
Itraconazole	HPMCAS	Hot-melt extrusion	In this study, they used surfactants like alpha-tocopherol PEG 1000 succinate, poloxamer 407, and poloxamer 188 as part of extrudates with itraconazole and HPMCAS polymer, resulting in enhancing the extrudability at 130°C instead of 170°C which is the typical temperature to extrude pure HPMCAS. It also showed an enhancement in the drug release in acidic conditions, from 8% in pure HPMCAS SD to 50% in surfactants containing HPMCAS SD (126).
Nifedipine	HPMCAS	Hot-melt extrusion	Nakamichi et al. prepared the enteric SD with HPMCAS using a twin-screw extruder. HPMCAS has a ductile character; it can be extruded quickly with a twin-screw extruder. It was discovered that HPMCAS prevents nifedipine from crystallizing in an aqueous condition. It also enhances the dissolution of nifedipine by the extrusion method (127).
Carbamazepine	HPMC HME 15LV	Hot melt extrusion	Carbamazepine SD prepared with HPMC HME 15 LV and Soluplus by the HME method exhibited low moisture absorption and better thermal stability, beneficial for long-term stability and high dissolution ability (128).
Ritonavir	HPMC HME 15 LV	Hot melt extrusion	The wide processing range of HPMC HME enables the exploration of the process parameter design space, which helps to study and reduce drug degradation for sensitive compounds like Ritonavir (129)

## 1.12 Problem statement

### *Abiraterone acetate in the treatment of prostate cancer*

Abiraterone acetate (ABTA) was approved for use in patients with metastatic castration-resistant prostate cancer (mCRPC) who had previously been treated with chemotherapy. The current marketed formulation of ABTA faces several challenges, including high doses (1000 mg/day), low bioavailability (less than 10% in fasting conditions), and high therapy cost. Moreover, the ABTA exhibits inter-individual pharmacokinetic variability and strong positive food effects when administered with low fat (7- and 5-fold increase in the  $C_{max}$  and  $AUC_{0-\infty}$ , respectively) and high fat (17- and 10-fold increase in the  $C_{max}$  and  $AUC_{0-\infty}$ , respectively) which requires the commercial drug product to be taken on the fasting stomach at least 2h before and 1h after meal to avoid the overexposures (130,131). However, it is of great interest to develop a new pharmaceutical formulation of ABTA that improves the solubility and bioavailability of ABTA, which could potentially allow food effect elimination, possibly dose reduction, and reduce the overall variability in absorption, such as formulation would meet higher standards in terms of both safety and convenience for the patients.

### ***Existing formulation strategies of ABTA***

A relatively limited number of publications detail various formulation strategies to enhance the oral delivery of ABTA. If a formulation can achieve the same pharmacokinetic profile and exposure as Zytiga® but is more efficient, addresses food effects, and reduces pill burden, cost, and lifestyle constraints, it becomes more favorable for patients. Herein, the approaches will be discussed and compared, emphasizing the existing gaps in the literature (130).

### ***ABT salt formation***

ABTA is the ester prodrug of ABT and should not be misconstrued as an acetate salt. The reported work exhibited that ABT HCl monohydrate was easily synthesized by extracting ABTA from crushed Zytiga® using ethanol, followed by filtration and recrystallization. The extracted ABTA solubilized in the methanol and HCl was incorporated, and after that, the solvent was slowly evaporated to obtain the ABT HCl monohydrate. The crystal packing of the ABTA salt differs significantly from the ABTA. Although there is no reported solubility data for ABT HCl monohydrate, it is anticipated to exhibit high solubility due to the dissociation of hydrochloride ions in aqueous environments, thereby enhancing its bioavailability through ABT supersaturation in the intestinal lumen. However, certain salts may precipitate in gastrointestinal fluid, reverting to their free acid and base forms, with slow redissolution owing to their very low aqueous



solubility. ABT HCl monohydrate holds promise due to its straightforward manufacturing process, which is suitable for commercial production. Nonetheless, the published data is preliminary and does not mention the in-vitro dissolution absorption data. Further investigation is also required to conclude its oral delivery efficacy (30,132).

### ***Nano-amorphous and wet-milled ABTA SD***

Particle size reduction is a proven approach to enhance bioavailability and mitigate the pharmaceutical food effect. Decreasing the crystal size of a drug augments its surface area, thereby enhancing dissolution rates, as per the Noyes-Whitney equation. Enhanced dissolution may result in improved drug absorption and decreased variability when the drug is taken alongside food. The bottom-up approach (nano-amorphous ABTA) and top-down approach (wet-milled ABTA) for diminishing the particle size of ABTA to enhance its dissolution and bioavailability have been explored. (133,134).

Nano-amorphous ABTA, produced via continuous flow precipitation, showed d50 and d90 values of 186 nm and 254 nm, respectively, with significantly enhanced dissolution compared to crystalline ABTA from wet milling, which had d50 and d90 values of 497 nm and 1050 nm. The nano-amorphous ABTA demonstrated an 8.3-fold and 2.9-fold increase in solubility in fasted-state and fed-state simulated intestinal fluids, respectively. This improved dissolution is attributed to its smaller particle size and amorphous nature, which mitigate the food effect and enhance dissolution rates compared to both wet-milled and unformulated ABTA (134).

The nano-amorphous ABTA formulation, which necessitates reconstitution with water before oral intake, results in a 'powder in a bottle' final dosage form (134). However, this mode of administration poses challenges in clinical practice, as patients are required to perform the reconstitution process independently, potentially leading to variability and inaccurate dosing on a day-to-day basis. This approach proves more complex for patients compared to the preferred oral dosage forms of tablets or capsules, such as Yonsa® or Zytiga® (135).

### ***SoluMatrix fine particle technology - Yonsa***

SoluMatrix fine particle technology, developed by iCeutica Inc., enhances the dissolution of poorly water-soluble drugs like ABTA by combining particle-size reduction and the incorporation of surfactants. This technology develops particles ranging from 200 to 800 nm, improving

bioavailability and reducing food effects. Yonsa®, a SoluMatrix ABTA formulation, was FDA-approved in May 2018 for mCRPC treatment at a daily dose of 500 mg, to be taken with or without food alongside 4 mg methylprednisone twice daily (136–138). Yonsa® does not infringe Johnson & Johnson's patent for Zytiga® due to its co-administration with methylprednisone. Yonsa® tablets, taken with or without food, offer more predictable absorption than Zytiga®. However, despite FDA approval for both fed and fasted states, Yonsa® is predominantly taken in the fasted state. This may be due to prescribing habits or patient preferences. While Yonsa® provides clear benefits over Zytiga®, limited clinical trial data may cause physicians to hesitate in prescribing it over Zytiga® (139).

### 1.13 Gaps in existing research and rationale for the present work

Prostate cancer is one of the most prevalent forms of cancers diagnosed in men around the world, with approximately 0.3 million estimated deaths per year. Among the treatments for prostate cancer, androgen deprivation therapy (ADT) effectively controls the disease, particularly during a phase where testosterone levels in the serum are suppressed (139). However, there is a subsequent phase characterized by castration resistance, during which the disease progresses despite continuous testosterone inhibition. This phase is referred to as metastatic castration-resistant prostate cancer (mCRPC), where prostate cancer continues to advance despite ADT. The treatment of mCRPC has significantly expanded with the addition of various drugs, including enzalutamide, sipuleucel-T, docetaxel, cabazitaxel, radium-223, and ABTA. The approval of ABTA for mCRPC has significantly improved the treatment of choice for prostate cancer. ABTA, combined with prednisone, has shown synergistic benefits and better outcomes in mCRPC patients pretreated with docetaxel. Thus, ABTA may be considered a primary drug of choice for prostate cancer, offering survival benefits, particularly in mCRPC cases.

Zytiga, the marketed formulation of ABTA, has achieved significant clinical and commercial success, but delivering ABTA orally remains highly challenging. It falls under the BCS class IV, characterized by extremely poor aqueous solubility ( $< 0.5 \mu\text{g/mL}$ ) as well as low permeability. Its pH-dependent solubility causes ABTA to precipitate when transitioning from the gastric fluid to the alkaline intestinal region, reducing solubility, hindering API dissolution, and impeding drug absorption across the intestinal membrane. Due to its characteristics, the oral bioavailability of ABTA in humans is estimated to be less than 10%. Consequently, a substantial daily dose of 1000

mg (four 250 mg tablets taken once daily) is necessary to achieve therapeutic blood levels. Following oral administration, approximately 88% of the administered drug is excreted unchanged through feces, and another 5% is excreted in urine. Consequently, over 90% of the administered drug is excreted and does not contribute to its intended therapeutic effects (136). Moreover, abiraterone acetate exhibits inter-individual pharmacokinetic variability and strong food effects when administered with low fat (7- and 5-fold increase in the  $C_{max}$  and  $AUC_{0-\infty}$ , respectively) and high fat (17- and 10-fold increase in the  $C_{max}$  and  $AUC_{0-\infty}$ , respectively) which requires the commercial tablet formulation drug product to be taken on the fasting stomach at least 2h before and 1h after meal to avoid the overexposures (130,131) Apart from that, there are various treatment-related adverse effects arising from the administration of ABTA, and prednisolone therapy comprised of cardiac issues (such as ischemic heart disease, myocardial infarction, supraventricular arrhythmias, and tachyarrhythmias), hepatotoxicity (characterized by abnormalities in liver function tests), hypokalemia, hypertension, and manifestations of fluid retention or edema.

To overcome all the limitations of the ABTA, there limited number of publications detailing oral formulation approaches for ABTA, and numerous strategies remain unexplored. Additionally, the existing approaches reveal inherent limitations, such as ABT hydrochloride salt has been developed to improve gastrointestinal solubility; there's still a lack of reported data on solubility and dissolution testing for this advancement. Moreover, in the case of nano-amorphous ABTA formulation requires reconstitution with water before oral intake, resulting in a 'powder in a bottle' dosage form. This self-reconstitution process can lead to dosing variability and inaccuracies in clinical practice. Although FDA-approved for administration with or without food, Yonsa® is predominantly taken in the fasted state, indicating a discrepancy in adherence to dosing recommendations. This may result from prescribing habits, patient preferences, or healthcare provider instructions. Despite Yonsa® offering advantages over Zytiga®, limited clinical trial data (only 84 days) may cause physicians to hesitate in prescribing it over Zytiga®.

This gap in knowledge underscores the pressing need for innovative solutions such as amorphous SD using polymeric carriers to effectively address the challenges associated with delivering poorly water-soluble drugs like ABTA via oral routes. This developed formulation will help in overcoming the drawbacks of the existing formulations. This study will help in enhancing the solubility and bioavailability, ability to take with food or without food, decreasing dose, and

reducing the frequency of administration, leading to better patient compliance

To meet the above gap, we proposed the following objectives:

### 1.14 Objectives of the present work

The following are the specific objectives of the thesis work.

**Objective 1:** Preparation and evaluation of ABTA amorphous SD using hydroxypropyl methylcellulose acetate succinate (HPMCAS) through solvent evaporation and granulation method, utilizing an industry-feasible and scalable approach.

To fulfill the above objective following studies were conducted:

- (i) The development and validation of simple, rapid, and sensitive analytical (UV and RP-HPLC) methods and bioanalytical (HPLC) methods for the quantification of ABTA and ABT during various phases of the development such as preformulation, formulation development, and characterization, stability, and animal studies
- (ii) Pre-formulation investigations were conducted on ABTA exploring various polymers. These studies encompassed solubility assessments in both buffered solutions and organic solvents, stability evaluations encompassing solution state, and comprehensive characterization utilizing techniques such as Fourier transform infrared spectroscopy (FT-IR), Differential Scanning calorimetry (DSC), X-ray diffraction (XRD), and Thermogravimetric analysis (TGA) for both the drug and the polymer. Compatibility studies were conducted to ascertain the drug's and the polymer's interaction. The Hansen solubility parameter and flory-huggins drug-polymer interaction approach would be used to predict the miscibility of ABTA with the selected polymer
- (iii) Development of the SD of the ABTA with different grades of HPMCAS 716 and HPMCAS 912 using solvent evaporation and granulation methods. Solubility studies, in-vitro, and bio-relevant dissolution studies of the optimized SD were conducted in different dissolution mediums (pH 1.2, pH 6.8, pH 4.5, FaSSIF, and FeSSIF).
- (iv) Precipitation inhibition studies of the optimized ABTA SD formulation were conducted in a FaSSIF media.
- (v) Optimized SD formulation was characterized using FTIR, DSC, XRD, TGA, and FE-SEM.

**Objective 2:** Preparation and evaluation of ABTA amorphous SD using hydroxypropyl methylcellulose hot melt extrusion (HPMC HME) through the Hot melt extrusion method.

To fulfill the above objective following studies were conducted:

- (i) Development of the SD of the ABTA with different grades of HPMC HME 15 LV and HPMC HME 100 LV using the HME method at different extrusion temperatures.
- (ii) Precipitation inhibition studies of the different ratios of the ABTA and HPMC HME were conducted in FaSSIF media
- (iii) Solubility studies, in-vitro, and bio-relevant dissolution studies of the optimized SD were conducted in different dissolution mediums (pH 1.2, pH 4.5, FaSSIF, and FeSSIF).
- (iv) Optimized SD was characterized using ATR- FTIR, DSC, XRD, TGA, and FE-SEM.

**Objective 3:** Pharmacokinetic evaluations of the optimized SD formulation of ABTA and free ABTA in animals. These studies encompassed the determination of various pharmacokinetic parameters, including plasma drug concentration, mean residence time, half-life, and area under the curve, utilizing the Phoenix WinNolin Certera™ software (Pharsight, U.S.A; version: 8.0)

### References

1. Society AC. 2024-Cancer-Facts-and-Figures-Acs 2024. p. 10–2. [statistics/annual-cancer-facts-and-figures/2024/2024-cancer-facts-and-figures-acr.pdf](https://www.aacr.org/press-releases/2024-cancer-facts-and-figures-acr)
2. Gala UH, Miller DA, Williams RO. Harnessing the Therapeutic Potential of Anticancer Drugs through Amorphous Solid Dispersions. *Biochimica Et Biophysica Acta - Reviews on Cancer*. 2020;1873(1):188319.
3. Zamboni WC, Torchilin V, Patri A, Hrkach J, Stern S, Nel A, et al. NCI alliance. 2014;18(12):3229–3241.
4. Wong CH, Siah KW, Lo AW. Estimation of Clinical Trial Success Rates and Related Parameters. *Biostatistics*. 2019;20(2):273–286.
5. Di L, Fish P V, Mano T. Bridging Solubility Between Drug Discovery and Development. *Drug Discovery Today* 2012;17(9):486–495.
6. Hoelder S, Clarke PA, Workman P. Discovery of Small Molecule Cancer Drugs: Successes, Challenges and Opportunities. *Molecular Oncology*. 2012;6(2):155–176.
7. Gupta SC, Sung B, Prasad S, Webb LJ, Aggarwal BB. Cancer Drug Discovery by

- Repurposing: Teaching New Tricks to Old Dogs. *Trends in Pharmacological Sciences* 2013;34(9):508–517.
8. Sawicki E, Schellens JHM, Beijnen JH, Nuijen B. Inventory of Oral Anticancer Agents: Pharmaceutical Formulation Aspects with Focus on the Solid Dispersion Technique. *Cancer Treatment Reviews*. 2016;50:247–263.
  9. Mazzaferro S, Bouchemal K, Ponchel G. Oral Delivery of Anticancer Drugs I: general considerations. *Drug Discovery Today*. 2013;18(1):25–34.
  10. Banna GL, Collovà E, Gebbia V, Lipari H, Giuffrida P, Cavallaro S, et al. Anticancer Oral Therapy: Emerging Related Issues. *Cancer Treatment Review*. 2010;36(8):595–605.
  11. Batlle JF, Arranz EE, De Castro Carpeño J, Sáez EC, Auñón PZ, Sánchez AR, et al. Oral Chemotherapy: Potential Benefits and Limitations. *Clinical and Translational Oncology*. 2004;6(6):335–340.
  12. Gauthier A, Ho M. Role of Sorafenib in the Treatment of Advanced Hepatocellular Carcinoma: An Update. *Hepatology Research*. 2013;43(2):147–154.
  13. Truong DH, Tran TH, Ramasamy T, Choi JY, Choi HG, Yong CS, et al. Preparation and Characterization of Solid Dispersion using A Novel Amphiphilic Copolymer to Enhance Dissolution and Oral Bioavailability of Sorafenib. *Powder Technology*. 2015;:260–283.
  14. Boudou-Rouquette P, Ropert S, Mir O, Coriat R, Billemonet B, Tod M, et al. Variability of Sorafenib Toxicity and Exposure over Time: A Pharmacokinetic/Pharmacodynamic Analysis. *The Oncologist*. 2012;17(9):1204–1212.
  15. Gelderblom H, Verweij J, Nooter K, Sparreboom A. Cremophor EL: The Drawbacks and Advantages of Vehicle Selection for Drug Formulation. *European Journal of Cancer*. 2001;37(13):1590–1598.
  16. Amidon GL, Lennernäs H, Shah VP, Crison JR. A Theoretical Basis for a Biopharmaceutic Drug Classification: The Correlation of in Vitro Drug Product Dissolution and in Vivo Bioavailability. *Pharmaceutical Research: An Official Journal of the American Association of Pharmaceutical Scientists*. 1995;12; 413–420.
  17. Savjani KT, Gajjar AK, Savjani JK. Drug Solubility: Importance and Enhancement Techniques. Aktay G, Du YZ, Torrado J, editors. *ISRN Pharmaceutics*. 2012;195727.
  18. Gallo JM. Pharmacokinetic/ Pharmacodynamic-Driven Drug Development. *Mount Sinai Journal of Medicine: A Journal of Translational and Personalized Medicine*.

- 2010;77(4):381–388.
19. Cragg GM, Newman DJ, Kingston DGI. Terrestrial Plants as a Source of Novel Pharmaceutical Agents. In: Liu HW (Ben), Mander L, editors. *Comprehensive Natural Products II*. Oxford: Elsevier; 2010; 5–39.
  20. Hearn BR, Shaw SJ, Myles DC - Microtubule Targeting Agents. In: Taylor JB, Triggle DJ, editors. *Comprehensive Medicinal Chemistry II* Oxford: Elsevier; 2007; 81–110.
  21. Baghel S, Cathcart H, O'Reilly NJ. Polymeric Amorphous Solid Dispersions: A Review of Amorphization, Crystallization, Stabilization, Solid-State Characterization, and Aqueous Solubilization of Biopharmaceutical Classification System Class II Drugs. *Journal of Pharmaceutical Sciences*. 2016;105(9):2527–2544.
  22. Szczurek J, Rams-Baron M, Knapik-Kowalczyk J, Antosik A, Szafraniec J, Jamróz W, et al. Molecular Dynamics, Recrystallization Behavior, and Water Solubility of the Amorphous Anticancer Agent Bicalutamide and its Polyvinylpyrrolidone Mixtures. *Molecular Pharmaceutics*. 2017;14(4):1071–1081.
  23. Bohr A, Nascimento TL, Harmankaya N, Weisser JJ, Wang Y, Grohganz H, et al. Efflux Inhibitor Bicalutamide Increases Oral Bioavailability of the Poorly Soluble Efflux Substrate Docetaxel in Co-Amorphous Anti-Cancer Combination Therapy. *Molecules*. 2019;24(2):1–13.
  24. Krishnaiah YSR. Pharmaceutical Technologies for Enhancing Oral Bioavailability of Poorly Soluble Drug. *Journal of Bioequivalence & Bioavailability*. 2010;2(2):028-036
  25. Savjani KT, Gajjar AK, Savjani JK. Drug Solubility : Importance and Enhancement Techniques. *ISRN Pharmaceutics*. 2012;1–10.
  26. Blagden N, de Matas M, Gavan PT, York P. Crystal Engineering of Active Pharmaceutical Ingredients to Improve Solubility and Dissolution Rates. *Advanced Drug Delivery Reviews*. 2007;59(7):617–630.
  27. Singh V. Nanosuspension : Way to Enhance the Bioavailability of Poorly Soluble Drug *International Journal of Current Trends in Pharmaceutical Research*. 2013;1(4):277–287.
  28. Patravale VB, Date AA, Kulkarni RM. Nanosuspensions: A Promising Drug Delivery Strategy. *Journal of Pharmacy and Pharmacology*. 2010;56(7):827–840.
  29. Ramyasree J, Hindustan AA, Chinthaguinjala H, Reshma T, Chenga Venkata HV, Yedire Bharath K. Solubility Enhancement of Drugs with Aid of Surfactants: Research Done Since

- Last Two Decades. *International Journal of Pharma and Bio Sciences*. 2020;10(5):11-16
30. Serajuddin ATM. Salt Formation to Improve Drug Solubility. *Advanced Drug Delivery Reviews* . 2007;59(7):603–616.
  31. Parikh RK, Mansuri N, Gohel M, Soniwala M. Dissolution Enhancement of Nimesulide Using Complexation and Salt Formation Techniques. *Indian Drugs*. 2005;42:149–154.
  32. Yadav A V., Shete AS, Dabke AP, Kulkarni P V., Sakhare SS. Co-crystals: A Novel Approach to Modify Physicochemical Properties of Active Pharmaceutical Ingredients. *Indian Journal of Pharmaceutical Sciences*. 2009;71(4):359–370.
  33. Rasool AA, Hussain AA, Dittert LW. Solubility Enhancement of Some Water-Insoluble Drugs in the Presence of Nicotinamide and Related Compounds. *Journal of Pharmaceutical Sciences*. 1991;80(4):387–393.
  34. Sekiguchi, K.; Obi, N.; Ueda Y. Studies on Absorption of Eutectic Mixture. II. Absorption of Fused Conglomerates of Chloramphenicol and Urea in Rabbits. *Chemical Pharmaceutical Bulletin*. 1970;(43):2091.
  35. Chiou WL, Riegelman S. Pharmaceutical Applications of Solid Dispersion Systems. *Journal of Pharmaceutical Sciences*. 1971;60(9):1281–1302.
  36. Van Duong T, Van den Mooter G. The Role of The Carrier in The Formulation of Pharmaceutical Solid Dispersions. Part I: Crystalline and Semi-crystalline Carriers. *Expert Opinion on Drug Delivery*. 2016;13(11):1583–1594.
  37. Van Duong T, Van den Mooter G. The Role of the Carrier in the Formulation of Pharmaceutical Solid Dispersions. Part II: Amorphous Carriers. *Expert Opinion on Drug Delivery*. 2016;13(12):1681–1694.
  38. Jadhav K, Pacharane S, Pednekar P, Koshy P, Kadam V. Approaches to Stabilize Amorphous Form - A Review. *Current Drug Therapy*. 2012;7:255–262.
  39. Vasconcelos T, Sarmiento B, Costa P. Solid Dispersions as Strategy to Improve Oral Bioavailability of Poor Water Soluble Drugs. *Drug Discovery Today*. 2007;12(23):1068–1075.
  40. Nair AR, Lakshman YD, Anand VSK, Sree KSN, Bhat K, Dengale SJ. Overview of Extensively Employed Polymeric Carriers in Solid Dispersion Technology. *AAPS PharmSciTech*. 2020;21(8) 309.
  41. Meng F, Gala U, Chauhan H. Classification Of Solid Dispersions: Correlation to (I)



- Stability And Solubility (II) Preparation and Characterization Techniques. Drug Development and Industrial Pharmacy. 2015;41(9):1401–1415.
42. Tejwani RW, Squibb B myers, Joshi H, Serajuddin A. Study of Phase Behavior of Poly (ethylene glycol) - Polysorbate B0 and Poly (ethylene glycol) -Polysorbate B0-Water Mixtures. Journal of Pharmaceutical Science. 2023; 89(89):946-950
  43. Janssens S, Van den Mooter G. Review: Physical Chemistry of Solid Dispersions. Journal of Pharmacy and Pharmacology. 2009;61(12):1571–1586.
  44. S. Kiho T. Yoshida Ikmsmusu. Physical Properties of Solid Dispersions Of Poorly Water-Soluble Drugs with Enteric Coating Agents. Chemical Pharmaceutical Bulletin. 1994;17(11):1460–1462.
  45. Arca HC, Mosquera-Giraldo LI, Bi V, Xu D, Taylor LS, Edgar KJ. Pharmaceutical Applications of Cellulose Ethers and Cellulose Ether Esters. Biomacromolecules. 2018;19(7):2351–2376.
  46. Schver GCRM, Nadvorny D, Lee PI. Evolution of Supersaturation from Amorphous Solid Dispersions in Water-Insoluble Polymer Carriers: Effects of Swelling Capacity and Interplay Between Partition and Diffusion. International Journal of Pharmaceutics. 2020;581:119292.
  47. Ueda K, Okada H, Zhao Z, Higashi K, Moribe K. Application of Solid-State <sup>13</sup>C Relaxation Time to Prediction of The Recrystallization Inhibition Strength of Polymers on Amorphous Felodipine At Low Polymer Loading. International Journal of Pharmaceutics. 2020;581:119300.
  48. Chavan RB, Rathi S, Jyothi VGSS, Shastri NR. Cellulose-Based Polymers in the Development of Amorphous Solid Dispersions. Asian Journal of Pharmaceutical Sciences. 2019;14(3):248–264.
  49. Bochmann ES, Neumann D, Gryczke A, Wagner KG. Micro-scale Solubility Assessments and Prediction Models for Active Pharmaceutical Ingredients in Polymeric Matrices. European Journal of Pharmaceutics and Biopharmaceutics 2019;141:111–120.
  50. Knopp MM, Chourak N, Khan F, Wendelboe J, Langguth P, Rades T, et al. Effect of Polymer Type and Drug Dose on the In Vitro and In Vivo Behavior of Amorphous Solid Dispersions. European Journal of Pharmaceutics and Biopharmaceutics. 2016;105:106–14.
  51. Nirika B, Hari Kumar S. Current Trends in Solid Dispersion: a Review. Journal of Drug

- Delivery & Therapeutics. 2011;14(3):80.
52. Vo CLN, Park C, Lee BJ. Current Trends and Future Perspectives of Solid Dispersions Containing Poorly Water-Soluble Drugs. *European Journal of Pharmaceutics and Biopharmaceutics* 2013;85(3):799–813.
  53. Dengale SJ, Grohganz H, Rades T, Löbmann K. Recent Advances in Co-Amorphous Drug Formulations. *Advanced Drug Delivery Reviews*. 2016;100:116–125.
  54. Ruff A, Fiolka T, Kostewicz ES. Prediction Of Ketoconazole Absorption using an Updated In Vitro Transfer Model Coupled to Physiologically Based Pharmacokinetic Modelling. *European Journal of Pharmaceutical Sciences*. 2017;100:42–55.
  55. Chegireddy M, Hanegave GK, Lakshman D, Urazov A, Sree KN, Lewis SA, et al. The Significance of Utilizing In Vitro Transfer Model and Media Selection to Study the Dissolution Performance of Weak Ionizable Bases: Investigation Using Saquinavir as a Model Drug. *AAPS PharmSciTech*. 2020;21(2):47.
  56. Pinto JMO, Rengifo AFC, Mendes C, Leão AF, Parize AL, Stulzer HK. Understanding the Interaction Between Soluplus® and Biorelevant Media Components. *Colloids and Surfaces B: Biointerfaces*. 2020;187:110673.
  57. Zhong Y, Jing G, Tian B, Huang H, Zhang Y, Gou J, et al. Supersaturation Induced by Itraconazole/Soluplus® Micelles Provided High GI Absorption In Vivo. *Asian Journal of Pharmaceutical Sciences*. 2016;11(2):255–264.
  58. Hancock BC, Zografi G. The Relationship Between the Glass Transition Temperature and the Water Content of Amorphous Pharmaceutical Solids. *Pharmaceutical Research*. 1994;11(4):471–477.
  59. Nokhodchi A, Ford JL, Rowe PH, Rubinstein MH. The Influence of Moisture Content on the Consolidation Properties of Hydroxypropylmethylcellulose K4M (HPMC 2208). *Journal of Pharmacy and Pharmacology*. 1996;48(11):1116–1121.
  60. Yu L. Amorphous Pharmaceutical Solids: Preparation, Characterization and Stabilization. *Advanced Drug Delivery Reviews*. 2001;48(1):27–42.
  61. Craig DQM, Royall PG, Kett VL, Hopton ML. The Relevance of the Amorphous State to Pharmaceutical Dosage Forms: Glassy Drugs and Freeze Dried Systems. *International Journal of Pharmaceutics*. 1999;179(2):179–207.
  62. Marsac PJ, Li T, Taylor LS. Estimation of Drug–Polymer Miscibility and Solubility in

- Amorphous Solid Dispersions using Experimentally Determined Interaction Parameters. *Pharmaceutical Research*. 2009;26(1):139–151.
63. Choudhari M, Damle S, Narayan R, Sunil S, Dubey K, Singhvi G. Emerging Applications of Hydroxypropyl Methylcellulose Acetate Succinate : Different Aspects in Drug Delivery and Its Commercial Potential. *AAPS PharmSciTech*. 2023;1–26.
  64. Curatolo W, Nightingale JA, Herbig SM. Utility of Hydroxypropylmethylcellulose Acetate Succinate ( HPMCAS ) for Initiation and Maintenance of Drug Supersaturation in the GI Milieu. 2009;26(6) 1491-1431.
  65. Warren DB, Benameur H, Porter CJH, Pouton CW. Using Polymeric Precipitation Inhibitors to Improve the Absorption of Poorly Water-Soluble Drugs: A Mechanistic Basis For Utility. *Journal of Drug Targeting*. 2010;18(10):704–731.
  66. Friesen DT, Shanker R, Crew M, Smithey DT, Curatolo WJ, Nightingale JAS. Hydroxypropyl Methylcellulose Acetate Succinate-Based Spray-Dried Dispersions: An Overview. *Molecular Pharmaceutics*. 2008;5(6):1003–1019.
  67. Luk E, Sandoval AJ, Cova A, Müller AJ. Anti-Plasticization of Cassava Starch by Complexing Fatty Acids. *Carbohydrate Polymers*. 2013;98(1):659–664.
  68. Wlodarski K, Sawicki W, Kozyra A, Tajber L. Physical Stability of Solid Dispersions with respect to Thermodynamic Solubility of Tadalafil in PVP-VA. *European Journal of Pharmaceutics and Biopharmaceutics*. 2015;96:237–246.
  69. Nagapudi K, Jona J. Amorphous Active Pharmaceutical Ingredients in Preclinical Studies: Preparation, Characterization, and Formulation. *Current Bioactive Compounds*. 2008;4(4):213–224.
  70. Paudel A, Worku ZA, Meeus J, Guns S, Van den Mooter G. Manufacturing of Solid Dispersions of Poorly Water Soluble Drugs by Spray Drying: Formulation and Process Considerations. *International Journal of Pharmaceutics*. 2013;453(1):253–284.
  71. Meng F, Trivino A, Prasad D, Chauhan H. Investigation and Correlation of Drug Polymer Miscibility and Molecular Interactions by Various Approaches for the Preparation of Amorphous Solid Dispersions. *European Journal of Pharmaceutical Science*. 2015;71:12–24.
  72. Kothari K, Ragoonanan V, Suryanarayanan R. The Role of Polymer Concentration on the Molecular Mobility and Physical Stability of Nifedipine Solid Dispersions. *Molecular*

- Pharmaceutics. 2015;12(5):1477–1484.
73. Mistry P, Mohapatra S, Gopinath T, Vogt FG, Suryanarayanan R. Role of the Strength of Drug-Polymer Interactions on the Molecular Mobility and Crystallization Inhibition in Ketoconazole Solid Dispersions. *Molecular Pharmaceutics*. 2015;12(9):3339–3350.
  74. Yanqing Shen Fei Lu JHYS, Guo S. Incorporation of Paclitaxel Solid Dispersions with Poloxamer188 or Polyethylene Glycol to Tune Drug Release From Poly( $\epsilon$ -Caprolactone) Films. *Drug Development and Industrial Pharmacy*. 2013;39(8):1187–1196.
  75. Jiménez de los Santos CJ, Pérez-Martínez JI, Gómez-Pantoja ME, Moyano JR. Enhancement of Albendazole Dissolution Properties using Solid Dispersions With Gelucire 50/13 And PEG 15000. *Journal of Drug Delivery Science and Technology*. 2017;42:261–272.
  76. Karolewicz B, Gajda M, Pluta J, Górniak A. Dissolution Study and Thermal Analysis of Fenofibrate–Pluronic F127 Solid Dispersions. *Journal of Thermal Analysis and Calorimetry*. 2016;125(2):751–757.
  77. Prasad, R.; Radhakrishnan, P.; Singh, S.K.; Verma PR. Furosemide - Soluplus® Solid Dispersion: Development and Characterization. *Recent Pat Drug Deliv Formul*. 2018;11:211–220.
  78. Tran P, Pyo Y chul, Kim D hyun, Lee S eun, Kim J ki, Park J sook. Overview of the Manufacturing Methods of Solid Dispersion Technology for Improving the Solubility of Poorly Water-Soluble Drugs and Application to Anticancer Drugs. 2019;1–26.
  79. Tachibana T, Nakamura A. A Method for Preparing An Aqueous Colloidal Dispersion of Organic Materials by Using Water-Soluble Polymers: Dispersion of B-Carotene by Polyvinylpyrrolidone. *Kolloid-Zeitschrift Und Zeitschrift Für Polymere*. 1965;203(2):130–133.
  80. Chen Y, Shi Q, Chen Z, Zheng J, Xu H, Li J, et al. Preparation and Characterization of Emulsified Solid Dispersions Containing Docetaxel. *Archives of Pharmacal Research*. 2011;34(11):1909–1917.
  81. Herbrink M, Schellens JHM, Beijnen JH, Nuijen B. Improving the Solubility of Nilotinib Through Novel Spray-Dried Solid Dispersions. *International Journal of Pharmaceutics* 2017;529(1):294–302.
  82. Biswal S, Sahoo J, Murthy PN, Giradkar RP, Avari JG. Enhancement of Dissolution Rate

- of Gliclazide using Solid Dispersions with Polyethylene Glycol 6000. *AAPS PharmSciTech*. 2008;9(2):563–570.
83. Kaur S, Jena SK, Samal SK, Saini V, Sangamwar AT. Freeze Dried Solid Dispersion of Exemestane: A Way to Negate an Aqueous Solubility and Oral Bioavailability Problems. *European Journal of Pharmaceutical Sciences*. 2017;107:54–61.
84. Elgindy N, Elkhodairy K, Molokhia A, Elzoghby A. Lyophilization Monophase Solution Technique for Preparation of Amorphous Flutamide Dispersions. *Drug Development and Industrial Pharmacy*. 2011;37(7):754–764.
85. Ghebremeskel AN, Vemavarapu C, Lodaya M. Use Of Surfactants As Plasticizers In Preparing Solid Dispersions of Poorly Soluble API: Selection Of Polymer-Surfactant Combinations Using Solubility Parameters and Testing the Processability. *International Journal of Pharmaceutics*. 2007;328(2):119–129.
86. Huang S, O'Donnell KP, Keen JM, Rickard MA, McGinity JW, Williams RO. A New Extrudable Form of Hypromellose: AFFINISOL™ HPMC HME. *AAPS PharmSciTech*. 2016;17(1):106–119. 87
87. Hot Melt Extrusion Process in Pharma Drug Formulation [cited 2024 Oct 11] Available from: <https://fabtechnologies.com/hot-melt-extrusion-process-in-pharmaceutical-drug-formulation/>
88. Agrawal AM, Dudhedia MS, Patel AD, Raikes MS. Characterization and Performance Assessment of Solid Dispersions Prepared by Hot Melt Extrusion and Spray Drying Process. *International Journal of Pharmaceutics*. 2013;457(1):71–81.
89. Maniruzzaman M, Boateng JS, Snowden MJ, Douroumis D. A Review of Hot-Melt Extrusion: Process Technology to Pharmaceutical Products. Sah H, Bolognese A, Murata Y, Segall AI, editors. *ISRN Pharmaceutics*. 2012;436763.
90. Matic J, Paudel A, Bauer H, Garcia RAL, Biedrzycka K, Khinast JG. Developing HME-Based Drug Products Using Emerging Science: a Fast-Track Roadmap from Concept to Clinical Batch. *AAPS PharmSciTech*. 2020;21(5)176.
91. Sonali D, Tejal S, Vaishali T, Tejal G. Silymarin-Solid Dispersions: Characterization and Influence of Preparation Methods on Dissolution. *Acta Pharmaceutica*. 2010;60(4):427–443.
92. Tran PHL, Tran TTD, Park JB, Lee BJ. Controlled Release Systems Containing Solid

- Dispersions: Strategies and Mechanisms. *Pharmaceutical Research*. 2011;28(10):2353–2378.
93. Miller JM, Beig A, Carr RA, Webster GK, Dahan A. The Solubility-Permeability Interplay when using Cosolvents for Solubilization: Revising the Way We Use Solubility-Enabling Formulations. *Molecular Pharmaceutics*. 2012;9(3):581–590.
  94. Six K, Verreck G, Peeters J, Brewster M, Van Den Mooter G. Increased Physical Stability and Improved Dissolution Properties of Itraconazole, a Class II Drug, by Solid Dispersions that Combine Fast- and Slow-Dissolving Polymers. *Journal of Pharmaceutical Sciences*. 2004;93(1):124–131.
  95. Newman A, Nagapudi K, Wenslow R. Amorphous Solid Dispersions: A Robust Platform to Address Bioavailability Challenges. *Therapeutic Delivery*. 2015;6(2):247–261.
  96. Psimadas D, Georgoulas P, Valotassiou V, Loudos G. Molecular Nanomedicine Towards Cancer : *Journal of Pharmaceutical Sciences*. 2012;101(7):2271–2280.
  97. Liu S, Li M, Jia L, Chen M, Du S, Gong J. Investigation of Drug-Polymer Miscibility, Molecular Interaction, and Their Effects on the Physical Stabilities and Dissolution Behaviors of Norfloxacin Amorphous Solid Dispersions. *Crystal Growth and Design*. 2020;20(5):2952–2964.
  98. Moseson DE, Parker AS, Beaudoin SP, Taylor LS. Amorphous Solid Dispersions Containing Residual Crystallinity: Influence of Seed Properties and Polymer Adsorption on Dissolution Performance. *European Journal of Pharmaceutical Sciences*. 2020;146:105276.
  99. Kapourani A, Vardaka E, Katopodis K, Kachrimanis K, Barmpalexis P. Crystallization Tendency of APIs Possessing Different Thermal and Glass Related Properties In Amorphous Solid Dispersions. *International Journal of Pharmaceutics*. 2020;579:119149.
  100. Monschke M, Kayser K, Wagner KG. Processing of polyvinyl acetate phthalate in hot-melt extrusion-preparation of amorphous solid dispersions. *Pharmaceutics*. 2020;12(4):337.
  101. Lapuk SE, Zubaidullina LS, Ziganshin MA, Mukhametzyanov TA, Schick C, Gerasimov A V. Kinetic stability of amorphous solid dispersions with high content of the drug: A fast scanning calorimetry investigation. *International Journal of Pharmaceutics*. 2019;562:113–123.
  102. Blaabjerg LI, Bulduk B, Lindenberg E, Löbmann K, Rades T, Grohgan H. Influence of Glass Forming Ability on the Physical Stability of Supersaturated Amorphous Solid

- Dispersions. *Journal of Pharmaceutical Sciences*. 2019;108(8):2561–2569.
103. Martinez-Garcia JC, Rzoska SJ, Drzozd-Rzoska A, Martinez-Garcia J, Mauro JC. Divergent Dynamics and the Kauzmann Temperature in Glass Forming Systems. *Scientific Reports*. 2014;4:5160.
  104. Rumondor ACF, Wikström H, Van Eerdenbrugh B, Taylor LS. Understanding The Tendency of Amorphous Solid Dispersions to Undergo Amorphous-Amorphous Phase Separation in the Presence of Absorbed Moisture. *AAPS PharmSciTech*. 2011;12(4):1209–1219.
  105. Li J, Hubert M, Pinnamaneni S, Tao L, Zhao J, Sharif S, et al. Effect of Moisture Sorption on Free Volume and Relaxation of Spray Dried Dispersions: Relation to Drug Recrystallization. *Journal of Pharmaceutical Sciences*. 2020;109(2):1050–1058.
  106. Chavan RB, Bhargavi N, Lodagekar A, Shastri NR. Near Infra Red Spectroscopy: A Tool for Solid State Characterization. *Drug Discovery Today*. 2017;22(12):1835–1843.
  107. Hongze Piao Liang Yang HPPWHS LF, Cui F. A Pre-Formulation Study of a Polymeric Solid Dispersion of Paclitaxel Prepared using A Quasi-Emulsion Solvent Diffusion Method to Improve the Oral Bioavailability in Rats. *Drug Development and Industrial Pharmacy*. 2016;42(3):353–363.
  108. WO2016108123A2.pdf. 2016.
  109. Undevia SD, Gomez-Abuin G, Ratain MJ. Pharmacokinetic Variability of Anticancer Agents. *Nature Reviews Cancer*. 2005;5(6):447–458.
  110. Moes JJ, Koolen SLW, Huitema ADR, Schellens JHM, Beijnen JH, Nuijen B. Pharmaceutical Development and Preliminary Clinical Testing of An Oral Solid Dispersion Formulation of Docetaxel. *International Journal of Pharmaceutics* 2011;420(2):244–250.
  111. Truong DH, Tran TH, Ramasamy T, Choi JY, Lee HH, Moon C, et al. Development of Solid Self-Emulsifying Formulation for Improving the Oral Bioavailability of Erlotinib. *AAPS PharmSciTech*. 2016;17(2):466–473.
  112. Wagner JG. Linear Pharmacokinetic Equations Allowing Direct Calculation of Many Needed Pharmacokinetic Parameters from the Coefficients and Exponents of Polyexponential Equations which have been Fitted to the Data. *Journal of Pharmacokinetics and Biopharmaceutics*. 1976;4(5):443–467.
  113. Chen H, Shien K, Suzawa K, Tsukuda K, Tomida S, Sato H, et al. Elacridar, A Third-

- Generation ABCB1 Inhibitor, Overcomes Resistance to Docetaxel in Non-Small Cell Lung Cancer. *Oncology Letters*. 2017;14(4):4349–4354.
114. Sawicki E, Verheijen RB, Huitema ADR, van Tellingen O, Schellens JHM, Nuijen B, et al. Clinical Pharmacokinetics of An Amorphous Solid Dispersion Tablet of Elacridar. *Drug Delivery and Translational Research*. 2017;7(1):125–131.
  115. Sawicki E, Schellens JHM, Beijnen JH, Nuijen B. Pharmaceutical Development of An Amorphous Solid Dispersion Formulation of Elacridar Hydrochloride for Proof-of-Concept Clinical Studies. *Drug Development and Industrial Pharmacy*. 2017;43(4):584–594.
  116. Shanholtz C. Acute Life-Threatening Toxicity of Cancer Treatment. *Critical Care Clinics*. 2001;17(3):483–502.
  117. FDA. SORAFENIB: FDA Prescribing Information. *NciGov*. 2007;1–17.
  118. Butreddy A. Hydroxypropyl Methylcellulose Acetate Succinate as an Exceptional Polymer for Amorphous Solid Dispersion Formulations: A Review From Bench To Clinic. *European Journal of Pharmaceutics and Biopharmaceutics*. 2022;177:289–307.
  119. Babu NR, Nagpal D, Ankola D, Awasthi R. Evolution of Solid Dispersion Technology: Solubility Enhancement Using Hydroxypropyl Methylcellulose Acetate Succinate: Myth or Reality? *Assay and Drug Development Technologies*. 2022;20(4):149–163.
  120. Winslow C, Nichols B, Novo D, Mosquera-Giraldo L, Taylor L, Edgar K, et al. Cellulose-Based Amorphous Solid Dispersions Enhance Rifapentine Delivery Characteristics in Vitro. *Carbohydrate Polymers*. 2017;182.
  121. Shah N, Iyer RM, Mair H juergen, Choi duks, Tian H, Diodone R, et al. Improved Human Bioavailability of Vemurafenib , a Practically Insoluble Drug , Using an Amorphous Polymer-Stabilized Solid Dispersion Prepared by a Solvent-Controlled Coprecipitation. 2013;102(3):967–981.
  122. Xie T, Taylor LS. Dissolution Performance of High Drug Loading Celecoxib Amorphous Solid Dispersions Formulated with Polymer Combinations. *Pharmaceutical Research*. 2016;33(3):739–750.
  123. Rampal, A., Singh, M., Mahajan, S., & Bedi N. Formulation and Characterization of HPMC and HPMCAS Based Solid Dispersions of Fenofibrate: A Comparative Study. *International Journal of Applied Pharmaceutics*, 2019;11(4):41–48.
  124. Jung J young, Il Shin K, Lee M, Song M, Kwon S. Enhanced Solubility Through Particle



- Size Control, Modification of Crystal Behavior, and Crystalline Form Changes in Solid Dispersion of Nifedipine. *Biotechnology and Bioprocess Engineering*. 2021;110:105–110.
125. Tanno F, Nishiyama Y, Kokubo H, Obara S. Evaluation of Hypromellose Acetate Succinate (HPMCAS) as a Carrier in Solid Dispersions. *Drug Development and Industrial Pharmacy*. 2004;30(1):9–17.
126. Solanki NG, Lam K, Gumaste SG, Shah A V, Serajuddin ATM. Effects of Surfactants on Itraconazole-HPMCAS Solid Dispersion Prepared by Hot-Melt Extrusion I : Miscibility and Drug Release. *Journal of Pharmaceutical Sciences*. 2018;1–13.
127. Nakamichi K, Nakano T, Izumi S, Yasuura H, Kawashima Y. The Preparation of Enteric Solid Dispersions with Hydroxypropylmethylcellulose Acetate Succinate using A Twin-Screw Extruder. *Journal of Drug Delivery Science and Technology*. 2004;14:193–198.
128. Wu H, Liu Y, Ci T, Ke X. Application of HPMC HME Polymer as Hot Melt Extrusion Carrier in Carbamazepine Solid Dispersion. *Drug Development and Industrial Pharmacy* 2020;46(12):1911–1918.
129. Kaushik R, O'Donnell KP, Singh G. Impact of Extrusion Process Parameters on Drug Recovery and Dissolution Performance of Solid Dispersions of Ritonavir and AFFINISOL<sup>TM</sup>HPMC HME. 2016, 1521383513
130. Schultz HB, Meola TR, Thomas N, Prestidge CA. Oral Formulation Strategies to Improve the Bioavailability and Mitigate the Food Effect of Abiraterone Acetate. *International Journal of Pharmaceutics*. 2020;577:119069.
131. Chi KN, Spratlin J, Kollmannsberger C, North S, Pankras C, Gonzalez M, et al. Food Effects on Abiraterone Pharmacokinetics in Healthy Subjects and Patients with Metastatic Castration-Resistant Prostate Cancer. *Journal of Clinical Pharmacology*. 2015;55(12):1406–1414.
132. Silveira RG, Cunha BN, Tenório JC, Alves de Aguiar DV, da Cruz Souza P, Vaz BG, et al. A Simple Alternative to Prodrug: The Hydrochloride Salt Monohydrate of the Prostate Anticancer Drug Abiraterone. *Journal of Molecular Structure*. 2019;1190:165–170.
133. Solymosi T, Tóth F, Orosz J, Basa-Dénes O, Angi R, Jordán T, et al. Solubility Measurements at 296 and 310 K and Physicochemical Characterization of Abiraterone and Abiraterone Acetate. *Journal of Chemical and Engineering Data*. 2018;63(12):4453–4458.
134. Solymosi T, Ötvös Z, Angi R, Ordasi B, Jordán T, Semsey S, et al. Development of An

- Abiraterone Acetate Formulation with Improved Oral Bioavailability Guided by Absorption Modeling Based on in Vitro Dissolution and Permeability Measurements. *International Journal of Pharmaceutics* 2017;532(1):427–434.
135. Ang JE, Olmos D, De Bono JS. CYP17 Blockade by Abiraterone: Further Evidence for Frequent Continued Hormone-Dependence in Castration-Resistant Prostate Cancer. *British Journal of Cancer*. 2009;100(5):671–675.
  137. Goldwater R, Hussaini A, Bosch B, Nemeth P. Comparison of a Novel Formulation of Abiraterone Acetate vs. the Originator Formulation in Healthy Male Subjects: Two Randomized, Open-Label, Crossover Studies. *Clinical Pharmacokinetics*. 2017;56(7):803–813.
  136. Hussaini A, Olszanski AJ, Stein CA, Bosch B, Nemeth P. Impact of an Alternative Steroid on the Relative Bioavailability and Bioequivalence of A Novel Versus the Originator Formulation of Abiraterone Acetate. *Cancer Chemotherapy and Pharmacology*. 2017;80(3):479–486.
  137. Papangelou A, Olszanski AJ, Stein CA, Bosch B, Nemeth P. The Effect of Food on the Absorption of Abiraterone Acetate from a Fine Particle Dosage Form: A Randomized Crossover Trial in Healthy Volunteers. *Oncology and Therapy*. 2017;5(2):161–170.
  138. Koziolk M, Alcaro S, Augustijns P, Basit AW, Grimm M, Hens B, et al. The Mechanisms of Pharmacokinetic Food-Drug Interactions – A Perspective From the UNGAP Group. *European Journal of Pharmaceutical Sciences*. 2019;134:31–59.
  139. Kirby M, Hirst C, Crawford ED. Characterising the Castration-Resistant Prostate Cancer Population: A Systematic Review. *International Journal of Clinical Practice*. 2011;65(11):1180–1192.

## **Chapter 2: Drug and Polymer Profile**

## 2.1. Abiraterone acetate

### 2.1.1. Introduction

In the early 1990s, Abiraterone (ABT) was synthesized at the Institute of Cancer Research, London, UK, for the treatment of prostate cancer (1). In 2004, Cougar Biotechnology was granted the right by British Technology Group to begin the commercial development of the ABT product (2). Johnson and Johnson bought Cougar Biotechnology in 2009, and the responsibility for developing and marketing the Zytiga®, which contains the ABT, was transferred to its subsidiary Janssen Biotech (1). In 2011, the US FDA approved ABTA for patients with mCRPC who had undergone prior chemotherapy. Subsequently, in 2012, it received approval for use in all patients with mCRPC. In February 2018, ABTA received approval for the treatment of mCSPC based on the findings of the LATITUDE study, a multinational, randomized, double-blind, and placebo-controlled phase 3 trial (3). ABTA (17-(3-pyridinyl) androsta-5,16-dien-3 $\beta$ -ol acetate) is an orally active prodrug of ABT. It inhibits the C-17, 20 lyases, and 17  $\alpha$ -hydroxylase enzymes (CYP 17), leading to reduce the androgen synthesis in adrenal gland-related tissues. The expression of the CYP17 enzyme is observed in tumor tissues of the testes, adrenal glands, and prostate, where it plays a vital role in the synthesis of androgens (4).

Some of the important drug information and properties of ABTA are listed below:

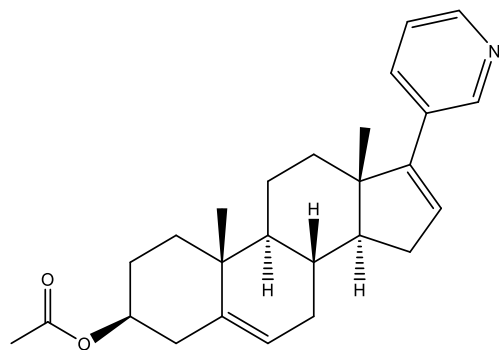
### 2.1.2. Physicochemical Properties

**Name:** Abiraterone acetate

**Chemical Name:** 17-(pyridin-3-yl) androsta-5,16-dien-3 $\beta$ -yl acetate

**Molecular formula:** C<sub>26</sub>H<sub>33</sub>NO<sub>2</sub>

**Chemical structure:**



**Molecular weight:** 391.55 g/mol

**Chemical class:** derivative of androstadienol

**Therapeutic class:** Anti-androgen

**Description:** Odorless, white to off-white crystalline powder

**Melting point:** 144-145 °C

**Solubility:** pH-dependent solubility, being practically insoluble within the pH range of 2–12 and slightly soluble within the pH range of 1–2

**pK<sub>a</sub>:** 5.19

**Partition coefficient:** 5.12

**BCS class:** IV (low solubility and low permeability)

**Marketed as:** Zytiga (250 mg and 500 mg film-coated tablet) and Yonsa (250 mg two times a day)

### 2.1.3. Mechanism of action

ABTA, a steroidal compound and a first-in-class drug, demonstrates a notable affinity for CYP17, with a remarkably low inhibition constant of 0.39 nM. This enzyme plays a crucial role in the biosynthesis of steroids, performing functions related to 17- $\alpha$ -hydroxylase and 17,20-lyase. Briefly, CYP17 exhibits catalytic activity and converts the pregnenolone and progesterone to their 17-hydroxy derivatives through 17 $\alpha$ -hydroxylase activity. This is followed by the formation of dehydroepiandrosterone (DHEA) and androstenedione by C17, 20 lyase activity. In the testes, 17 $\alpha$ -hydroxysteroid dehydrogenase transforms DHEA and androstenedione into testosterone, which is further converted to dihydrotestosterone (DHT) through the action of 3 $\beta$ -hydroxysteroid dehydrogenase/isomerase. The expression of CYP17 is observed in tissues within the testicles, prostate, and adrenal glands. Notably, its expression is 17 times greater in mCRPC compared to primary prostate tumors. ABT is the active metabolite of ABTA, which is produced upon hydrolysis and acts as an androgen biosynthesis inhibitor that inhibits 17  $\alpha$ -hydroxylase/ C17, 20-lyase (CYP17) (5). Furthermore, the production of androgen can be hindered by disrupting the activity of enzymes such as C17, 20-lyase, and C17 $\alpha$ -hydroxylase. The CYP 17 enzyme has a crucial role in the formation of cortisol from cholesterol and in the biosynthesis of androgen such as testosterone. This leads to the inhibition of testosterone in all tissues, concurrently reducing the synthesis of hormones like cortisol (6). The mechanism of action of ABTA is shown in Figure 2.1.

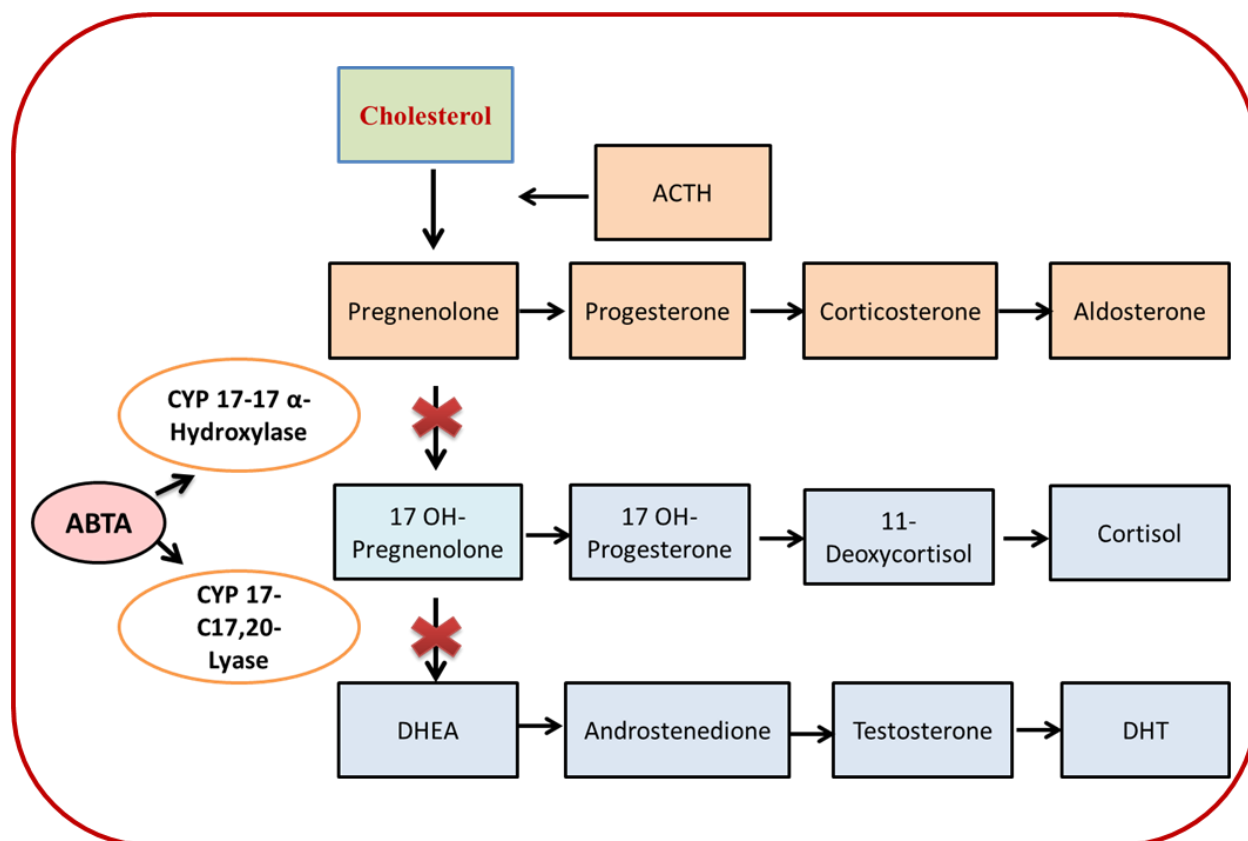


**Figure 2.1.** Mechanism of action of ABTA

#### 2.1.4. Tolerability and safety

ABTA (with or without prednisone) demonstrated an acceptable safety profile and was well tolerated in men with mCRPC, as evidenced by phase 3 trials, a combined safety analysis (1333 ABTA recipients vs. 934 placebo), and real-world data from the global Early Access Program (EAP) trial. Elderly patients tolerated ABTA similarly to younger patients (10).

#### 2.1.5. Adverse effect

Treatment-related adverse effects arising from the administration of ABTA and prednisolone therapy comprised cardiac issues (such as ischemic heart disease, myocardial infarction, supraventricular arrhythmias, and tachyarrhythmias), hepatotoxicity (characterized by abnormalities in liver function tests), hypokalemia, hypertension, and manifestations of fluid retention or edema. Selected adverse events such as hypertension, hypokalemia, and fluid retention seem to be associated with the mechanism of action of ABTA. The concurrent administration of a corticosteroid has been observed to decrease both the frequency and intensity of these adverse

events. The mechanism behind abiraterone acetate-induced hepatotoxicity remains unclear. Serious hepatotoxicity was observed in 1.1% of patients in the abiraterone acetate (with or without prednisone) group, compared to 0.6% in the placebo (with or without prednisone) group (11).

### 2.1.6. Pharmacokinetics Characters

#### **Absorption**

After oral administration of ABTA is rapidly absorbed and hydrolyzed to its main active metabolite ABT, this conversion typically occurs in the intestinal fluids. The reaction is enzymatic, involving enzymes like pancreatic cholesterol esterase and arylacetamide deacetylase. Consequently, hydrolysis takes place in the intestinal lumen and continues within intestinal and liver microsomes. After oral administration of ABTA in patients with mCRPC, it takes approximately 2h to reach the median time for maximum plasma ABT concentration. There is an observed accumulation of ABT at steady-state, resulting in a 2-fold higher exposure (steady-state AUC) compared to a single 1,000 mg dose of ABTA. Steady-state values for  $C_{max}$  and AUC were  $226 \pm 178$  ng/mL and  $993 \pm 639$  ng. h/mL in patients with mCRPC receiving a daily dose of 1,000 mg (12). Furthermore, the absolute bioavailability of ABT following Zytiga® administration has not been precisely determined, it is expected to be below 10% in the fasted condition.

#### **Effect of Food**

When ABTA is administrated in the presence of food, the systemic exposure of ABT is increased. Among healthy subjects, when a single dose of ABTA was given with a low-fat meal (7% fat, 300 calories), the  $C_{max}$  and  $AUC_{0-\infty}$  of ABT were roughly 7- and 5-fold higher, while with a high-fat meal (57% fat, 825 calories), the  $C_{max}$  and  $AUC_{0-\infty}$  of ABT were roughly 17- and 10-fold higher, respectively compared to overnight fasting. when a single dose of ABTA was administered either 2 hours after or 1 hour before a medium-fat meal (25% fat, 491 calories), the  $AUC_{0-\infty}$  of ABT was roughly 7-fold or 1.6-fold higher in comparison to overnight fasting (12,13).

#### **Distribution**

ABT exhibits high binding affinity (>99%) to the human plasma proteins, alpha-1 acid glycoprotein, and albumin. The apparent volume of distribution at steady state is  $19,669 \pm 13,358$  L (mean  $\pm$  SD) in adult (13).

#### **Elimination**

For individuals with mCRPC, the average terminal half-life of ABT in plasma is  $12 \pm 5$  hours (mean  $\pm$  SD) (12,13).

### **Metabolism**

After being administered orally in capsule form,  $^{14}\text{C}$ -ABTA undergoes hydrolysis in the intestinal lumen and continues in the intestinal and liver microsomes to produce ABT, its active metabolite. This conversion is likely facilitated by esterase activity, although the specific esterase involved has not been known, and it is not enabled by CYP. ABT yields two principle circulating metabolites in human plasma, ABT sulphate and N-oxide ABT sulphate, both contributing to around 43% of overall exposure each. Enzymes such as CYP3A4 and SULT2A1 are involved in the formation of N-oxide ABT sulfate (12,13).

### **Excretion**

After oral administration of  $^{14}\text{C}$ -ABTA, about 88% of the radioactive dose is found in feces, while approximately 5% is excreted in urine. The primary components identified in feces are unaltered ABTA and ABT, comprising about 55% and 22% of the administered dose, respectively (12,13).

#### **2.1.7. Dosage and administration**

In accordance with the EU regulations, ABTA is recommended in combination with prednisone and prednisolone to treat the mCRCP in men who exhibit either no symptoms or mild symptoms following the deficit of androgen deprivation and for those in whom chemotherapy is not clinically indicated. Additionally, it is prescribed for men whose disease condition has advanced either during or after docetaxel-based chemotherapy. In the USA and Japan, ABTA is administered with a combination of prednisone for the treatment of mCRPC. ABTA is advised to be taken at a daily dose of 1000 mg on an empty stomach or at least 2 h after a meal (14) and it is important to observe a strict restriction on the timing of the subsequent meal, ensuring that it is not consumed sooner than one hour after taking the medication, while prednisone or prednisolone is recommended at a daily dosage of 10 mg. The substantial impact of food on ABTA leads to increased exposure post-meal, prompting the manufacturer to establish precise dosing recommendations (6,12,13).

#### **2.1.8. Drug-Drug interaction**

Zytiga®, (ABTA) acts as an inhibitor for hepatic drug-metabolizing enzymes CYP2D6 and CYP2C8. In a drug-drug interaction study involving CYP2D6, the co-administration of dextromethorphan (a CYP2D6 substrate) with ABTA at a daily dose of 1000 mg and prednisone at 5 mg twice daily resulted in a 2.8-fold increase in  $C_{\text{max}}$  and a 2.9-fold increase in AUC for dextromethorphan. It is recommended to refrain from concurrently administering ABTA with



substrates of CYP2D6 characterized by a narrow therapeutic index, such as thioridazine. During a drug-drug interaction trial involving CYP2C8 in healthy subjects, the AUC of pioglitazone, a CYP2C8 substrate, showed a 46% increase when co-administered with a single dose of 1000 mg ABTA. In a specific drug interaction trial, the concurrent use of rifampin, a potent CYP3A4 inducer, resulted in a 55% reduction in abiraterone exposure. It is advisable to refrain from administering strong CYP3A4 inducers while undergoing Zytiga® treatment. If it becomes necessary to co-administer a strong CYP3A4 inducer, consider adjusting the dosing frequency of Zytiga® (15).

### **2.1.9. Marketed formulation**

The marketed formulation of ABTA is “Zytiga,” available in the form of 500 mg film-coated tablets and 250 mg uncoated tablets. Additionally, Yonsa, administered at a dosage of 250 mg twice daily, is another tablet form available in the market for mCRPC (1).

## **2.2. Hydroxypropyl methyl cellulose acetate succinate**

### **2.2.1. Introduction**

Hydroxypropyl methyl cellulose acetate succinate (HPMCAS) stands out due to its remarkable applications in the pharmaceutical dosage form. HPMCAS was introduced by Shin-Etsu Chemical Co. Ltd in Japan in 1986 to the commercial market for the first time, branding under the name of ACOAT-an enteric coating agent (16). HPMCAS is considered a safe polymer with higher chemical stability with an aversion to moisture accumulation (17,18). HPMCAS is part of many approved products and finds a listing in the FDA-IID. Recent publications have brought to light the exceptional capabilities of HPMCAS in preventing the crystallization of API and enhancing the solubility, dissolution rate, and oral bioavailability of poorly water-soluble drugs. Additionally, Curatolo et al. conducted a case study evaluating 41 polymeric carriers to assess their effectiveness in maintaining the supersaturation for nine poorly soluble drugs. Among all these carriers, HPMCAS emerged as the most effective carrier for inhibiting precipitation. However, despite these insights, there are currently comprehensive overviews on HPMCAS, particularly its applications in various formulations such as dry coating, amorphous nanoparticles, 3D printing technology, and the effect of pressurized carbon dioxide on HME and extrudates properties of HPMCAS, biomedical applications, and regulatory considerations (19).

HPMCAS is also called hypromellose acetate succinate. It is hydroxypropyl methylcellulose (HPMC) functionalized using a combination of acetic acid and monosuccinic acid esters (20). Figure 2.2 illustrates the chemical structure of the HPMCAS; this polymer chain is mainly composed of methoxy groups (-OCH<sub>3</sub>), acetyl groups (-COCH<sub>3</sub>), 2-hydroxypropoxy groups (-OCH<sub>2</sub>CH(CH<sub>3</sub>)OH), and succinyl groups (-COCH<sub>2</sub>CH<sub>2</sub>COOH) (21). Different grades of HPMCAS are available based on substitution patterns, primarily of acetyl (2.0–16.0%) and succinyl (4.0–28.0%) groups. The molecular weights of the HPMCAS range from 55,000 to 93,000 Da. The pK<sub>a</sub> of the succinate groups of HPMCAS is approximately 5, so it is mostly unionized at pH values below 4 and can be 50% ionized at pH values of 5 or higher. In HPMCAS, methoxy and acetate groups are hydrophobic, so they are water-insoluble when unionized in an acidic pH environment of pH < 5 (22). This property makes the use of HPMCAS possible in applications of an enteric polymer for achieving pH-dependent delayed-release (23). HPMCAS is amphiphilic in nature, where the hydrophobic region of the polymer interacts with the insoluble drug compound, while in an aqueous environment, the hydrophilic portion permits these structures to remain stable colloids (24).

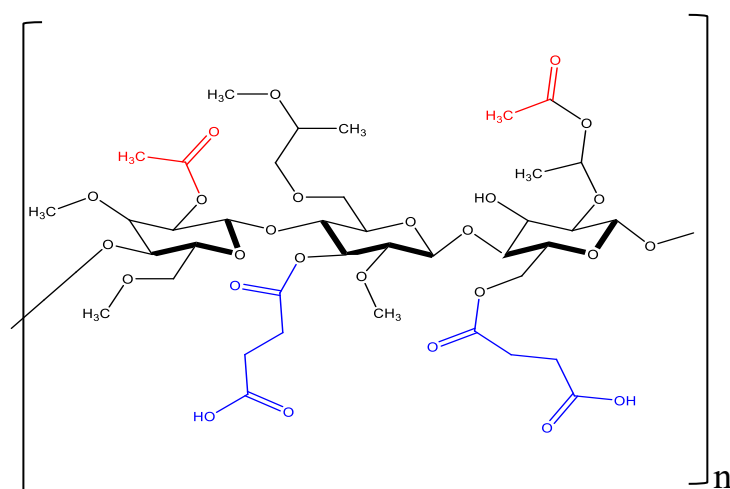


**Figure 2.2.** Chemical structure of HPMCAS

### 2.2.2. Chemistry of HPMCAS

For the synthesis of the HPMC, the process starts with cellulose, a polymer chain comprising the repeating unit of  $\beta$ -1,4-anhydroglucose. Here, swollen alkali cellulose is formed when the purified form of cellulose obtained from the wood pulp or cotton linters is reacted with the sodium hydroxide solution, which is more chemically reactive than untreated cellulose. After that, methyl

chloride and propylene oxide are reacted with alkali cellulose to form the HPMC. Post this, the generated HPMC is employed in a chemical process to give HPMCAS (25–28). Acetyl and succinyl groups are incorporated into the -OH groups of the HPMC backbone during the chemical synthesis of the HPMCAS. First, HPMC dissolves in the glacial acetic acid in a furnace. Then, HPMC esterification occurred by adding succinic and acetic anhydride in a reaction environment, i.e., sodium acetate, which acts as a catalyst. At the specific reaction time, the product paste is incorporated into the water where polymer (HPMCAS) is precipitated using stirring because water acts as a weak solvent. Following that, wash the polymer with the water by mixing/filtering it and then dry it. Granular and mid-sized particle grades are finalized by sieving, blending, and packing. Prior to sieving, mixing, and packaging, mills the material if it is of fine grade (25). Figure 2.3 depicts a schematic representation of (a) the synthesis of HPMC by reacting with cellulose in the presence of chloromethane and propylene oxide and (b) the formation of HPMCAS by the esterification of HPMC using succinic and acetic anhydride.

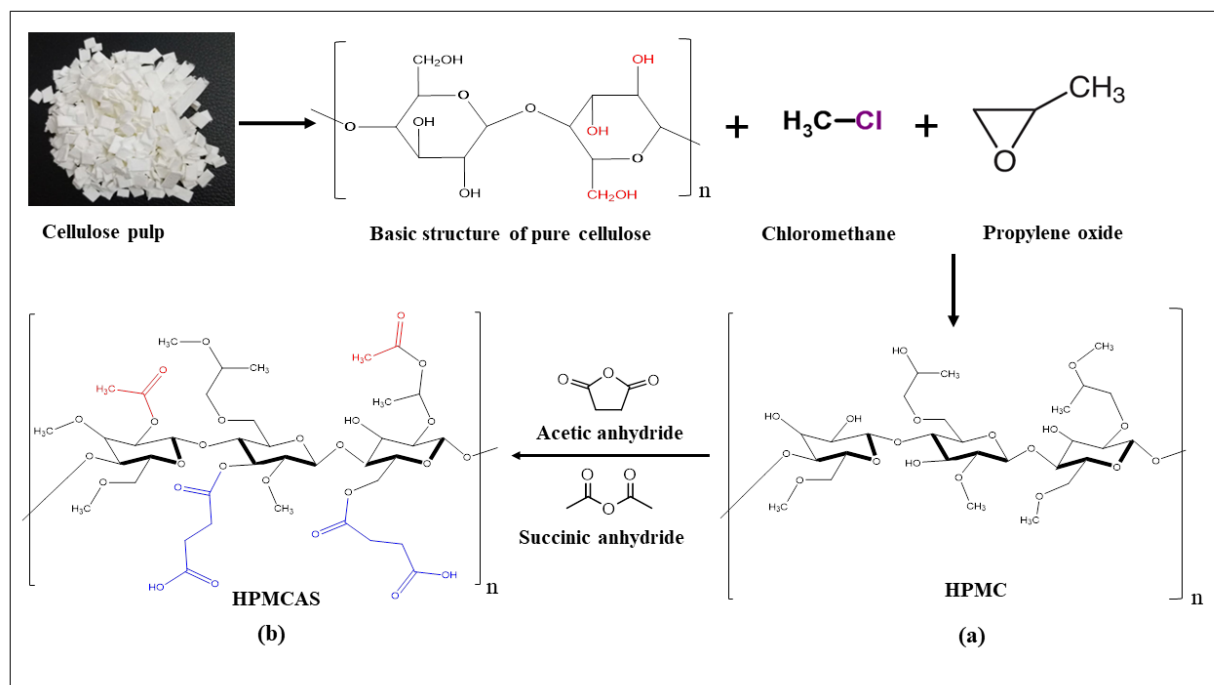


**Figure 2.3.** Schematic representation of (a) the synthesis of HPMC by reacting with cellulose in the presence of chloromethane and propylene oxide and (b) the formation of HPMCAS by the esterification of HPMC using succinic and acetic anhydride

### 2.2.3. Different grades of HPMCAS

The different available grades of HPMCAS are distinguished based on the ratio of succinyl to acetyl substituents on the HPMC skeleton, as shown in Table 2.1. HPMCAS 716, 912, 126 is permitted for use according to the USP-NF and the JPE (26). The side-chain substitution or the ratio of various substitutions will directly affect the hydrophilic-lipophilic balance of the polymer. Based on powder properties, some grades of HPMCAS are also available in fine powder form (AS-LF, AS-MF, AS-HF) and some in granular powder (AS-LG, AS-MG, AS-HG). The fine and granular form of the HPMCAS has a mean particle size of 5  $\mu\text{m}$  and 1 mm (27,28). HPMCAS is an anionic polymer that also shows pH-dependent solubility in an aqueous environment. By adjusting the substitution in the polymer structure dissolves over a wide pH range higher than 5.5. All grades are insoluble in acidic aqueous solutions and soluble in dilute caustic solutions (29,30).

### 2.2.4. Physicochemical properties of HPMCAS

HPMCAS is available in powder or granules with a white to off-white color and a faint acetic acid-like odor. HPMCAS is to be solubilized in various organic solvents such as methanol, acetone, methylene chloride, dichloromethane, and tetrahydrofuran. Table 2.1 lists the typical characteristics of different grades of HPMCAS polymer (23). Employing the solubility parameters has been a well-established practice, and it is a suitable technique for forecasting the interactions between polymers and carriers. The solubility parameter, according to Hansen, can be categorized into three components depending on the various interaction forces among the molecules in a condensed form. As a result, cohesive energy must be considered as the sum of contributions from hydrogen bonding, dispersion, and polar interaction forces (23). The total solubility parameter of HPMCAS is 29.1  $\text{MPa}^{1/2}$  calculated by the experimental method (31).

Each grade of HPMCAS differs in its moisture content, and the rate of moisture absorption directly depends on numerous factors, such as the substitution pattern of acetyl and succinyl groups, temperature, the initial level of moisture content, and relative humidity. The moisture dramatically influences the stability of SD since it can lower the  $T_g$  and consequently enhance molecular mobility, which causes drug crystallization. The onset of degradation temperature of HPMCAS is around 200°C which imparts a large computing window for drug formulation development. Each grade of HPMCAS shows a different  $T_g$ , which directly depends on the acetyl and succinyl substitution levels and the absorbed moisture content. According to the literature, polymers with a high  $T_g$  are more suited for SD because they have lower molecular mobility and impede

crystallization. The  $T_g$  tool can be used to quantify the stability of SD as a resistance of glasses to devitrification upon reheating, particularly above or close to the glass temperature point. Hancock et al. offer the  $T_g$ -50K criteria for storing SD, which, states that the temperature at which SD is stored must be at least 50 K lower than the  $T_g$  temperature because it has been seen that low molecular mobility can be identified in this temperature range (32). Table 2.1 shows the glass transition temperatures ( $T_g$ ) of HPMCAS grades (28,33). Additionally, the strength (S), Weakness (W), Opportunities (O), and Threats (T) (SWOT) analysis of HPMCAS showed in Figure 2.4

**Table 2.1.** Various properties of the different grades of HPMCAS

Different grades of HPMCAS	HPMCAS*			Ref
	716/L/LG & LF	912/M/MG & MF	126/H/HG & HF	
Appearances	White to off-white powders and granules			(34)
Molecular weight (g/mol)	114,700	103,200	75,100	(35)
Intermolecular interaction radius	10.06 J/cc <sup>0.5</sup>	10.76 J/cc <sup>0.5</sup>	9.85 J/cc <sup>0.5</sup>	
Hydrogen bonding	10.19 J/cc <sup>0.5</sup>	10.33 J/cc <sup>0.5</sup>	9.67 J/cc <sup>0.5</sup>	
Dispersive forces	17.77 J/cc <sup>0.5</sup>	16.73 J/cc <sup>0.5</sup>	18.09 J/cc <sup>0.5</sup>	(33)
Polar (dipole) interaction	11.87	12.37	12.76	
Solubility parameter (MPa <sup>0.5</sup> )	29.1			(23)
Glass transition temperature ( $T_g$ )	119-120 °C	120-130 °C	122-135°C	(28,33,34)
Thermal decomposition temperature ( $T_d$ )	258	267	276	(34)
pH solubility	5.5-6	6-6.5	> 6.8	
Acetyl content	5.0-9.0 %	7.0-11.0 %	10.0-14.0 %	
Succinate content	14.0-18.0 %	10.0-14.0 %	4.0-8.0 %	
Methoxy content	20.0-24.0 %	21.0-25.0 %	22.0-26.0 %	(28,33,34)
Hydroxypropyl content	5.0-9.0 %	5.0-9.0 %	6.0-10.0 %	
Water vapor permeability (0%/75% RH)	165 g/m <sup>2</sup> /24h	185 g/m <sup>2</sup> /24h	210 g/m <sup>2</sup> /24h	
Film strength (tensile strength at break MPa)	52	51	55	(28)
Film strength (Elongation %)	8.4	7.2	4.3	
Viscosity	2.4-3.6 mPa			
Loss on drying	≤ 5 %			
Residue on ignition	≤ 0.20 %			
Heavy metals	≤ 10 ppm			
Arsenic	≤ 2 ppm			(28,33–35)
Acetic acid	0.5 %			
IID base limit	560 mg/day			

Solubility in an organic solvent	Methanol, methanol/dichloromethane (1:2), ethanol/water (4:1), acetone, tetrahydrofuran, methylene chloride	(33)
Melt viscosity	< 100,000 at the temperature range of 170–200 °C	(34,35)
Hygroscopicity	<10 % at 25 °C, RH of approximately 100 %	
Mean Particle size for fine grade	5 µm	
Mean Particle size for granular grade	1 µm	(35)
Degree of polymerization	70	(28)

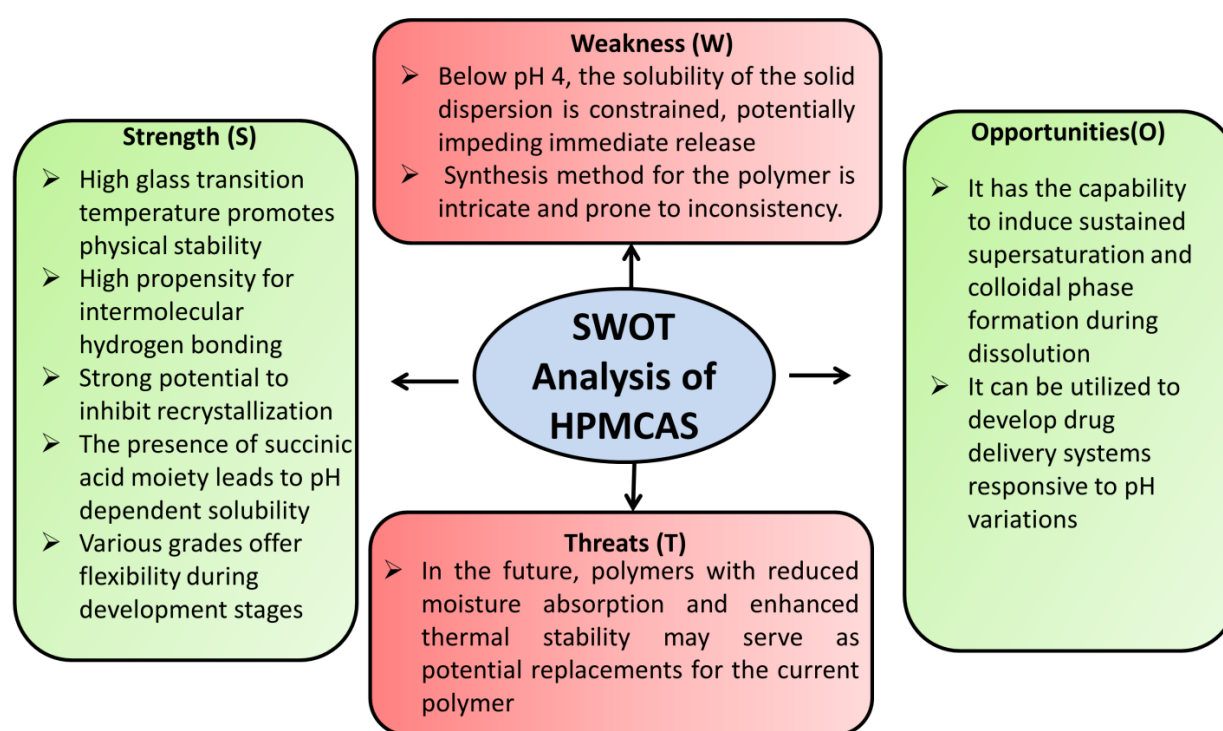


Figure 2.4.SWOT analysis of HPMCAS

### 2.2.5. Regulatory aspects for applications of HPMCAS

Even though cellulose-based polymer and their derivatives are assumed as inert materials, newly prepared cellulose derivatives may cause questions about their safety and toxicity depending on their interaction with API and the biological environment. However, the US FDA has included a list of substances that are GRAS in the Code of Federal Regulations (CFR). The agency has also kept a database of inactive ingredients (IID) for excipients authorized and used in marketed

products (20). In accordance with clause 201(s) of the Federal Food, Drug, and Cosmetic Act, Shin-Etsu has concluded that Shin-Etsu AQOAT®, HPMCAS is GRAS for the use for which it is intended (25). This notice is being submitted in compliance with 21 CFR Part 170; Subpart E. HPMCAS is permitted for use according to the USP-NF (26) and JP. The FDA-IID currently lists 560 mg of HPMCAS as the maximum amount that can be allowed in one tablet. HPMCAS is employed as an enteric coating material, and SD carriers (25). HPMCAS, considered safe, does not show any side effects in the toxicological studies (36).

The pharmacokinetic investigations show that after oral administration, related modified cellulose compounds, including the raw materials HPMC used to make the Shin-Etsu AQOAT® HPMCAS, have minimal absorption and are primarily eliminated in the feces. According to numerous researches on reproductive and developmental toxicity in rats, Shin-Etsu AQOAT® HPMCAS has not shown any hazardous effect on the rat fertility and reproductive system (25). In 1985, Hoshi et al. conducted various toxicological studies of the Shin-Etsu AQOAT® HPMCAS. They carried out general pharmacological studies on various experimental animals (such as mice, rats, rabbits, guinea pigs, frogs, and dogs) to confirm the safety of HPMCAS because it is anticipated that HPMCAS is a useful pharmaceutical excipient (17,36–39).

### **2.3. Hydroxypropyl methyl cellulose Hot melt extrusion (HPMC HME)**

#### **2.3.1. Introduction**

Hydroxypropyl methyl cellulose (HPMC) is a water-soluble polymer extensively employed in pharmaceutical formulations such as immediate-release and modified-release formulations. It is an amorphous polymer having high  $T_g$  from about 160-220°C. HPMC shows low decomposition temperature, exhibiting significant degradation temperature in the range of 200-250°C, depending upon the substitution (40). These high  $T_g$ , low degradation temperature and elevated melt viscosity possess significant obstacles in processing HPMC through HME. During the processing, the elevated melt viscosity of HPMC results in increased torque inside the extruder. While temperature elevation can mitigate both the melt viscosity and torque, it may also lead to degradation of the HPMC, and drugs utilized at high processing temperatures. These parameters limit the application of HPMC in HME. Current methods utilized to enhance the processability of HPMC often require the inclusion of significant levels of plasticizers and other additives (41). However, in certain cases, particularly with the amorphous system such as SD, this approach may lead to the

crystallization of the drug over time and upon exposure to water in the gastrointestinal tract, ultimately diminishing the dissolution and absorption rates, thereby reducing the bioavailability (42). HPMC has proven its effectiveness as a recrystallization inhibitor for stabilizing amorphous drugs; there is a pressing need to incorporate it into HME formulations without relying on plasticizers (43,44).

To improve this condition, Dow Chemical, a manufacturer of various cellulosic polymers, has introduced a range of new HPMC grades, branded as HPMC HME, designed for pharmaceutical researchers. These grades are formulated to be extruded through hot melt extruders at reduced processing temperatures due to their lower glass transition temperatures ( $T_g$ ) (117-128°C) (45) and enhanced 'melt flow' characteristics (43). Moreover, aside from enhancing processing via HME, the newly introduced HPMC HME polymers have been purported to retain their benefits as precipitation inhibitors after dissolution (44). HPMC HME polymers are specifically customized to meet the solubilization performance needs of APIs, whether for formulation via spray-dried dispersion (SDD) or HME. While HPMC is already known for its effectiveness in forming SD with APIs, HPMC HME enhances these advantageous properties by widening the thermal processing range and improving solubility in organic solvents. Additionally, the polymer's increased organosolubility offers benefits for utilizing HPMC in solvent spray drying applications. These combined attributes make HPMC HME an outstanding option for formulating poorly soluble drugs, such as those classified under the BCS as Class II and Class IV compounds. HPMC HME serves as a crucial tool for overcoming solubility challenges through various processing techniques (46).

HPMC HME, a hydroxypropyl methylcellulose compound, is engineered with a specialized polymer substitution structure that facilitates thermal processing. This characteristic makes HPMC HME particularly advantageous in pharmaceutical manufacturing techniques like HME, ideal for creating stable SDs containing poorly soluble APIs. HME, being a solvent-free, continuous manufacturing method, has demonstrated significant relevance in enhancing drug solubility within the pharmaceutical sector. The distinctive composition of HPMC HME enables the formation of robust SDs, leading to enhanced solubility and subsequent improvements in bioavailability for both immediate and controlled release formulations (46). Table 2.2 shows the difference between the traditional HPMC and HPMC HME.



**Table 2.2.** Difference between the traditional HPMC and HPMC HME (43,46)

HPMC	HPMC HME
High glass transition temperature (high Tg) (160°C to 210°C)	Low glass transition temperature (low Tg) (117°C–128°C)
Cellulosic polymers (HPMC, PVP) are not suitable for melt extrusion	HPMC HME is suitable for melt extrusion
The high glass transition temperature and low degradation temperature, together with the high melt viscosity and significant color change at elevated temperatures, make it challenging to process Hypromellose by HME.	Lower melt viscosity enables HPMC HME to be processed by HME without plasticizers, a feature which reduces formulation requirements, can improve physical stability, and may reduce toxicity. (Lower Tg, reduced melt viscosity, and reduced color change at elevated temperatures)
Improve the processability of Hypromellose require the use of high levels of plasticizer and other processing aids which for certain amorphous systems, including SD may result in crystallization of the drug during storage	HPMC HME has been shown to be an effective recrystallization inhibitor in stabilizing amorphous drugs which can enhance the bioavailability of poorly soluble compounds. Therefore, it is highly desirable to incorporate Hypromellose into a HME formulation without the use of plasticizers
High Moisture absorption	Low moisture absorption
High moisture uptake	Low moisture uptake

### 2.3.2. Chemistry of HPMC HME

HPMC HME is manufactured using traditional HPMC production methods, resulting in a distinct substitution architecture. This difference leads to HPMC HME having a considerably lower Tg (117°C–128°C) and melt viscosity compared to currently available HPMC grades, making it more suitable for thermal processing. The primary distinction between HPMC HME and standard HPMC lies in the degree of methoxy and hydroxypropyl substitution. A HPMC HME typically controls the methoxy substitution degree at 22%–27% and the hydroxypropyl substitution at 25%–32% (47).

### 2.3.3. Physicochemical properties of HPMC HME

HPMC HME is a water-soluble amorphous polymer, presented as a white to off-white powder and presently offered in three variants: HPMC HME 15 LV, HPMC HME 100 LV, and HPMC HME 4M. These variants vary in their molecular weights, as illustrated in Table 2.3. Depending on the

specific requirements of the formulation, the suitable grade can be chosen to effectively manage the degree of solubility enhancement while achieving the desired drug release profile. HPMC HME exhibits a  $T_g$  of approximately 115°C, yet it remains stable against thermal degradation at temperatures exceeding 250°C. This lower  $T_g$  widens the processing window for the polymer, while still ensuring the solid-state stability of amorphous SDs for poorly soluble drugs. HPMC HME exhibits unique thermal properties, with a lower glass transition temperature ( $T_g$ ) and reduced melt viscosity compared to other HPMC grades. This combination allows for processing by HME without the need for plasticizers, which can simplify formulations, improve physical stability, and potentially reduce toxicity. HPMC HME demonstrates thermal stability across a wide temperature range, it is advised to conduct extrusion at temperatures below 200°C to reduce color alteration and prevent degradation of molecular weight. The recommended highest and lowest extrusion temperatures for HPMC HME are presented in Table 2.3 to ensure effective processing with minimal color formation. For formulated systems, extrusion can be performed above or below these temperatures with slight adjustments to the process, depending on the specific materials involved (43,45,46).

The absorption of atmospheric moisture can profoundly affect the performance and structural integrity of a final drug product. HPMC HME demonstrates diminished moisture absorption in comparison to other HPMC grades and non-cellulosic materials typically employed in HME, thereby significantly mitigating potential adverse effects on product performance and physical stability. This beneficial attribute remains consistent regardless of the polymer's molecular weight. Minimizing moisture sorption is particularly critical for SDs, where the presence of water can act as a plasticizer, lowering the  $T_g$  and heightening the risk of structural instability. HPMC HME displays a lesser degree of  $T_g$  reduction as moisture content increases, in contrast to numerous other common HME polymers, thus reducing the impact of water on product performance (43,46).

**Table 2.3.** Various properties of the different grades of HPMC HME (46,47)

<b>HPMC HME</b>			
Different grades of HPMC HME	15LV	100LV	4M
Appearances	White to off-white powder		
Molecular weight	84	179.3	552.8
Intermolecular interaction radius	10.9	10.6	9.8
Hydrogen bonding	12.3	12.7	12.7

Dispersive forces	18	17.9	17.8
Polar (dipole) interaction	11.9	12.5	11.4
Solubility parameter (MPa <sup>0.5</sup> )	24.83	25.25	24.65
Glass transition temperature (T <sub>g</sub> )	117-120 °C		
Recommended lowest processing temperature of neat polymer	135 °C	145 °C	155 °C
Recommended Highest processing temperature of neat polymer	190 °C	195 °C	200°C
Particle Size D (0.1)	54.35	52.75	53.17
Particle Size D (0.5)	104.49	102.63	107.92
Particle Size D (0.9)	207.068	208.87	237.12
Thermal decomposition temperature (T <sub>d</sub> )	250 °C		
Bulk Density (g/cc)	0.42		
Tapped Density (g/cc)	0.55		
True Density (g/cc)	1.2		
Cloud Point (°C)	46		
Loss on Drying (%)	1-3		
Angle of Repose (°)	32		
CARR Index	23.64		

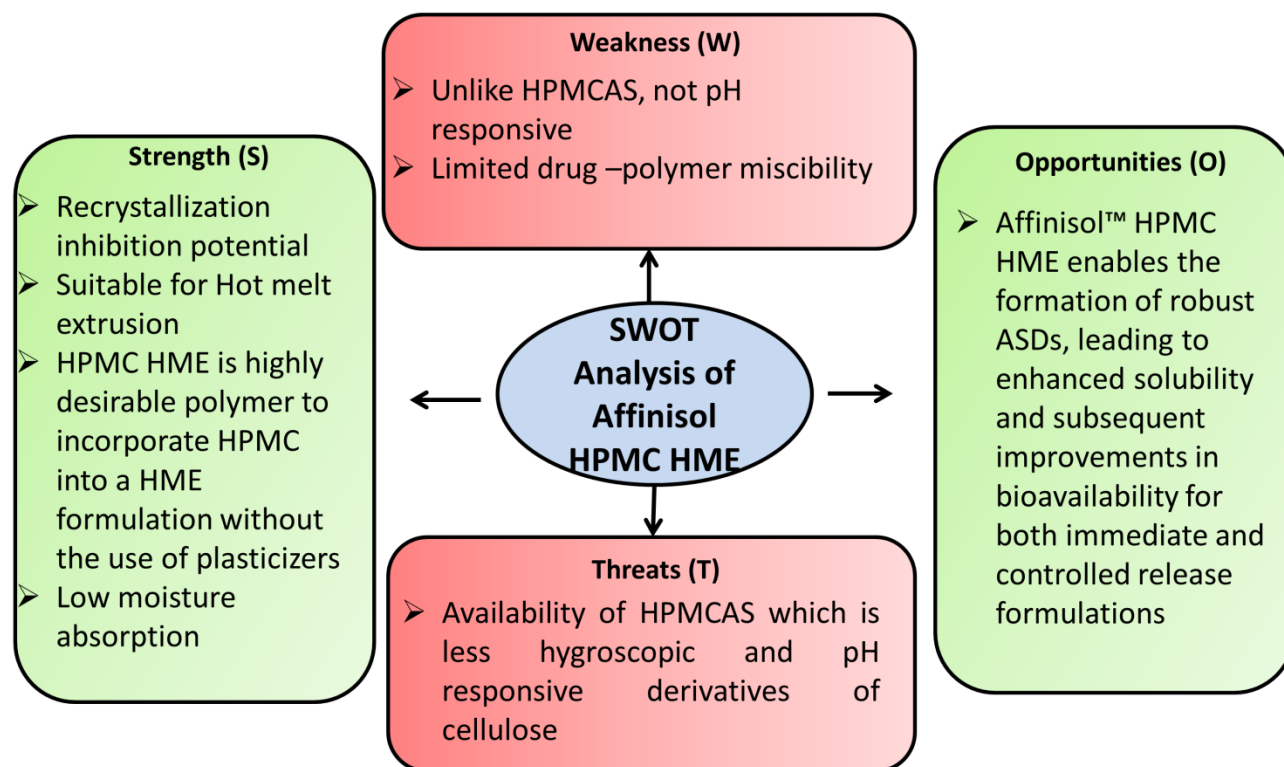


**Figure 2.5.** SWOT analysis of HPMC HME

#### 2.3.4. Toxicity study of HPMC HME

HPMC HME consists solely of hydroxypropyl methylcellulose without any added plasticizers or functional additives. Its hydroxypropyl and methoxy substitution ranges align with the extended substitution pattern (ESP) grades submitted to the U.S. FDA in GRAS Notice 000213 (2006). The GRAS assessment has confirmed that HPMC ESP grades can be utilized in food products, adhering to scientific standards, with a daily consumption level not exceeding 20 grams per individual. A specific type of HPMC called HME, which doesn't match the hydroxypropyl and methoxy substitution ranges listed in the USP/EP/JP standards, has undergone subchronic testing and was found to have a similar safety profile to existing HPMC grades. This means that HME can be used in food products and drug formulations, just like other HPMC grades, with the same maximum daily intake limit (46).

#### References

1. Schultz HB, Meola TR, Thomas N, Prestidge CA. Oral formulation strategies to improve

- the bioavailability and mitigate the food effect of abiraterone acetate. *International Journal of Pharmaceutics* 2020;577:119069.
2. The Institute of Cancer Research. *Abiraterone: A Story of Scientific Innovation and Commercial Partnership*. 2014.
  3. Fizazi K, Tran N, Fein L, Matsubara N, Rodriguez-Antolin A, Alekseev BY, et al. Abiraterone acetate plus prednisone in patients with newly diagnosed high-risk metastatic castration-sensitive prostate cancer (LATITUDE): final overall survival analysis of a randomised, double-blind, phase 3 trial. *The Lancet Oncology*. 2019;20(5):686–700.
  4. Agency EM, Kingdom U, Espan A, Universitario H, Hierro P De, Products H, et al. Oncologist of the Committee for Medicinal Products for Human Use. 2013;1032–1042.
  5. Sonpavde G, Attard G, Bellmunt J, Mason MD, Malavaud B, Tombal B, et al. The role of abiraterone acetate in the management of prostate cancer: A critical analysis of the literature. *European Urology*. 2011;60(2):270–278.
  6. Thakur A, Roy A, Ghosh A, Chhabra M, Banerjee S. Abiraterone acetate in the treatment of prostate cancer. *Biomedicine and Pharmacotherapy*. 2018;101:211–218.
  7. Ryan CJ, Smith MR, de Bono JS, Molina A, Logothetis CJ, de Souza P, et al. Abiraterone in Metastatic Prostate Cancer without Previous Chemotherapy. *New England Journal of Medicine*. 2013;368(2):138–148.
  8. Pierre Amarenco, Julien Bogousslavsky, Alfred Callahan 3rd, Larry B Goldstein, Michael Hennerici, Amy E Rudolph, Henrik Sillesen, Lisa Simunovic, Michael Szarek, K M A Welch, Justin A Zivin SP by AR in CL (SPARCL) I. Abiraterone and Increased Survival in Metastatic Prostate Cancer. *New England Journal of Medicine*. 2011;365:687–696.
  9. Fizazi K, Scher HI, Molina A, Logothetis CJ, Chi KN, Jones RJ, et al. Abiraterone acetate for treatment of metastatic castration-resistant prostate cancer: Final overall survival analysis of the COU-AA-301 randomised, double-blind, placebo-controlled phase 3 study. *The Lancet Oncology*. 2012;13(10):983–992.
  10. Sternberg CN, Castellano D, Daugaard G, Géczi L, Hotte SJ, Mainwaring PN, et al. Abiraterone acetate for patients with metastatic castration-resistant prostate cancer progressing after chemotherapy: Final analysis of a multicentre, open-label, early-access protocol trial. *The Lancet Oncology*. 2014;15(11):1263–1268.
  11. Date QS off, Number RMPV, Version S, Number E. European Union Risk Management

Plan Data lock point for current RMP 28 Apr 2022 Version number Final for Procedure EMEA / H / C / 002321 / II / 0072 – Health Authority Approval Date 06 July 2023 QPPV Name ( s ): QPPV Signature : Dr . Laurence Oster-Gozet. 2023.

12. Agency EM. Zytiga 250mg tablet: Summary of product characteristics. 2017.
13. Scott LJ. Abiraterone Acetate: A Review in Metastatic Castration-Resistant Prostate Cancer. *Drugs*. 2017;77(14):1565–1576.
14. Cornford P, Bellmunt J, Bolla M, Briers E, De Santis M, Gross T, et al. EAU-ESTRO-SIOG Guidelines on Prostate Cancer. Part II: Treatment of Relapsing, Metastatic, and Castration-Resistant Prostate Cancer. *European Urology*. 2017;71(4):630–642.
15. US. Highlighting Prescribing information : Zytiga (abiraterone acetate tablets) for oral use. 2011
16. Obara S, Tanno FK, Sarode A. Properties and Applications of Hypromellose Acetate Succinate (HPMCAS) for Solubility Enhancement Using Melt Extrusion. In: Repka MA, Langley N, DiNunzio J, editors. *Melt Extrusion: Materials, Technology and Drug Product Design*. New York, NY: Springer New York; 2013. 107–121.
17. N. Hoshi, H. Yano, K. Hirashima, H. Kitagawa YF. Toxicological Studies of Hydroxypropyl methylcellulose acetate succinate- Acute toxicity in rats and rabbits, and subchronic and chronic toxicities in rats. *The Journal of toxicological science*. 1970;10:147–185.
18. Shi SC, Su CC. Electrochemical behavior of hydroxypropyl methylcellulose acetate succinate as novel biopolymeric anticorrosion coating. *Materials Chemistry and Physics*. 2020;248:122929.
19. Choudhari M, Damle S, Narayan R, Sunil S, Dubey K, Singhvi G. Emerging Applications of Hydroxypropyl Methylcellulose Acetate Succinate : Different Aspects in Drug Delivery and Its Commercial Potential. *AAPS PharmSciTech*. 2023;1–26.
20. Chavan RB, Rathi S, Jyothi VGSS, Shastri NR. Cellulose based polymers in development of amorphous solid dispersions. *Asian Journal of Pharmaceutical Science*. 2019;14(3):248–264.
21. Brady J, Drig T, Lee PI, Li JX. Polymer properties and characterization. *Developing Solid Oral Dosage Forms: Pharmaceutical Theory and Practice: Second Edition*. 2017. 181–223.
22. Obara S, Kokubo H. Application of HPMC and HPMCAS to aqueous film coating of

- pharmaceutical dosage forms. *Aqueous Polymeric Coatings for Pharmaceutical Dosage Forms*. 2008;279–322.
23. Klar F, Urbanetz NA. Solubility parameters of hypromellose acetate succinate and plasticization in dry coating procedures. *Drug Development and Industrial Pharmacy*. 2016;42(10):1621–1635.
  24. Friesen DT, Shanker R, Crew M, Smithey DT, Curatolo WJ, Nightingale JAS. Hydroxypropyl Methylcellulose Acetate Succinate-Based Spray-Dried Dispersions: An Overview. *Molecular Pharmaceutics*. 2008;5(6):1003–1019.
  25. Carlson S, Nutrition A, Services H. Notice to US Food and Drug Administration of the Conclusion that the Intended Use of Shin-Etsu AQOAT® Hypromellose Acetate Succinate (HPMCAS) is Generally Recognized as Safe. 2020;(960):1-51
  26. Verlag. DA. USP 38 - NF 33 The United States Pharmacopeia and National Formulary 2015 Main edition plus Supplements 1 and 2. 1. Aufl. TA - TT -. Stuttgart SE -: Deutscher Apotheker Verlag Stuttgart; 2014.
  27. Kim SJ, Lee HK, Na YG, Bang KH, Lee HJ, Wang M, et al. A novel composition of ticagrelor by solid dispersion technique for increasing solubility and intestinal permeability. *International Journal of Pharmaceutics*. 2019;555:11–18.
  28. Shinetsu. Shinetsu NF Hypermellose Acetate Succinate Shin-Etsu AQOAT;Enteric Coating agent. 2005.
  29. Wang Y, Fang Y, Zhou F, Liang Q, Deng Y. The Amorphous Quercetin/Hydroxypropylmethylcellulose Acetate Succinate Solid Dispersions Prepared by Co-Precipitation Method to Enhance Quercetin Dissolution. *Journal of Pharmaceutical Sciences*. 2021;110(9):3230–3237.
  30. Ueda K, Higashi K, Yamamoto K, Moribe K. The effect of HPMCAS functional groups on drug crystallization from the supersaturated state and dissolution improvement. *International Journal of Pharmaceutics*. 2014;464(1):205–213.
  31. Carpentier P. The three dimensional solubility parameter and solvent diffusion coefficient their importance in surface coating formulation. 1967;1–104.
  32. Jelić D. Thermal Stability of Amorphous Solid Dispersions. *Molecules (Basel, Switzerland)*. 2021;26(1)238.
  33. AFFINISOL™ HPMCAS for Spray-Dried Dispersion (SDD) Solving the Insoluble.

- 2021;1–10.
34. AquaSolve Hydroxypropyl methylcellulose acetate succinate: Physical and chemical properties handbook. 2021;1–15.
  35. Butreddy A. Hydroxypropyl methylcellulose acetate succinate as an exceptional polymer for amorphous solid dispersion formulations: A review from bench to clinic. *European Journal of Pharmaceutics and Biopharmaceutics*. 2022;177:289–307.
  36. Hoshi, N., Ueno, K., Yano, H., Hirashima, K., & Kitagawa H. General pharmacological studies of hydroxypropylmethylcellulose acetate succinate in experimental animals. *The Journal of toxicological sciences*, 1985; 10 (2), 129–146.
  37. Hoshi N. Teratological studies of Hydroxypropyl methyl cellulose acetate succinate in rats. *The Journal of Toxicological Sciences*. 1985;10(II):203–226.
  38. Hoshi N. Teratological study of hydroxypropyl methylcellulose acetate succinate in rabbits. *The Journal of Toxicological Sciences*. 1985;10(II):227–234.
  39. Hoshi N. Studies of Hydroxypropylmethyl cellulose acetate succinate on fertility in rats. *The Journal of Toxicological Sciences*. 1985;10(II):187–201.
  40. Jani R, Patel D. Hot melt extrusion: An industrially feasible approach for casting orodispersible film. *Asian Journal of Pharmaceutical Science*. 2015;10(4):292–305.
  41. Bennett RC, Keen JM, Bi Y, Porter S, Dürig T, McGinity JW. Investigation of the interactions of enteric and hydrophilic polymers to enhance dissolution of griseofulvin following hot melt extrusion processing. *Journal of Pharmacy and Pharmacology*. 2015;67(7):918–938.
  42. Konno H, Handa T, Alonzo DE, Taylor LS. Effect of polymer type on the dissolution profile of amorphous solid dispersions containing felodipine. *European Journal of Pharmaceutics and Biopharmaceutics*. 2008;70(2):493–499.
  43. Huang S, O'Donnell KP, Keen JM, Rickard MA, McGinity JW, Williams RO. A New Extrudable Form of Hypromellose: AFFINISOL™ HPMC HME. *AAPS PharmSciTech*. 2016;17(1):106–119.
  44. Verreck G, Six K, Van den Mooter G, Baert L, Peeters J, Brewster ME. Characterization of solid dispersions of itraconazole and hydroxypropylmethylcellulose prepared by melt extrusion—part I. *International Journal of Pharmaceutics*. 2003;251(1):165–174.
  45. O'Donnell KP, Woodward WHH. Dielectric spectroscopy for the determination of the glass



- transition temperature of pharmaceutical solid dispersions. *Drug Development and Industrial Pharmacy*. 2015;41(6):959–968.
46. Dow Pharma & Food Solutions. AFFINISOL™ HPMC HME for Hot Melt Extrusion. :1–8.
  47. Khatri P, Katikaneni P, Desai D, Minko T. Evaluation of Affinisol® HPMC polymers for direct compression process applications. *Journal of Drug Delivery Science and Technology*. 2018;47:461–467.

# **Chapter 3: Analytical Method**

## **Development**

### 3.1. Introduction

Analytical methods are essential to formulation development, substantially impacting product development. A suitable analytical method is necessary for each stage of the drug and formulation development process to authenticate the completeness and quality of the procedure and final product. Analytical methods tailored to meet the specific requirements of each development stage are developed in a sequence. The analytical method should be simple, rapid, accurate, precise, and economical and should confirm stability, thereby accelerating the product development process. Hence, it is crucial to develop an analytical method for any drug molecule to characterize it before initiating the design of any drug delivery system. Developing and validating simple, sensitive, accurate, precise, and cost-effective analytical methods well suited for regular applications are essential for determining drugs in bulk, pre-formulation studies, in-vitro dissolution samples, stability studies, and in-vivo pharmacokinetic studies. In the present work, from the development of the Ultraviolet (UV) spectrophotometric method, suitable liquid chromatographic (LC) based analytical and bioanalytical methods were developed and validated to estimate ABTA in bulk and other samples. The developed analytical and bioanalytical methods were successfully applied to estimate ABTA in SD formulations, dissolution, stability, and biological samples.

### 3.2. Analytical methods reported for the estimation of ABTA

Few analytical and bioanalytical methods have been reported to estimate ABTA in bulk, formulation, and biological samples. A UV spectroscopic method has been reported for determining ABTA in tablet dosage form (1); however, the method is not fully validated per the ICH guidelines. Numerous chromatographic methods (RP-HPLC) have been described to separate and quantify ABTA, its degradation products, related substances, and impurities in bulk drugs, dosage forms, and biological specimens. These existing methods manifested various limitations, such as high operational cost, low sensitivity, variability in accuracy and precision, and higher retention time (2). For the biological samples, a few methods have been reported by liquid chromatography-tandem mass spectroscopy (LC-MS/MS), UV-ESI-IT-MS, and UPLC-MS/MS (3,4). Nevertheless, these methods come with a high cost, and not all laboratories with moderate funding have access to such facilities.

In the current investigation, it was necessary to quantitatively assess ABTA at various stages, including pre-formulation studies, evaluating and screening in-house developed SD formulations,

and pharmacokinetic studies of optimized formulations. We developed HPLC methods for formulation and biological samples to meet these requirements and validated them accordingly. Additionally, a straightforward, quick, and cost-effective UV spectroscopy method was devised for routine analyses, determining drug content, and the % assay of in-house developed amorphous SD formulations.

### **3.3. Method I: Ultraviolet (UV) Spectrophotometric method**

#### **3.3.1. Materials and methods**

ABTA has attained a generous gift sample from Biophore Pharmaceutical Pvt. Ltd, India. Sodium hydroxide, hydrogen peroxide, hydrochloric acid, and dibasic potassium phosphate ( $K_2HPO_4$ ) were procured from S.D Fine Chemical Pvt. Ltd. The solvents used for the research purpose were of HPLC grade, such as acetonitrile and methanol obtained from Merck. All other necessary chemicals were from reputed companies.

#### **3.3.2. Instruments**

An UV visible spectrophotometer (Jasco, Model V-750) is connected to a computer loaded with spectra manager (version 2) software, and absorbance measurements were conducted. The measurements were performed with matched micro quartz cuvettes featuring a 10 mm path length. Absorption spectra were recorded in the Spectrum mode, scanning from 200 to 800 nm at a medium scanning speed and 1 nm bandwidth.

#### **3.3.3. Method development**

In the initial study, various aqueous buffers (pH 1.2, pH 4.5, and pH 6.8) and solvents were systematically evaluated to establish a suitable UV-spectrophotometric method for the ABTA analysis. The media selection was based on drug solubility, method sensitivity, ease of sample preparation, cost-effectiveness, and applicability. The chosen drug solution was scanned within the 200-800 nm wavelength to identify the wavelength.

#### **3.3.4. Preparation of stock and calibration standards**

Dissolving 10 mg of the ABTA in 100 mL of buffer medium resulted as a stock solution with a concentration of ABTA (100  $\mu$ g/mL). To prepare different concentrations, aliquots of this stock solution were transferred into a series of 10 mL volumetric flasks, and each flask was filled to the mark with the respective media. For the calibration curve development, six different

concentrations of ABTA, ranging from 10 to 35  $\mu\text{g/mL}$ , were prepared in the selected media.

### 3.3.5. Analytical Method validation

The developed method was validated according to USP and ICH guidelines, assessing specificity, selectivity, linearity and range, precision, accuracy, limit of detection, limit of quantification, and robustness. To establish selectivity and specificity, a solution of ABTA (10  $\mu\text{g/mL}$ ) from the stock solution and a placebo mix containing excipients used in SD preparation (urea, HPMC, HPMCAS, lactose monohydrate, and mannitol) were prepared. These solutions were scanned from 200-800 nm to check for changes in absorbance at the specific wavelengths.

To validate the accuracy of the proposed analytical method, quality control (QC) samples were prepared at three different concentration levels (low-quality control (LQC; 12  $\mu\text{g/mL}$ ), medium-quality control (MQC; 22  $\mu\text{g/mL}$ ), and high-quality control (HQC; 32  $\mu\text{g/mL}$ )) using an independent stock solution, which were then analyzed to assess the accuracy of the method using two metrics: percentage relative error (RE%), which quantifies the deviation between the measured values and the true or expected values, and mean percentage recovery, which represents the average percentage of the analyte recovered from the sample matrix, reflecting the efficiency of the extraction and analytical processes, ensuring the reliability and suitability of the method for its intended application.

Precision was evaluated using various quality control (QC) drug concentration levels prepared from an independent stock solution, focusing on both inter-day and intra-day variations. For intra-day variation, different drug concentrations were prepared in triplicate at three different times throughout the day. To assess inter-day variation, the same procedure was repeated over three consecutive days. Precision was expressed as the relative standard deviation (% RSD).

To assess the linearity of the proposed method, six distinct series of drug solutions (ranging from 10 to 35  $\mu\text{g/mL}$  in the selected medium) were prepared from the stock solution and analyzed. The resulting data underwent least squares regression analysis. The limit of detection (LOD) and limit of quantification (LOQ) were calculated using the calibration standards, determined as  $3.3 \sigma/S$  and  $10 \sigma/S$ , respectively, where S represents the slope of the calibration curve and  $\sigma$  denotes the standard deviation of the y-intercept of the regression equation.

Robustness was evaluated by examining how slight variations in experimental parameters impacted the analytical performance of the method. This was tested by adjusting the pH of the medium by  $\pm 0.2$  units. Three different concentrations (LQC, MQC, and HQC) were prepared in media with the modified pH. The results for robustness were expressed as mean percentage recovery and percentage relative standard deviation (% RSD).

The stability of ABTA in the diluent medium was assessed using the validated UV-spectrophotometric method. Fresh quality control (QC) samples were prepared, and their spectra were recorded using the developed technique. All QC samples were analyzed at room temperature over a 24 h period. The stability of ABTA was quantified as the percentage mean recovery.

### 3.4. Result and discussion

In selecting the appropriate aqueous medium for the analysis of ABTA, several factors were considered, including drug solubility, method sensitivity, cost, ease of preparation, stability, and applicability to dissolution studies. Based on these criteria, a 100 mM hydrochloric acid buffer (pH 1.2) was chosen as the optimal medium. The UV spectrophotometric analysis revealed that ABTA exhibits maximum absorbance at a wavelength ( $\lambda_{\max}$ ) of 236 nm. When evaluating potential solvent media, the primary considerations were method sensitivity, ease of preparation, cost-effectiveness, and the broader applicability of the method for routine ABTA analysis. Attempts to improve method sensitivity by adding acetonitrile or methanol in various proportions to different aqueous media were unsuccessful. Ultimately, 100 mM hydrochloric acid (pH 1.2) was selected as the medium based on its stability, cost-effectiveness, ease of preparation, and suitability for the intended application of the method.

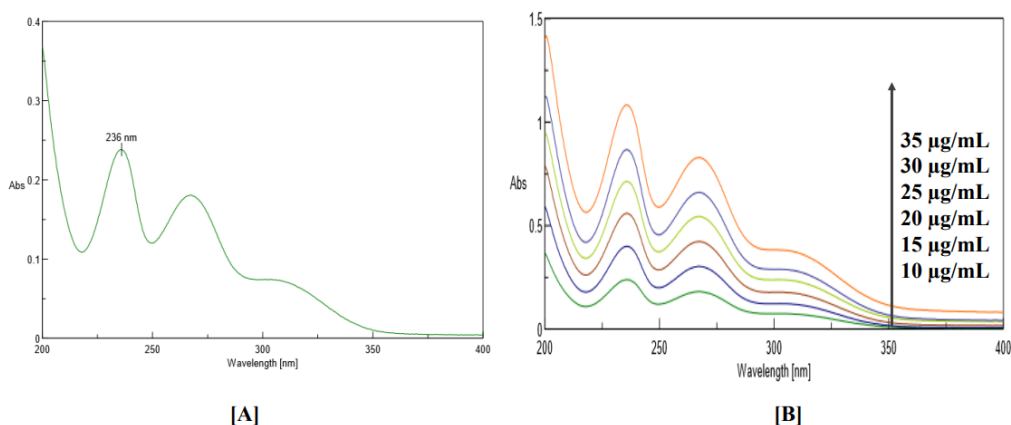


**Figure 3.1.** [A] UV absorption spectra (Concentration; 10 µg/mL) and [B] Overlay of ABTA at

different concentrations

**Table 3.1.** Calibration data of the ABTA developed UV-spectrophotometric method

Concentration ( $\mu\text{g/mL}$ )	Absorbance at 236 nm $\pm$ SD	% RSD
10 $\mu\text{g/mL}$	0.2277 $\pm$ 0.001	0.230
15 $\mu\text{g/mL}$	0.3603 $\pm$ 0.008	0.289
20 $\mu\text{g/mL}$	0.5053 $\pm$ 0.009	0.713
25 $\mu\text{g/mL}$	0.6333 $\pm$ 0.007	0.284
30 $\mu\text{g/mL}$	0.7613 $\pm$ 0.003	0.444
35 $\mu\text{g/mL}$	0.9130 $\pm$ 0.010	0.892

The presence of frequently used excipients did not affect the absorbance of ABTA. There were no alterations in the UV spectra of the drug when tested alongside these commonly used excipients in the examined media. The absorption spectrum for free ABTA closely matched that of the marketed formulation in the same media. The developed methods demonstrate high specificity and selectivity for ABTA, even in the presence of various common excipients, making them suitable for application across different dosage forms containing a diverse array of excipients.

The accuracy of the proposed method was studied to determine ABTA, as shown in Table 3.2. The mean absolute percentage recovery for the LQC, MQC, and HQC were found to be 99.58 %, 98.16 %, and 97.95 %, respectively. The % RSD was very low (less than 1.0 %), showing the accuracy of the proposed method. This method can accurately detect subtle variations in the drug concentration within the solution.

**Table 3.2.** Accuracy data of the proposed UV method for the determination of ABTA

Concentration ( $\mu\text{g/mL}$ )	Concentration ( $\mu\text{g/mL}$ )	Total concentration of drug found ( $\mu\text{g/mL}$ )	Mean Absolute recovery (%)	% RSD
LQC	12	11.95 $\pm$ 0.213	99.58 $\pm$ 0.057	0.715
MQC	22	21.59 $\pm$ 0.178	98.16 $\pm$ 0.123	0.917
HQC	32	31.35 $\pm$ 0.247	97.95 $\pm$ 0.025	0.489

Each result represents the average of six separate determinations

The precision of the proposed method was assessed by examining both intraday and interday precision. The % RSD for interday and intraday precision did not exceed 1.353 across all three QC concentrations, as illustrated in Table 3.3. The low % RSD values reflect the high precision of the

proposed method.

**Table 3.3.** Precision study results for the UV method

Concentration ( $\mu\text{g/mL}$ )	Intra-day repeatability RSD (%) (n =9)			Inter day Repeatability RSD (%) (n=27)
	Day 1	Day 2	Day 3	
QC standard				
LQC (12 $\mu\text{g/mL}$ )	0.885	0.804	1.353	0.797
MQC (22 $\mu\text{g/mL}$ )	0.379	0.402	0.738	0.581
HQC (32 $\mu\text{g/mL}$ )	0.253	0.134	0.369	0.247

The linearity range was 10-35  $\mu\text{g/mL}$  in the selected medium at 236 nm. The low values of the standard error of slope and intercept, as presented in Table 3.4, indicate the high precision of the proposed method. The high regression coefficient values demonstrate the excellent fit of the regression equations. Table 3.4 summarizes the various statistical data of the regression equations and validation parameters, further confirming the reliability and accuracy of the developed method.

**Table 3.4.** Statistical data of the regression equations and validation parameters

Regression analysis Parameters	Results
Linearity range	10-35 $\mu\text{g/mL}$
Regression equation	$y = 0.0272X - 0.0449$
Slope	0.0272
Intercept	- 0.0449
Regression coefficient	0.9994
95% Confidence limit of slope	0.0262 to 0.0280
Standard error of estimate	0.0067
Validation Parameters	
Linearity	10-35 $\mu\text{g/mL}$
Limit of Detection	0.9334 $\mu\text{g/mL}$
Limit of Quantification	2.8782 $\mu\text{g/mL}$
Precision (% RSD)	Intra-day repeatability (0.253-1.353) Inter-day repeatability (0.247-0.797)
Accuracy (% Mean recovery)	97.95-99.58

The LOD and LOQ were determined to be 0.9334  $\mu\text{g/mL}$  and 2.8782  $\mu\text{g/mL}$ , respectively,



demonstrating the sensitivity of the UV spectroscopic method. Changes in the pH of the selected media by  $\pm 0.2$  did not significantly impact the absorbance, with recovery values ranging from 98.14% to 102.47%, as detailed in Table 3.5. Additionally, the ABTA solution in the chosen diluent remained stable for 24 hours at room temperature, with recovery values between 99.47% and 100.58%, also shown in Table 3.5. These results indicate that the proposed method is reliable and stable for routine analysis.

**Table 3.5.** Robustness data of the proposed UV method

Concentration ( $\mu\text{g/mL}$ )	pH 1.1		pH 1.3		Stability Data (24 h)	
	% Mean absolute Recovery	% RSD	% Mean absolute Recovery	% RSD	% Mean absolute Recovery	% RSD
LQC (12 $\mu\text{g/mL}$ )	98.17 $\pm$ 0.347	1.213	99.42 $\pm$ 0.247	0.478	99.47 $\pm$ 0.415	1.112
MQC (22 $\mu\text{g/mL}$ )	101.58 $\pm$ 0.789	1.415	100.11 $\pm$ 0.318	0.714	100.58 $\pm$ 0.218	1.247
HQC (32 $\mu\text{g/mL}$ )	102.47 $\pm$ 0.684	1.789	98.14 $\pm$ 0.479	1.586	98.45 $\pm$ 0.514	0.989

The findings indicate that the suggested UV spectrophotometric approach offers a cost-effective, simple, rapid, sensitive, precise, and accurate method. It can reliably analyze ABTA in bulk form and formulations without being affected by commonly utilized excipients in SD.

### 3.5. Method II: Chromatographic analytical methods

#### 3.5.1. Materials and methods

ABTA has attained a generous gift sample from Biophore India Pharmaceutical Pvt. Ltd. Sodium hydroxide, hydrogen peroxide, hydrochloric acid, and dibasic potassium phosphate ( $\text{K}_2\text{HPO}_4$ ) were procured from S.D Fine Chemical Pvt. Ltd. The solvents used for the research purpose were of HPLC grade, such as acetonitrile and methanol obtained from Merck. HPLC grade water was obtained from the MiliQ system (Millipore GmbH, Germany) and was used for the analysis. Buffers were adequately filtered through a 0.22  $\mu\text{m}$  Millipore<sup>TM</sup> membrane filter (Merck, Darmstadt, Germany) and degassed using an ultrasonic bath for 30 min before use.

#### 3.5.2. Instrumentation and chromatographic conditions

HPLC-based analysis was conducted on Shimadzu LC-20AC liquid chromatography coupled with a photodiode array detector. This system comprises an autosampler, a column oven, and a quaternary gradient pump. LC-solution software was applied for data acquisition, process

monitoring, and system control. The developed HPLC method examined the degradation products of ABTA and related impurities. The separation was conducted on the Hypersil gold C<sub>18</sub> HPLC column (50mm x 4.6mm, particle size 5µm). The mobile phase mixture comprised acetonitrile and 0.01mM K<sub>2</sub>HPO<sub>4</sub> buffer (pH 6.5) in a ratio of 80:20 (v/v %). The injection volume was kept at 20µL with a flow rate of 1mL/min, the column temperature was set at 30°C for the analysis, and the analytes were detected at wavelength 254 nm.

### 3.5.3. Buffer Preparation

Accurately weigh 1.7g of 10 mM dipotassium hydrogen phosphate (K<sub>2</sub>HPO<sub>4</sub>) and dissolve in the 1000 mL MilliQ water. The solution was mixed properly and then adjusted to pH 6.5 ± 0.05 with 1% acetic acid. This given buffer preparation was degassed and filtered through a 0.22 µm Millipore filter under vacuum.

### 3.5.4. Preparation of stock and standard solution

Accurately weigh and transfer about 50 mg of ABTA into a 50 mL volumetric flask and dilute with 25 ml of acetonitrile. This solution was sonicated for 2-3 min and make up the volume up to the mark. The prepared sample was filtered through a 0.22 µm syringe filter before injecting the sample into the column.

### 3.5.5. Preparation of sample solution

The working sample solution of different concentrations was prepared and diluted with acetonitrile from the stock solution. After that, this solution was filtered through a 0.22 µm syringe filter before sampling into the system.

### 3.5.6. Analytical method development using Quality by design

#### (i) Step1: Analytical Target Profile (ATP) and Critical Analytical Attributes (CAA)

ATP outlines the quality attributes of the developed targeted analytical method. To develop an effective RP-HPLC chromatographic method for assessing ABTA, consider various factors of ATP such as a sample, type of method, instrument requirement, nature of the specimen, standard preparation, sample of preparation, and application of the method. To fulfill the objectives after completing the ATP, the theoretical plate, retention time, and tailing factor were considered CAA (5,6).

#### (ii) Step 2: Risk Assessment

Risk assessments were implemented to determine the impact of several elements on the ATP. Risk analysis was carried out by estimating the risk-associated factors during the investigation and using the Ishikawa fishbone diagram to determine the potential factors in the HPLC method shown in Figure 3.2. After that, the evaluation was done with the individual risk factor allotted to low, medium, and high grades. Furthermore, factor screening studies were conducted for the chosen parameters, and optimization studies were performed to characterize the analytical design space. After that, these studies were postulated on the control strategy for continuous method improvement (7).

### (iii) Step 3: Factor Screening Studies

A five-factor, eight-run FFD was carried out to determine the CMP/ CPP (column temperature, volume of acetonitrile, flow rate, pH, and injection volume) critically impacting the selected CAA (i.e., theoretical plate, tailing factor, and retention time). As illustrated in Table 3.6, the design matrix enlisting the five independent factors was examined at low (-1) and high (+1) levels, respectively. This study computed eight experimental runs in randomized order using a resolution V design. A mathematical statistics investigation was related to the design, which included the main and possible interaction effects. Furthermore, the main parameters of the factor screening studies are half-normal plots and the Pareto charts. These were carried out by qualitatively identifying each variable's impact on the chosen CAA (8).

**Table 3.6.** Design matrix enlisting the selected factor using FFD

Factor	Name	Units	Type	Low actual	High Actual	Low coded	High Coded
A	pH	Number	Numeric	5.50	6.50	-1	+1
B	Volume of acetonitrile	%	Numeric	80	90	-1	+1
C	Injection volume	μL	Numeric	10	20	-1	+1
D	Flow rate	mL/min	Numeric	0.8	1	-1	+1
E	Column temperature	°C	Numeric	25	35	-1	+1

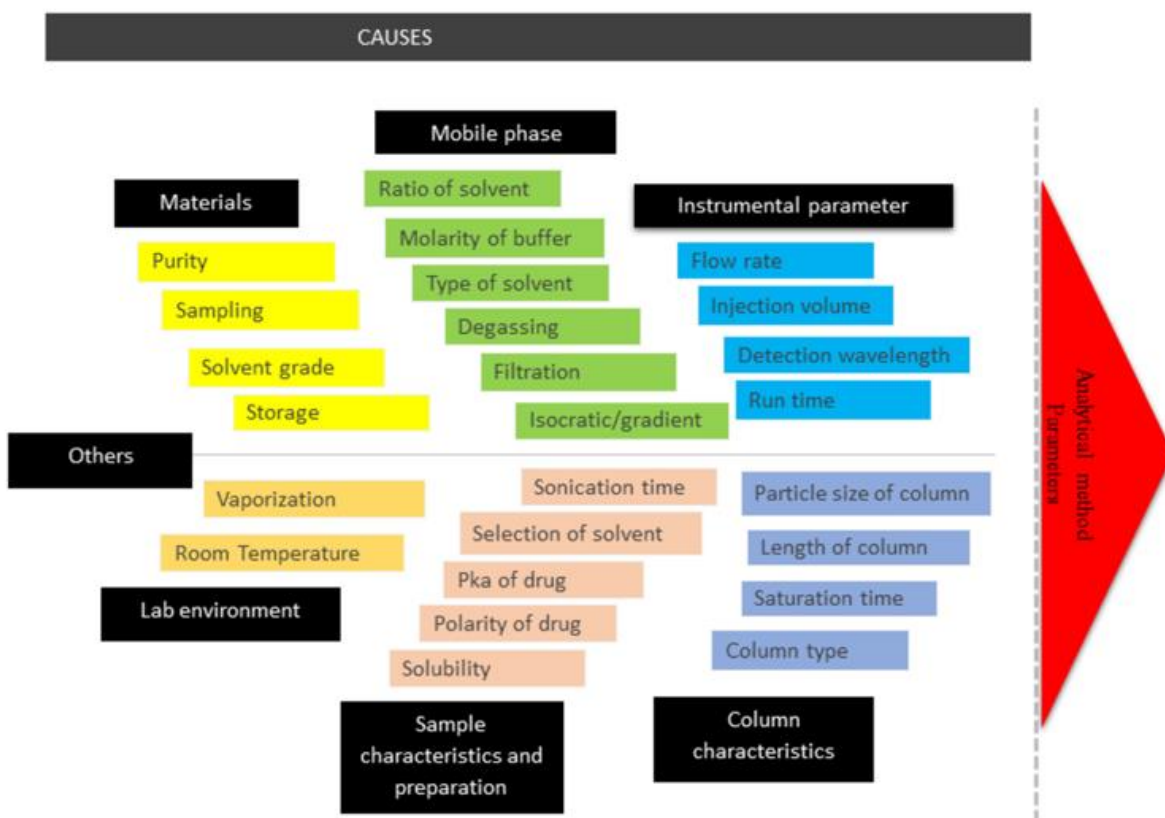


**Figure 3.2.** Ishikawa Fishbone diagram to determine the potential factors in the HPLC method development

#### (iv) Step 4: Method Optimization Studies

Based on the FFD, the volume of acetonitrile, the pH of the aqueous buffer, and the flow rate were selected as significant CMP that was methodically optimized by a second-order face-centered CCD. As shown in Table 3.7, the factors are enlisted at various stages, i.e., low (-1) and high (+1). The outline of the design matrix as per the CCD with a total of 17 experimental runs containing quintuplicate trials at the center points runs (9). A standard concentration of  $5\mu\text{g/mL}$  drug solution was applied in the entire run, which was evaluated for CAA, such as theoretical plate, tailing factor, and retention time.

**Table 3.7.** Design matrix enlisting the selected factor using CCD

Factor	Name	Units	Type	Low actual	High Actual	Low coded	High Coded
A	pH	Number	Numeric	5.50	6.50	-1	+1
B	Volume of Acetonitrile	%	Numeric	80	90	-1	+1

D	Flow rate	mL/min	Numeric	0.8	1	-1	+1
---	-----------	--------	---------	-----	---	----	----

### (v) Step 5: Optimization, Data Analysis and Model Validation

Design-Expert version-7.0.0 software was employed for the data evaluation, optimization, and validation of the model. The second-order quadratic polynomial model was used to assess the main effect and interaction effect. Analysis of variance (ANOVA) is the primary tool for selecting the mathematical model. Apart from that, the lack of fit analysis and the coefficient of correlation ( $R^2$ ), adjusted  $R^2$  ( $R^2$ -adj), and predictive  $R^2$  ( $R^2$ -pred) were designated as the model estimation parameters. The regression model is poorly attuned when the lack of fit is greater than the random pure error (P-value  $>0.05$ ). The 2D-counter and 3D-response surface plots were used to detect the factor-response relationship and plausible interaction effect. Estimating the efficient chromatographic method performance is based on the numerical optimization and desirability function by interchanging the different CAAs, minimizing the tailing factor retention time, and increasing the theoretical plate (10).

### 3.5.7. Validations of Analytical Methods

#### (a) System Suitability

The system suitability was applied to ensure whether the instrumentation was appropriate for actual chromatographic requirements. It was assessed by injecting six replicates of the standard solution of ABTA. Retention time, theoretical plate, tailing factor, and % relative standard deviation (RSD) were estimated from the chromatogram. The system suitability parameters, i.e., theoretical plate number higher than 2000, tailing factor  $\leq 2$ , and %RSD  $\leq 2$  %, were accepted according to the analytical guidelines (11).

#### (b) Linearity and range

The standard solution was injected to determine the linearity of the method in various concentration levels. It was prepared in the 0.5-10  $\mu\text{g/mL}$  range for ABTA using HPLC at 254 nm. The graph of the calibration curve of different concentration levels of the samples was plotted between peak area versus concentration. Moreover, the slope, regression coefficient, and intercept were evaluated by the linear regression equation (12).

#### (c) Accuracy

The accuracy of the established method was defined in terms of the mean percentage recovery method. In this method, three different quality control (QC) levels of ABTA concentration at

Lower quality control (LQC: 0.75 µg/mL), Medium quality control (MQC: 3.5 µg/mL), and Higher quality control (HQC: 8.5 µg/mL) were prepared from the standard solution and analyzed. The accuracy was evaluated regarding % RSD  $\leq$  2 %, which was accepted according to the analytical guidelines (13,14).

### **(d) Precision**

Precision was estimated by two methods: inter-day precision and intra-day precision. Furthermore, intraday precision or repeatability was determined at a different time interval on the same day with three different concentrations, such as (LQC: 0.75 µg/mL, MQC:3.5 µg/mL, HQC:8.5 µg/mL) in triplicates. Moreover, interday or intermediate precision was assessed by injecting the same triplicates of three different concentrations and analyzed over multiple days. The precision was estimated in terms of % RSD  $\leq$  2 %, which was accepted according to the analytical guidelines (15).

### **(e) Sensitivity**

The sensitivity of the developed method was assessed in terms of the limit of detection (LOD) and limit of quantification (LOQ). The evaluation of LOD and LOQ is based on the signal-to-noise (S/N) ratio of the response of the analyte in the calibration standard according to the ICH guidelines. The ideal S/N ratio should be greater than 10 for the lower LOQ and greater than 3 for the LOD (16).

### **(f) Selectivity**

Selectivity was determined by preparing the standard solution of ABTA in the respective media with or without an excipient. These prepared samples were injected into the HPLC in triplicates and evaluated %RSD  $\leq$  2 % was accepted as per the analytical guidelines.

### **(g) Robustness**

According to the ICH guidelines, the term robustness is the ability of the analytical procedure to be unaffected by slight but deliberate alterations in the experimental factors. Here, different parameters were selected for the proposed experiments, such as the flow rate, mobile phase mixture, column oven temperature, and pH. The developed method was assessed by slight changes in the operating conditions, i.e., column oven temperature ( $\pm$  25 to 30°C), flow rate ( $\pm$  0.8 to 1.2 mL/min), the mobile phase mixture ( $\pm$  2%), and pH of the Buffer (6.3 and 6.7) (17).

### **(h) Solution stability**

The solution stability was evaluated by storing the ABTA 5 µg/mL solution at room temperature

for different intervals (0h, 4h, 12h, 24h, and 48h) to observe any variation in the peak areas. The % RSD of ABTA was determined for the initial time interval at 48h.

### **3.5.8. Specificity and Forced degradation study**

As per the ICH guidelines, ICHQ1 (R2) recommended the stress and forced degradation study to examine the specificity of the method. The forced degradation study involves several pathways, such as oxidation, hydrolysis, thermal, humidity, and photolysis. The forced degradation studies were carried out with ABTA standard solution to check impurities, % assay, and % degradation of the sample in different stress conditions (18).

#### **(a) Acid and Base Hydrolysis and Hydrolytic Conditions Induced Degradation**

For the preparation of the sample, 1mL of standard stock solution was added to 10mL measuring flasks, adding 2mL diluent, and further volume was adjusted up to the mark with 0.1 N HCl/ 0.1 N NaOH/water separately. This sample was subjected to a water bath at 60°C for 24h. After 24h, this given drug solution was diluted with the diluent, mixed well, and filtered with a 0.45µm syringe filter. These samples were injected into the HPLC system, and the % recovery assay was calculated.

#### **(b) Oxidative Condition Induced Degradation**

For the preparation of the sample, 1mL of standard stock solution was added to 10mL measuring flasks, adding 2mL diluent, and further volume was adjusted up to the mark with 30% H<sub>2</sub>O<sub>2</sub> separately. This sample was subjected to room temperature for 24h. After 24h, this given drug solution was diluted with the diluent, mixed well, and filtered with a 0.45µm syringe filter. These samples were injected into the HPLC system, and the % recovery assay was calculated.

#### **(c) Thermal Condition-Induced Degradation**

For the preparation of the sample, 1mL of standard stock solution was added into the 10mL of the measuring flask, and further volume was adjusted up to the mark with a diluent. This sample was subjected to dry heat at 60°C for 24h in an oven, respectively. After 24h, this given drug solution was diluted with the diluent, mixed well, and filtered with a 0.45µm syringe filter. This sample was injected into the HPLC system, and the % recovery assay was calculated.

#### **(d) Photolytic Condition-Induced Degradation**

For the preparation of the sample, 1mL of standard stock solution was added into the 10 mL of the measuring flask, and further volume was adjusted up to the mark with a diluent. This sample was subjected to UV light (200h/m<sup>2</sup> and 1.2 million x 1h) for 24h in an oven, respectively. After 24h,

this given drug solution was diluted with the diluent, mixed well, and filtered with a 0.45 $\mu$ m syringe filter. This sample was injected into the HPLC system, and the % recovery assay was calculated.

### **(e) Humidity Condition-Induced Degradation**

For the preparation of the sample, 1mL of standard stock solution was added into the 10mL of the measuring flask, and further volume was adjusted up to the mark with a diluent. This sample was subjected to the humidity chamber at 40°C/75% R.H. for 24h in an oven, respectively. After 24h, this given drug solution was diluted with the diluent, mixed well, and filtered with a 0.45 $\mu$ m syringe filter. This sample was injected into the system, and the % recovery assay was calculated.

### **3.5.9. Application of the method**

SD was prepared by the simple melting method using urea as the carrier. In brief, ABTA and urea were mixed in different proportions, i.e., 1:1, 1:2, and 1:3 in a china plate and warmed up on a paraffin bath at 60°C temperature. The given blend was transferred to a plate and cooled at room temperature. The given solidified mass having different proportions was dried and passed across sieve number #60. Furthermore, the developed S.D. was subjected to solubility profiling. Briefly, the weight ratio of ABTA: urea (1:2) showed that the solubility of the drug in the SD was enhanced compared to pure drug. Therefore, to estimate ABTA, we selected a 1:2 weight ratio of SD and dissolved it in acetonitrile with the help of sonication (2-3min). Afterward, before injecting the prepared sample into the HPLC system, it should be filtered via a 0.22 $\mu$ m syringe filter.

## **3.6. Result and discussions**

### **3.6.1. Preliminary Method Development Studies**

The main criteria of analytical QBD are to obtain a good peak shape with less run time and attain accuracy, and the precision parameter with the % RSD  $\leq$  2 % was accepted as per the analytical guidelines, resulting in a robust process reducing the variableness. The mobile phase condition was optimized so that drugs can elute in less run time. Most of the existing methods define the usage of mobile phase mixture, including various solvent systems such as methanol, acetonitrile, ammonium acetate, and phosphate buffer, along with different pH, column chemistry (C<sub>8</sub> and C<sub>18</sub>), variable flow rate, different column temperature settings, injection volume, etc. for separation of ABTA, its degradation properties and impurities. It was proposed to prepare a rapid, simple, and sensitive liquid chromatographic method to quantify ABTA. Primarily, different mobile phase



mixtures were tried using acetonitrile, methanol, and a buffer comprising ammonium formate, ammonium acetate, and potassium phosphate (various strengths 10mM, 20mM, and 30mM) with variable pH (between 5 and 7) and different flow rates (between 0.8 and 1.2mL/min). From the reported studies, it can be concluded that the molecule is sensitive to pH. The retention time increases when the pH decreases from 6.5 to 5.5. At pH 6.0 and pH 6.5, the retention time almost remains constant. It was observed that the peak shape was not perfect while using the combination of methanol as an organic modifier at pH 5.5. The various ratios of K<sub>2</sub>HPO<sub>4</sub> (pH 6.5): acetonitrile were carried out, depicting that increasing the concentration of buffer leads to increasing the retention time of ABTA. These preliminary studies recommended that the selection of acetonitrile and K<sub>2</sub>HPO<sub>4</sub> (pH 6.5) be an appropriate mixture of mobile phases with fast chromatographic separation with low tailings factor, better resolution, and high theoretical plate count.

### 3.6.2. Implementation of QbD

#### (a) Risk Assessment Studies

The risk evaluation matrix studies were established upon investigating literature reports and pondering the research team exercise, and various critical input parameters were examined. Every method parameter had different levels of risk. From the Ishikawa diagram, preliminary studies were carried out; critical parameters were chosen to facilitate further studies like molarity of buffer (mM), the volume of acetonitrile, and pH as method variables, whereas the flow rate (mL/min), injection volume (μL), column temperature having the most significant effect on system suitability parameters. Furthermore, the column dimension was kept steady throughout the entire study for the development and validation of the RP-HPLC method.

#### (b) Factor screening studies

FFD is a factor screening design that was performed on the selected CMP. FFD was evaluated by selecting the first-order polynomial model to determine the main and interaction effects. The response variables were determined by generating the first-order polynomial equation. Furthermore, the coefficients b<sub>1</sub> to b<sub>3</sub> illustrate the coefficient of the linear model term of selected factors during screening studies, i.e., A, B, C, and the coefficient b<sub>0</sub> stands for the intercept term according to equation (3.1).

$$Y = b_0 + b_1 A + b_2 B + b_3 C \quad \dots \text{Equation (3.1)}$$

The polynomial coefficient was produced from each selected CAA during screening studies, expressing the substantial interaction effect between the factors. As shown in Figure 3.3, the Pareto

charts and half-normal plots represent the impact of CMP/ CPP on method CAA. Pareto ranking studies declare that the volume of acetonitrile, pH, and flow rate highly influence the selected CAA. This CMP/ CPP (volume of acetonitrile, pH, and flow rate) was analyzed for further optimization studies.

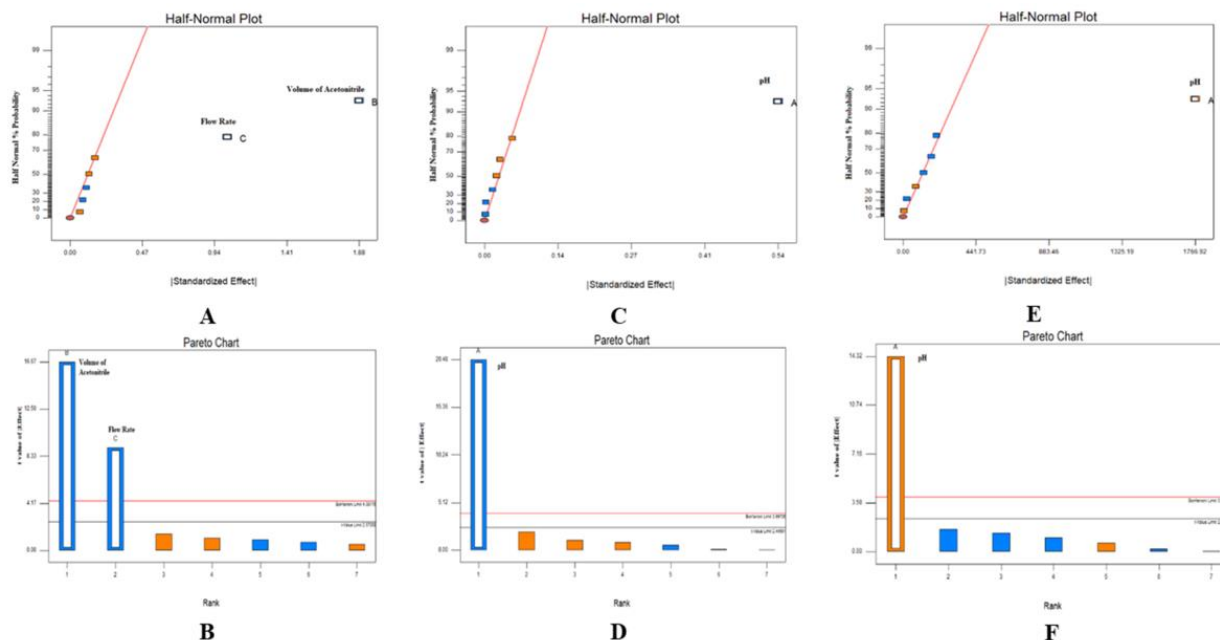


**Figure 3.3.** Half-normal plots and Pareto charts of various critical analytical attributes (CAA), i.e., Retention time (A and B), Tailing factors (C and D), and theoretical plate (E and F)

### (c) Method optimization studies and response surface mapping

The CCD was used for the method optimization studies, and the following data was examined by deciding the second-order polynomial model for depicting the main and interaction effects. The CCD was applied to optimize chromatographic requirements by studying the impact of various factors such as pH (A), the volume of acetonitrile (B), and flow rate (C) on the retention time of ABTA (R1), a tailing factor of ABTA (R2) and a theoretical plate of ABTA (R3). As illustrated in Table 3.8, the three factors affect the different responses, i.e., retention time, theoretical plate, and tailing factor of ABTA.

**Table 3.8.** Experimental design CCD for each run and response

Run	Factors			Response		
	pH	Volume of Acetonitrile (%)	Flow Rate (mL/min)	Retention time (min)	Tailing Factor	Theoretical plate

1	6.00	80.00	0.90	5.58	1.29	1920
2	6.00	90.00	0.90	3.43	1.25	1630
3	6.00	85.00	1.00	4.52	1.27	1856
4	5.50	85.00	0.90	4.89	1.69	1587
5	5.50	90.00	1.00	2.49	1.58	1487
6	6.50	80.00	0.80	5.55	1.03	3225
7	6.00	85.00	0.90	5.57	1.26	1789
8	5.50	80.00	1.00	4.41	1.63	1386
9	6.50	90.00	1.00	2.73	1.10	2935
10	5.50	90.00	0.80	3.61	1.59	1394
11	6.00	85.00	0.90	5.57	1.25	1880
12	6.00	85.00	0.90	5.55	1.13	1895
13	5.50	80.00	0.80	5.59	1.59	1418
14	6.50	90.00	0.80	3.82	1.09	2837
15	6.00	85.00	0.80	5.10	1.12	1790
16	6.50	80.00	1.00	4.74	0.995	3647
17	6.50	85.00	0.90	5.05	1.10	2896

Design Expert 7.0 software was employed to validate the model by analysis of variance (ANOVA). As shown in Table 3.9, the values of different parameters, such as PRESS value, % CV, standard deviation, mean,  $R^2$ ,  $R^2$ -adj,  $R^2$ -pred, and adequate precision. For considering PRESS value, the quadratic model was chosen for the theoretical plate, tailing factor, and retention time of ABTA. Adequate precision states that if the signal-to-noise ratio is higher than 4, the model is fitted. Table 3.9 shows that all obtained values are in an adequate signal. Apart from that, the high adjusted  $R^2$  value and low standard deviation (% CV) revealed a good association between the experimental data and the fitted model.

**Table 3.9.** ANOVA results of CCD

<b>Response</b>	<b>SD</b>	<b>Mean</b>	<b>% CV</b>	<b>PRESS</b>	<b><math>R^2</math></b>	<b><math>R^2</math>- adj</b>	<b><math>R^2</math>- pred</b>	<b>Adequate precision</b>	<b>P- value</b>
Retention time	0.27	4.60	5.81	2.81	0.971	0.933	0.837	15.76	0.001
Tailing Factor	0.06	1.29	4.94	0.16	0.967	0.924	0.819	13.02	0.002
Theoretical plate	134	2110	6.35	9.669	0.986	0.968	0.893	20.87	0.001

The coefficient analysis was carried out by estimating the model with Equation 3.2, produced according to the second-order quadratic polynomial equation for each CAA.

$$Y = b_0 + b_1A + b_2B + b_3C + b_4A^2 + b_5B^2 + b_6C^2 + b_7AB + b_8AC + b_9BC \quad \dots\text{Equation 3.2}$$

Whereas Y represents the values of each CAA,  $b_0$  indicates the intercept of the produced polynomial model,  $b_1$  to  $b_3$  represents the coefficient of the linear model term,  $b_4$  to  $b_6$  stands for the coefficient of the quadratic model term,  $b_7$  to  $b_9$  stands for the coefficient of the quadratic interaction term between the factor A, B, and C respectively. Actual components and factors show the final second-order quadratic polynomial equation, which can be applied to predict the response of given levels of each factor, such as the retention time of ABTA (R1 shown in equation 3.3), the tailing factor of ABTA (R2 shown in equation 3.4) and a theoretical plate of ABTA (R3 shown in equation 3.5).

$$R1 = +5.37 + 0.080*A - 0.97*B - 0.47*C + 0.032*A*B + 0.062*A*C - 0.041*B*C - 0.23*A^2 - 0.69*B^2 - 0.38*C^2 \quad \dots\dots\dots\text{Equation 3.3}$$

$$R2 = +1.24 - 0.28*A + 7.400E-003*B + 0.014*C + 0.026*A*B - 7.625E-003*A*C - 1.125E003*B*C + 0.14*A^2 + 0.012*B^2 - 0.058*C^2 \quad \dots\dots\dots\text{Equation 3.4}$$

$$R3 = +1809.68 + 856.93*A - 160.60*B + 34.81*C - 184.65*A*B + 19.88*A*C + 12.69*B*C + 465.72*A^2 - 2.03*B^2 + 46.79*C^2 \quad \dots\dots\dots\text{Equation 3.5}$$

The positive values in Equations 3.3, 3.4, and 3.5 illustrate a favorable impact on optimization, while negative values depict an inverse correlation between the factors and response. The response surface analysis estimated the degree of interaction between the CMPs and the CAA. The 3D response surface and 2D counterplots in Figure 3.4 (a-f) illustrate the effect of pH, the volume of acetonitrile, and flow rate on the retention time. The decrease in the volume of acetonitrile and flow rate increases the retention time. It was observed that curvilinear rises in retention time up to the intermediate levels, followed by gradual decreases at a high level. Furthermore, the acetonitrile and buffer pH were observed as the optimum retention time value at intermediate levels. Figure 3.5 (a-f) shows the 3D response surface and 2D counter plots representing the effect of buffer pH, the volume of acetonitrile, and flow rate on the tailing factor. A sharp “rising ridge” type of 3D response surface plot was observed for the tailing factor due to the combined effect of flow rate

and volume of acetonitrile. Wherein the reduction in the value of the tailing factor was observed with a decrease in flow rate and volume of acetonitrile.

On the contrary, the decrease in buffer pH increased the tailing factor's value. The 3D response surface and 2D counterplots, illustrated in Figure 3.6 (a-f), show the effect of buffer pH, the volume of acetonitrile, and the flow rate on the theoretical plate. In the curvilinear trend, the interaction between the buffer pH and the volume of acetonitrile was inversely analogous. The increase in pH revealed a sharp increment in the value of the theoretical plate. Meanwhile, the increase in the volume of acetonitrile showed a reduction in the value of the theoretical plate.

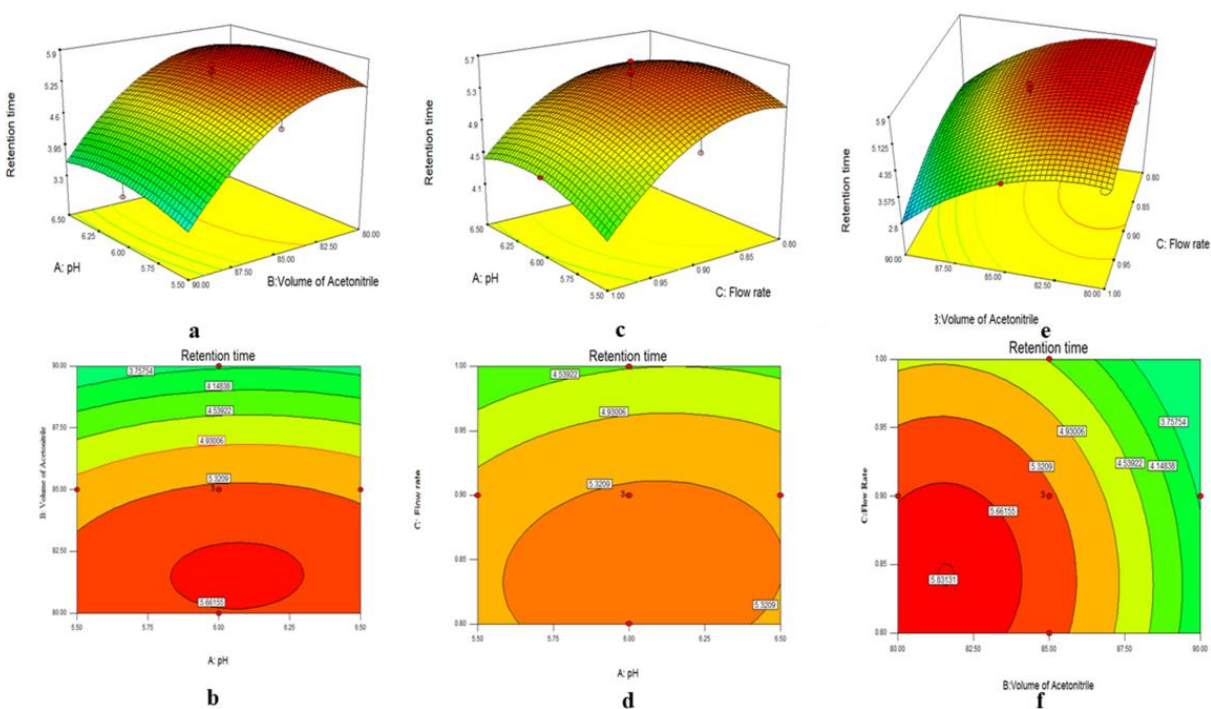


**Figure 3.4.** 3D response surface and 2D contour plots viewing the influence of CMP, viz., pH (A), Volume of acetonitrile (B), and Flow rate (C) on the retention time as the CAA

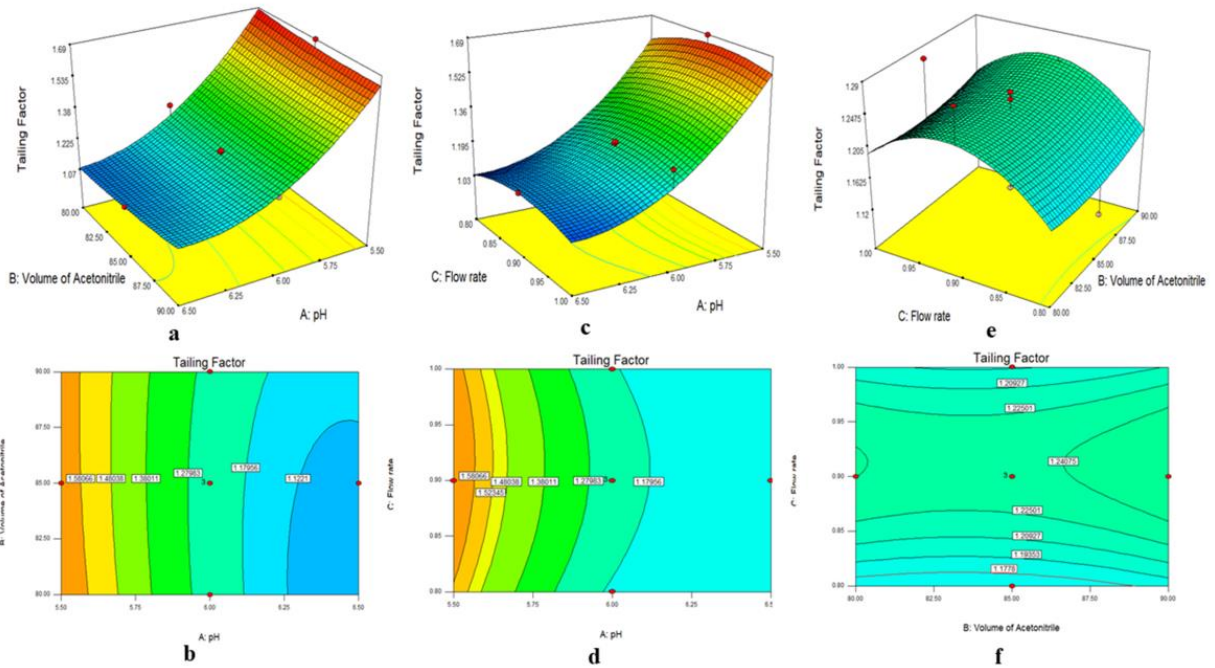


**Figure 3.5.** 3D response surface and 2D contour plots viewing the influence of CMP, viz., pH (A), Volume of acetonitrile (B), and Flow rate (C) on the tailing factor as the CAA

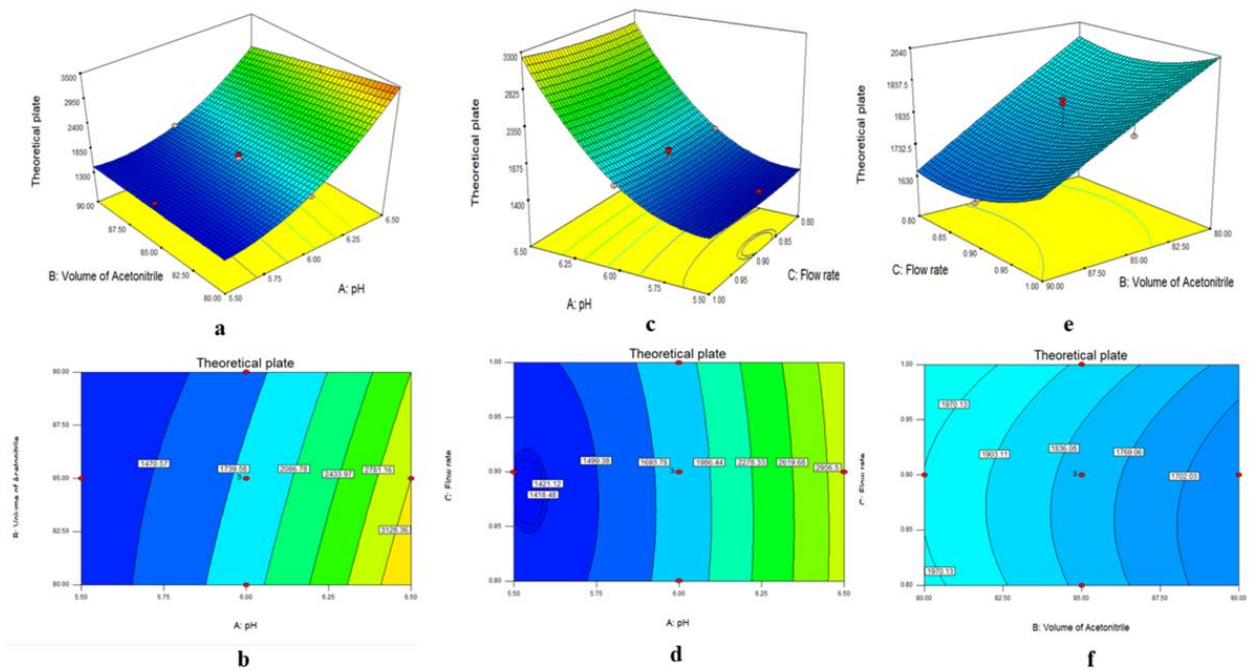


**Figure 3.6.** 3D response surface and 2D contour plots viewing the influence of CMP, viz., pH (A), Volume of acetonitrile (B), and Flow rate (C) on the theoretical plate as the CAA.

**(d) Optimum chromatographic condition**

The search for an optimum chromatographic solution was performed using numerical optimization with different CAAs to acquire the desired goal, i.e., minimization of retention time, peak tailing, and maximization of the theoretical plate desirability function close to 1. The developed RP-HPLC chromatographic optimized method was shown at mobile phase composition comprising the 80:20 v/v ratios of acetonitrile and  $K_2HPO_4$  at pH (6.5), the flow rate of 1 mL/min, which evaluated the desirability value of 4.72 min of retention time, 1.0 tailing factor and 3554 theoretical plates. The overlay plot is shown in Figure 3.7. The blank sample and ABTA containing chromatograms were evaluated using an optimized RP-HPLC method, as shown in Figure 3.8 (a and b).

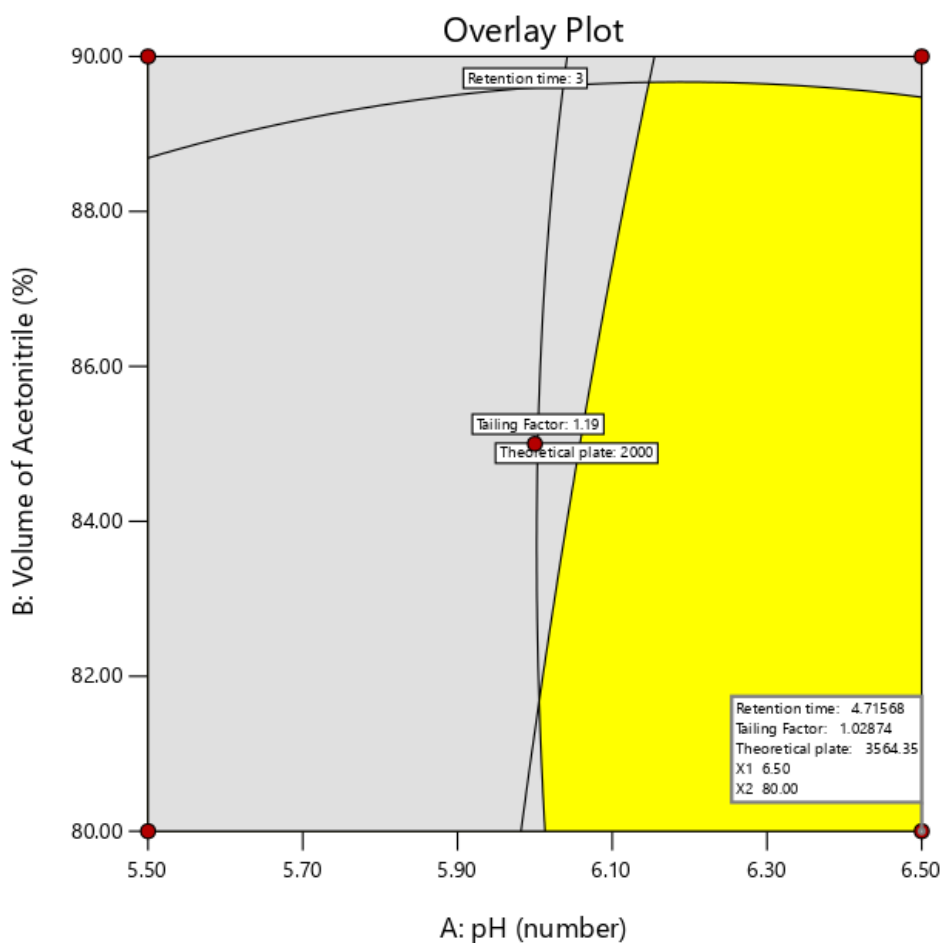


**Figure 3.7.** Overlay plot illustrating the optimal analytical design space

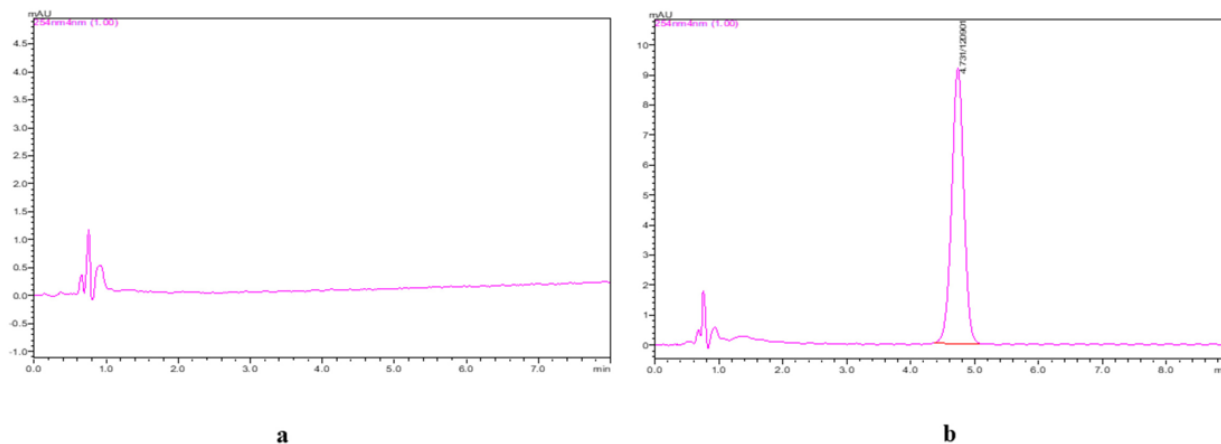


**Figure 3.8.** (a) Chromatogram of the blank sample, (b) Chromatogram of ABTA

### 3.6.3. Analytical method validation

#### (a) Linearity and range

The calibration curve of ABTA plotted in the given concentration range of 0.5-10  $\mu\text{g/mL}$  showed good linearity with a high value of the correlation of coefficient ( $r^2 = 0.9998$ ). The data shows that all results occurred under the specified acceptance criteria, representing the high degree of closeness between the experimental and observed data.

#### (b) Accuracy

Accuracy describes the closeness of the agreement to the actual value. The data presented in Table 3.10 outline the accuracy data for the various QC samples of ABTA, showing the percent mean recovery data from 100 % and 101%, with % RSD less than 2%.

**Table 3.10.** Accuracy results of the developed HPLC method

Concentration ( $\mu\text{g/mL}$ )	Amount Recovered ( $\mu\text{g/mL}$ ) $\pm$ SD	% RSD	Mean % Recovery $\pm$ SD	Accuracy (% Bias)
LQC (0.75 $\mu\text{g/mL}$ )	0.756 $\pm$ 0.009	1.19	101 $\pm$ 1.13	0.80
MQC (3.5 $\mu\text{g/mL}$ )	3.51 $\pm$ 0.030	0.857	100 $\pm$ 0.791	0.285
HQC (8.5 $\mu\text{g/mL}$ )	8.63 $\pm$ 0.014	0.166	101 $\pm$ 0.589	1.53

#### (c) Precision

The developed analytical method showed the intra-day and inter-day precision data, designating them as the high value of percent recovery of ABTA ranging from 100 to 101%, with %RSD being less than 2%. The data are presented in Table 3.11 for inter-day and intra-day precision of the



optimized method containing different QC samples of ABTA.

**Table 3.11.** Intra-day repeatability and Inter-day repeatability (% RSD) data of the different QC samples of the developed HPLC method of ABTA

Concentration ( $\mu\text{g/mL}$ )	Intra-day repeatability RSD (%) (n =9)			Inter day Repeatability RSD (%) (n=27)
	Day 1	Day 2	Day 3	
LQC (0.75 $\mu\text{g/mL}$ )	0.366	0.592	0.552	0.479
MQC (3.5 $\mu\text{g/mL}$ )	0.966	1.026	1.343	0.996
HQC (8.5 $\mu\text{g/mL}$ )	0.843	1.092	1.176	0.967

#### (d) LOD and LOQ

The established analytical method of ABTA has LOD and LOQ as 0.0978  $\mu\text{g/mL}$  and 0.3260  $\mu\text{g/mL}$ , respectively.

#### (e) Selectivity

The selectivity was confirmed as no distractive peak from the placebo solution was observed at the retention time of the ABTA. It was indicated the % RSD of a was below 2.0%.

#### (f) Robustness

Robustness was estimated by modifying the various chromatographic conditions, like a change in the mobile phase mixture ratio, flow rate, column temperature, and injection volume. No significant difference was observed between the various CAAs, i.e., tailing factor, retention time, and theoretical plate. The robustness of the developed method has been confirmed by changing the variable conditions, and the observed values are within the acceptance criteria. According to the analytical guidelines, the acceptance criteria for % RSD  $\leq$  2%, theoretical plate number higher than 2000, and tailing factor  $\leq$  2. The robustness data of ABTA are depicted in Table 3.12.

**Table 3.12.** Robustness results of the developed RP-HPLC method of ABTA

Sr.no	Condition	Retention time	Tailing factor	Theoretical plate	% RSD
1.	Standard sample	4.73	1.05	2822	1.49
2.	Flow rate (0.8 mL/min)	5.36	1.24	3216	1.57
3.	Flow rate (0.9 mL/min)	4.96	1.21	2895	1.70
4.	Flow rate (1.2 mL/min)	4.16	1.16	2956	1.48
5.	Mobile phase ratio variation	4.90	1.13	2789	1.46

(82:18)					
6.	Mobile phase ratio variation	4.62	1.26	2870	1.52
(78:22)					
7.	Temperature (25 °C)	4.79	1.08	2956	1.36
8.	Temperature (30 °C)	4.76	1.06	2789	1.48
9.	pH 6.3	4.63	1.06	2787	1.50
10.	pH 6.7	4.80	1.03	2841	1.36

### (g) System suitability

The system suitability observed no significant differences between the various critical analytical attributes, i.e., tailing factor, retention time, and a theoretical plate of the standard solution of ABTA (5 µg/mL) after injecting six times. Furthermore, % RSD ≤ 2 % was observed within the acceptance criteria. The system suitability data of ABTA are presented in Table 3.13.

**Table 3.13.** System suitability of ABTA

Parameter (n =6)	Mean ± SD	% RSD
Peak area	126064 ± 2254	1.79
Retention time	4.73 ± 0.0131	0.277
Theoretical plate	2821 ± 9.43	0.334
Tailing Factor	1.03 ± 0.0168	1.64

### (h) Solution stability

The solution stability studies showed that the standard solution of ABTA was stable at room temperature for 24 h.

### 3.6.4. Forced degradation studies

The degradation studies of ABTA were conducted to determine the stability of the drug under different stress-accelerated conditions such as acidic, basic, H<sub>2</sub>O<sub>2</sub>, and hydrolytic, subjected to heat, humidity, and photolytic conditions. The chromatograms are documented for each degradation, and % recovery was calculated. From the results, it was determined that the drug was stable in oxidation, thermal, photolytic, humidity, and hydrolytic conditions and degraded in acidic and basic conditions. It is observed that the ABTA is not split into ABT in the complete validation process. In acidic and basic degradation conditions, ABTA degraded to ABT (known impurity). The retention time of ABTA is 4.81 min, and the ABT retention time is 2.66 min, as depicted in

the HPLC chromatogram Figure 3.9. The experimental data were presented in Table 3.14, and chromatograms were shown in Figure 3.10 (a to h).

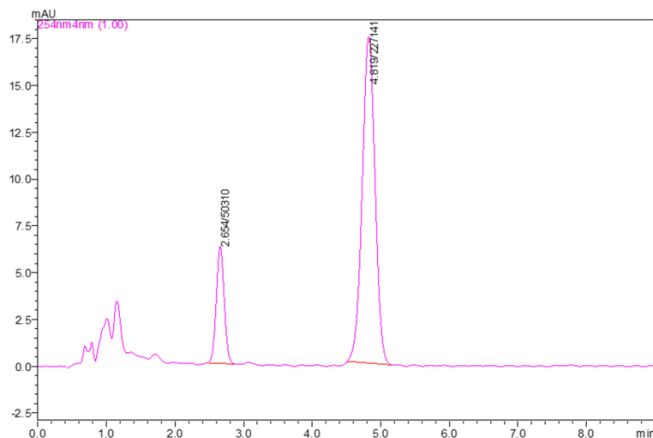


**Figure 3.9.** Chromatograms of ABT and ABTA (10 µg/mL)

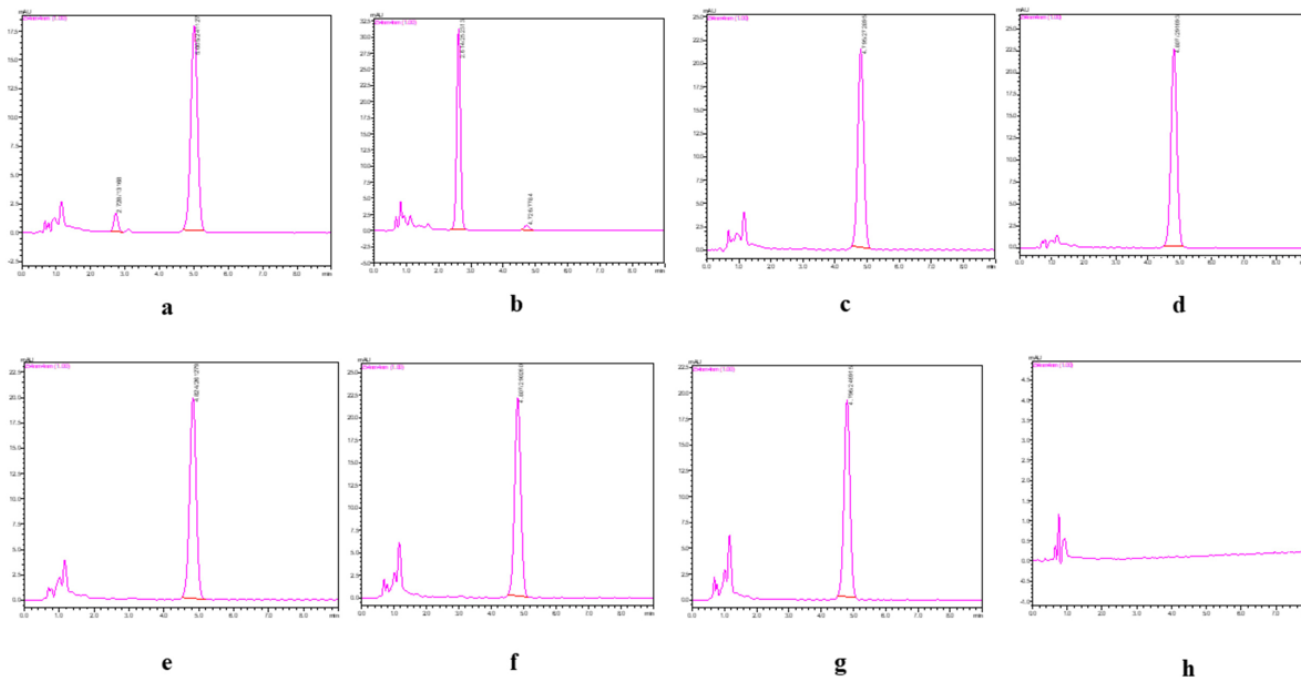


**Figure 3.10.** Chromatogram for the different stress conditions studied under (a) Acidic condition (0.1 N HCl), (b) Basic condition (0.1 N NaOH), (c) Oxidation (30 % H<sub>2</sub>O<sub>2</sub>), (d) Thermal (Hot air oven) (e) U.V. light (f) Humidity (g) Hydrolytic (h) blank sample

**Table 3.14.** Forced degradation study of ABTA

Stress condition	Solvent	Temperature	Sampling time	% Recovery ± SD	% Recovery ± SD
------------------	---------	-------------	---------------	-----------------	-----------------

				(After 12h)	(After 24h)
Blank sample	Diluent	-	-	100.25 ± 0.01	100.49 ± 0.07
Acid Hydrolysis	0.1 N HCl	60 °C	12 h,24 h	83.45 ± 0.41	54.16 ± 0.24
Base Hydrolysis	0.1 N NaOH	60 °C	12 h,24 h	65.75 ± 0.39	35.06 ± 0.45
Thermal degradation	Diluent	60 °C	12 h,24 h	98.34 ± 0.78	95.14 ± 0.87
Oxidative degradation	30% H <sub>2</sub> O <sub>2</sub>	RT	12 h,24 h	95.31 ± 0.58	90.47 ± 0.48
Photolytic degradation	Diluent	UV light	12 h,24 h	89.64 ± 0.38	85.24 ± 0.42
Hydrolytic degradation	Diluent	60 °C	12 h,24 h	99.66 ± 0.58	97.25 ± 0.52
Humidity degradation	Diluent	40°C, 75 %RH	12 h,24 h	99.27 ± 0.45	97.57 ± 0.57

### 3.6.5. Application of the method

Figure 3.11 depicts the chromatogram of ABTA in SD formulation. The given chromatogram indicated no significant alteration occurred in the retention time of ABTA with the nonappearance of unwanted peaks from the urea. This illustrates the selectivity of the developed RP-HPLC method for quantifying ABTA in SD formulation.

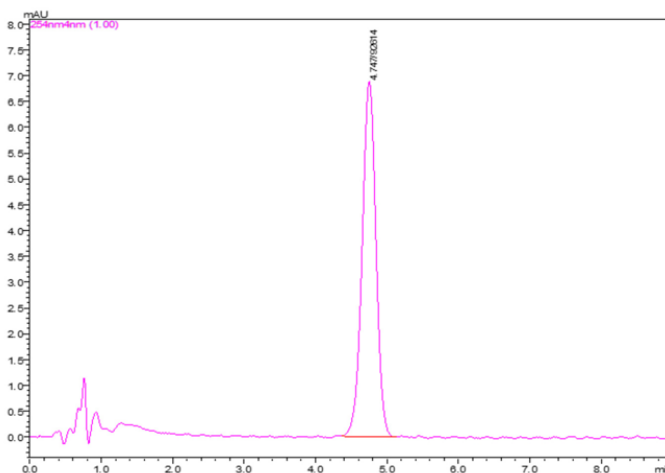


**Figure 3.11.** Chromatograms of ABTA in SD formulations

### 3.7. Chromatographic Bioanalytical methods

ABTA is hydrolyzed in plasma to ABT, the active metabolite. ABT inhibits 17 $\alpha$ -hydroxylase CYP17, an enzyme crucial for androgen biosynthesis, which is expressed in testicular, adrenal, and prostatic tumor tissues. The present study developed a simultaneous RP-HPLC bioanalytical method to quantify both ABTA and ABT. However, due to the rapid hydrolysis, ABTA levels

were often below the quantification limit in most plasma samples. Hence, ABT plasma concentration was determined in most of the reports.

Consequently, only ABT plasma concentrations were reported, aligning with regulatory recommendations to assess pharmacokinetics. While regulatory agencies prefer measuring parent compounds for sensitivity, they accept bioequivalence evaluations based on metabolites for drugs like ABTA, where parent drug detection is challenging. In this study, we devised a concurrent approach for quantifying both ABTA and ABT by assessing the extent of complete hydrolysis from ABTA to ABT within plasma while also checking the parent drug detection.

### 3.7.1. Materials and methods

ABTA has attained a generous gift sample from Biophore India Pharmaceutical Pvt. Ltd. Sodium hydroxide, hydrogen peroxide, hydrochloric acid, and dibasic potassium phosphate ( $K_2HPO_4$ ) were procured from S.D Fine Chemical Pvt. Ltd. The solvents used for the research purpose were of HPLC grade, such as acetonitrile and methanol obtained from Merck. HPLC grade water was obtained from the MiliQ system (Millipore GmbH, Germany) and was used for the analysis. Buffers were adequately filtered through a 0.22 Millipore<sup>TM</sup> membrane filter (Merck, Darmstadt, Germany) and degassed using an ultrasonic bath for 30 min before use.

### 3.7.2. Instrumentation and chromatographic conditions

HPLC-based analysis was conducted on Shimadzu LC-20AC liquid chromatography coupled with a UV-Visible detector. This system is composed of an autosampler, a column oven, and a quaternary gradient pump. Lab solution software was applied for data acquisition, process monitoring, and system control. The separation was conducted on the Hypersil gold C<sub>18</sub> HPLC column (50mm x 4.6mm, particle size 5 $\mu$ m). An isocratic mobile phase consisting of acetonitrile and 10 mM  $K_2HPO_4$  buffer in a ratio of 34:66 (v/v %). The buffer pH was adjusted to 3.0 using orthophosphoric acid. The injection volume was kept at 50 $\mu$ L with a flow rate of 1mL/min, the column temperature was set at 30°C for the analysis, and the analytes were detected at wavelength 254nm.

### 3.7.3. Bioanalytical method development

Before starting the simultaneous bioanalytical method development of ABTA and ABT, firstly synthesize the ABT from the ABTA and characterize by using the FTIR-ATR, <sup>1</sup>H NMR, and mass

spectroscopy

#### **3.7.4. Synthesis of ABT from ABTA**

ABTA (200 mg) was dissolved in a 6 mL methanolic sodium hydroxide solution (153.45 mg) with continuous stirring at room temperature. Monitor the reaction using thin-layer chromatography to confirm the formation of the product. Neutralize the reaction using 4N Hydrochloric acid. A precipitation occurs, filter the product, dry it, and check the TLC. The desired product was confirmed using FTIR-ATR, <sup>1</sup>H NMR, and mass spectroscopy.

#### **3.7.4. Collection of plasma**

The research protocols (Protocol no.417/P.O./be/2001/CPCSEA) received approval from the Institutional Animal Ethical Committee (IAEC) at BITS Pilani before initiating the study. Male Wistar rats, deemed healthy, were sourced from the Central Animal Facility at BITS, Pilani, Rajasthan, India. These rats were housed in standard plastic cages under controlled conditions (maintained at 23 ± 2°C, 60 ± 5% RH, and subjected to a 12-hour light-dark cycle) and provided with standard laboratory pellet food and water ad libitum. Blood samples were collected from the retro-orbital sinus of the male Wistar rats into 2mL polypropylene centrifuge tubes containing 30 µL of a 10% w/v solution of EDTA. Subsequently, the blood-EDTA mixture underwent centrifugation at 8000 rpm for 10 minutes at 4°C. The resulting clear supernatant plasma was pooled into fresh tubes and stored at -20°C until further utilization.

#### **3.7.5. Preparation of standard, stock solution, calibration, and quality control standards**

The primary stock solution of ABTA and ABT was prepared at a concentration of 1000 µg/mL by dissolving the compounds in methanol. This study utilized an internal standard (IS) as itraconazole, with a 200 µg/mL stock solution prepared in methanol. The stock solution of the ABTA, ABT, and IS was stored at 4°C and was found to be stable for one month. The ABTA and ABT standard solutions were diluted to give spiking standard solutions of 2, 2.5, 5, 7.5, 10, 15, 20, 25, 30, 40, 45, and 50 µg/mL, respectively. Calibration samples of ABTA (500, 1000, 1500, 2000, 3000, 3500, 4000, 5000 ng/mL) and ABT (200, 500, 1000, 1500, 2000, 3000, 4000, 5000 ng/mL) were prepared by spiking ABTA and ABT of spiking standard solution into 100 µL rat plasma.

#### **3.7.6. Extraction procedure**

The protein precipitation and liquid-liquid extraction were assessed for the extraction of ABTA

and ABT from rat plasma. Tert-butyl methyl ether (TBME), diethyl ether, chloroform, and ethyl acetate were tried for the liquid-liquid extraction. Furthermore, several water-miscible organic solvents (acetonitrile and methanol) were used in different ratios to extract ABTA and ABT from plasma to assess plasma protein precipitation. The extraction efficiency was assessed by comparing the chromatographic peak areas of non-biological standard samples with the biological plasma samples with spiked drugs at the same concentration level.

### 3.7.7. Sample preparation by protein precipitation techniques

A protein precipitation procedure was used to extract ABTA and ABT from the rat plasma. 85  $\mu\text{L}$  of pooled rat plasma was spiked with 5  $\mu\text{L}$  of ABTA, 5  $\mu\text{L}$  of ABT, and 5  $\mu\text{L}$  of ITZ (20  $\mu\text{g}/\text{mL}$ ) (I.S.). The samples were vortexed for 5 min. Then, 1000  $\mu\text{L}$  of methanol was added to precipitate the protein, followed by centrifugation for 10 min at 14,000 rpm at 4°C. The methanol was separated and placed in a vacuum oven at 40°C until the entire methanol was completely evaporated. The residue was reconstituted in 100  $\mu\text{L}$  of the 80:20 mixtures of methanol and buffer (pH 3.0), followed by vortex mixing and centrifugations (10,000 rpm, 10min). A 0.22  $\mu\text{m}$  nylon syringe filter was used to filter the supernatant, and 50  $\mu\text{L}$  of the resultant solution was injected into the HPLC system.

### 3.7.8. Method validation parameters

The method was validated for linearity, specificity, accuracy, precision (both intraday and interday), and stability in accordance with bioanalytical method validation. The calibration samples were freshly prepared and analyzed in triplicates on three consecutive days. Linearity of the calibration curve was obtained by plotting the peak area ratio (area of ABTA/ area of IS or area of ABT/ area of IS) for plasma and a peak area for tissues against the corresponding concentration of ABTA and ABT. Selectivity, which assesses the method for any interferences from the sample matrix, endogenous substance, degradants, and sample blanks due to reagents added during the sample processing, was investigated by processing six independent sources of the rat plasma and analyzing them with the proposed method. Quality control (QC) standards of ABTA were independently prepared at the following concentration levels: Lower limit of quantification (LLOQ = 500 ng/mL), LQC = 750  $\mu\text{g}/\text{mL}$ , MQC= 2500 ng/mL, and HQC=4500 ng/mL concentration levels. Furthermore, QC standards of ABT were independently prepared at the LLOQ = 200 ng/mL, LQC = 750  $\mu\text{g}/\text{mL}$ , MQC= 2500 ng/mL, and HQC= 4500 ng/mL concentration levels. Accuracy,

recovery, and precision (interday and intraday) were determined on QC standards of ABTA (500, 750, 2500, and 4500 ng/mL) and ABT (200, 750, 2500, and 4500 ng/mL) prepared freshly in five replicates on three consecutive days. Precision was calculated as % RSD, and accuracy was expressed as % bias, the percent deviation from the nominal value.

### 3.8. Results and Discussion

#### 3.8.1. Synthesis of ABT from ABTA

ABTA undergoes hydrolysis in the basic medium. This reaction involves breaking the ester bond in ABTA to yield ABT and acetic acid. The hydrolysis reaction typically occurs in the presence of a base, such as sodium hydroxide (NaOH). This basic medium helps to facilitate the hydrolysis of the ester bond. The synthesized ABT should be characterized to confirm its identity using analytical techniques such as ATR-FTIR, NMR (nuclear magnetic resonance), and HRMS. The ATR-FTIR spectrum of the ABTA showed a major peak at  $1730\text{ cm}^{-1}$  (indicating C=O stretching) and  $1239\text{ cm}^{-1}$  (indicating C-O stretching). Conversely, the spectrum of ABT exhibited a prominent peak at  $3342\text{ cm}^{-1}$ , corresponding to OH-stretching, while the characteristic peaks for C=O stretching and C-O stretching, as seen in Figure 3.12, were absent. Despite this, it was confirmed that the ester prodrug of ABTA had effectively undergone conversion to ABT.

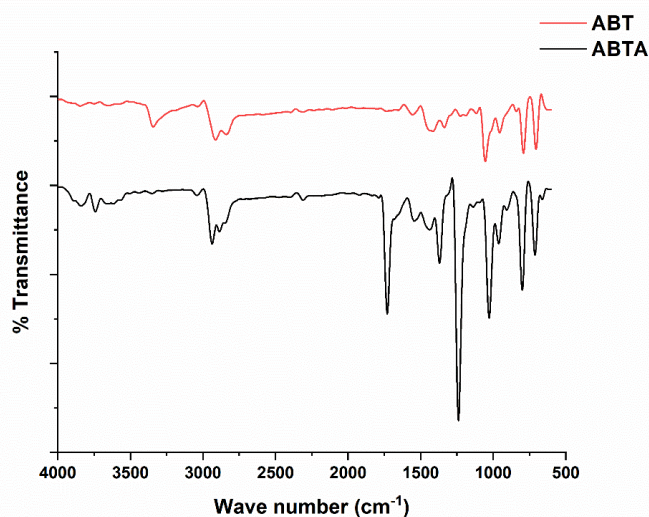


**Figure 3.12.** FTIR-ATR spectrum of ABTA and ABT

In  $^1\text{H}$  NMR, all the characteristic peak was observed in ABT compared with the ABTA; only one group disappeared in the case of ABT (1-2 ppm shift) due to the absence of proton H in the acetate group, shown in Figure 3.13. It was concluded that ester prodrug ABTA was successfully converted to ABT. Figure 3.14 shows the HRMS spectrum of the synthesized ABT, which



confirms the formation of ABT from ABTA.

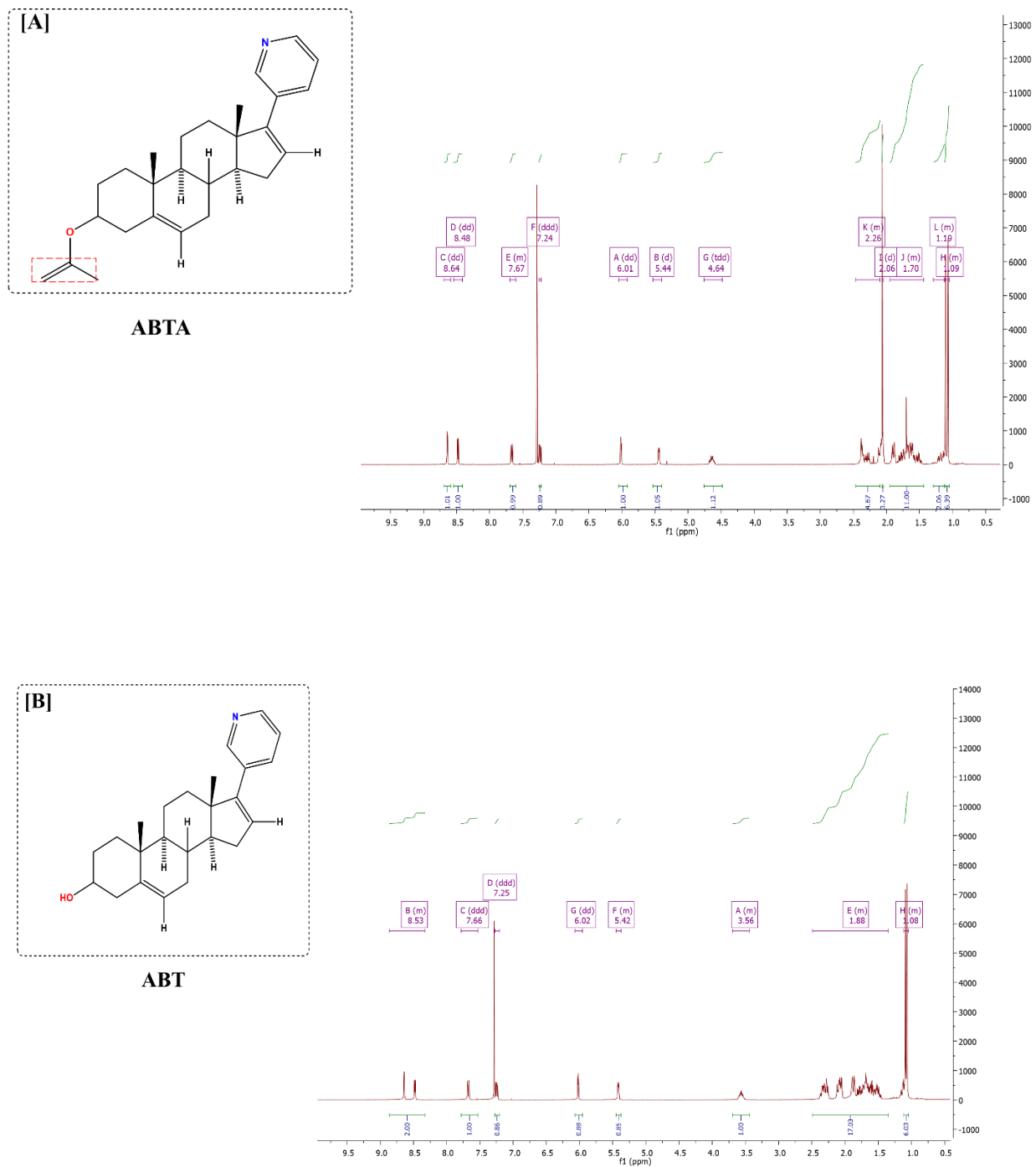


**Figure 3.13.** [A]  $^1\text{H}$  NMR spectrum of the ABTA [B]  $^1\text{H}$  NMR spectrum of the synthesized ABT

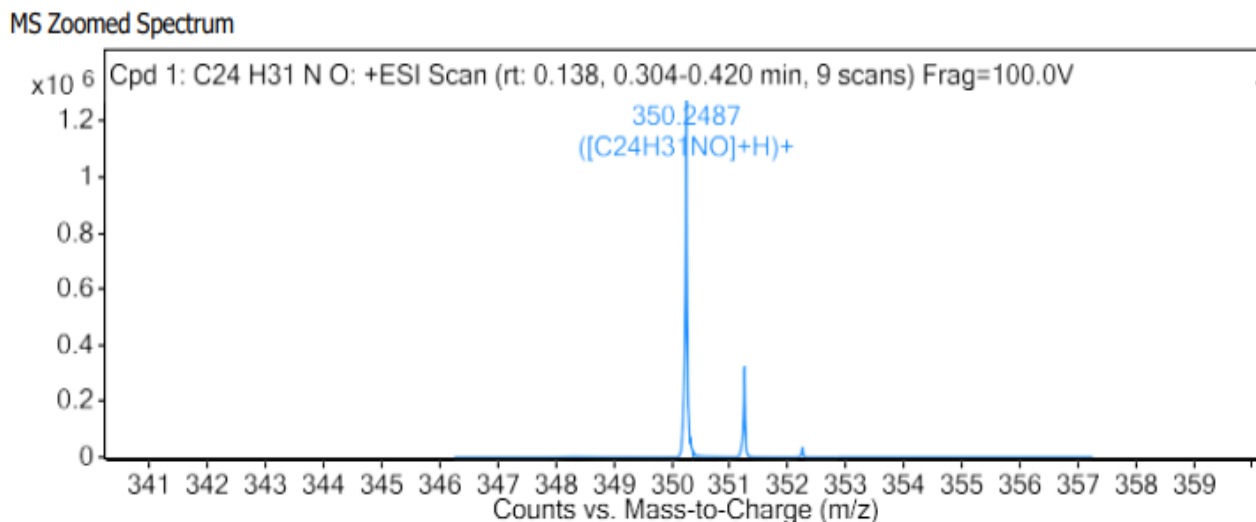


**Figure 3.14.** HR-MS spectrum of the synthesized ABT

### 3.8.2. Bioanalytical method development

#### 3.8.2.1. Optimization of the Chromatographic conditions

The analytical method development involved assessing various chromatographic settings to determine the optimal mobile phase composition, column selection, flow rate, and injection volume for accurately measuring ABTA and ABT levels in rat plasma. The chromatographic settings were optimized using information obtained throughout the development of the analytical method. Using a Hypersil gold C<sub>18</sub> HPLC column (50mm x 4.6mm, particle size 5µm), the mobile phase mixture was comprised of acetonitrile and 0.01mM K<sub>2</sub>HPO<sub>4</sub> buffer (pH 3.0) in a ratio of 34:66 (v/v %), 1mL/min flow rate, 50 µL injection volume, and 30°C column temperature was the final optimized separation techniques for the quantification of ABT, and ABTA. The retention times for the ABT, ABTA, and IS were 6.21 min, 27.73 min, and 14.2 min, respectively, with a total run duration of 32 min. A typical chromatogram of blank plasma and ABTA, ABT, and IS are shown in Figure 3.15[A] and Figure 3.15 [B].

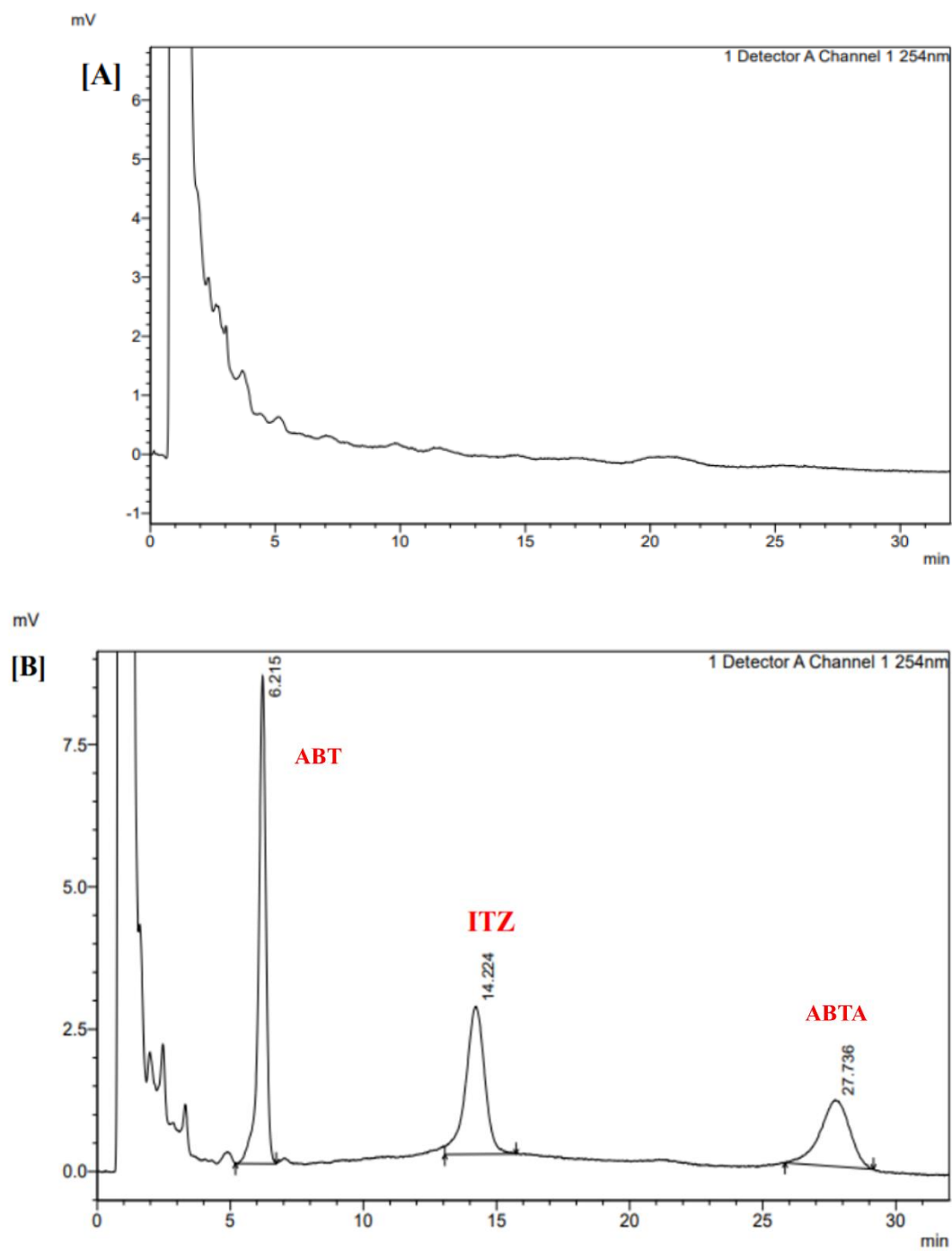


**Figure 3.15.** Typical chromatogram of [A] Blank rat Plasma [B] blank rat plasma spiked with ABT, ABTA, and ITZ

### 3.8.2.2. Optimization of sample preparation method

Cleaning the plasma sample is a critical aspect of bioanalytical method development, as it directly impacts the sensitivity and selectivity of the method. The recovery of a predetermined analyte concentration after employing sample extraction methods is termed the extraction efficiency of the analytical process. Enhanced extraction efficiency leads to a more accurate procedure. Among the various techniques utilized for drug extraction, the protein precipitation method yields the highest recovery rates. Figure 3.15 shows the extraction efficiency of ABT and ABTA in different organic solvents.

**Table 3.15.** Extraction efficiency of the ABT and ABTA in different organic solvents

Solvent	Quantity of solvent ( $\mu\text{L}$ )	Vortex time (min)	Centrifugation (Speed (rpm), time (min))	% Recovery ABT	% Recovery ABTA
<b>Protein precipitation extraction</b>					
<b>Methanol</b>	1000	5	10,000, 10	82 %	79 %
<b>Acetonitrile</b>	1000	5	10,000, 10	75 %	72 %
<b>Liquid-Liquid extraction</b>					
<b>Diethyl ether</b>	1000	5	10,000, 10	24 %	10 %
<b>TBME</b>	1000	5	10,000, 10	17 %	12 %
<b>Ethyl acetate</b>	1000	5	10,000, 10	61 %	52 %
<b>Chloroform</b>	1000	5	10,000, 10	18 %	10 %

### 3.8.2.3. Method validation parameters

The peak area ratios of ABT to IS at different concentrations in plasma were plotted to generate a calibration curve that exhibited linearity in the concentration range of 200-5000 ng/mL with high regression coefficient of 0.9991, indicating good reproducibility. Furthermore, The peak area ratios of ABTA to IS at different concentrations in plasma were plotted to generate a calibration curve that exhibited linearity in the concentration range of 500-5000 ng/mL with high regression coefficient of 0.9927. Figure 3.16 illustrates the linear regression calibration curve of both ABT and ABTA. Table 3.16 displays the regression data for the calibration curve of ABT and ABTA.

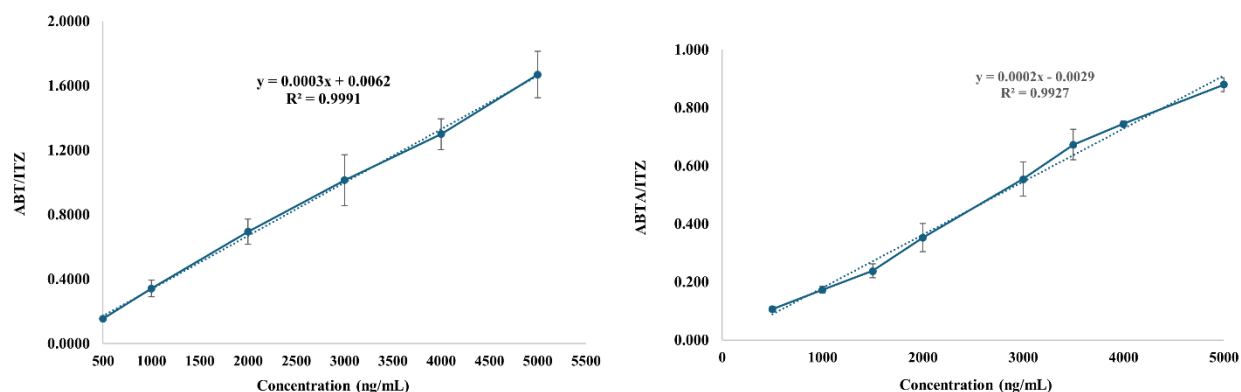


**Figure 3.16.** Linear regression calibration curve of ABT and ABTA

**Table 3.16.** Linear regression data for the calibration curve of ABT and ABTA in rat plasma (n=6).

Parameters	ABT	ABTA
Range (ng/mL)	200-5000	500-5000
Correlation coefficient	0.9991	0.9927
Slope	0.0003	0.0002
Intercept	0.0062	-0.0029
LLOQ (ng/mL)	200	500

Tables 3.17 and 3.18 list the QC values of LQC, MQC, and HQC, including the LLOQ, for interday and intraday precision and accuracy. All the values for these QC samples were found to be within the acceptable range, thus rendering the method suitable for the quantification of ABT and ABTA in the biological matrices shown in Table 3.17 and 3.18 (% RSD  $\leq \pm 15\%$  at LQC, MQC, and HQC while,  $\leq \pm 20$  for LLOQ)

**Table 3.17:** Precision (% RSD) and accuracy (% bias) of the ABT in the rat plasma samples at QC concentrations of the calibration ranges

Level	Nominal Conc. (ng/mL)	Inter-day			
		Measured concentration Mean $\pm$ SD	% Accuracy	Precision % RSD	Accuracy % bias
LLOQ	200	200.96 $\pm$ 14.86	100.48 $\pm$ 7.43	7.40	0.48
LQC	750	756.80 $\pm$ 12.79	100.91 $\pm$ 1.70	1.69	0.90

Level	Nominal Conc. (ng/mL)	Measured concentration Mean $\pm$ SD	% Accuracy	Precision % RSD	Accuracy % bias
MQC	2500	2576.45 $\pm$ 56.68	103.06 $\pm$ 2.26	2.20	3.05
HQC	4500	4552.24 $\pm$ 247.20	101.16 $\pm$ 5.49	5.43	1.16
<b>LLOQ</b>	200	201.19 $\pm$ 28.72	100.6 $\pm$ 14.36	14.28	0.59
<b>LQC</b>	750	758.50 $\pm$ 31.83	101.13 $\pm$ 4.24	4.20	1.13
<b>MQC</b>	2500	2559.40 $\pm$ 231.38	102.38 $\pm$ 9.25	9.04	2.38
<b>HQC</b>	4500	4569.67 $\pm$ 226.39	101.55 $\pm$ 5.03	4.95	1.54

**Table 3.18.** Precision (% RSD) and accuracy (% bias) of the ABTA in the rat plasma samples at QC concentrations of the calibration ranges

Level	Nominal Conc. (ng/mL)	Measured concentration Mean $\pm$ SD	% Accuracy	Precision % RSD	Accuracy % bias
<b>LLOQ</b>	500	494.07 $\pm$ 38.45	98.81 $\pm$ 7.68	7.78	-1.18
<b>LQC</b>	750	748.86 $\pm$ 28.10	99.85 $\pm$ 3.74	3.75	-0.15
<b>MQC</b>	2500	2508.57 $\pm$ 159.33	100.34 $\pm$ 6.37	6.35	0.34
<b>HQC</b>	4500	4523.17 $\pm$ 252.13	100.51 $\pm$ 5.60	5.57	0.51
<b>LLOQ</b>	500	492.19 $\pm$ 43.85	98.44 $\pm$ 8.76	8.91	-1.56
<b>LQC</b>	750	732.12 $\pm$ 100.78	97.62 $\pm$ 13.43	13.77	-2.38
<b>MQC</b>	2500	2566.48 $\pm$ 172.82	102.66 $\pm$ 6.91	6.73	2.66
<b>HQC</b>	4500	4564.64 $\pm$ 461.43	101.44 $\pm$ 10.25	10.11	1.43

### 3.9. Conclusions

A sensitive simultaneous bioanalytical was developed to quantify ABT and ABTA in rat plasma at 200 ng/mL and 500 ng/mL. It could be successfully utilized in pharmacokinetic studies to quantify ABT and ABTA in rat plasma.

### References

1. Annapurna MM, Pradhan DP, Chaitanya RK. New Spectrophotometric Techniques for the determination of Abiraterone acetate (A Steroidal Inhibitor) in Tablets. *Journal of Chemical and Pharmaceutical Science*. 2017;10(2):768–770.
2. Chandra Reddy BJ, Sarada NC. Development and validation of a novel RP-HPLC method for stability-indicating assay of Abiraterone acetate. *Journal of Liquid Chromatography*

- Related Technologies. 2016;39(7):354–363.
3. Martins V, Asad Y, Wilsher N, Raynaud F. A validated liquid chromatographic-tandem mass spectroscopy method for the quantification of abiraterone acetate and abiraterone in human plasma. *Journal of Chromatography B*. 2006;843(2):262–267.
  4. Belleville T, Noé G, Huillard O, Thomas-Schoemann A, Vidal M, Goldwasser F, et al. A HPLC-fluorescence method for the quantification of abiraterone in plasma from patients with metastatic castration-resistant prostate cancer. *Journal of Chromatography B*. 2015;989:86–90.
  5. Fukuda IM, Pinto CFF, Moreira CDS, Saviano AM, Lourenço FR. Design of experiments (DOE) applied to pharmaceutical and analytical quality by design (QbD). *Brazilian Journal of Pharmaceutical Sciences*. 2018;54:1–16.
  6. Peraman R, Bhadraya K, Reddy YP. Analytical Quality by Design: A Tool for Regulatory Flexibility and Robust Analytics. *International Journal Analytical Chemistry*. 2015.
  7. Jadhav ML, Tambe SR. Implementation of QbD Approach to the Analytical Method Development and Validation for the Estimation of Propafenone Hydrochloride in Tablet Dosage Form. *Chromatography Research International*. 2013;1–9.
  8. Singh B, Kumar R, Ahuja N. Optimizing drug delivery systems using systematic “design of experiments.” Part I: Fundamental aspects. *Critical Reviews in Therapeutic Drug Carrier Systeme*. 2005;22(1):27–105.
  9. Politis SN, Colombo P, Colombo G, Rekkas DM. Design of experiments (DoE) in pharmaceutical development. *Drug Development and Industrial Pharmacy*. 2017;43(6):889–901.
  10. Jain A, Sharma T, Sharma G, Khurana RK, Katare OP, Singh B. QbD-Driven Analytical Method Development and Validation for Raloxifene Hydrochloride in Pure Drug and Solid Oral Dosage Form. *Analytical Chemistry Letters*. 2019;9(4):463–477.
  11. Pradhan R, Krishna K V., Wadhwa G, Taliyan R, Khadgawat R, Kachhawa G, et al. QbD-driven development and validation of HPLC method for determination of Bisphenol A and Bis-sulphone in environmental samples. *International Journal of Environmental Analytical Chemistry*. 2020;100(1):42–54.
  12. Technical Requirements for Registration of Pharmaceuticals for Human Use: The ICH Process. 2013:447–460.

13. Bhatt D, Thatavarthi P, Rajkamal B. Analytical Method Development and Validation for the Estimation of Canagliflozin in Bulk and Formulation by RP- HPLC. *International Journal of Pharmaceutical Sciences and Drug Research*. 2018;10(03):139–143.
14. Kumar PA, Thirupathi D, Kumar YR, Jayashree A. Simultaneous determination of related organic impurities of Ibuprofen and Paracetamol in combination solid dosage form by Rp-HPLC with Qbd approach. *Oriental Journal of Chemistry*. 2017;33(3):1461–1468.
15. Shantanu Damle, Manisha Choudhari Gautam Singhvi, Ranendra Narayan Saha SKD. Development and Validation of Reverse-Phase High-Performance Liquid Chromatography Method for Estimation of Itraconazole through Hydroxypropyl Methylcellulose Acetate Succinate based Polymeric Films using Quality by Design principles. 2021.
16. Krishna KV, Saha RN, Singhvi G, Dubey SK. Pre-clinical pharmacokinetic-pharmacodynamic modelling and biodistribution studies of donepezil hydrochloride by a validated HPLC method. *RSC Advances*. 2018;8(44):24740–24749.
17. Rignall A. ICHQ1A(R2) Stability Testing of New Drug Substance and Product and ICHQ1C Stability Testing of New Dosage Forms. *ICH Guidelines*. 2017;3–44.
18. Blessy M, Patel RD, Prajapati PN, Agrawal YK. Development of forced degradation and stability indicating studies of drugs—A review. *Journal of Pharmaceutical Analysis*. 2014;4(3):159–165.



# **Chapter 4: Preformulation Studies**

### 4.0. Introduction

Drug discovery and development is an expensive process, so it is necessary to characterize the drug molecules in depth to successfully develop an economic and commercially viable product with the desired quality, safety, and efficacy. Preformulation is a group of studies that focus on the physicochemical properties of a drug candidate alone and in combination with excipients that could affect the development of a dosage form and the drug performance. This preformulation study provides important information for formulation design. Preformulation reduces the development time and cost considerably and reduces the possible challenges during formulation development (1). The objective of the pre-formulation study is to develop an elegant, stable, effective, and safe dosage form by establishing the physicochemical parameters of drug substances, a kinetic rate profile, compatibility with the other ingredients, and identifying the possible risk for the drug and formulation. Among these properties, drug solubility in various solvents and buffers, partition coefficient, dissolution rate, polymorphic forms, and stability in both solid and solution states play important roles in formulating stability and efficacy. ABTA is an anticancer drug for the treatment of metastatic castration-resistant prostate cancer. As our research objectives involve the formulations of SD for ABTA appropriate studies can provide information about the drug candidates and help in designing the SD undertaken.

### 4.1. Experimental

#### 4.1.1. Materials and methods

ABTA (purity 99%) was generously gifted by Biophore India Pharmaceuticals Pvt. Ltd, India. HPMCAS 716, HPMCAS 912, and Startab were supplied as gift samples from Colorcon Asia Pvt. Ltd, India. Soya lecithin and sodium taurocholate were procured from the SRL. Mannitol and citric acid were purchased from Himedia. Lactose monohydrate and Colloidal silicon dioxide were supplied from Lubrizol. Magnesium stearate was procured from CDH. Analytical grade HPLC solvents such as acetone, methanol, dichloromethane, and acetonitrile were procured from Merck. All other necessary chemicals were purchased from standard companies.

#### 4.1.2. Instruments and equipment

Digital analytical balance (Mettler-Toledo) was used for all the weighing. An orbital shaker incubator (MAC instrument, India), vortex mixer (Spinix India), and Remi cooling centrifuge were used for the solubility studies in different buffers and solvents. All pH measurements were

conducted using a portable pH meter (Eutech) after calibrations. Characterization and drug-excipient compatibility studies were carried out using Attenuated total reflectance -Fourier Transform Infrared (ATR-FTIR) Spectroscopy (Bruker, USA; with Opus software), Differential Scanning Calorimetry (DSC-60 with 60WS thermal analyzer; integrating software: TA -60WS collection monitor, ver1.51; analysis software: TA-60; Shimadzu Japan), Thermal gravimetric analysis (TGA; Shimadzu TA 60 instrument operated with TA 60 software) Powder X-ray diffraction (PXRD; Rigaku mini flex II diffractometer), ultra-violet visible spectrophotometer (Jasco, Model V-750) is connected to a computer loaded with spectra manager (version 2) software, HPLC (Shimadzu LC-20AC liquid chromatography coupled with a photodiode array detector) was used.

### **4.1.3. Buffers Compositions**

#### **pH 1.2**

To prepare a hydrochloric acid buffer solution with a pH of 1.2, 8.5 mL of concentrated hydrochloric acid (approximately 37% w/w) was measured. The measured acid was then poured into a 1000 mL volumetric flask containing about 900 mL of distilled water. The solution was mixed thoroughly to ensure even distribution. Finally, the solution was diluted to the final volume of 1000 mL with distilled water and mixed again to achieve a uniform solution.

#### **pH 4.5**

56.5 mM of monobasic sodium phosphate was dissolved in water. The pH was adjusted to 4 using 5 N sodium hydroxide or phosphoric acid (2).

#### **pH 6.8**

Disodium hydrogen phosphate (28.20 g) and potassium dihydrogen phosphate (11.45 g) were dissolved in sufficient water to produce a final volume of 1000 mL.

### **Biorelevant media**

#### **Fasted state simulated intestinal fluid (FaSSIF, pH 6.5)**

3.43 gm of sodium dihydrogen phosphate and 6.18 gm of sodium chloride were dissolved in 1000 mL of water. Then, 1.54 gm of sodium taurocholate was added to the mixture. Separately, 482.92 mg of lecithin was dissolved in 4 mL of dichloromethane and then added to the mixture. The resulting emulsion was turbid and yellow in color. This emulsion was kept on a magnetic stirrer overnight to remove traces of methylene chloride. The pH was then adjusted to 6.5 with 1N NaOH (3).

### **Fed state simulated intestinal fluid (FeSSIF, pH 5.0)**

11.87 gm of sodium chloride was dissolved in 1000 mL of water. Then, 8.65 gm of acetic acid was added to the mixture. Following this, 8.25 gm of sodium taurocholate was incorporated into the solution. Separately, 2.41 gm of lecithin was dissolved in 10 mL of dichloromethane and then added to the mixture. The resulting emulsion was turbid and yellow in color. This emulsion was kept on a magnetic stirrer overnight to remove traces of methylene chloride. Finally, the pH was adjusted to 5.0 with 1N NaOH (3).

### **4.1.4. Bulk Characterization**

ABTA was visually observed for physical characterization, such as color. Further identification of ABTA was conducted by using the ATR-FTIR and UV spectrum, DSC and TGA thermogram and PXRD pattern were also generated.

Dissolving 10 mg of the ABTA in 100 mL of buffer medium resulted in a stock solution with a concentration of ABTA (100  $\mu\text{g/mL}$ ), which was analyzed by UV spectrophotometric method. To prepare different concentrations, aliquots of this stock solution were transferred into a series of 10 mL volumetric flasks, and each flask was filled to the mark with the respective media. The UV Spectrum of the ABTA was recorded (4).

The free ABTA spectrum was recorded using ATR-FTIR spectroscopy (Bruker, USA) operated with Opus software. The spectra were collected in the region from 400-4000  $\text{cm}^{-1}$  with a 1  $\text{cm}^{-1}$  resolution and averaged over 100 scans.

Thermal analysis by DSC was conducted by taking 2-3 mg of ABTA placed in a perforated aluminum crucible and an empty pan as a reference for the measurement. The sample was then heated from 30 to 250  $^{\circ}\text{C}$  at 10  $^{\circ}\text{C}/\text{min}$  under a nitrogen atmosphere with a 50 mL/min flow rate.

PXRD testing of ABTA was performed using a Rigaku mini flex II diffractometer with incident radiation of Cu K $\alpha$  produced at 40 kV and 30 mA, applying a scanning rate of 2 $^{\circ}/\text{min}$  with a 2  $\Theta$  range of 10-60 $^{\circ}$ .

TGA analysis was conducted by weighing between 8-10 mg of ABTA, loaded into platinum crucibles, and subjected to heating from 30 to 400  $^{\circ}\text{C}$  at a rate of 10  $^{\circ}\text{C}/\text{min}$  under a nitrogen atmosphere with a flow rate of 50 mL/min.

### 4.1.4. Solubility studies

The solubility of ABTA in various buffers and solvents was determined by using the shake flask method. Excessive quantities of free ABTA were introduced into vials containing various buffers, i.e., water, 0.1N HCl (pH 1.2), pH 6.8 (phosphate buffer), and biorelevant media such as fasted-state simulated intestinal fluid (FaSSIF, pH 6.5), and fed-state simulated intestinal fluid (FeSSIF, pH 5.0) and solvents such as DMSO, acetonitrile, methanol, acetone, isopropyl alcohol, ethyl acetate, chloroform, dichloromethane for the solubility studies. These vials were then placed on an orbital shaker and continuously stirred for 8h at a controlled temperature of  $37 \pm 0.5^{\circ}\text{C}$ , allowing equilibrium to be reached. At different time points up to 8h, samples were centrifuged, and precise aliquots of the supernatant samples were collected, filtered, and subsequently subjected to analysis using RP-HPLC.

### 4.1.5. Stability studies

Solution state stability study was evaluated in the water, 0.1 N HCl, pH 4.5, pH 6.8, FaSSIF and FeSSIF. A known concentration of ABTA (10  $\mu\text{g}/\text{mL}$ ) in different media and the solution kept at room temperature and freeze conditions in 10mL volumetric flasks in triplicate. At different time intervals (0, 1h, 2h, 3h, 4h, 5h, 6h, 8h, 10h, and 12h), samples were withdrawn and analyzed using the developed RP-HPLC method, which was described in Chapter 3. The % log drug remaining to be degraded was plotted against time, and the degradation rate constant was determined.

### 4.1.6. Drug-excipient computability studies

In these studies, ABTA was admixed with various potential excipients HPMCAS 716, HPMCAS 912, HPMC HME 15LV, HPMC HME 100LV, and lactose monohydrate for the SD formulation. The binary mixture was prepared in a 1:1 ratio by geometric mixing and stored at room temperature for 1 month. The samples were analyzed by DSC and FTIR immediately after the preparation of this mixture. After 1 month, the same sample was analyzed by DSC and PXRD, FTIR to evaluate any compatibility issues between the drug and excipients. Furthermore, the mixtures were evaluated for any physical changes, such as color and formation of a lump.

## 4.2. Results and Discussions

### 4.2.1. Bulk Characterization

ABTA appears as an off-white odorless crystalline powder. The free ABTA displayed the

absorption bands with maxima at  $\lambda$  of 236 nm in the UV spectrum for a concentration of 10  $\mu\text{g/mL}$  in 100 mM hydrochloric acid medium (pH 1.2), shown in Figure 7.1. Similar results have been reported in the literature (4).

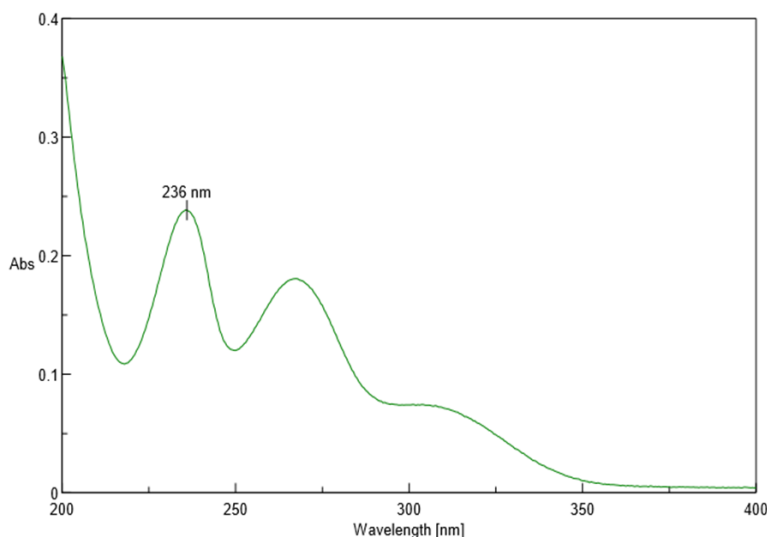


**Figure 4.1.** UV absorption spectrum of ABTA

In the DSC thermogram of free ABTA powder (Figure 4.2 A), a distinct endothermic peak was detected at 147.16 °C, closely aligning with the reported melting point of ABTA at 147 °C, thus confirming its crystalline nature (5). Figure 4.2 [B] illustrates characteristic absorption bands of crystalline ABTA at 2935.68  $\text{cm}^{-1}$ , 1731  $\text{cm}^{-1}$ , 1533  $\text{cm}^{-1}$ , and 1240  $\text{cm}^{-1}$ , corresponding to aromatic C-H stretching, C=O stretching, C=N stretching (pyridine ring vibration), and C-O stretching, respectively, further confirming the identification of ABTA (6). In PXRD analysis, free ABTA powder exhibited distinct peaks at 12.1°, 14.9°, 15.2°, 16.05°, 18.4°, 19.07°, and 21.8° (Figure 4.2 [C]), indicating its crystalline structure (7). The TGA thermogram of ABTA (Figure 4.2 [D]) revealed its thermal stability up to 300 °C (8).

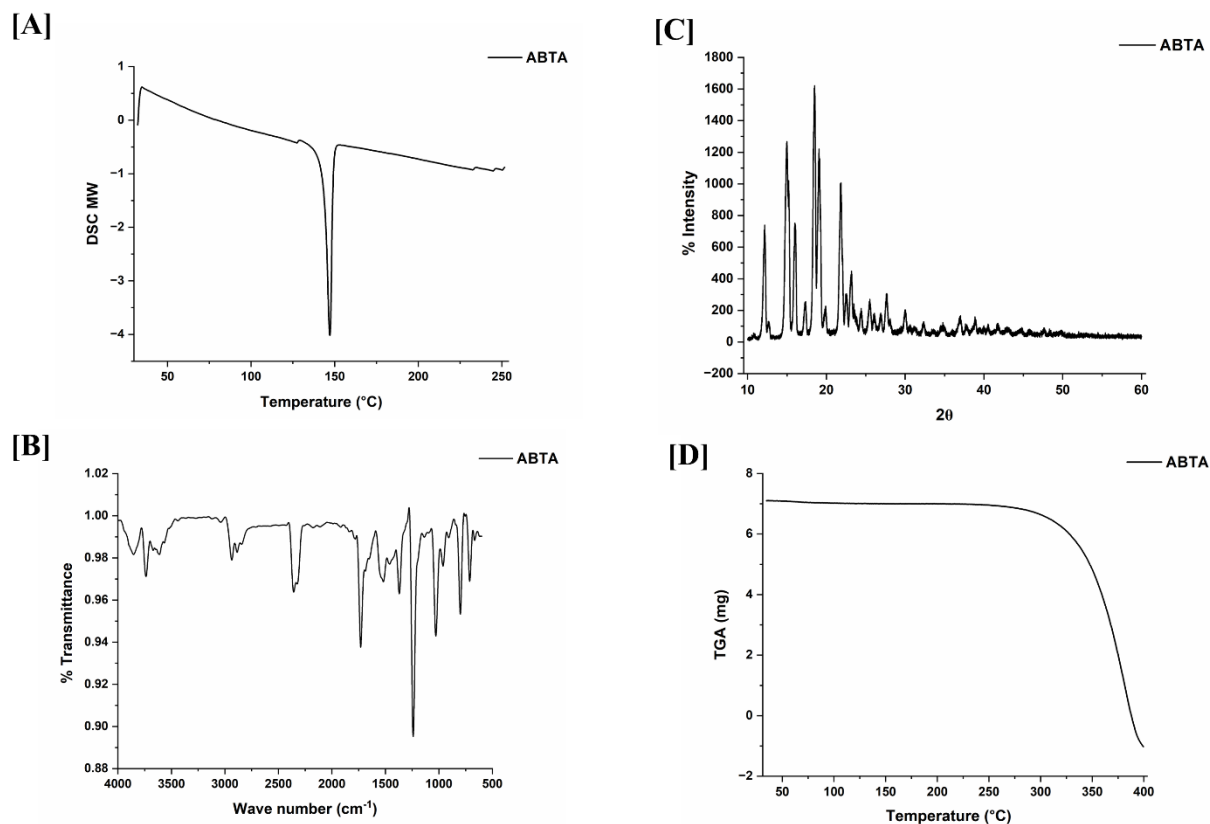


**Figure 4.2.** [A] DSC thermogram; [B] ATR-FTIR spectrum; [C] PXRD pattern; [D] TGA thermogram of ABTA

### 4.2.3. Solubility studies

ABTA, being a weak base with aromatic nitrogen and a pKa of 5.19, exhibits pH-dependent solubility, as shown in Figure 4.3 (7). Its solubility in pH 1.2 and pH 6.8 phosphate buffer was found to be 136.70  $\mu\text{g/mL}$ , and 0.512  $\mu\text{g/mL}$ , respectively. In water, ABTA solubility was approximately 1.012  $\mu\text{g/mL}$ . With its lipophilic nature, ABTA solubility was determined in biorelevant media with lipophilic environments like FaSSIF and FeSSIF, resulting in approximately 5.07  $\mu\text{g/mL}$  and 82.2  $\mu\text{g/mL}$ , respectively. Most organic solvents, including dichloromethane, chloroform, ethyl acetate, isopropyl alcohol, and acetone, exhibited higher solubility (more than 360  $\text{mg/mL}$ ), as illustrated in Figure 4.4.

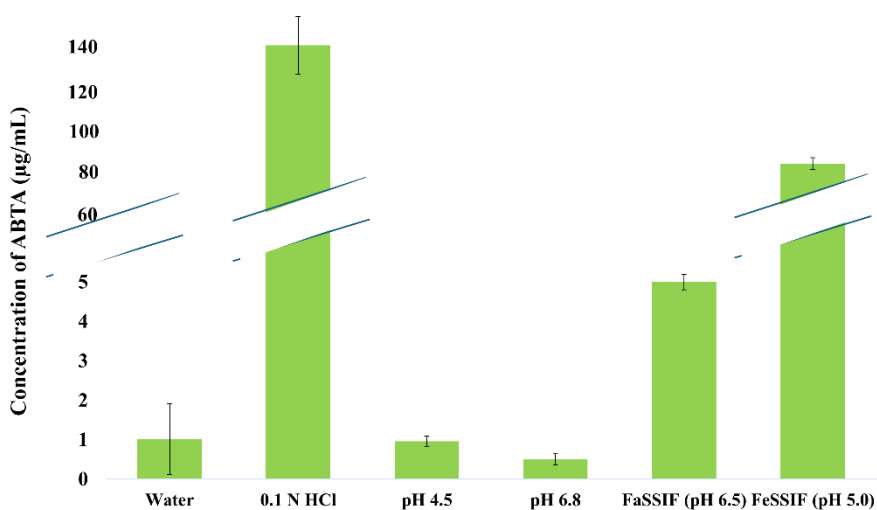


**Figure 4.3.** Solubility of ABTA in various aqueous buffers

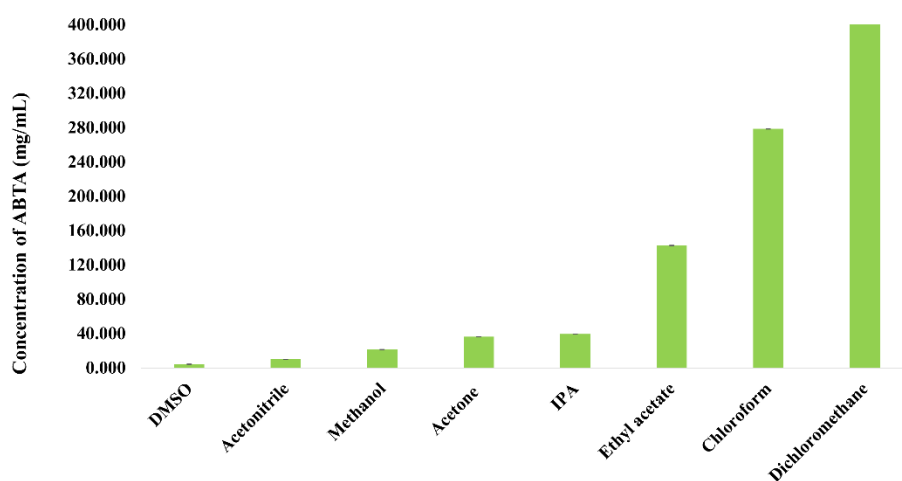


**Figure 4.4** Solubility of ABTA in different organic solvents

#### 4.2.4. Stability study

The solution stability study of ABTA was conducted at  $37 \pm 0.5$  °C as depicted in Figure 4.5. Degradation further depended on pH, with the degradation rate constant (K) increasing as pH shifted from acidic to neutral. Additionally, in biorelevant media, FeSSIF and FaSSIF exhibited higher solution stability at t90% more than 75h compared to the other solution media. ABTA exhibited the least solubility in pH 4.5 buffer. The logarithm of the percentage of drug remaining to be degraded was plotted against time under different pH conditions, and the corresponding K



values were calculated, as shown in Figure 4.5 and Table 4.1. These results indicated that the drug in water and pH 4.5 buffer should not be stored beyond 6h. Hence, this stability information can be utilized for our in-vitro dissolution studies and hold time for sample analysis.

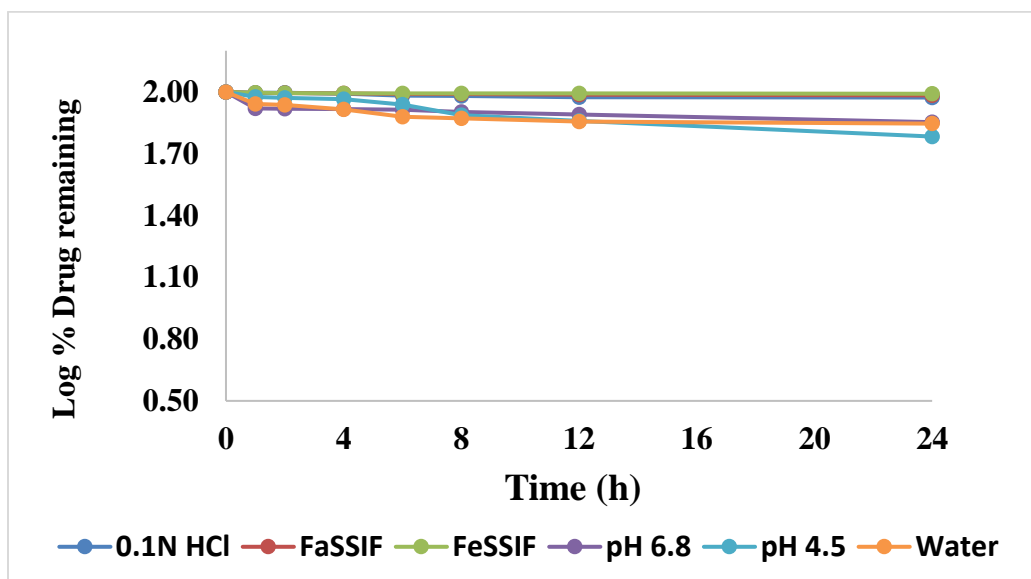


**Figure 4.5:** Solution stability study of ABTA at different aqueous buffers and Biorelevant media at  $37 \pm 0.5$  °C

**Table 4.1.** Solution state stability data of ABTA at different aqueous buffers and biorelevant media

pH	R <sup>2</sup>	K	t <sub>90%</sub> (h)
Water	0.6357	0.0117	8.97
0.1 N HCl	0.7593	0.0027	38.13
pH 4.5	0.9643	0.017	6.18
pH 6.8	0.6861	0.0087	10.04
FeSSIF (pH 5.0)	0.5072	0.0006	152.52
FaSSIF (pH 6.5)	0.8282	0.0013	76.26

#### 4.2.5. Drug excipient compatibility study

DSC provides valuable insights into physical and chemical changes within a system over time and temperature, including parameters like melting point, glass transition temperature, and thermal stability. The study of pure drug, excipients, and their physical mixture through DSC did not reveal

any incompatibility, as depicted in Figure 4.6. The exothermic peak of ABTA remained largely intact in most cases, with slight broadening or shifting to higher or lower temperatures. These variations in peak shape and enthalpy might be attributed to impurities present in the samples, rather than indicating incompatibility, as they could arise from the blending of the drug and excipients, which reduces the purity of each component in the mixture (5,8).

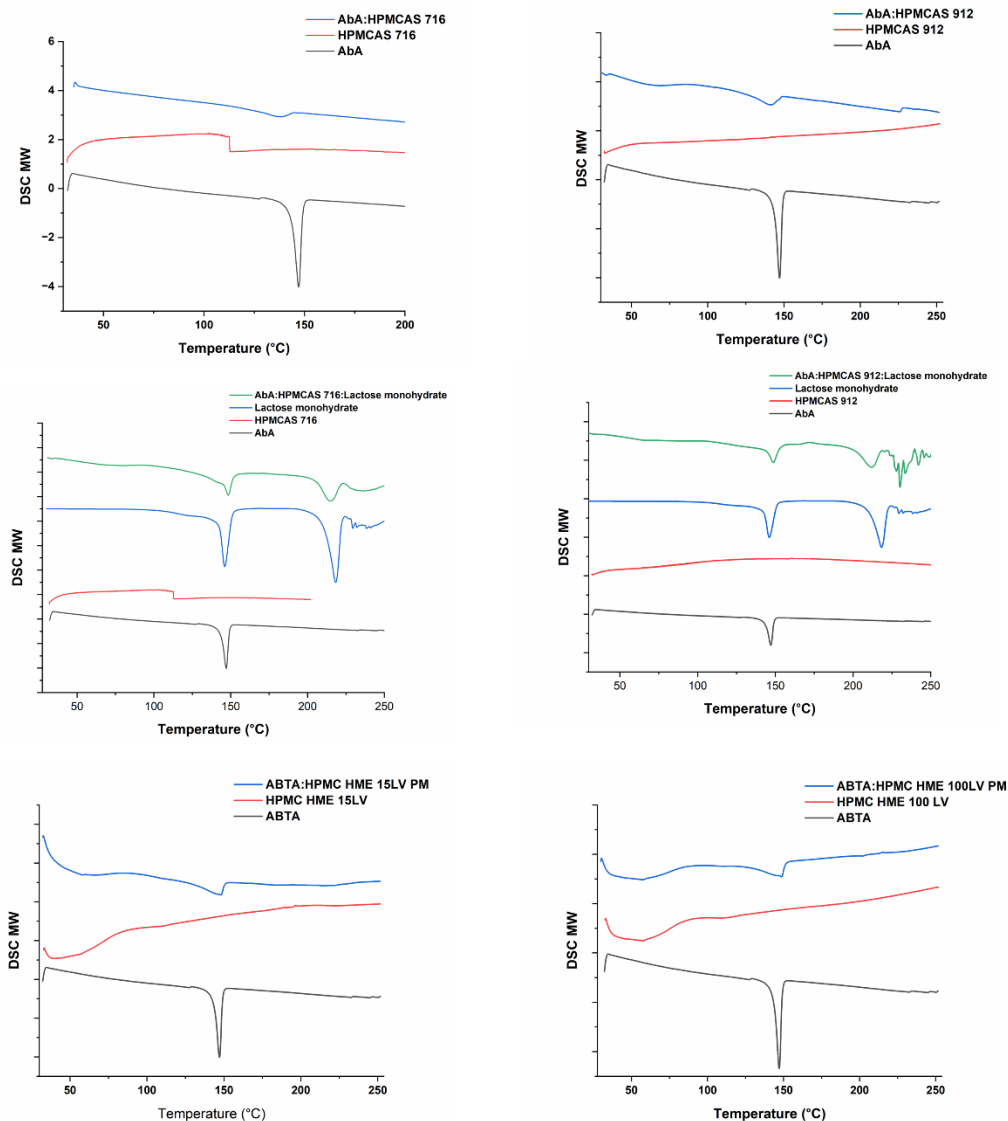


**Figure 4.6:** DSC thermogram of ABTA, HPMCAS 716, HPMCAS 912, Lactose monohydrate, HPMC HME 15LV and HPMC HME 100LV

Additionally, the FTIR spectra of drug-excipient mixtures reaffirmed the absence of any

incompatibility between ABTA and the excipients, as evidenced by the retention of all characteristic bands of ABTA across all investigated mixtures, as depicted in Figure 4.7.

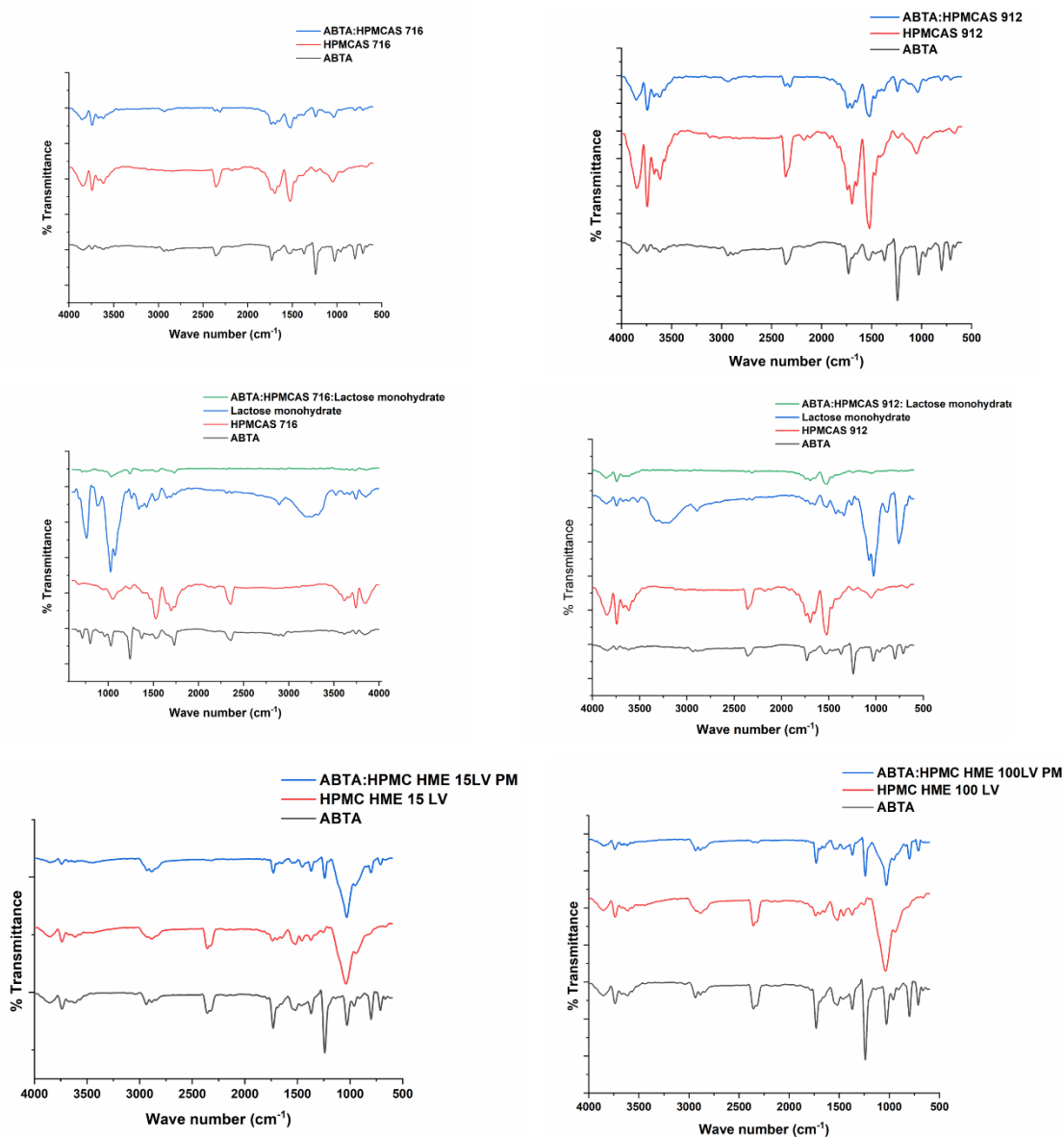


**Figure 4.7:** FTIR spectrum of ABTA, HPMCAS 716, HPMCAS 912, Lactose monohydrate, HPMC HME 15 LV and HPMC HME 100LV

### 4.3.Conclusion

The ABTA sample underwent comprehensive identification tests and displayed solubility in aqueous buffers that varied depending on pH. It exhibited higher solubility in organic solvents like

dichloromethane, chloroform, ethyl acetate, isopropyl alcohol, and acetone. Degradation was found to be pH-dependent, with the degradation rate constant (K) increasing as pH shifted from acidic to neutral. Drug-excipient compatibility studies conducted through DSC and FTIR indicated no significant interaction between ABTA and the selected excipients. The preformulation studies yielded valuable insights for selecting excipients and solvents for SD preparation, as well as determining optimal storage conditions for both the pure drug and formulations.

### References

1. Chaurasia G. a Review on Pharmaceutical Preformulation Studies in Formulation and Development of New Drug Molecules. *International Journal of Pharmaceutical Sciences and Research*. 2016;7(6):2313.
2. USPNF. Dissolution test tablet. 2020;0–2.
3. Klein S. The use of biorelevant dissolution media to forecast the in vivo performance of a drug. *AAPS Journal*. 2010;12(3):397–406.
4. Annapurna MM, Pradhan DP, Chaitanya RK. New Spectrophotometric Techniques for the determination of Abiraterone acetate ( A Steroidal Inhibitor ) in Tablets. *Journal of chemical and pharmaceutical sciences*. 2017;10(2):768–770.
5. Yahya BA, Bawazir AS, Shaikh SS, Dehghan MH, Jalil MA. Fabrication and characterization of  $\beta$ -cyclodextrin-based nano sponges for delivery of abiraterone acetate. *Journal of Medical Pharmaceutical and Allied Sciences*. 2021;10(6):4050–4056.
6. Sokol MB, Nikolskaya ED, Yabbarov NG, Zenin VA, Faustova MR, Belov A V., et al. Development of novel PLGA nanoparticles with co-encapsulation of docetaxel and abiraterone acetate for a highly efficient delivery into tumor cells. *Journal of Biomedical Materials Research - Part B Applied Biomaterials*. 2019;107(4):1150–1158.
7. Liu Y, Li Y, Xu P, Shen Y, Tang B, Wang Q. Development of Abiraterone Acetate Nanocrystal Tablets to Enhance Oral Bioavailability: Formulation Optimization, Characterization, In Vitro Dissolution and Pharmacokinetic Evaluation. *Pharmaceutics*. 2022;14(6)1134.
8. Stolarczyk EU, Łaszcz M, Leś A, Kubiszewski M, Kuziak K, Sidoryk K, et al. Design and molecular modeling of abiraterone-functionalized gold nanoparticles. *Nanomaterials*. 2018;8(9)641.

**Chapter 5: Formulation of**  
**Abiraterone acetate-HPMCAS based**  
**Solid Dispersion**

**5.0.Introduction**

Abiraterone acetate (ABTA) was approved by the USFDA in 2011 for treating metastatic castration-resistant prostate cancer. When ABTA is administered orally, it is converted into its active metabolite, abiraterone (ABT), through hydrolysis in the intestinal lumen (1). ABT inhibits the enzymes C-17,20 lyase and 17  $\alpha$ -hydroxylase (CYP 17), reducing androgen synthesis in tissues related to the adrenal glands (2,3). The drug has been highly successful in prolonging the lives of patients who have prostate cancer. Zytiga, the marketed formulation of ABTA, has achieved significant clinical and commercial success, but delivering orally ABTA remains highly challenging. It falls under the BCS class IV, characterized by extremely poor aqueous solubility ( $< 0.5 \mu\text{g/mL}$ ) as well as low permeability (4). Its pH-dependent solubility causes ABTA to precipitate when transitioning from the gastric fluid to the alkaline intestinal region, reducing solubility, hindering API dissolution, and impeding drug absorption across the intestinal membrane. Due to its characteristics, the oral bioavailability of ABTA in humans is estimated to be less than 10%. Consequently, a substantial daily dose of 1000 mg (four 250 mg tablets taken once daily) is necessary to achieve therapeutic blood levels (5). Moreover, ABTA shows significant inter-individual pharmacokinetic variability and strong food effects, with a 7- and 5-fold increase in  $C_{\text{max}}$  and  $\text{AUC}_{0-\infty}$  for low-fat meals and 17- and 10-fold for high-fat meals (6). Therefore, the commercial tablet must be taken on an empty stomach (2 h before and 1 h after a meal) to avoid overexposure (5).

Furthermore, to overcome the above drawbacks of ABTA, a few existing approaches to ABTA have been discussed in the literature. However, this approach reveals the inherent limitations, such as ABT hydrochloride salt, which has been developed to improve gastrointestinal solubility; there's still a lack of reported data on solubility and dissolution testing for this advancement (7). Moreover, nano-amorphous ABTA formulation requires reconstitution with water before oral intake, resulting in a 'powder in a bottle' dosage form. This self-reconstitution process can lead to dosing variability and inaccuracies in clinical practice (4). Although FDA-approved for administration with or without food, Yonsa® is predominantly taken in the fasted state, indicating a discrepancy in adherence to dosing recommendations. It may result from prescribing habits, patient preferences, or healthcare provider instructions. Despite Yonsa® offering advantages over Zytiga®, limited clinical trial data (only 84 days) may cause physicians to hesitate in prescribing it over Zytiga® (4).

Therefore, developing a formulation that enhances solubility, dissolution, and bioavailability is necessary while eliminating food effects and potentially allowing dose reduction. Such a formulation would meet higher standards for patient convenience by improving bioavailability and reducing side effects. Among the numerous ways to increase solubility by amorphization, SD has shown to be the most effective strategy in which API is homogeneously distributed in a polymeric matrix (8). However, there is a risk involved with utilizing an SD since the amorphous API can transform back into a more stable crystalline form. In SD formulations, several strategies are employed to mitigate the risk of recrystallization.

Consequently, choosing an appropriate polymer for SDs becomes a crucial step, as it not only enhances the API solubility and the rate of the dissolution of the SDs but also hinders the undesirable API precipitation (9). Previous studies have revealed that cellulosic polymers play a vital role in SD in maintaining supersaturation by inhibiting crystallization and keeping the drug molecules in a dissolved state for a prolonged period (10,11). Furthermore, cellulosic polymer chains interact with the API molecules, forming hydrogen bonds, reducing their mobility, and preventing them from precipitating out of the solution (11). The utilization of a high-energy form of the API and enhanced release properties, when combined with a hydrophilic/amphiphilic cellulosic polymer, are possibilities for the improved in vivo performance of SDs (12).

HPMCAS, the cellulose succinate derivative chosen for this study, has been utilized as a carrier in the SD. It enhances the solubility and improves the bioavailability of poorly water-soluble drugs (13). HPMCAS is amphiphilic, comprising acetic acid and succinic acid ester of hydroxypropyl methylcellulose. HPMCAS is available in 3 distinct grades, i.e., HPMCAS 716, HPMCAS 912, and HPMCAS 126, differentiated by the acetyl and succinyl substituents ratio on the HPMC backbone (9). Additionally, HPMCAS aids in sustaining drug supersaturation by inhibiting precipitation, thereby enhancing dissolution rate and extent in aqueous environments (9).

The objective of the present work was to improve the solubility, dissolution, and bioavailability of the poorly water-soluble ABTA using SD technology. To meet this objective, ABTA SD was prepared using solvent evaporation and solvent granulation methods employing the different grades of the HPMCAS. Hansen solubility parameter and Flory-Huggins drug-polymer interaction approach were used to predict the miscibility of ABTA with the selected polymer HPMCAS. The

ability of the HPMCAS to impede the crystallization of ABTA was investigated via the precipitation inhibition study. The solubility and dissolution were assessed using saturation solubility studies and in-vitro and bio-relevant dissolution studies. The physicochemical characterization of ABTA SD was evaluated by ATR-FTIR, PXRD, DSC, TGA, and Field emission-scanning electron microscopy (FE-SEM).

### 5.1. Materials and Methods

ABTA (purity 99%) was gifted by Biophore India Pharmaceuticals Pvt. Ltd, India. HPMCAS 716, HPMCAS 912, and Startab were supplied as gift samples from Colorcon Asia Pvt. Ltd, India. Soya lecithin and sodium taurocholate were procured from the SRL. Mannitol and citric acid were purchased from Hi-media. Lactose monohydrate and Colloidal silicon dioxide were supplied from Lubrizol. Magnesium stearate was procured from CDH. Analytical grade HPLC solvents such as acetone, methanol, dichloromethane, and acetonitrile were procured from Merck. All other necessary chemicals were purchased from an approved supplier.

### 5.2. Drug-polymer miscibility predictions

Drug–polymer miscibility is critical for successfully formulating a physically stable SD. Mathematical theories, such as the Hansen solubility parameters and Flory–Huggins interaction parameter ( $\chi$ ), are employed to predict drug-polymer miscibility (14–16).

#### 5.2.1. Hansen solubility parameter approach

The van Krevelen and Hoftyzer group contribution method was used to determine the Hansen solubility parameter ( $\delta$ ) of drugs (ABTA) and polymers (HPMCAS) using their chemical structure, as shown in Figure 5.1 (17).

The three primary Hansen parameters were calculated for each molecule: (i) dispersion forces amongst the molecule ( $\delta_d$ ), (ii) dipolar intermolecular forces amongst the molecule ( $\delta_p$ ), (iii) hydrogen bonding energy amongst the molecule ( $\delta_h$ ). The overall solubility parameter ( $\delta_t$ ), typically expressed in MPa<sup>0.5</sup>, was determined by aggregating all three Hansen parameters as depicted in equation (5.1).

$$\delta_t^2 = \delta_d^2 + \delta_p^2 + \delta_h^2 \quad (5.1)$$

The  $\delta_d$ ,  $\delta_p$ ,  $\delta_h$  can be calculated by following formulas:



$$\delta_d = \frac{\epsilon F_{di}}{V} \quad (5.2)$$

$$\delta_p = \frac{\sqrt{\epsilon F_{pi}^2}}{V} \quad (5.3)$$

$$\delta_h = \sqrt{\frac{\epsilon E_{hi}}{V}} \quad (5.4)$$

$F_{di}$  and  $F_{pi}$  are molar attraction forces of dispersive interaction and dipole-dipole interaction,  $E_{hi}$  is hydrogen bonding forces, and  $V$  is the molar volume, respectively.

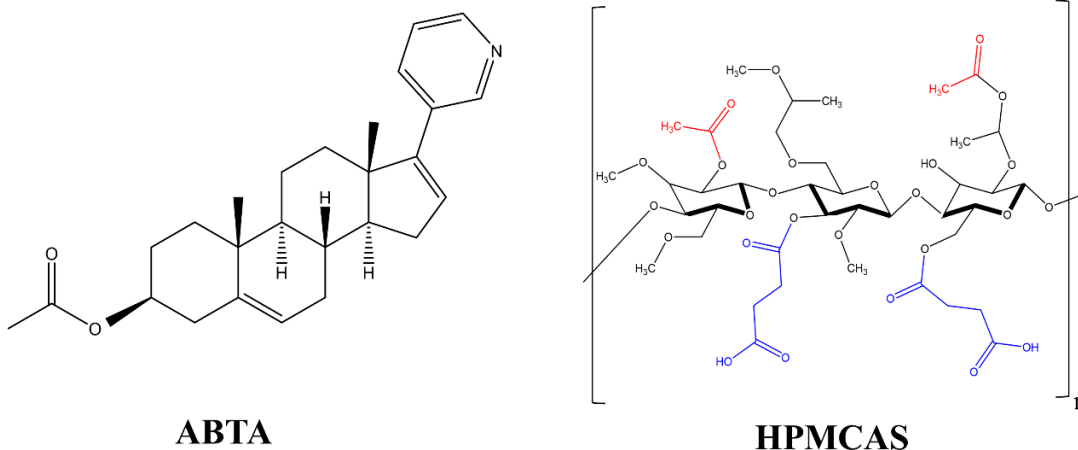


**Figure 5.1.** Chemical structure of ABTA and HPMCAS

### 5.2.2. Flory-Huggin's drug-polymer interaction approach

F-H drug-polymer interaction parameter ( $\chi$ ) is determined by the difference between the solubility parameters of drugs and polymers and calculated using equation 5.5.

$$\chi = \frac{v_{site} (\delta_{polymer} - \delta_{drug})^2}{RT} \quad (5.5)$$

In this equation,  $V_{site}$  represents the hypothetical lattice volume, while  $T$  denotes temperature,  $R$  stands for the gas constant,  $\delta_{drug}$  and  $\delta_{polymer}$  signify the solubility parameters of the drug and polymer, respectively (18).

### 5.3. Preparation and optimization of ABTA-SD formulation

ABTA-SD formulation was prepared using two different methods: solvent evaporation and solvent granulation. Both methods utilized organic solvents such as acetone. In the solvent granulation method, mannitol, citric acid, lactose monohydrate, and aerosil were used as an adsorbent.

### 5.3.1. Solvent evaporation method

In the solvent evaporation method, the SD of ABTA was prepared in the different weight ratios (1:1 to 1:10) of the drug: polymers, respectively. The ABTA and HPMCAS 716/ 912 were dissolved in acetone, following continuous mixing on a magnetic stirrer at 500 rpm to produce a clear solution. After that, the solvent was evaporated at room temperature. The obtained solid residue was pulverized using a porcelain mortar and pestle. The formulated SDs were collected, triturated, sieved, and stored in desiccators until further analysis. Table 5.1 details the compositions of the ABTA physical mixture (PM) and SD.

**Table 5.1.** Composition of ABTA PM and SD prepared by solvent evaporation method

Ingredients/ Formulation code	A1	A2	A3	A4	A5	A6	B1	B2	B3	B4	B5	B6
ABTA	250	166.67	125	250	166.67	125	250	166.67	125	250	166.67	125
HPMCAS 716	250	333.33	375	-	-	-	250	333.33	375	-	-	-
HPMCAS 912	-	-	-	250	333.33	375	-	-	-	250	333.33	375
Acetone (mL)	-	-	-	-	-	-	5	5	5	5	5	5
Total (mg)	500	500	500	500	500	500	500	500	500	500	500	500

**A1-A6:** PM of ABTA using HPMCAS 716 and 912; **B1-B6:** SD of ABTA using HPMCAS 716 and 912

### 5.3.2. Solvent granulation method

ABTA-SD formulations were prepared using the solvent granulation method. These formulations used different polymeric carriers, such as HPMCAS 716 and 912, with various adsorbents. During formulation development, several adsorbents, such as citric acid, mannitol, aerosil, and lactose monohydrate, were screened in different ratios for SD preparation. Among these, lactose monohydrates exhibited favorable adsorption properties and desirable flow characteristics, making them the adsorbent for SD preparation. Table 5.2 details the compositions of the ABTA-SD formulations. Acetone served as the solvent for dissolving the drug and carriers. In brief, the solvent granulation method entailed dissolving ABTA and HPMCAS 716 or 912 in acetone, then gradually adding this solution onto adsorbents to facilitate solvent evaporation. The formulated SDs were collected, sieved, and stored in desiccators until further analysis.

**Table 5.2.** Compositions of ABTA PM and SD prepared by Solvent Granulation method

<b>Ingredients/ Formulation code</b>	<b>P1</b>	<b>P2</b>	<b>P3</b>	<b>P4</b>	<b>P5</b>	<b>P6</b>	<b>F1</b>	<b>F2</b>	<b>F3</b>	<b>F4</b>	<b>F5</b>	<b>F6</b>
ABTA	166.66	125	100	166.66	125	100	166.66	125	100	166.66	125	100
HPMCAS 716	166.66	250	300	-	-	-	166.66	250	300	-	-	-
HPMCAS 912	-	-	-	166.66	250	300	-	-	-	166.66	250	300
Lactose monohydrate	166.66	125	100	166.66	125	100	166.66	125	100	166.66	125	100
Acetone (mL)	-	-	-	-	-	-	5	5	5	5	5	5
Total (mg)	500	500	500	500	500	500	500	500	500	500	500	500

**P1-P6:** PM of ABTA using HPMCAS 716 and 912 along with lactose monohydrate; **F1-F6:** SD of ABTA using HPMCAS 716 and 912 along with lactose monohydrate

### 5.3.3. Physical Mixtures

Physical mixtures (PMs) of ABTA (shown in Table 5.2) were formulated using geometric mixing with the different ratios of the drug and polymer with adsorbent in the mortar and pestle with less force, confirming that no grinding was employed during the process. The PMs were collected, sieved, and stored in desiccators until further analysis.

### 5.4. Solubility studies

Excessive quantities of free ABTA, PM of HPMCAS 716 and 912 (A1-A6; P1-P6), SD of HPMCAS 716 or 912 prepared from solvent evaporation and solvent granulation method were introduced into vials containing the distilled water, pH 1.2, pH 6.8, fasted-state simulated intestinal fluid (FaSSIF, pH 6.5) and fed-state simulated intestinal fluid (FeSSIF, pH 5.0) for the solubility studies. These vials were then placed on an orbital shaker and continuously stirred for 8h at a controlled temperature of  $37 \pm 0.5$  °C, allowing equilibrium to be reached. After 8h, precise aliquots of the samples were extracted, filtered, and subsequently subjected to analysis using RP-HPLC.

### 5.5. Precipitation inhibition assay

A precipitation inhibition study was conducted to evaluate the effect of HPMCAS in preventing precipitation and maintaining the supersaturation of ABTA. Supersaturation was induced by the

addition of 2 mL of ABTA solution (6 mg/mL in methanol) to 100 mL of FaSSIF (pH 6.5) precipitation media. All experiments were conducted at  $37 \pm 0.5^\circ\text{C}$  for 120 min at 200 rpm. In this experiment, the HPMCAS (716 and 912) was pre-dissolved in the precipitation media to assess the potential. In contrast, a precipitation media without polymer was employed as a control. The concentration of ABTA was calculated in the presence and absence of polymer at predetermined time intervals and quantified by the RP-HPLC. For ABTA precipitation inhibition, HPMCAS 716 or 912 were studied at a weight ratio of 1:2 (ABTA/HPMCAS) in a binary mixture; this ratio was selected based on the maximum solubility of the ABTA (10,19). The particle size of the precipitate was assessed through dynamic light scattering (DLS) using a Malvern Zeta Sizer (Nano ZS, Malvern Instruments, U.K.) at a temperature of  $25^\circ\text{C}$  as part of the precipitation inhibition study. Samples were removed from the precipitation inhibition study after 10, 30, 60, 120, and 180 min for further particle size evaluation (19).

### **5.6. Solid-state characterization of SD**

#### **5.6.1. Differential scanning calorimetry (DSC)**

To determine the crystallinity, the free ABTA, HPMCAS 716, HPMCAS 912, lactose monohydrate, ABTA-PM, and ABTA-SD were analyzed by DSC using the Shimadzu TA 60 DSC system operating with TA 60 software. The sample was placed in a perforated aluminum crucible and an empty pan as a reference for the measurement and then heated from 30 to  $250^\circ\text{C}$  at  $10^\circ\text{C}/\text{min}$  under a nitrogen atmosphere with a 50 mL/min flow rate. This study aimed to examine the thermal behavior of the drug and investigate drug-polymer interactions.

#### **5.6.2. Thermogravimetric analysis (TGA)**

TGA analysis was conducted utilizing a Shimadzu TA 60 instrument operated with TA 60 software. TGA was employed to assess the stability of the drug/polymer blend. Below  $150^\circ\text{C}$ , any weight reduction was considered dehydration, with the change in weight reflecting the moisture content. Each sample (free ABTA, HPMCAS 716, HPMCAS 912, Lactose monohydrate, ABTA-PM, and ABTA-SD) weighing between 8-10 mg, were loaded into platinum crucibles and subjected to heating from 30 to  $400^\circ\text{C}$  at a rate of  $10^\circ\text{C}/\text{min}$ , under a nitrogen atmosphere with a flow rate of 50 mL/min.

#### **5.6.3. Powder X-ray diffraction (PXRD)**

PXRD testing was performed using a Rigaku mini flex II diffractometer with incident radiation of Cu K $\alpha$  produced at 40 kV and 30 mA, applying a scanning rate of 2°/min with a 2  $\Theta$  range of 10-60°. PXRD analysis examined the crystallinity in the free ABTA, HPMCAS 716, HPMCAS 912, Lactose monohydrate, ABTA-PM, and ABTA-SD.

### **5.6.4. Attenuated total reflectance Fourier transform infrared spectroscopy (ATR-FTIR)**

ATR-FTIR spectra determined the distinguishing possible interactions between the API and polymer. The free ABTA, HPMCAS 716, HPMCAS 912, Lactose monohydrate, ABTA-PM, and ABTA-SD spectrum were recorded using ATR-FTIR spectroscopy (Bruker, USA) operated with Opus software. The spectra were collected in the region from 400-4000 cm<sup>-1</sup> with a 1 cm<sup>-1</sup> resolution and averaged over 100 scans.

### **5.6.5. Field emission scanning electron microscopy (FE-SEM)**

The FE-SEM determined the shape and surface characteristics of the free ABTA and ABTA SD formulations. The samples were prepared by mounting them on aluminum stubs and vacuum coating them with gold using a sputter coating machine (Leica Ultra Microtome EM UC7). Then, the coated samples were placed in the FE-SEM for the morphological analysis.

### **5.7. Determination of ABTA content**

The concentration of ABTA in the SD was quantified using RP-HPLC (Shimadzu) analysis. This analysis was conducted on a Hypersil Gold C18 column (50\*4.6 mm \*5 $\mu$ m) with a mobile phase consisting of acetonitrile and dibasic potassium phosphate (0.01 mM) buffer in an 80:20 ratio. The pH of the mobile phase was adjusted to 6.5, and the flow rate was set at 1.0 mL/min, while the injection volume was 20  $\mu$ L. The detection wavelength was 254 nm, and the column temperature was maintained at 40 °C (20).

### **5.8. Dissolution studies**

#### **5.8.1. In-vitro dissolution studies**

In-vitro dissolution studies of ABTA and SD were performed in various dissolution media, such as pH 1.2, pH 6.8, and pH 4.5, to evaluate the rate and extent of the drug from the dissolution of SD, and this was compared with the pure drug dissolution. Additionally, the dissolution behavior pattern in these various media was investigated. Specifically, for the pH 4.5 dissolution media, 0.25% sodium lauryl sulphate was incorporated, as per its specification in the official monograph.

The USP II apparatus was employed for the dissolution testing. Numerous researchers have utilized smaller volumes and modified apparatus for drug dissolution studies. Therefore, in our investigations, an in-house modified USP II dissolution apparatus was utilized to examine drug dissolution from both the SD and free ABTA. In brief, 10 mg of ABTA and ABTA SD (equivalent to 10 mg of ABTA) sample was added to 250 mL of pH 1.2, pH 6.8 media, and pH 4.5 maintained at  $37 \pm 0.5$  °C and stirred at 150 rpm. Samples were withdrawn at predetermined time points (5, 10, 15, 30, 45, 60, and 120 min), and an equal volume of fresh media was added. The withdrawn samples were filtered through a 0.45- $\mu$ m syringe filter and examined using RP-HPLC.

### 5.8.2. Bio-relevant dissolution studies

The biorelevant dissolution media aim to replicate the physiological conditions of the gastrointestinal tract, thus aiding in the prediction of a drug's behavior and dissolution within the human body. These studies play a pivotal role in forecasting in vivo performance and can offer valuable insights into how a formulation behaves in the gastrointestinal tract. The biorelevant dissolution studies can be critical when a drug shows a food effect. The food effects refer to the influence of the food on the absorption and pharmacokinetics of a drug after oral administration.

Given that ABTA exhibits a food effect, it is imperative to investigate its dissolution under FaSSIF, pH 6.5, and FeSSIF, pH 5.0 media. The free ABTA and ABTA SD (F2 and F5) (equivalent to 10 mg of ABTA) sample was added to 250 mL of FaSSIF and FeSSIF media maintained at 37 °C and stirred at 150 rpm. Samples were collected at scheduled intervals (5, 10, 15, 30, 45, 60, and 120 min), followed by adding an equal volume of fresh media. The collected samples underwent filtration through a 0.45- $\mu$ m syringe filter before being subjected to RP-HPLC analysis.

### 5.8.3. Mathematical analysis of in-vitro and bio-relevant dissolution data

The dissolution profiles of both free ABTA and the optimized formulation ABTA-SD were assessed using several parameters: percent dissolution efficiency (% DE) and mean dissolution time (MDT). Additionally, DDSolver software was used to conduct mathematical modeling of the dissolution profiles. Various models were employed to determine which one best represented the dissolution data, utilizing  $R^2$  (correlation coefficient), AIC (Akaike information criterion), and MSC (model selection criteria) as criteria for selection.

### **5.9. Preparation of tablet dosage form of ABTA from SD formulation**

The ABTA tablets from the SD were prepared using the dry granulation method. SD of ABTA and fillers such as lactose monohydrate, startab, and colloidal silicon dioxide were accurately weighed. Each excipient was individually screened through mesh size #40 and was thoroughly blended. Subsequently, magnesium stearate, a lubricant, was introduced last and thoroughly blended by passing through a #40 mesh size. The formulation mixture was then compressed into tablets using a rotary tableting machine (mini tablet compressing machine). The tablet weighed 645-685 mg, with 100 mg of ABTA. The content of ABTA was precisely determined using RP-HPLC.

#### **5.9.1. In-vitro dissolution studies of the tablet dosage form of ABTA from SD formulation**

For measuring the release of ABTA tablets, it is recommended to use the paddle method at a rotating speed of 50 rpm in a dissolution II apparatus (Electrolab, India) with a temperature set at  $37 \pm 0.5$  °C. Briefly, ABTA, the ABTA-SD tablets of F2 and F5 were introduced in the dissolution vessel containing 900 mL dissolution media. The procedure included operating at a rotation speed of 50 rpm and maintaining a  $37 \pm 0.5$  °C temperature. As specified in the monograph, the dissolution medium consists of a pH of 4.5, with a concentration of 56.5 mM and 0.25% (w/v) SLS. At specified time intervals (5, 10, 15, 30, 45, 60, and 120 min), approximately 5 mL samples were withdrawn, and an equivalent volume of fresh media was added to ensure the maintenance of sink conditions. These withdrawn samples underwent filtration using a 0.45- $\mu$ m syringe filter before being analyzed using RP-HPLC.

### **5.10. Stability studies**

Optimized ABTA SD formulations were stored in sealed amber glass bottles for three months (90 days) in stability chambers under accelerated conditions ( $40 \pm 2$  °C and  $75 \pm 5$  % RH). The stability study was assessed by examining physical characteristics (color), % assay, DSC, and PXRD both at initially and after three months at accelerated conditions

### **5.11. Result and discussion**

#### **5.12. Drug-solubility parameter approach**

A critical aspect of formulating stabilized SDs involves achieving a single homogeneous phase wherein the drug and polymer are thermodynamically compatible. The thermodynamic miscibility

of ABTA with the specified polymers (HPMCAS 716 and 912) was investigated by determining Hansen solubility parameters, employing the van Krevelen and Hoftyzer group's contribution method. Due to its relative simplicity, this method of calculating solubility parameters and applying them to SDs remains widely utilized. Group contribution methods are often employed to avoid time-consuming tests and potential inaccuracies in results. In this method, when the solubility parameter between a drug and a polymer differs by less than  $7 \text{ MPa}^{1/2}$ , a system is said to be miscible, or when both compounds have similar  $\Delta\delta$  values. However, a system is immiscible if  $\Delta\delta$  is more than  $10 \text{ MPa}^{1/2}$  (14). Estimation of the solubility parameter of HPMCAS 716 and 912 and ABTA using the Hansen group contribution theory is shown in Table 5.3 and Table 5.4.

**Table 5.3.** Estimation of solubility parameter of ABTA using the Hansen group contribution theory

Structural Group	Frequency	$F_d$	$F_p$	$E_h$	$V_m$	$F_d$	$F_p$	$E_h$	$V_m$
		$(\text{M.J./m}^3)^{0.5}$	$(\text{M.J./m}^3)^{0.5}$	(j/mol)		$(\text{M.J./m}^3)^{0.5}$	$(\text{M.J./m}^3)^{0.5}$	(j/mol)	
		Mol	Mol			mol	Mol		
--CH <sub>3</sub>	3	420	0	0	33.5	1260	0	0	100.5
CH <sub>2</sub>	7	270	0	0	16.1	1890	0	0	112.7
>CH	5	80	0	0	-1	400	0	0	-5
>C<	1	-70	0	0	19.2	-70	0	0	-19.2
=CH	8	200	0	0	13.5	1600	0	0	108
=C<	3	70	0	0	-5.5	210	0	0	-16.5
-N	1	20	0	0	5	20	0	0	5
-COO	1	390	490	7000	18	390	490	7000	18
					<b>Total</b>	5700	490	7000	303.5
						$\delta_d = 18.78$	$\delta_p = 0.072$	$\delta_h = 4.80$	
						19.38			
<b>Total solubility parameter</b>									

**Table 5.4.** Estimation of solubility parameter of HPMCAS using the Hansen Group Contribution theory

HPMCAS	Polar forces	Dispersive forces	Hydrogen bonding	Total solubility parameters
	$\Delta p$	$\Delta d$	$\delta h$	
HPMCAS 716	11.87	17.77	10.19	23.67
HPMCAS 912	12.37	16.73	10.33	23.22



**Table 5.5.** Estimated solubility parameter and Flory–Huggins drug-polymer interaction parameter values derived for HPMCAS and ABTA

Drug/Excipient	Hansen solubility parameter	$\Delta\delta$ (MPa <sup>1/2</sup> ) ( $\delta_{\text{HPMCAS}} - \delta_{\text{ABTA}}$ )	Flory Huggins drug-polymer interaction parameter ( $\chi$ )
ABTA	19.38	-	
HPMCAS 716	23.67	4.29	2.00
HPMCAS 912	23.22	3.85	1.61

As evident from Table 5.5,  $\Delta\delta$  between the ABTA and HPMCAS was below 7 MPa<sup>1/2</sup>, suggesting favorable miscibility between them. Utilizing these solubility parameter values for the drug-polymer system at 25 °C, also calculated the F-H interaction parameter ( $\chi$ ). The value of  $\chi$  relates to the square of the difference in solubility parameters computed from group contributions at 25 °C using Equation 5.3. This equation illustrates that if the drug and polymer solubility characteristics are similar, the interaction parameters will be close to zero. A low value of  $\chi$  indicates a smaller enthalpy of mixing and more negative free energy, facilitating mixing; thus, a value closer to zero signifies a more vital interaction between the drug and the polymer (16). The interaction parameter value for the ABTA-HPMCAS system, as shown in Table 5.4, is close to zero, indicating miscibility between them.

### 5.13. Preparation of SD by solvent evaporation and solvent granulation

The SD of ABTA was prepared using the solvent evaporation method, employing different weight ratios of ABTA to HPMCAS (716/912) ranging from 1:1, 1:2, 1:4: 1:6, 1:8 to 1:10. In the preparation of SD, acetone was used as a solvent for the solubilization of ABTA and HPMCAS. After the acetone was evaporated, retrieving the formulation became challenging due to the formation of a film, which was attributed to an increase in the concentration of HPMCAS. Additionally, the uneven distribution of the drug within the film is illustrated in Figure 5.2.



**Figure 5.2.** ABTA-SD prepared from the solvent evaporation method

This film containing ABTA SD was evaluated for the solubility studies in water across the various weight ratios 1:1 to 1:10, revealing that the 1:2 ratios exhibited the highest solubility, with no further increase in solubility observed beyond ratios of 1:3 to 1:10. Consequently, for further investigation, weight ratios of 1:1 to 1:3 for ABTA and HPMCAS (716 and 912) were selected for SD preparation.

In the SD preparation method, the challenges that occurred in the solvent evaporation method were encountered by employing the solvent granulation method incorporating various adsorbents, including citric acid, mannitol, aerosil, and lactose monohydrate. In this method, ABTA and HPMCAS (716/912) were initially dissolved in acetone, and then this solution was added to the adsorbent, followed by solvent evaporation.

#### **5.14. Solubility studies**

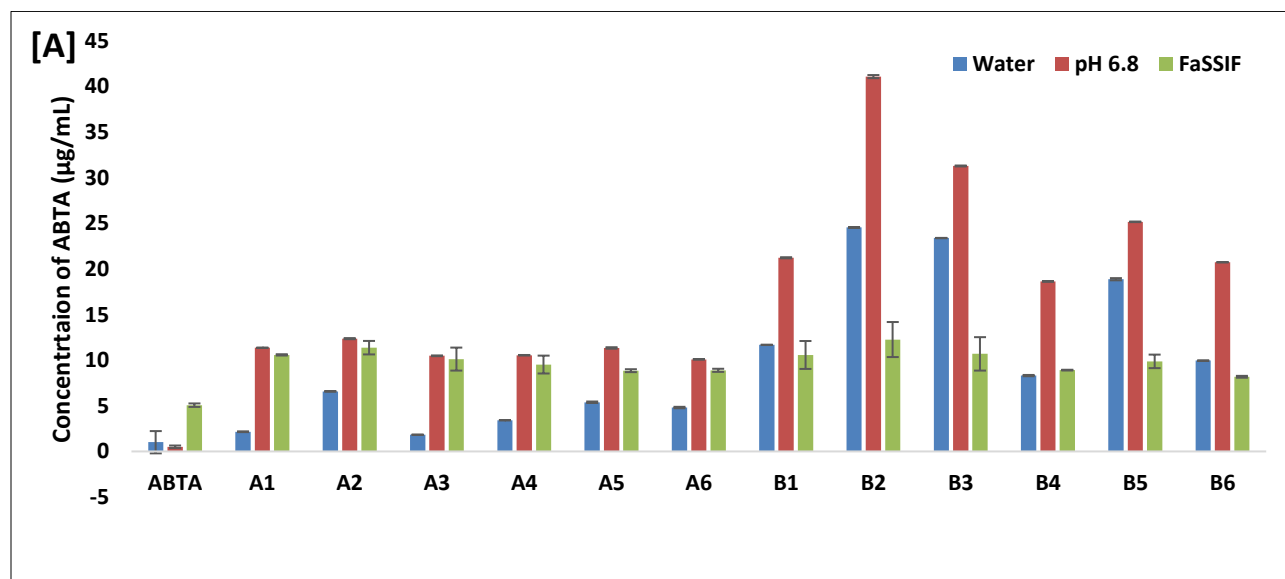
The solubility of free ABTA in water was approximately 1.012  $\mu\text{g/mL}$ . ABTA solubility varies with pH, with a solubility of 136.70  $\mu\text{g/mL}$  in pH 1.2. At pH 6.8, the solubility of free ABTA was 0.510  $\mu\text{g/mL}$ . In FaSSIF and FeSSIF, the solubility of free ABTA was around 5.07  $\mu\text{g/mL}$  and 82.20  $\mu\text{g/mL}$ , respectively.

In this study, SD was prepared using different grades of HPMCAS polymer, i.e., 716 and 912,

which enhanced the solubility of the ABTA. In Figure 5.3 [A and B] the PM (A1-A6) of ABTA, exhibited a slight enhancement in solubility in various media. The solubility of ABTA SD (B1-B6) using HPMCAS (716 and 912) prepared via solvent evaporation method exhibited higher solubility compared to the free ABTA shown in Table 5.6 and Figure 5.3 [A and B].

**Table 5.6.** Solubility studies of the ABTA PM and SD

	Water ( $\mu\text{g/mL}$ ) $\pm$ SD	pH 6.8 ( $\mu\text{g/mL}$ ) $\pm$ SD	pH 1.2 ( $\mu\text{g/mL}$ ) $\pm$ SD	FaSSiF ( $\mu\text{g/mL}$ ) $\pm$ SD	FeSSiF ( $\mu\text{g/mL}$ ) $\pm$ SD
<b>ABTA</b>	1.01 $\pm$ 1.22	0.51 $\pm$ 0.14	136.7 $\pm$ 10.34	5.07 $\pm$ 0.19	82.20 $\pm$ 1.58
<b>A1</b>	2.16 $\pm$ 0.04	11.36 $\pm$ 0.01	120.3 $\pm$ 0.02	10.58 $\pm$ 0.07	97.21 $\pm$ 0.23
<b>A2</b>	6.58 $\pm$ 0.02	12.36 $\pm$ 0.06	180.7 $\pm$ 0.04	11.37 $\pm$ 0.74	100.48 $\pm$ 3.88
<b>A3</b>	1.83 $\pm$ 0.03	10.48 $\pm$ 0.04	126.7 $\pm$ 0.03	10.12 $\pm$ 1.26	100.35 $\pm$ 1.92
<b>A4</b>	3.42 $\pm$ 0.01	10.54 $\pm$ 0.03	121.58 $\pm$ 0.06	9.52 $\pm$ 0.98	87.46 $\pm$ 1.10
<b>A5</b>	5.39 $\pm$ 0.08	11.34 $\pm$ 0.08	179.26 $\pm$ 0.01	8.85 $\pm$ 0.16	84.92 $\pm$ 0.01
<b>A6</b>	4.81 $\pm$ 0.08	10.09 $\pm$ 0.01	160.96 $\pm$ 0.01	8.89 $\pm$ 0.17	84.57 $\pm$ 0.76
<b>B1</b>	11.68 $\pm$ 0.02	21.22 $\pm$ 0.06	201.7 $\pm$ 0.09	10.57 $\pm$ 1.53	105.25 $\pm$ 0.96
<b>B2</b>	24.54 $\pm$ 0.05	41.07 $\pm$ 0.17	256.0 $\pm$ 0.01	12.26 $\pm$ 1.92	108.84 $\pm$ 7.23
<b>B3</b>	23.38 $\pm$ 0.02	31.28 $\pm$ 0.05	213.0 $\pm$ 0.01	10.69 $\pm$ 1.83	108.71 $\pm$ 0.56
<b>B4</b>	8.31 $\pm$ 0.07	18.63 $\pm$ 0.01	218.13 $\pm$ 0.01	8.91 $\pm$ 0.04	95.01 $\pm$ 0.29
<b>B5</b>	18.87 $\pm$ 0.12	25.16 $\pm$ 0.03	230.14 $\pm$ 0.04	9.87 $\pm$ 0.74	96.42 $\pm$ 1.35
<b>B6</b>	9.95 $\pm$ 0.01	20.73 $\pm$ 0.01	212.06 $\pm$ 0.09	8.18 $\pm$ 0.10	88.75 $\pm$ 4.04



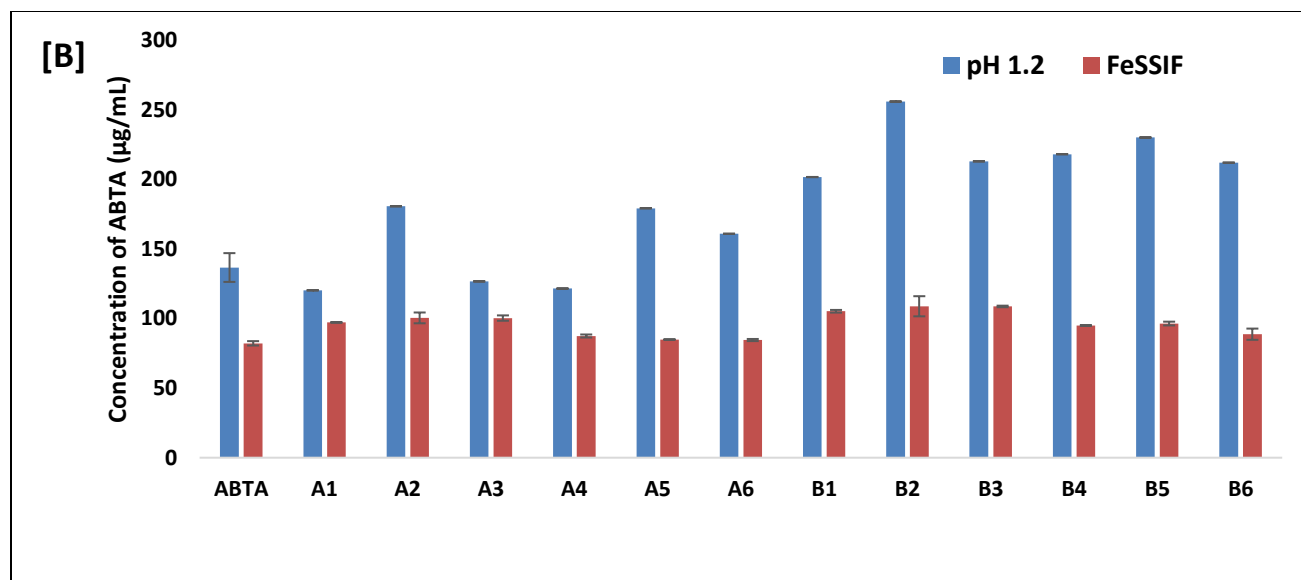


**Figure 5.3** The solubility profiles of all ABTA-SD formulations and PM in different media

After that, solubility studies of the ABTA SD with different adsorbents (citric acid, mannitol, aerosil, and lactose monohydrate) were evaluated in different media. Among these adsorbents, ABTA SD prepared with lactose monohydrate demonstrated higher solubility in different media compared to the other adsorbents. The PM (P1-P6) of ABTA, with the same carriers in the same proportion, exhibited a slight enhancement in solubility in various media.

**Table 5.7.** Solubility studies of ABTA PM and SD with lactose monohydrate

	Water (µg/mL) ±SD	pH 6.8 (µg/mL) ±SD	pH 1.2 (µg/mL) ±SD	FaSSIF (µg/mL) ±SD	FeSSIF (µg/mL) ±SD
<b>ABTA</b>	1.013 ± 1.223	0.51 ± 0.145	136.70 ± 10.34	5.07 ± 0.199	82.20 ± 1.58
<b>P1</b>	2.406 ± 0.606	2.413 ± 0.627	155.84 ± 6.355	9.90 ± 0.476	93.46 ± 1.982
<b>P2</b>	4.480 ± 0.095	4.977 ± 5.236	154.14 ± 0.971	10.42 ± 0.093	101.76 ± 0.244
<b>P3</b>	3.143 ± 1.525	3.135 ± 1.048	148.28 ± 1.329	10.24 ± 0.043	100.69 ± 0.129
<b>P4</b>	2.914 ± 0.135	1.018 ± 0.077	143.01 ± 4.697	8.85 ± 0.166	88.54 ± 1.00
<b>P5</b>	3.796 ± 0.096	2.752 ± 2.029	142.89 ± 0.179	9.52 ± 0.981	88.98 ± 0.280
<b>P6</b>	3.136 ± 0.083	2.264 ± 0.112	138.26 ± 5.696	8.89 ± 0.175	86.67 ± 1.693
<b>F1</b>	16.99 ± 1.962	12.88 ± 1.102	214.20 ± 7.625	10.30 ± 0.053	104.10 ± 1.997
<b>F2</b>	26.49 ± 1.692	26.75 ± 3.597	235.73 ± 2.053	12.83 ± 0.426	109.92 ± 1.091
<b>F3</b>	19.95 ± 1.813	20.70 ± 5.491	233.03 ± 1.742	10.32 ± 0.633	102.64 ± 1.811
<b>F4</b>	15.56 ± 1.373	14.31 ± 2.675	197.21 ± 2.463	10.09 ± 0.219	92.16 ± 0.386
<b>F5</b>	21.34 ± 2.405	19.12 ± 1.142	218.04 ± 1.512	11.92 ± 0.681	95.08 ± 0.995
<b>F6</b>	19.52 ± 2.525	16.04 ± 0.751	213.87 ± 4.290	10.61 ± 0.868	94.96 ± 0.328

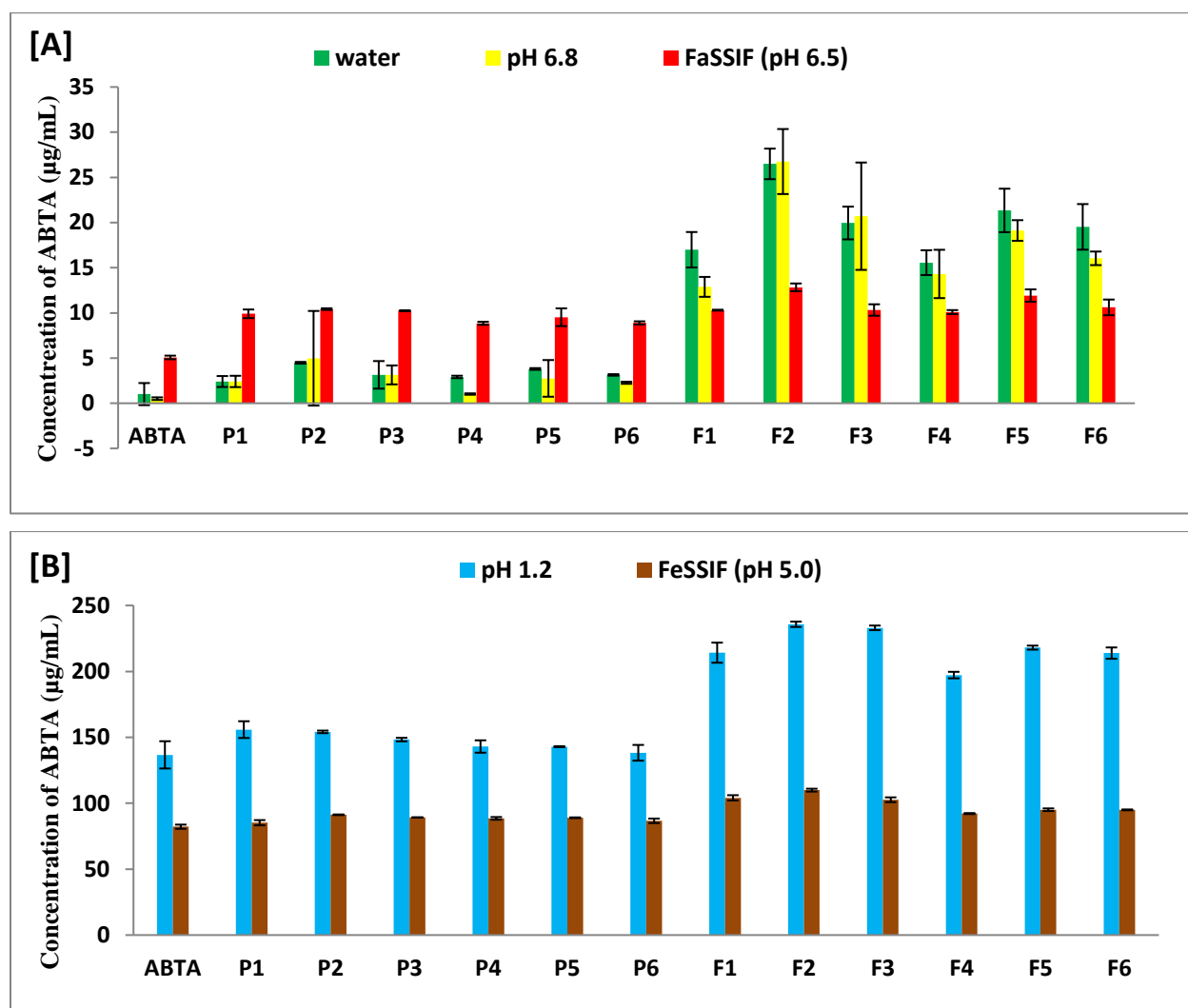


**Figure 5.4.** The solubility profiles of all ABTA-SD and PM along with lactose monohydrate in different media

The solubility of ABTA in SD using HPMCAS 716 and 912 with lactose (1:2:1) ratios exhibited higher solubility among all SD as shown in Table 5.7. The solubility of SD., i.e., F2 and F5 formulation in distilled water, pH 6.8, 0.1 N HCl (pH 1.2), FaSSIF (pH 6.5), and FeSSIF (pH 5.0) were observed to be 26-fold, 52-fold, 1.72-fold, 2.53-fold, 1.33-fold and 21-fold, 38-fold, 1.6-fold, 2.35-fold, and 1.16- fold respectively higher than the free ABTA.

The solubility of ABTA in the HPMCAS 716 was higher than the HPMCAS 912, indicating the substantial impact of acetate and succinate substitution. However, HPMCAS 716, a cellulose

succinate derivative containing the 14-18% succinate and 5-9% acetate group, imparts hydrophilicity. In contrast, HPMCAS 912 polymer with 10-14% succinate group and 7-11% acetate group exhibits hydrophobicity, as an increase in the acetate group corresponds to hydrophobicity, while an increase in the succinate group correlates with hydrophilicity (21). The enhanced solubility of ABTA in HPMCAS 716 polymer can be attributed to its hydrophilic nature compared to HPMCAS 912 (22). The solubility profiles of all ABTA-SD formulations and PM are shown in Figure 5.3 and 5.4

### 5.15. Precipitation inhibition effect

The effectiveness of cellulose succinate derivatives was evaluated by preventing and maintaining the supersaturation state of ABTA. The concentration of ABTA initially declined and continued to decrease over time, as depicted in Figure 5.5. However, the presence of pre-dissolved HPMCAS 716 and 912 polymers demonstrated a notable recrystallization inhibition effect, as the concentration of ABTA in the media remained elevated throughout the 180-min period. In this study, ABTA was chosen with either HPMCAS 716 or 912 at weight ratios of 1:2. This ratio was selected based on the maximum solubility of ABTA observed in various media. Upon inducing supersaturation of ABTA in the absence of polymer, instantaneous and complete precipitation could be observed in the first 10 min; this phenomenon is attributed to the “spring” effect. The presence of pre-dissolved HPMCAS 716 and 912 polymers provided a pronounced and stable supersaturation. This study demonstrated that the HPMCAS 716 and 912 acted as “parachute” to impede the crystal nucleation and growth. Therefore, HPMCAS is characterized as an amphiphilic molecule encompassing both hydrophilic and hydrophobic groups, demonstrating a recrystallization inhibition effect. The presence of pre-dissolved HPMCAS with ABTA demonstrated a “spring and parachute effect”.

It was further explained that the adsorption of the hydrophobic groups of these polymers onto the crystal surface of hydrophobic APIs could hinder the drug's crystal growth. Consequently, polymers with hydrophobic characteristics, such as HPMCAS, exhibited a strong affinity with hydrophobic drugs, leading to their superior recrystallization inhibition effect. However, the HPMCAS 912 polymer, possessing a higher hydrophobic nature, showed greater effectiveness in inhibiting precipitation than HPMCAS 716 (22).

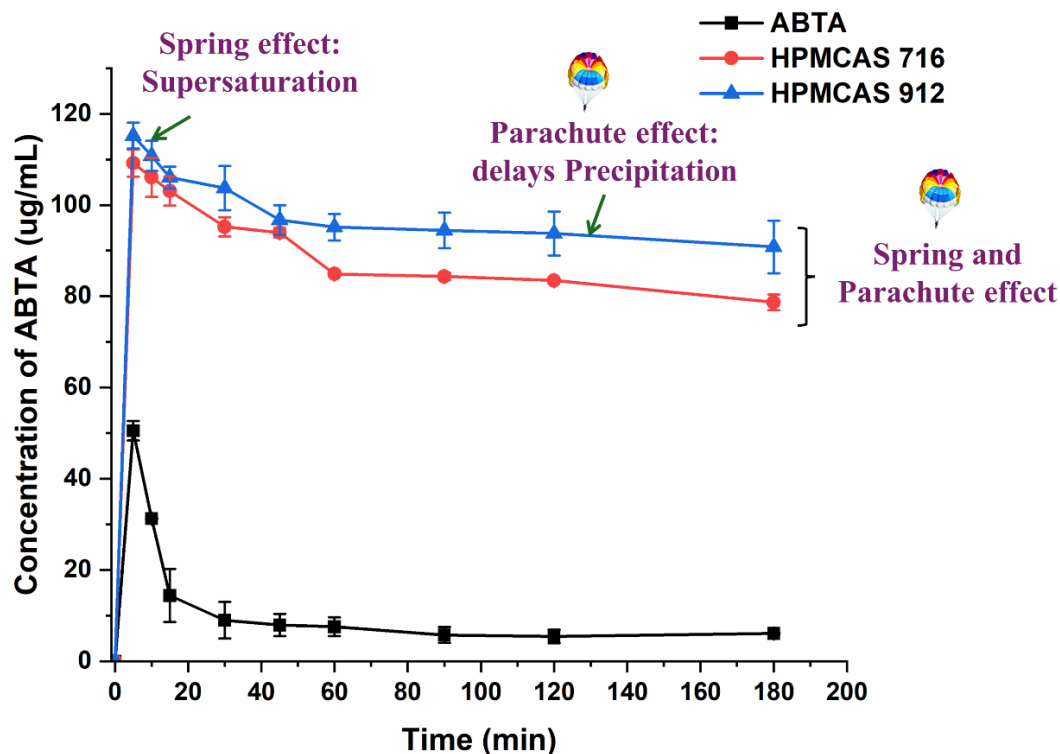


**Figure 5.5.** Precipitation inhibition assay of supersaturated ABTA in FaSSIF (pH 6.5) in the presence of pre-dissolved HPMCAS 716 and 912 (mean  $\pm$  S.D, n = 3)

The above conclusion was confirmed through particle size monitoring of pre-dissolved HPMCAS 716 and 912. The size of precipitates formed during induced precipitation was assessed using dynamic light scattering (DLS). As depicted in Figure 5.6, in the absence of a pre-dissolved polymer, the ABTA exhibited recrystallization within the first 10 min, evident from a notable increase in particle size up to 4500 nm. Conversely, in the presence of pre-dissolved, HPMCAS 716 and 912 maintained a particle size of around 150-400 nm without substantial growth throughout the precipitation inhibition study, i.e., 180 min. The polydispersity index (PDI) value was significantly changed (0.576-1.000) in the free ABTA without the pre-dissolved polymer. Conversely, in the presence of pre-dissolved polymer maintained a PDI of around 0.229-0.418 nm throughout the study, leading to the superior recrystallization inhibition effect.

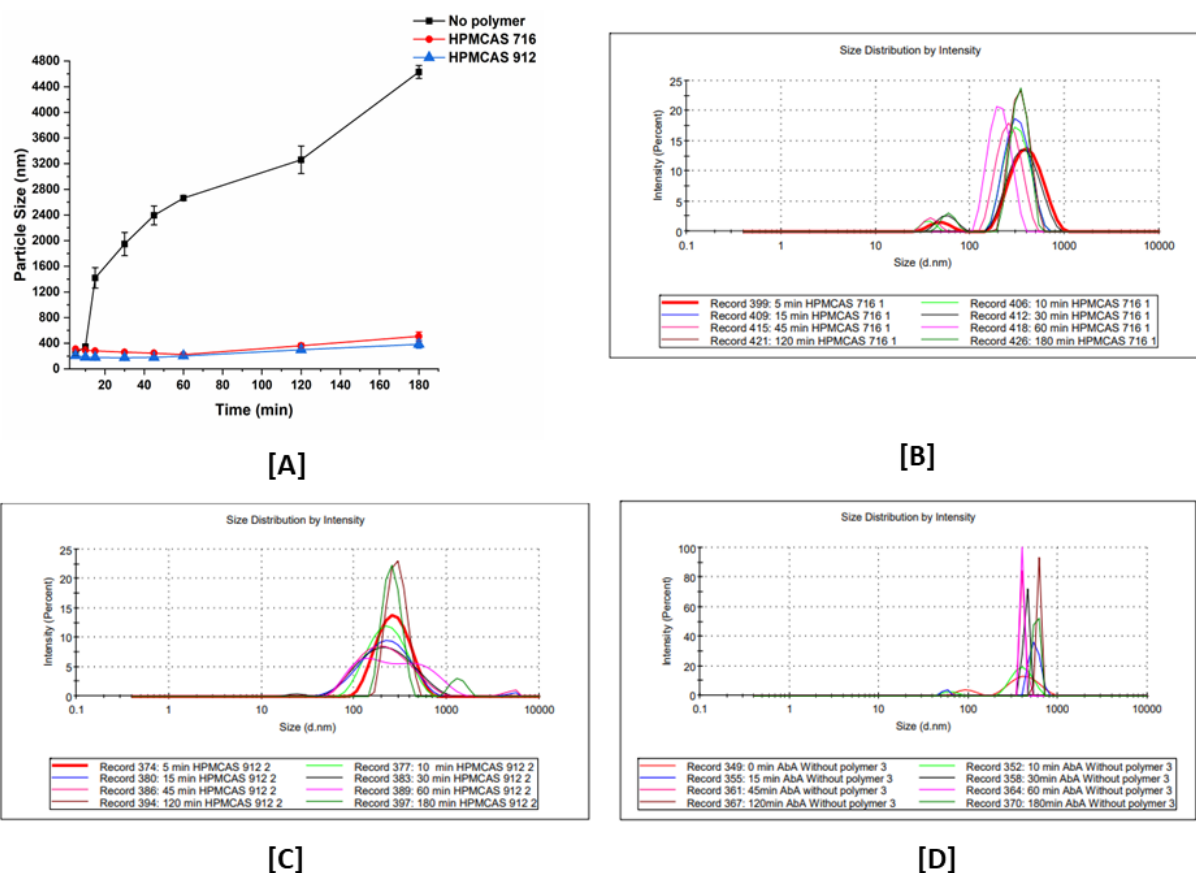


**Figure 5.6.** [A] Particle size graph of supersaturated ABTA in FaSSIF (pH 6.5) in the presence of pre-dissolved HPMCAS 716 and 912 (mean  $\pm$  S.D, n = 3); Evolution of particle size during supersaturation condition; [B] in the presence of HPMCAS 716; [C] in the presence of HPMCAS 912 [D] in the absence of HPMCAS 716 and 912

## 5.16.Characterization of the developed formulation

### 5.16.1. Differential Scanning Calorimetry

The thermograms of free ABTA bulk powder, HPMCAS 716, HPMCAS 912, Lactose monohydrate, ABTA-PM, and ABTA-SD are represented in Figure 5.7 [A]. The thermogram of the free ABTA bulk powder showed an endothermic peak at 147.16 °C corresponding to its melting point of ABTA, indicating its crystalline nature. The HPMCAS 716 and 912 displayed the glass transition temperature ( $T_g$ ) at 112.06 °C and 130.83 °C respectively. The lactose monohydrate displayed two prominent endothermic peaks; one signifies the dehydration of lactose at 146.04°C, and the other at 218.28 °C corresponds to the melting of lactose. The ABTA-PM showed the



endothermic peak of ABTA/lactose monohydrate. However, the endothermic peak disappeared in ABTA-SD, indicating the transformation of the ABTA from crystal form to amorphous form. However, the F2 and F5 formulations showed the endothermic peak corresponding at 146.04°C and 218.28 °C to the lactose monohydrate, not the ABTA. Additionally, ABTA-SD prepared with HPMCAS 716 and 912, excluding lactose monohydrate, exhibited the absence of the ABTA endothermic peak in the thermogram, as illustrated in Figure 5.7 [B]. This confirms that the endothermic peak observed in the F2 and F5 formulations originated from lactose monohydrate. Generally, reducing the crystallinity of a drug enhances its dissolution and solubility since less energy is needed to disrupt the crystal lattice.

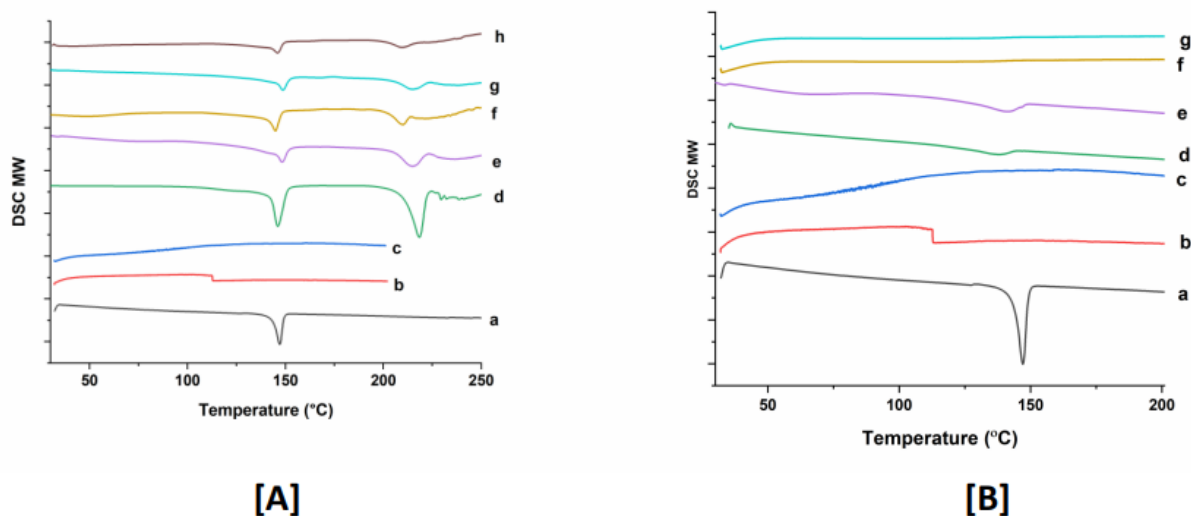


**Figure 5.7.** DSC thermogram of [A] (a) ABTA; (b) HPMCAS 716; (c) HPMCAS 912; (d) Lactose monohydrate; (e) P2; (f) P5; (g) F2; (h) F5; [B] (a) ABTA; (b) HPMCAS 716; (c) HPMCAS 912; (d) ABTA: HPMCAS 716 PM without lactose monohydrate; (e) ABTA: HPMCAS 912 PM without lactose monohydrate; (f) ABTA: HPMCAS 716 SD without lactose monohydrate; (g) ABTA: HPMCAS 912 SD without lactose monohydrate.

### 5.16.2. Powder X-ray Diffraction

The PXRD patterns of free ABTA, HPMCAS 716, HPMCAS 912, lactose monohydrate, ABTA-PM, and ABTA-SD formulation are shown in Figure 5.8 [A and B]. ABTA powder exhibited multiple distinctive peaks at 12.1°, 14.9°, 15.2°, 16.05°, 18.4°, 19.07°, and 21.8° which indicated the crystallinity of ABTA. Furthermore, HPMCAS 716 and HPMCAS 912 exhibited the amorphous PXRD pattern, while lactose monohydrate showed a crystalline PXRD pattern with

distinctive peaks at  $12.5^\circ$  and  $16.5^\circ$ . ABTA-PM showed the characteristics peak of both ABTA and lactose monohydrate in Figure 5.8 [B]. The diffraction peaks specific to ABTA disappeared completely, leaving only the distinctive diffraction peaks of lactose monohydrate (in the blue line). It suggests the amorphous dispersion of ABTA in ABTA SD, as shown in Figure 5.8 [A], which aligns well with the findings from the DSC results.

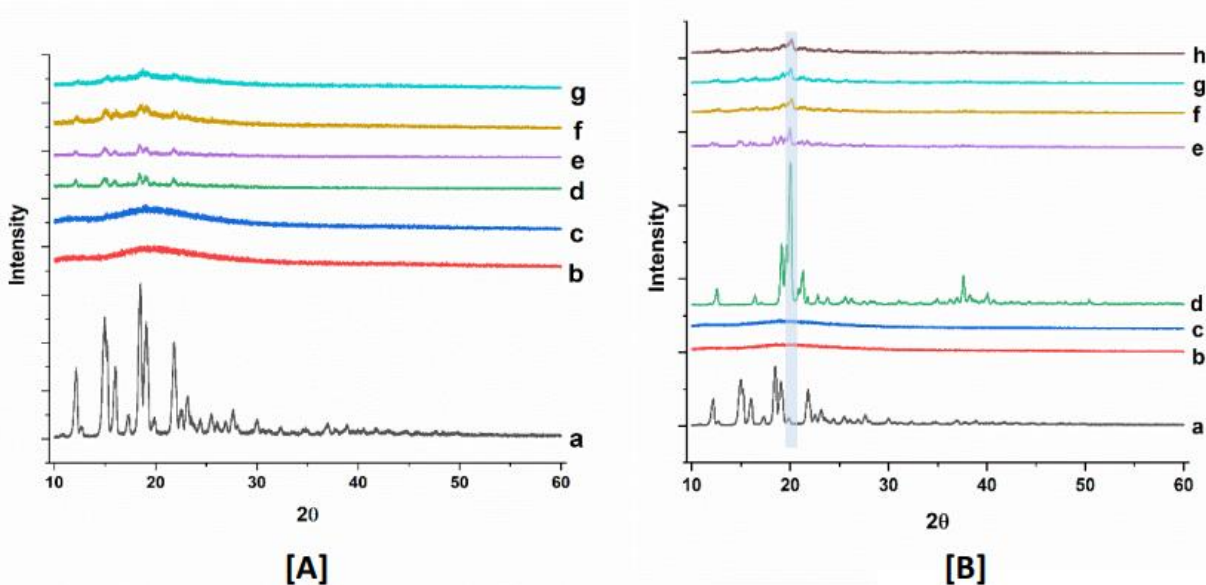


**Figure 5.8.** PXRD pattern of [A] (a) ABTA; (b) HPMCAS 716; (c) HPMCAS 912; (d) PM of ABTA with HPMCAS 716 without lactose monohydrate (e) PM of ABTA with HPMCAS 912 without lactose monohydrate (f) SD of ABTA with HPMCAS 716 without lactose; (g) SD of ABTA with HPMCAS 912 without lactose monohydrate; [B] (a) ABTA; (b) HPMCAS 716; (c) HPMCAS 912; (d) Lactose monohydrate; (e) P2; (f) P5; (g) F2; (h) F5

### 5.16.3. Thermal Gravimetric analysis

The thermo-gravimetric (TGA) profiles of ABTA, HPMCAS 716, HPMCAS 912, lactose monohydrate, ABTA-PM, and ABTA-SD are illustrated in Figure 5.9. TGA experiments were carried out to verify the impact of moisture or residual solvent on the SD systems. This analysis offers insights into storage and stability and unveils potential incompatibilities between the drug and excipients. Here, the studies revealed that ABTA, HPMCAS 716, HPMCAS 912, lactose monohydrate, ABTA-PM, and ABTA-SD were thermally stable within  $300^\circ\text{C}$ , which indicated that ABTA does not show any degradation and incompatibilities between the drug and excipients. Additionally, no trace of residual solvent (acetone) was observed in the ABTA-SD system

prepared using the solvent granulation method.

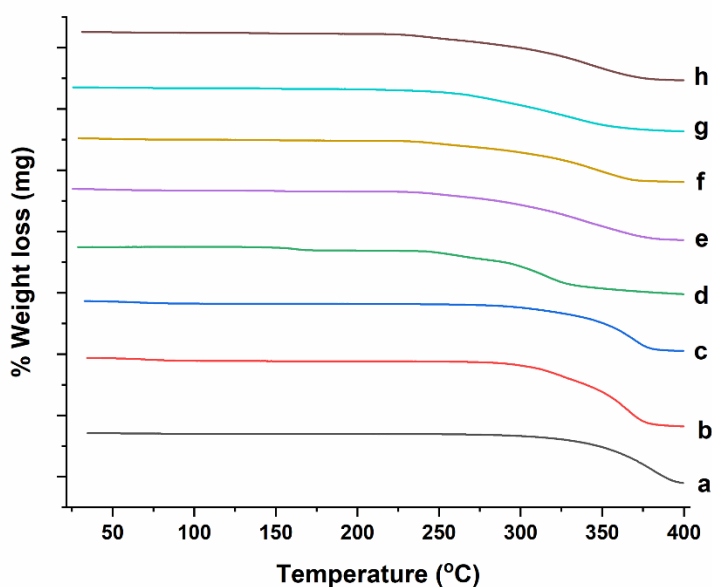


**Figure 5.9.** TGA of (a) ABTA; (b) HPMCAS 716; (c) HPMCAS 912; (d) Lactose monohydrate; (e) P2; (f) P5; (g) F2; (h) F5

#### 5.16.4. Attenuated total reflectance Fourier transform infrared spectroscopy (ATR-FTIR)

The ATR-FTIR of ABTA, HPMCAS 716, HPMCAS 912, lactose monohydrate, ABTA-PM, and ABTA-SD were obtained to investigate the physicochemical interaction between ABTA and carriers in the SD formulation as illustrated in Figure 5.10. The characteristic absorption bands of crystalline ABTA are depicted at  $1731\text{ cm}^{-1}$ ,  $1533\text{ cm}^{-1}$ , and  $1240\text{ cm}^{-1}$ , which corresponds to the C=O stretching, C=N stretching (pyridine ring vibration), and C-O stretching, respectively. The IR spectra of HPMCAS 716 and HPMCAS 912 showed characteristic peaks at  $3606\text{ cm}^{-1}$ ,  $2358\text{ cm}^{-1}$ ,  $1745\text{ cm}^{-1}$ ,  $1646\text{ cm}^{-1}$ , and  $1455\text{ cm}^{-1}$ , which resembles the O-H stretching, C-O stretching, C=O stretching, C=C stretching, and CH<sub>3</sub> stretching respectively. Meanwhile, the IR spectra of lactose monohydrate displayed O-H stretching at  $3280\text{ cm}^{-1}$  (broad peak) and doublet peak at  $1070\text{ cm}^{-1}$  and  $1030\text{ cm}^{-1}$ , respectively, corresponding to the C-C stretching. PM (P2 and P5) of ABTA/HPMCAS 716/912/lactose monohydrate presented all the leading bands of the three compounds. Furthermore, the intensity decreases, and disappearances of ABTA peak in the IR spectrum of ABTA SD suggest molecular interactions, potentially involving hydrogen bonding between ABTA and HPMCAS.

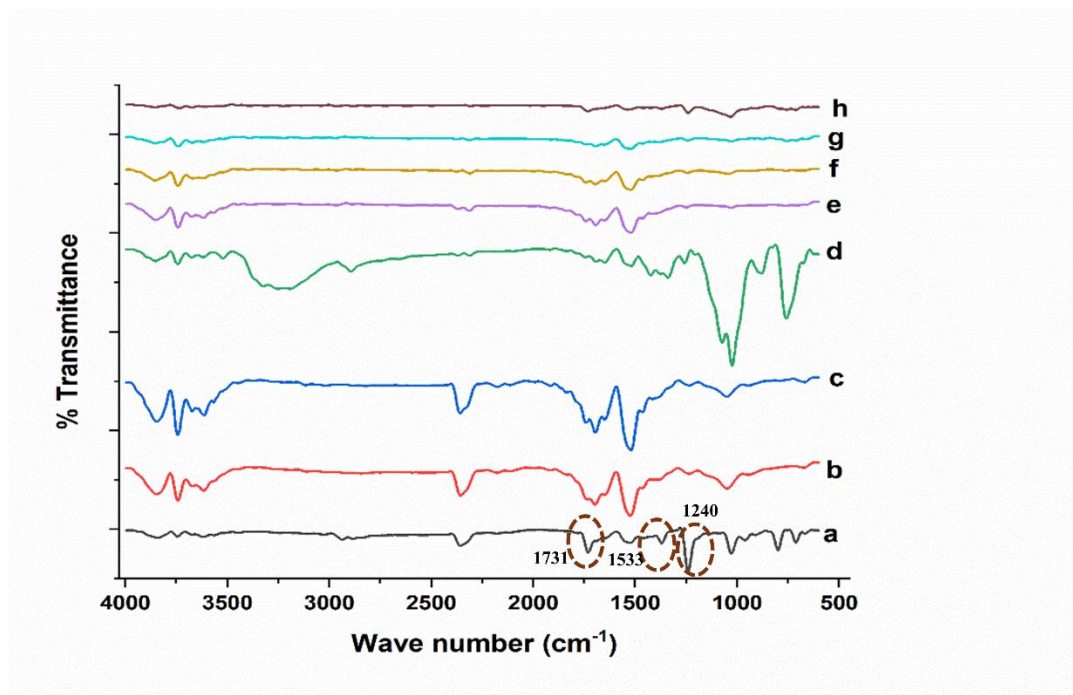


**Figure 5.10.** FTIR-ATR Spectra of (a) ABTA; (b) HPMCAS 716; (c) HPMCAS 912; (d) Lactose monohydrate; (e) P2; (f) P5; (g) F2; (h) F5

#### 5.16.5. Field emission-scanning electron microscopy (FE-SEM)

The ABTA and ABTA-SD surface morphologies were evaluated using FE-SEM and are represented in Figure 5.11. ABTA was observed as irregularly shaped crystals, indicating a crystalline form, while in the case of optimized ABTA with HPMCAS 716 (F2) and HPMCAS 912 (F5) SD formulation showing irregularly shaped without the existence of the crystals of ABTA fragments, which signifies the transformation of the crystalline drug form into the amorphous state during the formation of ABTA SD with HPMCAS.

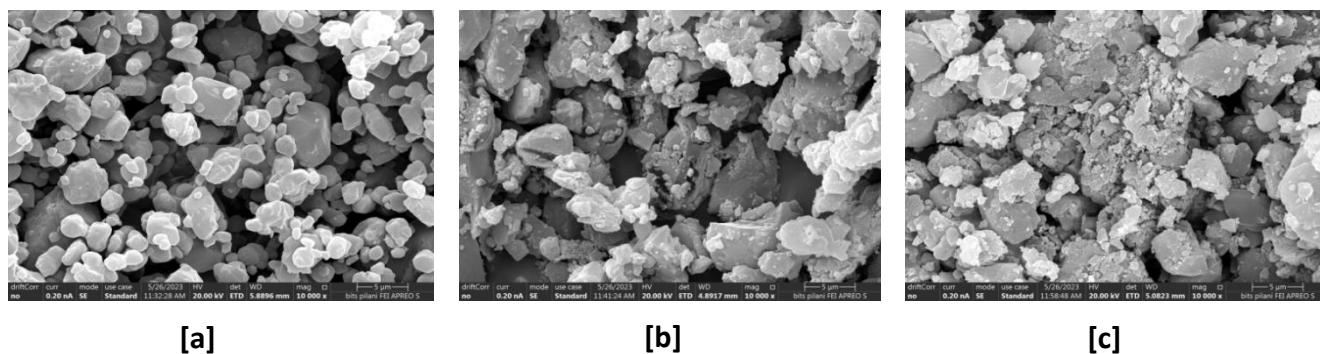


**Figure 5.11.** FE-SEM images of [a] ABTA; [b] F2; and [c] F5

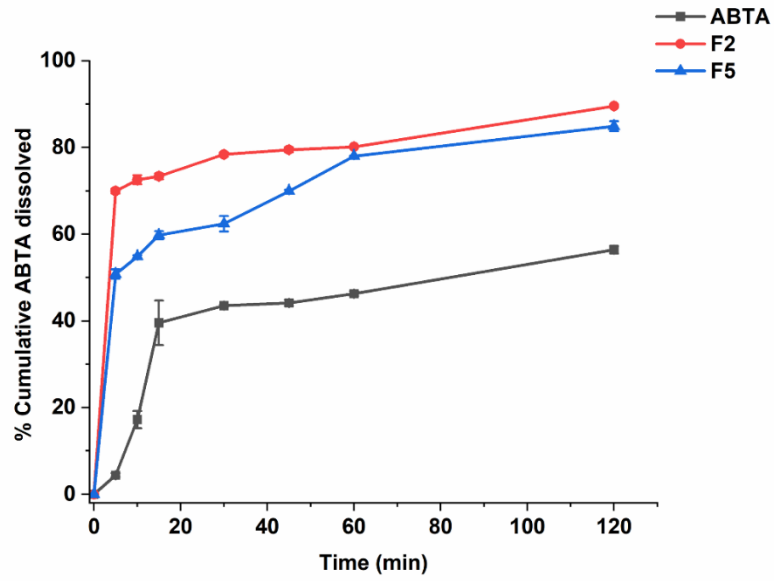
## 5.17. Dissolution studies

### 5.17.1. In-vitro dissolution studies

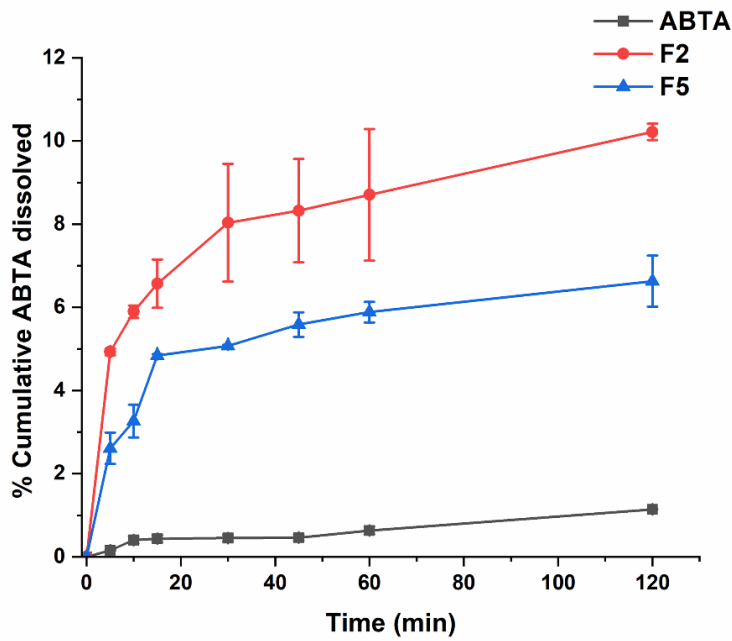
In-vitro dissolution experiments were undertaken to examine the improved drug-dissolved patterns of the SD formulation compared to free ABTA. Assessing the dissolution behavior of the SD formulation provides insights into their potential performance in vivo. The in-vitro dissolution profiles of the crystalline ABTA and ABTA SD were evaluated across various pH conditions, including pH 1.2, pH 6.8, and pH 4.5, as shown in Figure 5.12. Free ABTA showed an inadequate dissolution rate, with only 1.14 % at pH 6.8 and 56.41% at pH 1.2 after 120 min. Furthermore, according to the monograph, the in-vitro dissolution profile of ABTA was specified at pH 4.5 with 0.25% SLS; however, only 58.39 % of ABTA was dissolved after 120 min. These findings suggest potential factors contributing to this poor dissolution behavior, such as poor wettability and particle agglomeration, evidenced by the observed floating of the drug powder on the media's surface. Therefore, improving the dissolution behavior of ABTA is imperative to facilitate rapid and high absorption. From Figure 5.12, ABTA SDs have considerably increased the dissolution rate of ABTA compared to the free ABTA in all buffer media. In pH 1.2, the dissolution rate of ABTA of F2 and F5 SD formulations was 89.54 % and 84.88 % in 120 min, suggesting that drug dissolution significantly increased by 1.58 and 1.50 times compared to the Free ABTA shown in Figure 5.12 [A]. In pH 6.8, the dissolution rate of ABTA of F2 and F5 SD formulations was 10.22 % and 6.33% in 120 min, shown in Figure 5.12 [B], suggesting that drug dissolution increased by 8.97 and 5.61 times compared to the Free ABTA.

When the dissolution of ABTA SD F2 and F5 formulation was performed in pH 4.5, rapid dissolution of the drug from the SD formulation occurred, reaching an initial plateau within 5 min, the maximum drug dissolved of 83.75 % in F2 and 73.52 % in F5 was obtained in 15min, and at the end of 120 min, 88.25 % in F2 and 80.02 % in F5 was observed compared to the crystalline ABTA shown in Figure 5.12 [C]. However, the F2 formulation exhibited superior drug dissolution compared to the F5 formulation, attributed to the variance in the HPMCAS polymer grades—specifically 716 and 912. A more significant dissolution of ABTA was noted with HPMCAS 716 compared to HPMCAS 912, highlighting the significant influence of acetate and succinate substitution. The degree of succinate substitution in HPMCAS directly correlates with dissolution; thus, higher succinate substitution yields increased dissolution. HPMCAS 716, with 14-18%

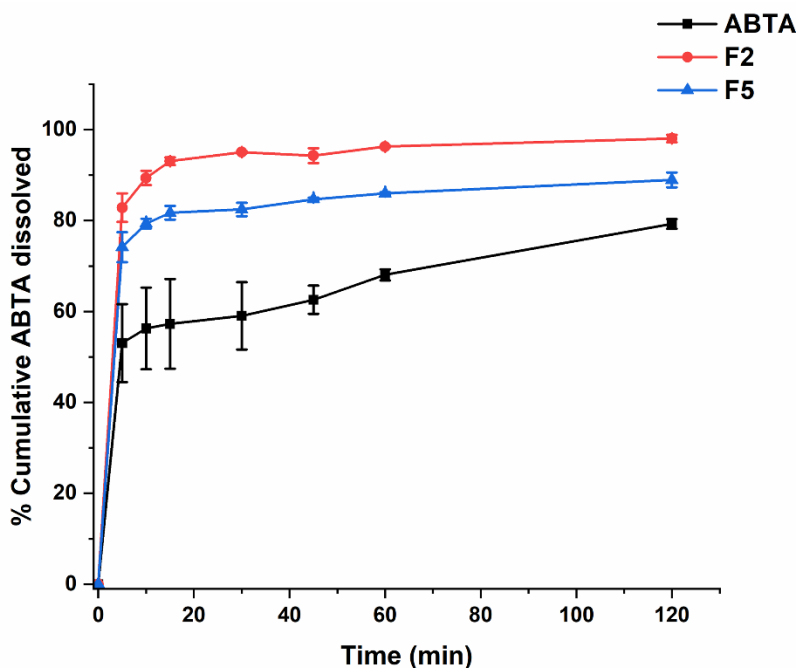
succinate substitution, demonstrated enhanced dissolution relative to HPMCAS 912, which contains 10-14% succinate substitution.



[A]



[B]



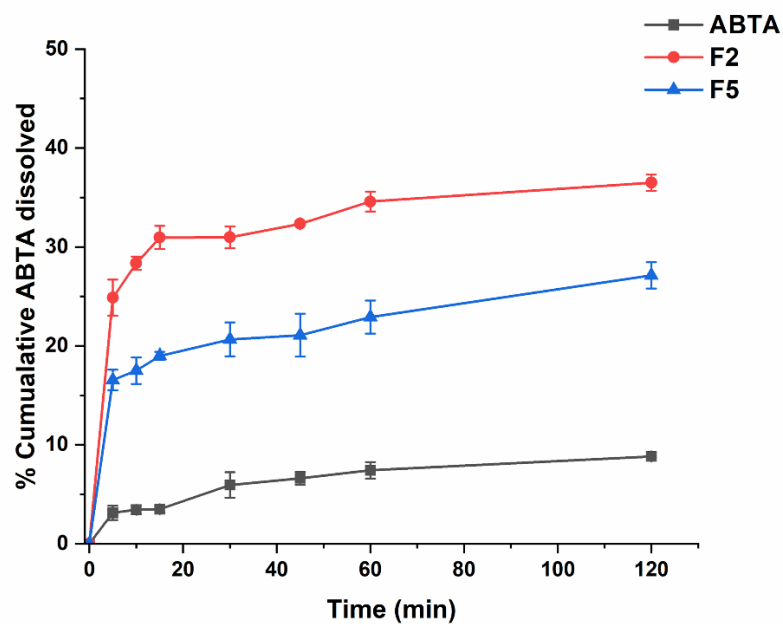
[C]

**Figure 5.12.** The in-vitro dissolution profile of ABTA and SD formulation (F2 and F5) in different buffer media [A] pH 1.2 [B] pH 6.8; [C] pH 4.5

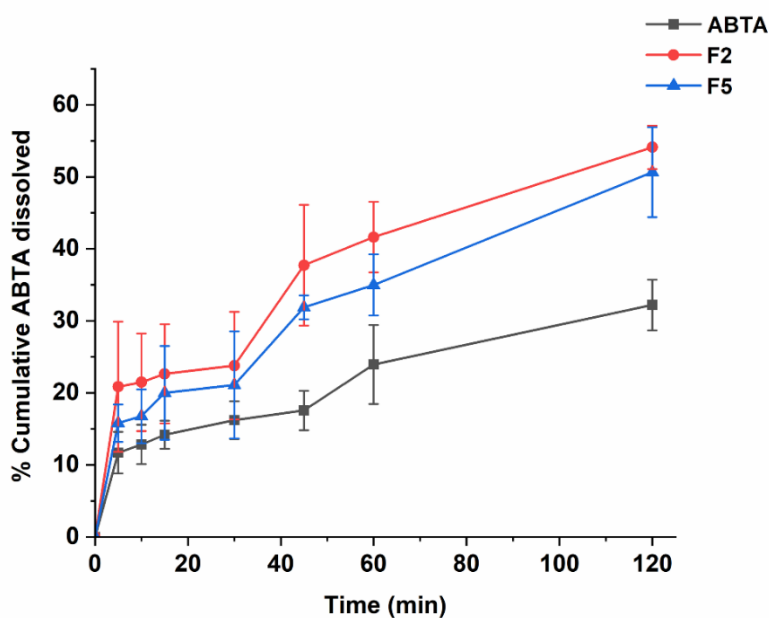
### 5.17.2. Biorelevant dissolution studies

Bio-relevant dissolution studies can be critical when a drug shows a food effect. The food effects refer to the influence of the food on the absorption and pharmacokinetics of a drug after oral administration. Given that ABTA exhibits a food effect, it is imperative to investigate its dissolution under varied food conditions. Here, biorelevant dissolution profiles of the crystalline ABTA and ABTA SD were evaluated in FaSSIF (pH 6.5) and FeSSIF (pH 5.0), as shown in Figure 5.13 [A and B]. When the dissolution of ABTA of F2 and F5 SD formulation was performed in FaSSIF (pH 6.5) and FeSSIF (pH 5.0), the drug rapidly dissolved from the SD formulation. In the case of FaSSIF dissolution media, the highest drug dissolved of 36.50 % in F2 and 27.13 % in F5 was obtained in 120 min, suggesting that the drug dissolution was increased by 4.13 and 3.07 times compared to the crystalline ABTA. Furthermore, in FeSSIF dissolution media, the highest drug dissolved of 54.10 % in F2 and 50.64 % in F5 was obtained in 120 min, suggesting that the drug dissolution was increased by 1.68 and 1.58 times compared to the crystalline ABTA. The F2 formulation shows higher drug dissolution in both the media FaSSIF and FeSSIF compared to the

F5 due to the succinoyl substitution.



[A]



[B]

**Figure 5.13.** In-vitro dissolution profile of ABTA and SD formulation [F2 and F5] in different buffer media [A] FaSSIF (pH 6.5); [B] FeSSIF (pH 5.0)



### 5.17.3. Mathematical analysis of in-vitro and bio-relevant dissolution data

The dissolution parameters, such as R<sup>2</sup>-adjusted, DE, MDT, AIC, and MSC, were calculated using the Microsoft Excel add-in DDSolver for both ABTA and the optimized formulation ABTA-SD (F2 and F5) across various dissolution media. The results are summarized in Table 5.5. It was observed that the dissolution models for the free ABTA and optimized ABTA-SD formulations (F2 and F5) demonstrated a better fit with the Korsmeyer Peppas models in pH 1.2, pH 4.5, pH 6.8, FaSSIF, and FeSSIF respectively as detailed in Table 5.8. The DE for the optimized ABTA-SD formulation (F2 and F5) was higher than the free ABTA, whereas the MDT for the optimized formulation of ABTA SD (F2 and F5) had a faster rate of dissolution than the free ABTA, as illustrated in Table 5.8.

**Table 5.8.** Dissolution parameters of ABTA and ABTA SD in dissolution media

Formulation	Model	R <sup>2</sup> -adjusted	AIC	MSC	MDT	DE
<b>Dissolution media</b>		<b>pH 1.2</b>				
ABTA	Korsmeyer Peppas	0.8284	53.02	1.05	27	0.437
F2	Korsmeyer Peppas	0.9961	27.32	3.40	13.85	0.792
F5	Korsmeyer Peppas	0.9839	37.39	2.58	19.42	0.711
<b>Dissolution media</b>		<b>pH 4.5</b>				
ABTA	Korsmeyer Peppas	0.9963	22.36	3.45	7.91	0.599
F2	Korsmeyer Peppas	0.9966	27.68	3.38	5.96	0.860
F5	Korsmeyer Peppas	0.9988	17.19	4.47	7.73	0.768
<b>Dissolution media</b>		<b>pH 6.8</b>				
ABTA	Korsmeyer Peppas	0.8979	-17.18	1.73	50.98	0.007
F2	Korsmeyer Peppas	0.9672	27.68	2.12	22.31	0.083
F5	Korsmeyer Peppas	0.9661	17.19	2.17	20.87	0.055
<b>Dissolution media</b>		<b>FaSSIF (pH 6.5)</b>				
ABTA	Korsmeyer Peppas	0.9549	11.10	2.16	22.17	0.072
F2	Korsmeyer Peppas	0.9935	17.33	3.13	12.66	0.326

<b>F5</b>	Korsmeyer Peppas	0.9907	14.25	3.04	21.97	0.222
<b>Dissolution media</b>		<b>FeSSIF (pH 5.0)</b>				
<b>ABTA</b>	Korsmeyer Peppas	0.8903	38.25	1.39	29.95	0.242
<b>F2</b>	Korsmeyer Peppas	0.9764	37.05	2.47	25.02	0.402
<b>F5</b>	Korsmeyer Peppas	0.9648	35.21	2.70	28.45	0.341

### 5.18. Preparation of ABTA tablet dosage form from SD and in-vitro dissolution study

The content uniformity of the ABT SD was between the ranges of  $95.50 \pm 4.43\%$  to  $99.34 \pm 2.18\%$ . The ABTA SD tablets were fabricated through dry granulation, wherein excipients and ABTA SD were blended and sieved through mesh #40 before compression. ABTA tablet was prepared from the ABTA SD of F2 formulation (F17), ABTA SD of F5 formulation (F18), and in-house prepared tablet of free ABTA without the use of HPMCAS 716 and 912 polymers (F21). The ABTA SD tablet composition is shown in Table 5.9.

**Table 5.9.** The composition of the ABTA SD tablet from ABTA SD

	F17	F18	F21
<b>Element</b>	<b>Weigh (mg)</b>	<b>Weigh (mg)</b>	<b>Weigh (mg)</b>
SD of ABTA (F2)	435	-	-
SD of ABTA (F5)	-	467	-
ABTA	-	-	100
Lactose monohydrate	-	-	335
Startab	185	185	185
Colloidal Silicon dioxide	15	15	15
Magnesium stearate	15	15	15

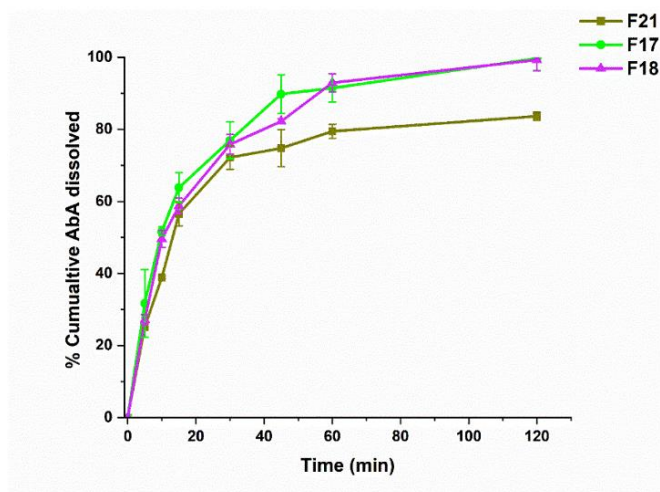


**Figure 5.14.** In-vitro dissolution profile of in-house prepared ABTA tablet (F21) and ABTA SD tablet dosage form prepared from SD (F17) and (F18) in pH 4.5

The ABTA SD tablets of F17 and F18 exhibited more excellent dissolution rates than the in-house prepared ABTA tablets of F21, as illustrated in Figure 5.14. Dissolution parameters, including  $R^2$ -adjusted, DE, MDT, AIC, and MSC, using Microsoft Excel add-in DDSolver for in-house prepared tablets (F21), ABTA SD of F2 formulation (F17), and ABTA SD of F5 formulation (F18) in different dissolution media summarized in Table 5.10. It was observed that the dissolution models for the ABTA SD of F2 formulation (F17) and ABTA SD of F5 formulation (F18) demonstrated a better fit with the first-order models, whereas in-house prepared tablets (F21) good fit with the Korsmeyer Peppas model in pH 4.5. Furthermore, optimized ABTA-SD formulation (F17) and ABTA-SD formulation (F18) showed higher dissolution efficiency than an in-house prepared tablet (F21), shown in Table 5.10

**Table 5.10.** Dissolution parameter of ABTA SD tablet in pH 4.5 dissolution media

Formulation	Model	$R^2$ -adjusted	AIC	MSC	MDT	DE
F21	Korsmeyer Peppas	0.9193	52.58	1.55	17.43	0.715
F17	First order	0.9785	43.32	2.92	19.93	0.831
F18	First order	0.9753	44.37	2.84	21.08	0.818

### 5.19. Stability studies of the developed formulation

Physical stability is a significant challenge in the development of SD. Ensuring good miscibility

between the drug and polymer, as well as enhancing drug-polymer interactions, is crucial for improving SD stability. After 90 days of stability studies, selected ABTA SD formulations (F2 and F5) were analyzed using physical characteristics, drug content, DSC, and PXRD, with results compared to initial results. The optimized formulation showed no change in color over the 90 days compared to the initial results. The % assay of the optimized formulation remained within the range of  $95.38 \pm 0.389$  to  $101.45 \pm 1.345$  after 90 days of the stability study. The DSC thermograms and PXRD patterns at 0 days and 90 days under accelerated conditions are shown in Figure 5.15. These stability studies confirmed that the ABTA did not recrystallize, and the ABTA SD (F2 and F5) formulations remained in an amorphous form for the entire 90-day period under accelerated conditions, as illustrated in Figure 5.15.

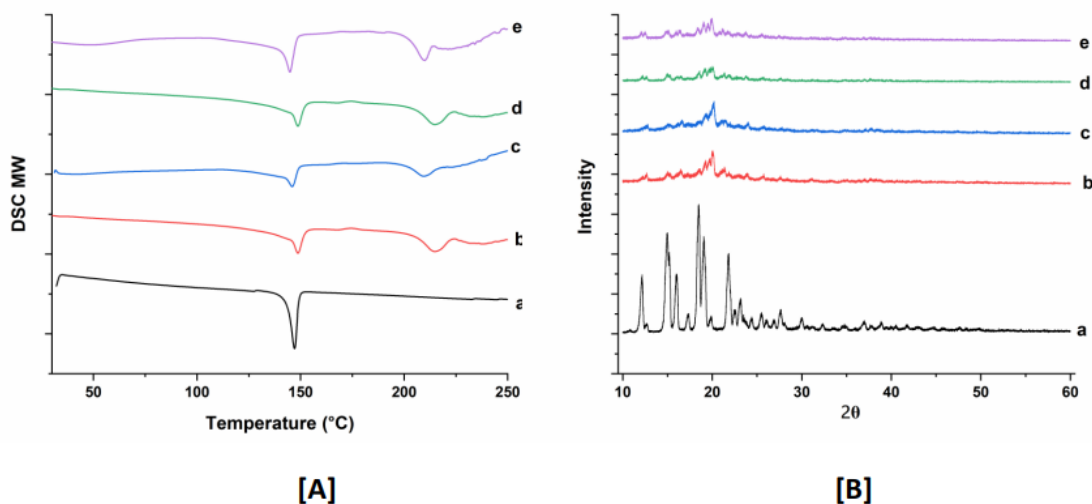


**Figure 5.15.** DSC thermogram [A] and PXRD patterns [B] of (a) ABTA; (b) F2 (0 days); (c) F5 (0 days); (d) F2 (90 days); (e) F5 (90 days)

### 5.20. Conclusion

Formulating SD has emerged as a promising approach to enhancing the pharmaceutical properties of poorly water-soluble active pharmaceutical ingredients. A stable SD of ABTA was effectively developed using HPMCAS polymer. Given its favorable dissolution characteristics, the formulation containing ABTA: HPMCAS: lactose monohydrate in a ratio of 1:2:1 is anticipated to serve as a novel formulation for oral absorption. The Hansen solubility parameters suggest that the solubility parameter ( $\Delta\delta$ ) between the ABTA and HPMCAS was below  $7 \text{ MPa}^{1/2}$ , suggesting

good miscibility. HPMCAS is one of the best precipitation inhibitors for maintaining the supersaturation of ABTA, demonstrating the spring and parachute phenomenon. The DSC, PXRD, and FTIR studies confirmed the amorphization of the ABTA during the SD formation. The in-vitro dissolution study showed that the dissolution rate of ABTA SD was enhanced in all dissolution media compared to free ABTA. The stability investigation revealed that ABTA SD did not transform into a crystalline form, potentially attributed to the superior crystal inhibition property of HPMCAS.

**References**

1. Stappaerts J, Geboers S, Snoeys J, Brouwers J, Tack J, Annaert P, et al. Rapid conversion of the ester prodrug abiraterone acetate results in intestinal supersaturation and enhanced absorption of abiraterone: In vitro, rat in situ and human in vivo studies. *European Journal of Pharmaceutics and Biopharmaceutics*. 2015;90:1–7.
2. Acharya M, Bernard A, Gonzalez M, Jiao J, De Vries R, Tran N. Open-label, phase I, pharmacokinetic studies of abiraterone acetate in healthy men. *Cancer Chemotherapy and Pharmacology*. 2012;69(6):1583–1590.
3. Attard G, Reid AHM, Auchus RJ, Hughes BA, Cassidy AM, Thompson E, et al. Clinical and Biochemical Consequences of CYP17A1 Inhibition with Abiraterone Given with and without Exogenous Glucocorticoids in Castrate Men with Advanced Prostate Cancer. *The Journal of Clinical Endocrinology & Metabolism*. 2012;97(2):507–516.
4. Schultz HB, Meola TR, Thomas N, Prestidge CA. Oral formulation strategies to improve the bioavailability and mitigate the food effect of abiraterone acetate. *International Journal of Pharmaceutics*. 2020;577:119069.
5. Solymosi T, Ötvös Z, Angi R, Ordasi B, Jordán T, Semsey S, et al. Development of an abiraterone acetate formulation with improved oral bioavailability guided by absorption modeling based on in vitro dissolution and permeability measurements. *International Journal of Pharmaceutics*. 2017;532(1):427–434.
6. Chi KN, Spratlin J, Kollmannsberger C, North S, Pankras C, Gonzalez M, et al. Food effects on abiraterone pharmacokinetics in healthy subjects and patients with metastatic castration-resistant prostate cancer. *Journal of Clinical Pharmacology*. 2015;55(12):1406–1414.
7. Silveira RG, Cunha BN, Tenório JC, Alves de Aguiar DV, da Cruz Souza P, Vaz BG, et al.

- A simple alternative to prodrug: The hydrochloride salt monohydrate of the prostate anticancer drug abiraterone. *Journal of Molecular Structure*. 2019;1190:165–170.
8. Baghel S, Cathcart H, O'Reilly NJ. Polymeric Amorphous Solid Dispersions: A Review of Amorphization, Crystallization, Stabilization, Solid-State Characterization, and Aqueous Solubilization of Biopharmaceutical Classification System Class II Drugs. *Journal of Pharmaceutical Sciences*. 2016;105(9):2527–2544.
  9. Ueda K, Higashi K, Yamamoto K, Moribe K. The effect of HPMCAS functional groups on drug crystallization from the supersaturated state and dissolution improvement. *International Journal of Pharmaceutics*. 2014;464(1):205–213.
  10. Ravikumar AA, Kulkarni PK, Osmani RAM, Hani U, Ghazwani M, Fatease A Al, et al. Carvedilol Precipitation Inhibition by the Incorporation of Polymeric Precipitation Inhibitors Using a Stable Amorphous Solid Dispersion Approach: Formulation, Characterization, and In Vitro In Vivo Evaluation. *Polymers*. 2022;14(22):4977.
  11. Warren DB, Benameur H, Porter CJH, Pouton CW. Using polymeric precipitation inhibitors to improve the absorption of poorly water-soluble drugs: A mechanistic basis for utility. *Journal of Drug Targeting*. 2010;18(10):704–731.
  12. Jha DK, Shah DS, Amin PD. Effect of Hypromellose Acetate Succinate Substituents on Miscibility Behavior of Spray-dried Amorphous Solid Dispersions: Flory–Huggins Parameter Prediction and Validation. *Carbohydrate Polymer Technologies and Application*. 2021;2:100137.
  13. Ueda K, Higashi K, Yamamoto K, Moribe K. Inhibitory effect of hydroxypropyl methylcellulose acetate succinate on drug recrystallization from a supersaturated solution assessed using nuclear magnetic resonance measurements. *Molecular Pharmaceutics*. 2013;10(10):3801–3811.
  14. Simões MF, Pereira A, Cardoso S, Cadonau S, Werner K, Pinto RMA, et al. Five-Stage Approach for a Systematic Screening and Development of Etravirine Amorphous Solid Dispersions by Hot-Melt Extrusion. *Molecular Pharmaceutics*. 2020;17(2):554–568.
  15. Greenhalgh DJ, Williams AC, Timmins P, York P. Solubility parameters as predictors of miscibility in solid dispersions. *Journal of Pharmaceutical Sciences*. 1999;88(11):1182–1190.
  16. Mukesh S, Joshi P, Bansal AK, Kashyap MC, Mandal SK, Sathe V, et al. Amorphous Salts

- Solid Dispersions of Celecoxib: Enhanced Biopharmaceutical Performance and Physical Stability. *Molecular Pharmaceutics*. 2021;18(6):2334–2348.
17. Van Krevelen DW, Te Nijenhuis K. Cohesive Properties and Solubility. Vol. i, Properties of Polymers. 2009. 189–227.
  18. Zhao Y, Inbar P, Chokshi HP, Malick AW, Choi DS. Prediction of the Thermal Phase Diagram of Amorphous Solid Dispersions by Flory–Huggins Theory. *Journal of Pharmaceutical Sciences*. 2011;100(8):3196–3207.
  19. Butreddy A, Sarabu S, Almutairi M, Ajjarapu S, Kolimi P, Bandari S, et al. Hot-melt extruded hydroxypropyl methylcellulose acetate succinate based amorphous solid dispersions: Impact of polymeric combinations on supersaturation kinetics and dissolution performance. *International Journal of Pharmaceutics*. 2022;615:121471.
  20. Choudhari M, Donthi M, Damle S, Singhvi G, Saha R, Dubey S. Implementation of Quality by Design Approach for Optimization of RP-HPLC Method for Quantification of Abiraterone Acetate in Solid Dispersion in Forced Degradation Studies. *Current Chromatography*. 2022;09(1):2213-2414.
  21. Choudhari M, Damle S, Narayan R, Sunil S, Dubey K, Singhvi G. Emerging Applications of Hydroxypropyl Methylcellulose Acetate Succinate : Different Aspects in Drug Delivery and Its Commercial Potential. *AAPS PharmSciTech*. 2023;1–26.
  22. Ueda K, Higashi K, Yamamoto K, Moribe K. The effect of HPMCAS functional groups on drug crystallization from the supersaturated state and dissolution improvement. *International Journal of Pharmaceutics*. 2014;464(1–2):205–213.

**Chapter 6: Formulation of**  
**Abiraterone acetate-HPMC HME-**  
**based Solid Dispersion**



**6.0. Introduction**

The characteristics and limitations of ABTA, along with the shortcomings of existing research, are addressed in Chapters 1 and 5. Among all the existing approaches, amorphous solid dispersion (SD) with polymeric carriers, where the drug can be dispersed in the polymeric matrix in an amorphous state, is a particularly effective strategy for significantly enhancing the solubility and bioavailability of ABTA. Solvent evaporation, spray drying, and KinetiSol have been employed as typical methodologies for the preparation of ABTA SD in recent years (1). Consequently, the Hot melt extrusion (HME) method was used for the manufacturing of the SD of ABTA for the first time explored with the polymeric carriers. HME is a suitable technique for large-scale industrial manufacturing and has recently gained considerable attention in the pharmaceutical industry due to its versatility, continuous operation, cost-effectiveness, and solvent-free process technology (2,3).

The prevalence of poorly soluble drugs in development pipelines and commercial products drives the formulator to select HME to prepare SDs. HME involves vigorous mixing of the molten API with polymeric carriers under the optimized temperature, yielding a uniformly dispersed product with anticipated characteristics (4). Critical considerations in HME include the glass transition temperature ( $T_g$ ) of the polymeric carriers and the melting temperature of the API. The interaction between the API and polymeric carriers is vital to prevent API recrystallization. Several parameters affect the quality of extruded products, such as drug-polymer ratios, extrusion temperature, screw rotating speed, and materials residence time. HME enables the transformation of an API into an amorphous form or dispersing it into highly fine particles. Successful development of bioavailable dispersions through HME requires careful selection of polymeric carriers and thorough assessment of the SD's physicochemical properties, stability, and performance (5).

Cellulosic polymers, HPMC widely utilized in SD development through spray drying and solvent evaporation methods, offered advantages in stabilizing amorphous drugs, enhancing drug release, inhibiting crystalline nucleation, and improving bioavailability (6). It has been observed that conventional HPMC was not suitable for HME due to high  $T_g$  (160 -210 °C) and high melt viscosity, which generates high torque within the extruder during processing and significant color changes at elevated temperatures, which requires unique formulation to overcome the processing

difficulties (7). Current techniques to improve the processability of HPMC often require high levels of plasticizers and aids, which can cause drug crystallization and reduced bioavailability during storage. To address this, Dow Chemical Company introduced HPMC HME, a new grade of HPMC with a lower T<sub>g</sub> (117-128 °C) and improved melt flow, allowing extrusion at lower temperatures while enhancing bioavailability and acting as a precipitation inhibitor after dissolution (8,9).

The objective of the current study was to improve the solubility, dissolution, and bioavailability of the poorly water-soluble ABTA. To achieve this objective, the ABTA SD was prepared via the HME process with the different ratios of ABTA, an HPMC HME, and at different extrusion temperatures (120°C, 140°C, and 160°C). The Hansen solubility parameter method was used to predict the in-silico drug-polymer miscibility before the preparation of SD. Furthermore, the ability of the HPMC HME to improve solubility and inhibit crystallization would also be determined through phase solubility and precipitation inhibition study. The study examined the effect of different grades of HPMC HME (15 LV and 100 LV), and HME process variables on solubility, stability, dissolution, and solid-state characterization using tools such as DSC, PXRD, ATR-FTIR, TGA, and FE-SEM.

### 6.1. Materials and methods

ABTA (purity 99%) was gifted by Biophore India Pharmaceuticals Pvt. Ltd, India. Affinisol™ HPMC HME (15 LV and 100 LV) were supplied as gift samples from Colorcon Asia Pvt. Ltd, India. Soya lecithin and sodium taurocholate were procured from the SRL. Analytical grade HPLC solvents such as acetone, methanol, dichloromethane, and acetonitrile were procured from Merck. All other necessary chemicals were purchased from an approved supplier.

### 6.2. ABTA-polymer miscibility predictions

Drug–polymer miscibility is a critical consideration for the successful formulation of a physically stable SD. Mathematical theories, such as the Hansen solubility parameters and Flory–Huggins interaction parameter ( $\chi$ ), are employed to predict drug-polymer miscibility (10–12).

#### 6.2.1. Hansen solubility parameter approach

The van Krevelen and Hoftyzer group contribution method was used to determine the Hansen solubility parameter ( $\delta$ ) of ABTA using their chemical structure, as shown in Figure 5.1. The three

primary Hansen solubility parameters of ABTA were calculated for each molecule: (i) dispersion forces amongst the molecule ( $\delta_d$ ), (ii) dipolar intermolecular forces amongst the molecule ( $\delta_p$ ), (iii) hydrogen bonding energy amongst the molecule ( $\delta_h$ ). The Hansen solubility parameters for HPMC HME (15 LV and 100LV) (Figure 6.1) were obtained from Dupont Pharma's solution brochure for HPMC HME.

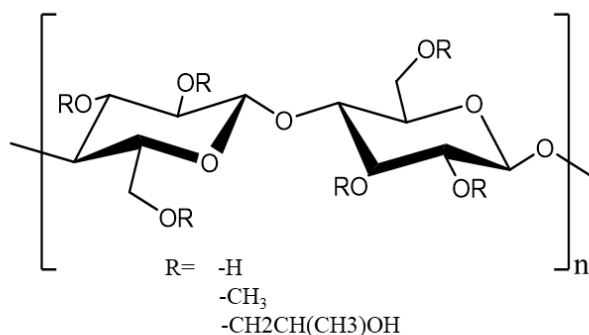


**Figure 6.1.** Structure of HPMC HME

The total solubility parameter ( $\delta_t$ ) is mostly expressed in  $\text{MPa}^{0.5}$ , calculated by grouping all three Hansen parameters shown in equation (6.1).

$$\delta_t^2 = \delta_d^2 + \delta_p^2 + \delta_h^2 \quad (6.1)$$

The  $\delta_d$ ,  $\delta_p$ ,  $\delta_h$  can be calculated by following formulas:

$$\delta_d = \frac{\epsilon F_{di}}{V} \quad (6.2)$$

$$\delta_p = \frac{\sqrt{\epsilon F_{pi}^2}}{V} \quad (6.3)$$

$$\delta_h = \sqrt{\frac{\epsilon E_{hi}}{V}} \quad (6.4)$$

where  $F_{di}$ ,  $F_{pi}$  are molar attraction forces of dispersive interaction, dipole-dipole interaction, and  $E_{hi}$  is hydrogen bonding forces, and  $V$  is the molar volume, respectively.

### 6.2.2. Flory-Huggin's drug-polymer interaction approach

Flory-Huggins (F-H) drug-polymer interaction parameter ( $\chi$ ) is determined by the difference between the solubility parameters of drugs and polymers and calculated using equation 6.5.

$$\chi = \frac{v_{site} (\delta_{polymer} - \delta_{drug})^2}{RT} \quad (6.5)$$

In this equation,  $V_{site}$  represents the hypothetical lattice volume, while  $T$  denotes temperature,  $R$

stands for the gas constant,  $\delta_{\text{drug}}$  and  $\delta_{\text{polymer}}$  signify the solubility parameters of the drug and polymer, respectively. (13).

### 6.3. Precipitation inhibition study

A precipitation inhibition study was conducted to evaluate the effect of HPMC HME in preventing precipitation and maintaining the supersaturation of ABTA. Supersaturation was induced by the addition of 2 mL of ABTA solution (6 mg/mL in methanol) to 100 mL of FaSSIF (pH 6.5) precipitation media. All experiments were conducted at  $37 \pm 0.5^\circ\text{C}$  for 120 min at 200 rpm. In this experiment, the HPMC HME (15LV and 100LV) was pre-dissolved in the precipitation media to assess the potential. In contrast, a precipitation media without polymer was employed as a control. The concentration of ABTA was calculated in the presence and absence of polymer at predetermined time intervals and quantified by the RP-HPLC. HPMC HME was studied at different weight ratios of 1:1, 1:1.5, and 1:2 (ABTA/HPMC HME) in binary mixtures. The particle size of the precipitate was assessed through dynamic light scattering (DLS) using a Malvern Zeta Sizer (Nano ZS, Malvern Instruments, U.K.) as part of the precipitation inhibition study. Samples were removed from the precipitation inhibition study after 10, 30, 60, and 120 min. (14).

### 6.4. Preparation of ABTA-SD via the HME method

The HME formulations, comprising ABTA and HPMC HME, were processed using a HAAKE MiniCTW (Thermo Scientific) equipped with twin rotating screws. Various ratios of ABTA and HPMC HME binary blends were prepared. These PM of ABTA and HPMC HME were then extruded through the 1 mm diameter die at different extrusion temperatures ( $120^\circ\text{C}$ ,  $140^\circ\text{C}$ , and  $160^\circ\text{C}$ ) at 50 rpm speed, and the obtained extrudates were further cooled at room temperature. Table 6.1 displays the compositions of ABTA SD prepared by the HME method. Finally, the extrudates were ground into a powdered form, sieved through a #40 ASTM mesh, and stored in desiccators for subsequent physicochemical characterization.

**Table 6.1:** Compositions of SD of ABTA prepared by HME method

Formulation code	Temperature $^\circ\text{C}$	ABTA: HPMC HME 15LV	ABTA (gm)	HPMC HME 15 LV (gm)
ABTA/SD/1	120			
ABTA/SD/2	140	1:1	2.5	2.5
ABTA/ SD/3	160			

ABTA/SD/4	120			
ABTA/SD/5	140	1:1.5	2	3
ABTA/SD/6	160			
ABTA/SD/7	120			
ABTA/SD/8	140	1:2	1.66	3.33
ABTA/SD/9	160			
<b>Formulation code</b>	<b>Temperature °C</b>	<b>ABTA: HPMC HME 100 LV</b>	<b>ABTA (gm)</b>	<b>HPMC HME 100LV (gm)</b>
ABTA/ SD/10	140	1:1	2.5	2.5
ABTA/ SD/11	160			
ABTA/ SD/12	140	1:2	1.66	3.33
ABTA/ SD/13	160			

## 6.5. Solid state characterization of the developed SD

### 6.5.1. Differential scanning calorimetry (DSC)

The DSC analysis was evaluated to determine the crystallinity, drug-polymer miscibility, melting temperature, and  $T_g$  of free ABTA, HPMC HME, and all ABTA SD formulations. In a nitrogen atmosphere, DSC was performed using the Shimadzu TA 60 DSC system, operated with TA 60 software. The sample, weighing 3-5 mg, was loaded into an aluminum crucible, while an empty pan served as a reference during the measurement. Thermograms were obtained by heating the samples from 30 to 250 °C at the scan rate of 10 °C/min under a nitrogen atmosphere with a flow rate of 50 mL/min

### 6.5.2. Powder X-ray diffraction (PXRD)

The PXRD testing was performed using a Rigaku mini flex II diffractometer with incident radiation of Cu K $\alpha$  produced at 40 kV and 30 mA, applying a scanning rate of 2°/min with a  $2\theta$  range of 10-60°. PXRD was analyzed for crystallinity in the free ABTA, HPMC HME, and all ABTA SD formulations.

### 6.5.3. Attenuated total reflectance fourier transform infrared spectroscopy (ATR-FTIR)

The ATR-FTIR spectra determined the distinguishing possible interactions between the API and polymer. The free ABTA, HPMC HME and all ABTA SD formulations spectrum were recorded using ATR-FTIR spectroscopy (Bruker, USA) operated with Opus software. The spectra were collected in the region from 400-4000  $\text{cm}^{-1}$  with a 1  $\text{cm}^{-1}$  resolution and averaged over 100 scans.

#### **6.5.4. Thermogravimetric analysis**

TGA analysis was conducted utilizing a Shimadzu TA 60 instrument operated with TA 60 software. TGA was employed to assess the stability of the drug/polymer blend. Below 150 °C, any weight reduction was considered dehydration, with the change in weight reflecting the moisture content. Each sample (free ABTA, HPMC HME 15 LV, HPMC HME 100 LV, and ABTA-SD) weighing between 8-10 mg, was loaded into platinum crucibles and subjected to heating from 30 to 400 °C at a rate of 10 °C/min, under a nitrogen atmosphere with a flow rate of 50 mL/min.

#### **6.5.5. Field emission scanning electron microscopy (FE-SEM)**

The FE-SEM determined the morphological behavior of the free ABTA and all ABTA SD formulations. The samples were prepared by mounting them on aluminum stubs and vacuum coating them with gold using a Sputter coating machine (Leica Ultra Microtome EM UC7). Then, the coated samples were placed in the SEM for the morphological analysis.

#### **6.6. Solubility determination of ABTA SD**

For the determination of the solubility, excessive quantities of free ABTA and all ABTA SD formulations prepared from the HME method were introduced into vials containing distilled water, pH 1.2, pH 6.8, FaSSIF, and FeSSIF. These vials were then placed on an orbital shaker and continuously stirred for 8h at a controlled temperature of  $37 \pm 0.5$  °C, allowing equilibrium to be reached. After 8h, precise aliquots of the samples were extracted, filtered, and subsequently subjected to analysis using RP-HPLC. All tests were performed in triplicates.

#### **6.7. Effect on viscosity with change in pH and HPMC HME polymer concentration**

The effect on viscosity with changing pH and varying HPMC HME polymer concentrations (15 LV and 100 LV) was evaluated at 1.33% (w/v) and 2.66% (w/v) in different pH environments, specifically pH 1.2, pH 4.5, pH 6.8, water, FaSSIF (pH 6.5), and FeSSIF (pH 5.0). The HPMC HME dispersion in different pH was evaluated using a Rheometer MCR 91 (Anton Paar). The study was conducted using a parallel plate, and the sample analysis was performed with a sample gap of 0.2 mm at a constant shear rate of  $50 \text{ s}^{-1}$ . The sample temperature was controlled at  $25 \pm 2$  °C.

#### **6.8. Dissolution studies**

##### **6.8.1. In-vitro dissolution studies**

In-vitro dissolution studies of ABTA were performed in dissolution media, such as pH 1.2, and pH 4.5, to evaluate the rate and extent of the drug from the dissolution of SD, and this was compared with the pure drug dissolution. Additionally, the dissolution behavior pattern in these various media was investigated. Specifically, for the pH 4.5 dissolution media, 0.25% SLS was incorporated, as per its specification in the official monograph of ABTA. ABTA showed solution stability in pH 1.2 and pH 4.5 dissolution media. The USP II apparatus was employed for the dissolution testing. Numerous researchers have utilized smaller volumes and modified apparatus for drug dissolution studies. Therefore, in our investigations, an in-house modified USP II dissolution apparatus was utilized to examine drug dissolution from both the SD and pure drug. In brief, equivalent to 10 mg of free ABTA and all ABTA SD samples were added to 250 mL of pH 1.2 and pH 4.5 with 0.25 % SLS maintained at 37 °C and stirred at 150 rpm, and sink conditions were maintained throughout the experiment in both the dissolution media. Samples were withdrawn at predetermined time points (5, 10, 15, 30, 45, 60, and 120 min), and an equal volume of fresh media was added. The withdrawn samples were filtered through a 0.45- $\mu$ m syringe filter and examined using RP-HPLC.

### **6.8.2. Bio-relevant dissolution studies**

Given that ABTA exhibits a food effect, it is imperative to investigate its dissolution under fasted-state simulated intestinal fluid (FaSSIF, pH 6.5) and fed-state simulated intestinal fluid (FeSSIF, pH 5.0) media. In brief, equivalent to 10 mg of free ABTA and ABTA SD sample was added to 250 mL of FaSSIF and FeSSIF media maintained at 37 °C and stirred at 150 rpm. Samples were collected at scheduled intervals (5, 10, 15, 30, 45, 60, and 120 min), followed by adding an equal volume of fresh media. The collected samples underwent filtration through a 0.45- $\mu$ m syringe filter before being subjected to RP-HPLC analysis.

### **6.8.3. Mathematical analysis of in-vitro and bio-relevant dissolution data**

The dissolution profiles of both free ABTA and the optimized formulation ABTA SD were assessed using several parameters: percent dissolution efficiency (% DE) and mean dissolution time (MDT). Additionally, DD Solver software was used to analyze and evaluate the dissolution profiles by applying various mathematical models. Various models were employed to determine which one best fitted the dissolution data, utilizing  $R^2$  (correlation coefficient), AIC (Akaike information criterion), and MSC (model selection criteria) as criteria for selection.

## 6.9. Stability studies

Optimized ABTA SD formulations were stored in sealed amber glass bottles for three months (90 days) in stability chambers under accelerated conditions ( $40 \pm 2$  °C and  $75 \pm 5\%$  relative humidity). Stability was assessed by examining physical characteristics (color), % assay, in-vitro dissolution, DSC, and PXRD both initially and after three months.

## 6.10. Result and discussions

### 6.11. Drug-solubility parameter approach

A critical aspect of formulating stabilized SDs involves achieving a single homogeneous phase wherein the drug and polymer are thermodynamically compatible. The thermodynamic miscibility of ABTA with the specified polymers (HPMC HME 15 LV and HPMC HME 100 LV) was investigated by determining Hansen solubility parameters, employing the van Krevelen and Hoftyzer group's contribution method. Due to its relative simplicity, this method of calculating solubility parameters and applying them to SDs remains widely utilized. Group contribution methods are often employed to avoid time-consuming tests and potential inaccuracies in results. In this method, when the solubility parameter between a drug and a polymer differs by less than 7  $\text{MPa}^{1/2}$ , a system is said to be miscible, or when both compounds have similar  $\Delta\delta$  values. However, a system is immiscible if  $\Delta\delta$  is more than 10  $\text{MPa}^{1/2}$  (10). Estimation of the solubility parameter of HPMC HME 15 LV and HPMC HME 100 LV using the Hansen group contribution theory has been shown in Table 6.2. The solubility parameters of ABTA were calculated using the Hansen group contribution theory, as discussed earlier in Chapter 3.

**Table 6.2.** Estimation of Solubility Parameter of HPMC HME using the Hansen Group Contribution theory

HPMCAS	Polar forces	Dispersive forces	Hydrogen bonding	Total solubility parameters
	$\Delta p$	$\Delta d$	$\delta h$	
HPMC HME 15 LV	11.9	18	12.3	24.83
HPMC HME 100LV	12.5	17.9	12.7	25.25

**Table 6.3.** Estimated solubility parameter and Flory–Huggin's drug-polymer interaction parameter values derived for ABTA and HPMC HME

Drug/Excipient	Hansen solubility parameter	$\Delta\delta$ ( $\text{MPa}^{1/2}$ ) ( $\delta_{\text{HPMC HME}} - \delta_{\text{ABTA}}$ )	Flory Huggins drug-polymer interaction parameter ( $\chi$ )
----------------	-----------------------------	--	---



ABTA	19.38	-	-
HPMC HME 15 LV	24.83	5.45	3.24
HPMC HME 100 LV	25.25	5.87	3.76

As evident from Table 6.3,  $\Delta\delta$  between the ABTA and (HPMC HME 15LV and 100 LV) was below  $7 \text{ MPa}^{1/2}$ , suggesting favorable miscibility between them. Utilizing these solubility parameter values for the drug-polymer system at  $25 \text{ }^\circ\text{C}$ , also calculated the F-H interaction parameter ( $\chi$ ). The value of  $\chi$  relates to the square of the difference in solubility parameters computed from group contributions at  $25 \text{ }^\circ\text{C}$  using Equation 6.3. This equation illustrates that the interaction parameters will be close to zero if the drug and polymer solubility characteristics are similar. A low value of  $\chi$  indicates a smaller enthalpy of mixing and more negative free energy, facilitating mixing; thus, a value closer to zero signifies a more vital interaction between the drug and the polymer (12). However, the interaction parameter value for the ABTA-HPMC HME system, as shown in Table 6.3, is close to zero, indicating miscibility between them.

### 6.12. Precipitation inhibition effect

The effectiveness of the HPMC HME was evaluated by maintaining the supersaturated state of ABTA. The concentration of free ABTA initially declined and continued to decrease over time, as illustrated in Figure 6.2 [A and B]. However, the presence of pre-dissolved HPMC HME observed a notable recrystallization inhibition effect, as the concentration of ABTA in the media remained elevated throughout the 120-min period. Upon inducing supersaturation of ABTA in the absence of polymer, instantaneous and complete precipitation could be observed in the first 10 min; this phenomenon is attributed to the “spring” effect. The presence of pre-dissolved HPMC HME provided a pronounced and stable supersaturation. This study exhibited that the HPMC HME (15 LV and 100 LV) acted as a “parachute” to impede crystal nucleation and growth. The presence of pre-dissolved HPMC HME with ABTA demonstrated a “spring and parachute effect”. The ABTA to HPMC HME ratios of 1:2 for both 15 LV and 100 LV demonstrated a significantly higher recrystallization inhibition effect compared to the 1:1 and 1:1.5 ratios, respectively. As shown in Figure 6.2 [A and B], increasing the concentration of HPMC HME enhances the recrystallization inhibition effect. This occurs because the higher viscosity of HPMC HME reduces the mobility of drug molecules in the media. The above conclusion was confirmed by the particle size monitoring of ABTA pre-dissolved HPMC HME (15LV and 100 LV). The size of precipitates formed during

induced precipitation was assessed using dynamic light scattering (DLS). As shown in Figures 6.3 [A and B], in the absence of the pre-dissolved polymer, the ABTA exhibited recrystallization within the first 10 min, which is evident from a notable increase in particle size of up to 3000 nm. Conversely, in the presence of pre-dissolved, HPMC HME (15 LV and 100 LV) maintained a particle size of around 150-400 nm without substantial growth throughout the precipitation inhibition study i.e., 120 min. The polydispersity index (PDI) value was significantly changed (0.512-1.000) in the free ABTA without the pre-dissolved polymer. Conversely, in the presence of pre-dissolved polymer maintained a PDI of around 0.304-0.567 nm throughout the study, leading to the superior recrystallization inhibition effect.

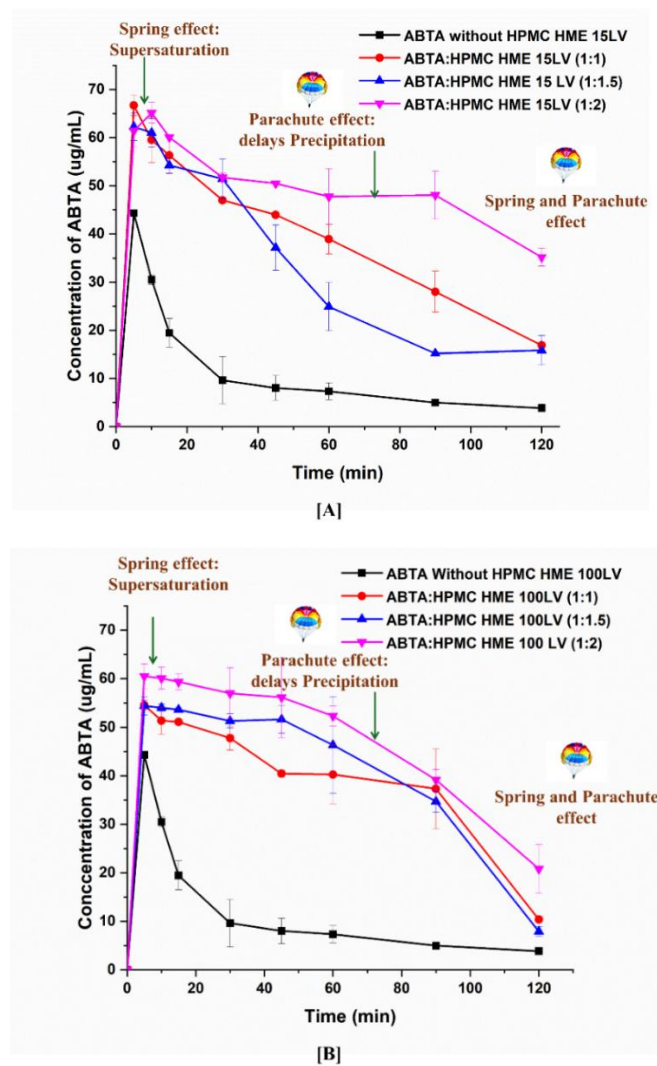


**Figure 6.2.** Precipitation inhibition assay of supersaturated ABTA in FaSSIF pH 6.5 in the

presence of the pre-dissolved [A] HPMC HME 15 LV and [B] HPMC HME 100 LV (mean  $\pm$  SD, n=3)

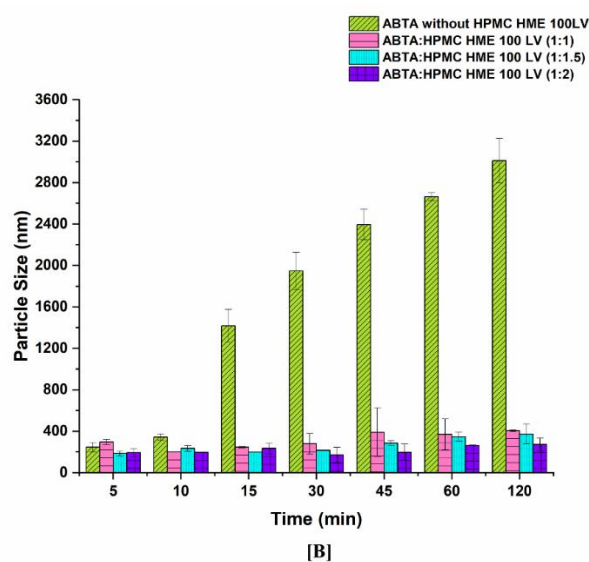
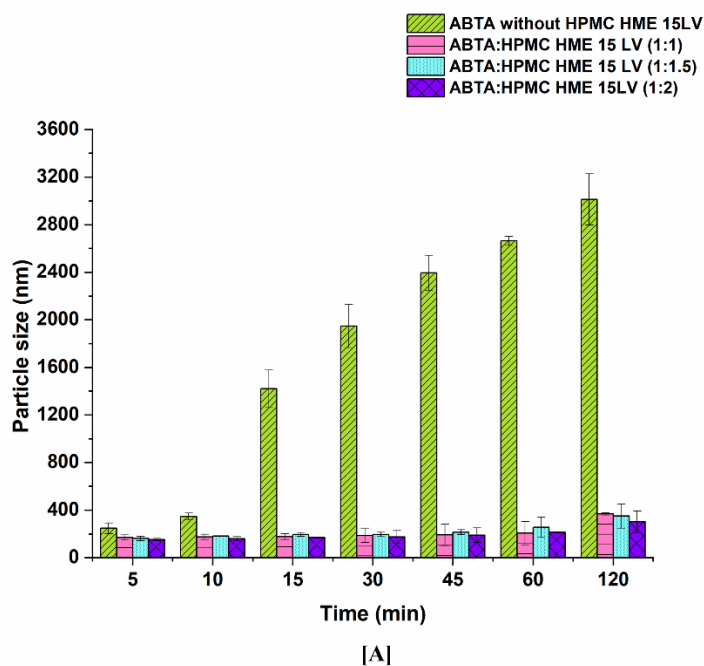


**Figure 6.3.** Particle size graph of supersaturated ABTA in FaSSIF (pH 6.5) in the presence of pre-dissolved [A] HPMC HME 15LV and, [B] HPMC HME 100LV at different concentrations (mean  $\pm$  S.D, n = 3)

### 6.13. Preparation of ABTA-SD via Hot-melt extrusion method

For the preparation of ABTA SD using the different ratios of ABTA and HPMC HME (15 LV and 100 LV) prepared through the hot melt method, but this preparation method was not suitable due to the formation of the hard extrudate, which changed the color of formulation indicating the degradation and lacked proper homogeneity which was shown in Figure 6.4 [A]. Moreover, this formulation incorporated different plasticizers, such as span 20 and docusate sodium, which led to the formation of the sticky mass, as illustrated in Figure 6.4 [B]. However, this indicated that the chosen formulation methods were inadequate for producing the desired ABTA SD. The challenges that occurred in the hot melt method with plasticizers were addressed by employing the HME method in SD preparation. The HME instrument for the preparation of SD is shown in Figure 6.5. The preparation of ABTA SD with HME using the HPMC HME (15 LV and 100 LV) polymer forming the extrudates. Finally, these given extrudates were grinded to form powdered material and sieved using #40 ASTM mesh.



**[A]**



**[B]**




**Figure 6.4.** Preparation of ABTA SD with hot melt method [A] and with the plasticizers [B]













**Figure 6.5.** HME instrument for the preparation of ABTA SD

ABTA SD with HPMC HME (15 LV and 100 LV) at different weight ratios (1:1, 1:1.5, and 1:2) were prepared by HME. The extrusion temperature for the HME process should always be equal to or greater than the 15°C-melting point of the drug, which is 147.46 °C for ABTA. Based on the literature and melting point of the ABTA, three different extrusion temperatures, 120°C, 140°C, and 160°C, were selected for the preparation of ABTA SD with HPMC HME 15LV, respectively. Additionally, for ABTA SD with HPMC HME 100 LV, the extrusion temperatures were set at 140°C and 160°C, respectively. Table 6.4 represents the extrusion process temperature with different ratios of ABTA and HPMC HME 15 LV and 100 LV SD formulations. We avoided using the 120°C temperature for ABTA SD with HPMC HME 100 LV due to the formation of white exudate, indicating inadequate mixing between the drug and polymer. It's crucial to note that the color of the extrudate during the process plays an important role. Here, transparent or light yellow extrudates are preferred, while white extrudates suggest poor blending, and dark-colored ones may indicate drug degradation.

**Table 6.4.** Extrusion process temperature with different ratios of ABTA and HPMC HME 15 LV and 100 LV SD formulations

Formulation code	ABTA: HPMC HME 15LV Ratios	Temperature °C	Appearance
ABTA/SD/1	1:1	120	
ABTA/SD/2		140	
ABTA/SD/3		160	

ABTA/SD/4		120	
ABTA/SD/5	1:1.5	140	
ABTA/SD/6		160	
ABTA/SD/7		120	
ABTA/SD/8	1:2	140	
ABTA/SD/9		160	
Formulation code	ABTA: HPMC HME 100LV Ratios	Temperature °C	Appearance
ABTA/SD/10	1:1	140	
ABTA/SD/11		160	
ABTA/SD/12	1:2	140	
ABTA/SD/13		160	

## 6.14. Characterization of the developed formulation

### 6.14.1. Differential Scanning Calorimetry (DSC)

The thermogram of the free ABTA, HPMC HME (15 LV and 100 LV), and ABTA SD formulation are represented in Figure 6.6. The thermogram of the free ABTA showed an endothermic peak at 147.16 °C corresponding to the melting point of ABTA, indicating its crystalline nature shown in Figure 6.6 [A-E]. The thermogram for HPMC HME 15LV and HPMC HME 100 LV displayed the  $T_g$  at 92.42 °C and 74.34 °C, shown in Figure 6.6 [A-E]. ABTA SD formulation extruded at a temperature of 120 °C, showed the endothermic peak of the ABTA shown in Figure 6.6 [A-C]. This indicates that ABTA did not convert from a crystalline to an amorphous form, likely due to inadequate mixing of the drug and polymer during the HME process. ABTA SD at 140 °C and 160 °C extrusion temperature, did not generate the endothermic peak of the ABTA illustrated in Figure 6.6 [A-E], confirming that the ABTA was completely converted from the crystalline form to the amorphous form during the HME. This is due to the intimate mixing between the drug and

polymer, promoting the strong interaction among them. Generally, reducing a drug crystallinity typically enhances its dissolution and solubility, as it requires less energy to break down the crystal lattice (15).

#### 6.14.2. Powder X-ray diffraction

The PXRD patterns of free ABTA, HPMC HME 15 LV, HPMC HME 100 LV, and ABTA SD formulation are shown in Figure 6.7 [A-E]. ABTA powder exhibited multiple distinctive peaks at  $12.1^\circ$ ,  $14.9^\circ$ ,  $15.2^\circ$ ,  $16.05^\circ$ ,  $18.4^\circ$ ,  $19.07^\circ$ , and  $21.8^\circ$  which indicated the crystallinity of ABTA. Furthermore, HPMC HME 15 LV and HPMC HME 100 LV exhibited amorphous PXRD patterns. In the ABTA SD formulation, i.e., ABTA/ SD/1, ABTA/ SD/4, and ABTA/SD/7 prepared with the HME method at the extrusion temperature of  $120^\circ\text{C}$ , the characteristics of the diffraction peak of the free ABTA showed the crystallinity shown in Figure 6.7 [A-C] due to the inadequate mixing of the ABTA and HPMC HME 15LV and 100LV. However, at the extrusion temperature of  $140^\circ\text{C}$  and  $160^\circ\text{C}$  in ABTA SD formulations, the characteristics diffraction peak of ABTA in all the formulations disappeared, and broad amorphous halo patterns were obtained, as shown in Figure 6.7 [A-E], which relates to the DSC results. The DSC and PXRD analyses verified that the state of ABTA in the ABTA SD formulations was not only physically mixed but revealed amorphous dispersion, and there may be a strong interaction between the drug and polymer that caused these changes.

#### 6.14.3. Attenuated total reflectance fourier transform infrared spectroscopy (ATR-FTIR)

The ATR- FTIR of free ABTA bulk powder, HPMC HME 15 LV, HPMC HME 100LV, and ABTA SD were obtained to investigate the physicochemical interaction between ABTA and carriers in the SD formulation, as illustrated in Figure 6.8 [A-E]. As illustrated in Figure 6.8 [A-E], the characteristics absorption bands of crystalline ABTA depicted at  $2935.68\text{ cm}^{-1}$ ,  $1731\text{ cm}^{-1}$ ,  $1533\text{ cm}^{-1}$ , and  $1240\text{ cm}^{-1}$  which corresponds to the aromatic C-H stretching, C=O stretching, C=N stretching (pyridine ring vibration) and C-O stretching respectively. The ATR-FTIR spectra of HPMC HME 15LV and 100 LV showed characteristic peaks at  $1049\text{ cm}^{-1}$  and  $1373\text{ cm}^{-1}$  of C-O stretching and C-O-H bending, respectively shown in Figure 6.8 [A-E]. However, the ABTA SD formulation prepared with the HME at different extrusion temperatures observed that the intensity decreases and disappearances of ABTA suggest the molecular interaction.

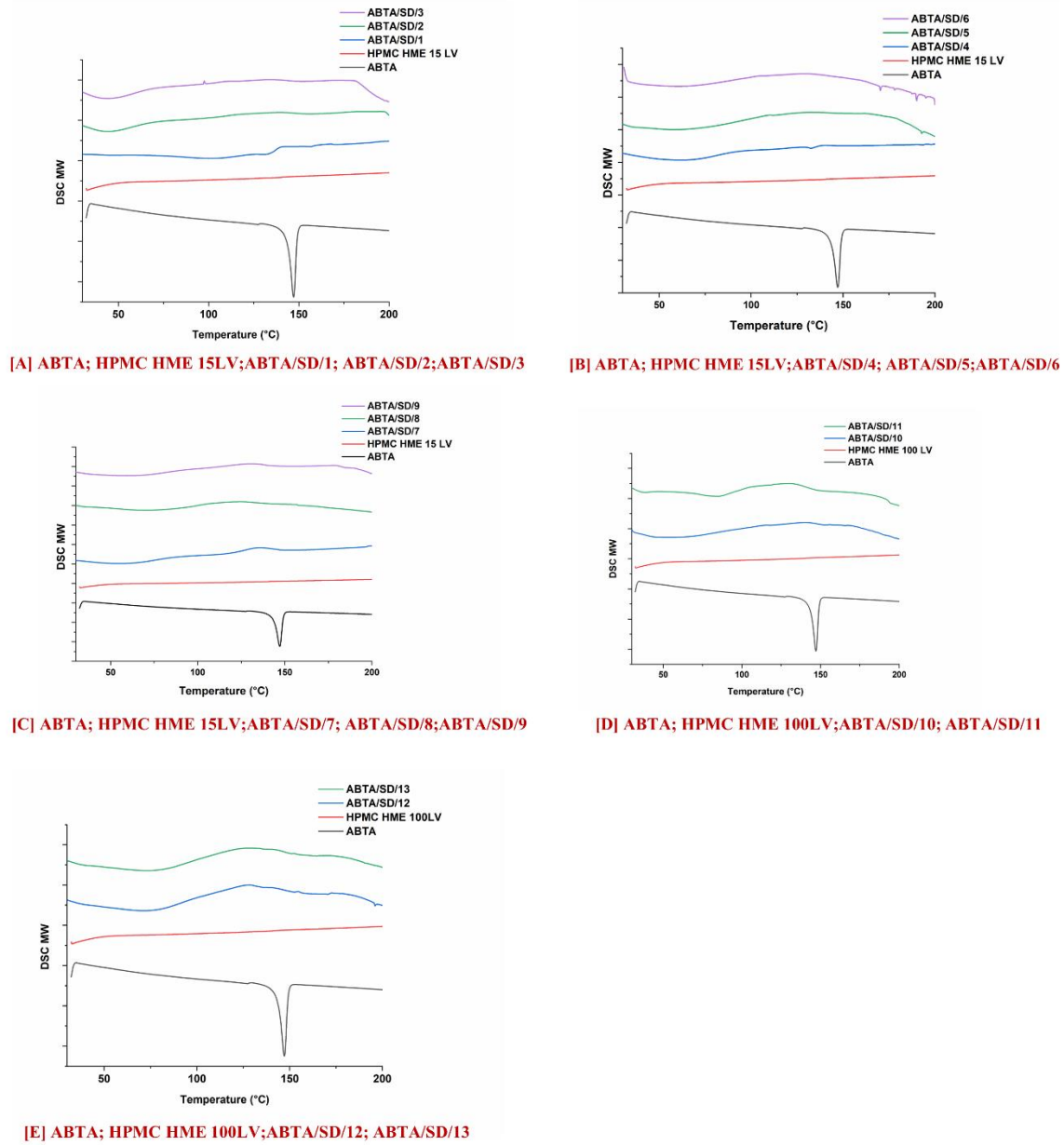
**6.14.4. Thermogravimetric analysis (TGA)**

TGA profiles of ABTA, HPMC HME 15 LV, HPMC HME 100 LV, and ABTA-SD are illustrated in Figure 6.9. The melting point of ABTA is 147.16 °C. As shown in Figure 6.9, ABTA does not exhibit any significant weight loss below 300 °C, indicating that it does not undergo substantial decomposition at temperatures below this threshold. The studies revealed that ABTA, HPMC HME 15 LV, HPMC HME 100 LV, and ABTA-SD are thermally stable up to 300 °C, indicating that ABTA does not degrade and is compatible with the excipients. Consequently, the extrusion process temperatures of 120°C, 140°C, and 160°C used for the preparation of SD should not cause any degradation of ABTA.

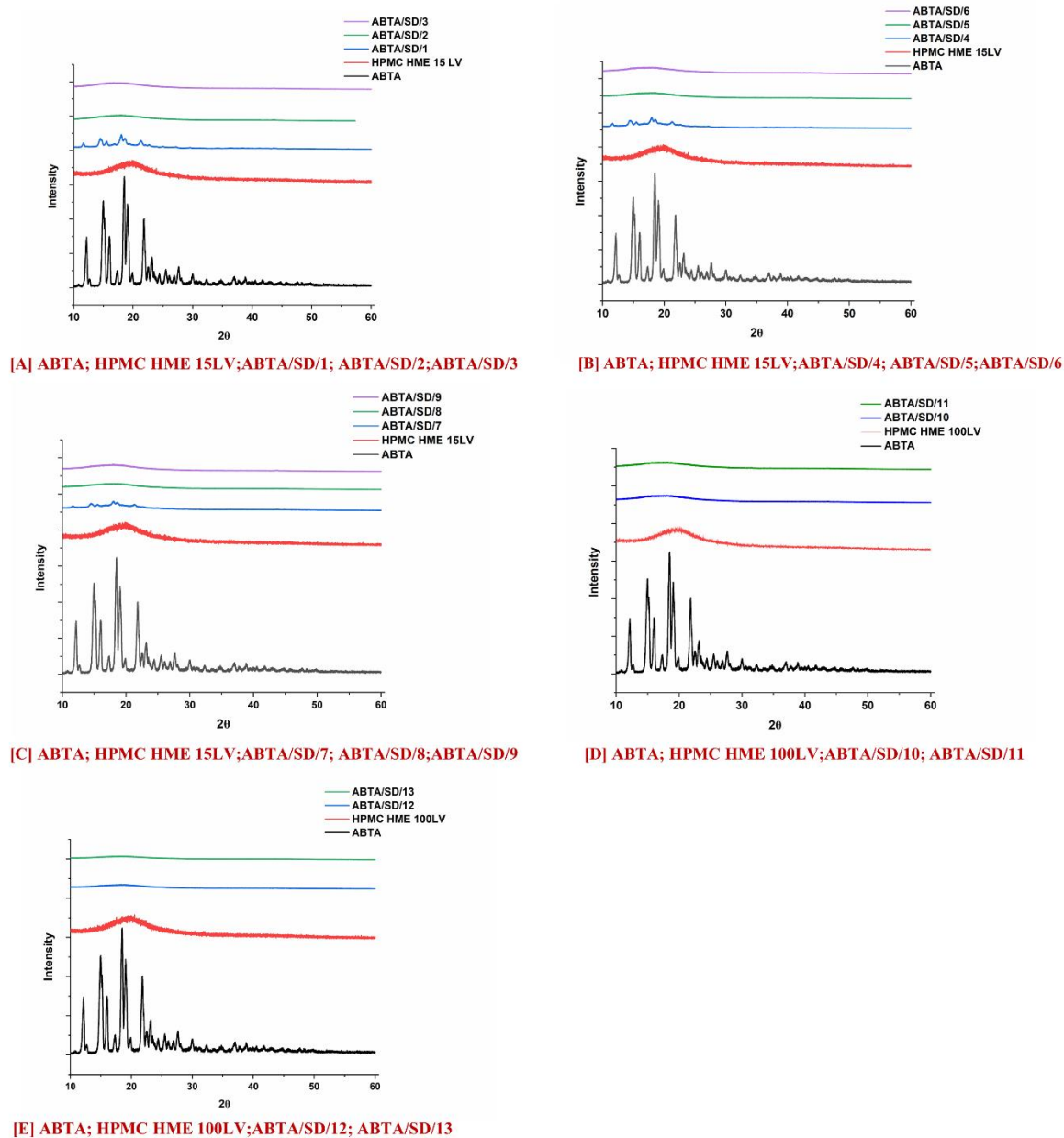
**6.14.5. Field Emission Scanning Electron Microscopy (FE-SEM)**

The ABTA and ABTA SD surface morphologies were observed using FE-SEM and are illustrated in Figure 6.10. ABTA was observed as irregularly shaped crystals, indicating a crystalline form shown in Figure 6.10 (n). In the case of all ABTA SD formulations showing the disappearance of the crystals of ABTA fragments shown in Figure 6.10 (a-m), which signifies the transformation of the crystalline drug form into the amorphous state during the formation of ABTA SD with HPMC HME. The main reason for changing the crystalline form to an amorphous form is the intimate mixing between the ABTA and HPMC HME 15 LV and 100 LV.

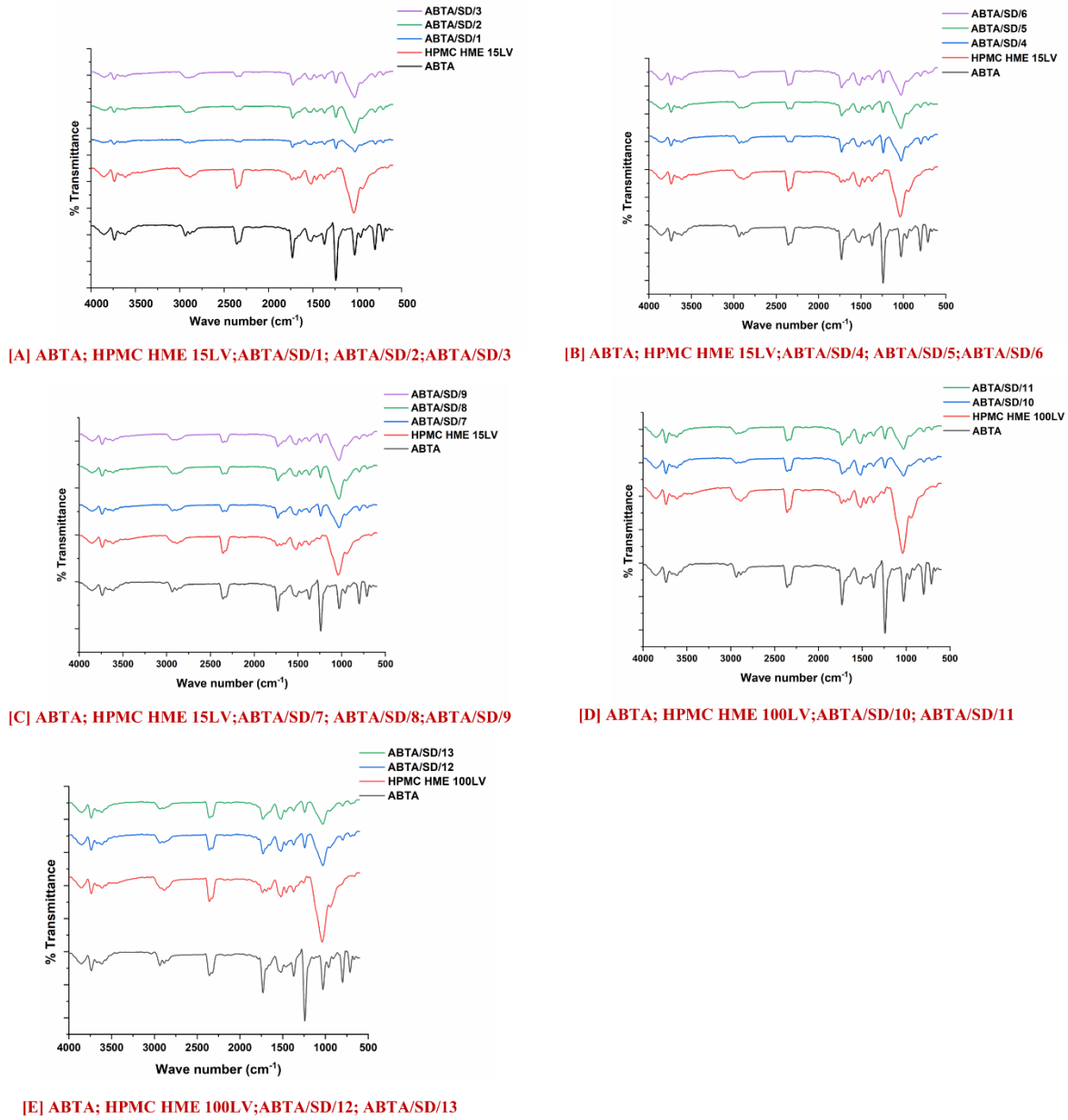




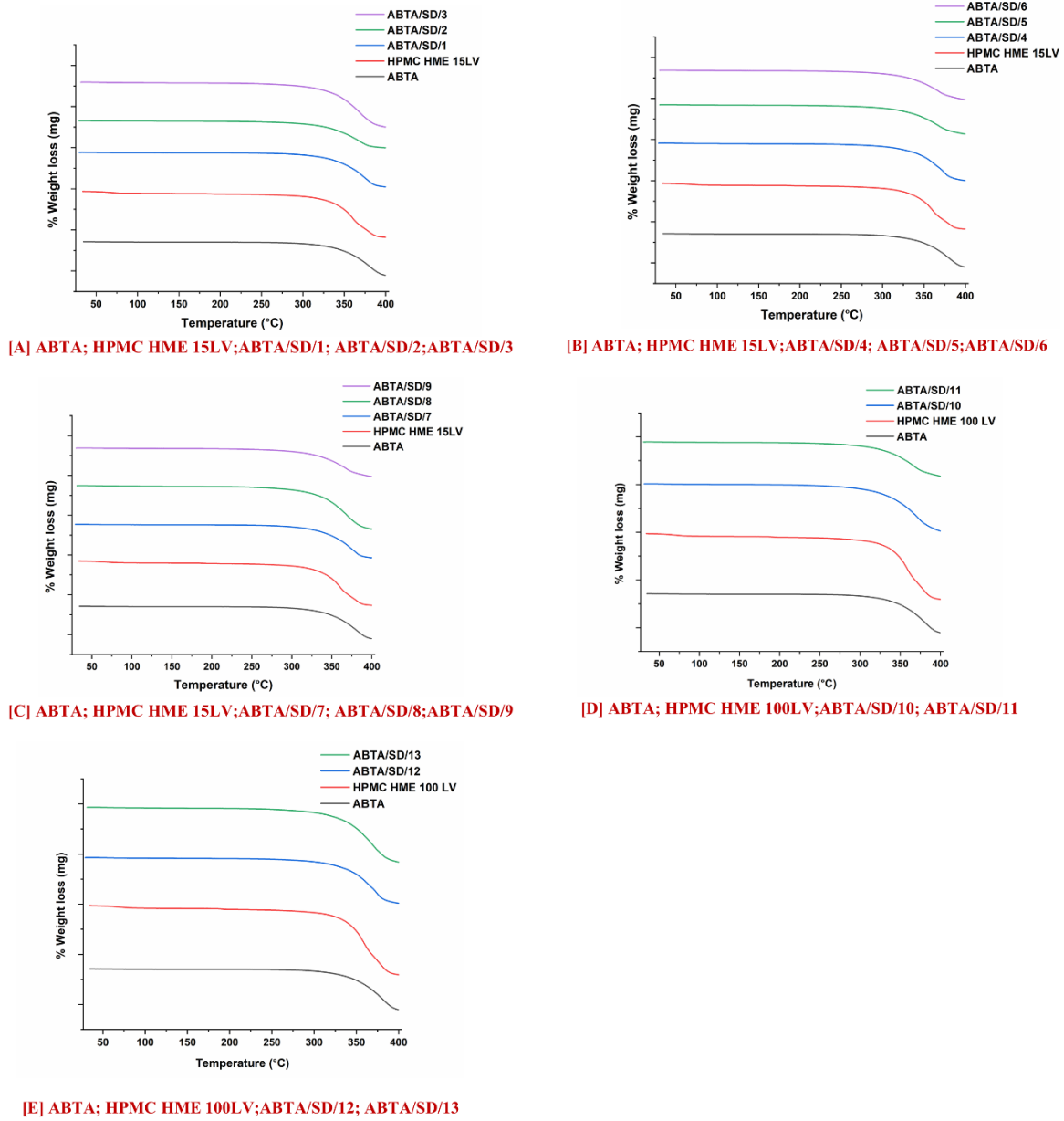
**Figure 6.6.** DSC thermograms of ABTA SD formulations with HPMC HME (15LV and 100LV)



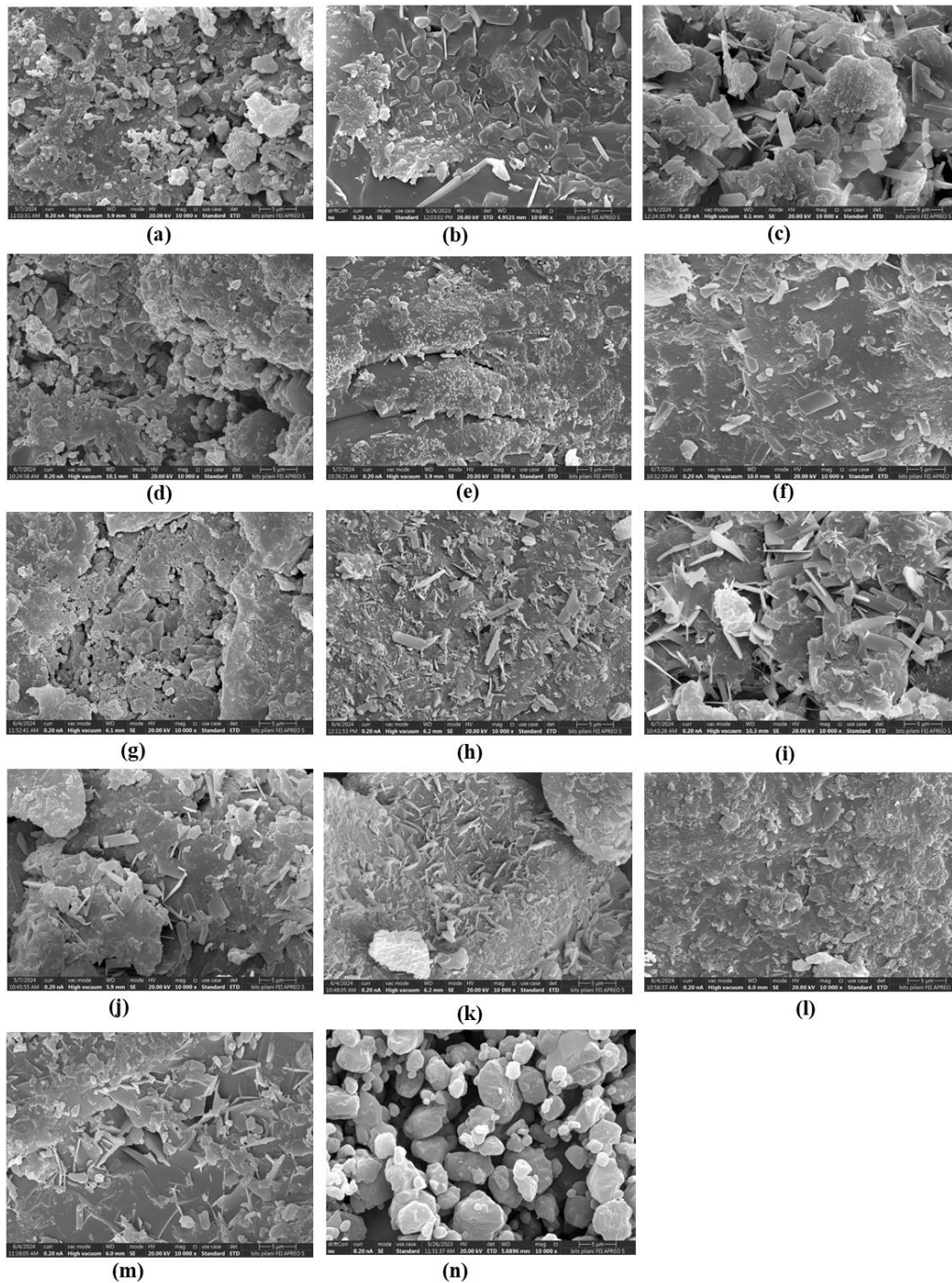
**Figure 6.7.** PXR D patterns of ABTA SD formulations with HPMC HME (15LV and 100LV)



**Figure 6.8.** FTIR of ABTA SD formulations with HPMC HME (15LV and 100LV)



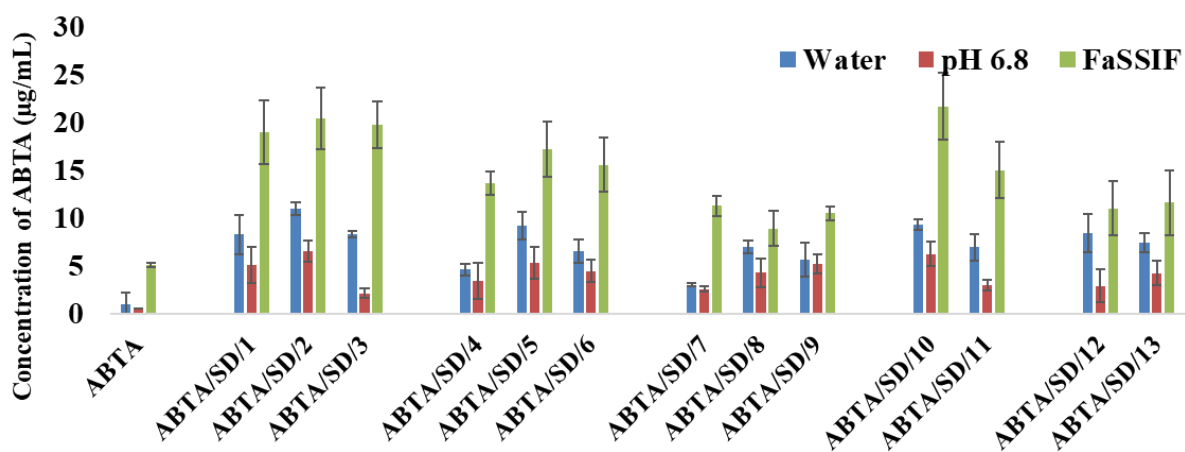
**Figure 6.9.** TGA of ABTA SD formulations with HPMC HME (15LV and 100LV)



**Figure 6.10.** FE-SEM images of (a) ABTA/SD/1; (b) ABTA/SD/2; (c) ABTA/SD/3; (d) ABTA/SD/4; (e) ABTA/SD/5; (f) ABTA/SD/6; (g) ABTA/SD/7; (h) ABTA/SD/8; (i) ABTA/SD/9; (j) ABTA/SD/10; (k) ABTA/SD/11; (l) ABTA/SD/12; (m) ABTA/SD/13; (n) ABTA

### 6.15. Solubility studies

The solubility of free ABTA in water was found to be approximately 1.012  $\mu\text{g/mL}$ . ABTA solubility varies with pH, with a solubility of 136.70  $\mu\text{g/mL}$  in 0.1 N HCl. At pH 6.8, the solubility of free ABTA was 0.510  $\mu\text{g/mL}$ . In FaSSIF and FeSSIF, the solubility of free ABTA was around 5.07  $\mu\text{g/mL}$  and 82.20  $\mu\text{g/mL}$ , respectively. In this investigation, ABTA SD formulations were prepared using the HME method with different grades of HPMC HME (15 LV and 100 LV) at various extrusion temperatures (120  $^{\circ}\text{C}$ , 140  $^{\circ}\text{C}$ , and 160  $^{\circ}\text{C}$ ). These formulations notably enhanced ABTA solubility across all media (Table 6.5), including water (3.01  $\mu\text{g/mL}$  -10.96  $\mu\text{g/mL}$ ), 0.1 N HCl (480.25  $\mu\text{g/mL}$ -574.22  $\mu\text{g/mL}$ ), pH 6.8 (3.0  $\mu\text{g/mL}$  -6.52  $\mu\text{g/mL}$ ), FaSSIF (8.91  $\mu\text{g/mL}$  -21.68  $\mu\text{g/mL}$ ), and FeSSIF (82.45  $\mu\text{g/mL}$ - 128.51  $\mu\text{g/mL}$ ) compared to free ABTA (see Figure 6.11 A and B). The solubility of ABTA in all formulations showed improvement compared to free ABTA, as illustrated in Table 6.6, represented as fold changes compared to free ABTA. However, no significant differences were observed among the polymer ratios and extrusion temperatures formulations. Consequently, further investigations, including in vitro dissolution studies, were conducted for all ABTA SD formulations.



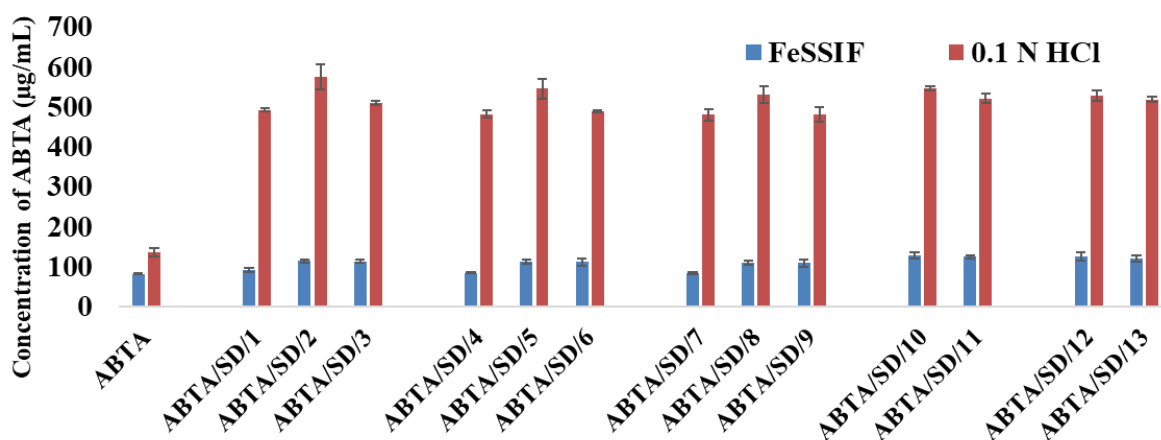


**Figure 6.11.** Solubility studies of free ABTA and ABTA SD formulation at different extrusion temperatures in different media [A] water, pH 6.8 and FaSSIF; [B] FeSSIF, and 0.1 N HCl (pH 1.2)

Moreover, the increase in solubility achieved through HME can be attributed to several key mechanisms. Firstly, the process leads to a reduction in particle size, resulting in a larger surface area available for solubility. Secondly, forming an amorphous state of the drug enhances solubility by disrupting the ordered crystalline structure. Thirdly, the intimate mixing of the drug and polymer promotes strong interactions such as the formation of the hydrogen bonding between the drug and polymer and improving wetting properties. Finally, the prevention of drug recrystallization maintains enhanced solubility over time.

**Table 6.5.** Solubility of ABTA SD formulations in different buffer media

ABTA SD	Water	pH 6.8	0.1 N HCl	FaSSIF	FeSSIF
ABTA	1.01 ± 1.22	0.51 ± 1.29	136.07 ± 10.34	5.07 ± 0.199	82.2 ± 1.58
ABTA/SD/1	8.26 ± 2.03	5.12 ± 1.89	492.49 ± 4.61	18.96 ± 3.36	91.49 ± 4.47
ABTA/SD/2	10.96 ± 0.68	6.52 ± 1.15	574.22 ± 31.74	20.38 ± 3.21	114.14 ± 5.05
ABTA/SD/3	8.29 ± 0.35	2.12 ± 0.51	510.22 ± 4.65	19.74 ± 2.44	113.46 ± 3.33
ABTA/SD/4	4.59 ± 0.62	3.42 ± 1.86	482.24 ± 9.82	13.67 ± 1.21	84.1 ± 1.36
ABTA/SD/5	9.16 ± 1.46	5.28 ± 1.66	545.24 ± 24.13	17.24 ± 2.89	112.86 ± 6.02
ABTA/SD/6	6.52 ± 1.24	4.44 ± 1.69	489.82 ± 2.86	15.58 ± 2.87	111.78 ± 9.98
ABTA/SD/7	3.01 ± 0.12	2.54 ± 0.27	480.25 ± 14.25	11.25 ± 1.09	83.76 ± 2.08
ABTA/SD/8	6.98 ± 0.65	4.25 ± 1.53	531.24 ± 20.72	8.91 ± 1.85	110.19 ± 4.86
ABTA/SD/9	5.63 ± 1.74	5.19 ± 1.04	481.74 ± 17.72	10.48 ± 0.69	110.07 ± 9.14
ABTA/SD/10	9.28 ± 0.58	6.22 ± 1.27	546.74 ± 4.56	21.68 ± 3.52	128.42 ± 7.28
ABTA/SD/11	6.93 ± 1.39	3 ± 0.56	521.47 ± 12.71	15.01 ± 2.95	125.51 ± 3.67
ABTA/SD/12	8.43 ± 2.03	2.89 ± 1.72	527.95 ± 12.96	11 ± 2.81	126.06 ± 9.91
ABTA/SD/13	7.42 ± 0.99	4.22 ± 1.27	518.72 ± 5.65	11.6 ± 3.39	121.24 ± 8.4

**Table 6.6.** Solubility of ABTA SD formulations expressed as fold changes compared to free ABTA

ABTA SD	Water	pH 6.8	0.1 N HCl	FaSSIF	FeSSIF
ABTA/SD/1	8.18-fold	5.70-fold	3.60-fold	3.74-fold	1.11-fold
ABTA/SD/2	10.8-fold	7.25-fold	4.20-fold	4.02-fold	1.39-fold
ABTA/SD/3	8.21-fold	2.40-fold	3.74-fold	3.90-fold	1.38-fold
ABTA/SD/4	4.55-fold	3.76-fold	3.53-fold	3.70-fold	1.03-fold
ABTA/SD/5	9.07-fold	5.81-fold	3.99-fold	3.41-fold	1.37-fold
ABTA/SD/6	6.49-fold	4.88-fold	3.58-fold	3.07-fold	1.36-fold
ABTA/SD/7	2.99-fold	2.70-fold	3.51-fold	2.22-fold	1.02-fold
ABTA/SD/8	6.92-fold	4.67-fold	3.89-fold	1.76-fold	1.34-fold
ABTA/SD/9	5.58-fold	5.71-fold	3.52-fold	2.14-fold	1.34-fold
ABTA/SD/10	9.19-fold	6.84-fold	4.0-fold	4.28-fold	1.56-fold
ABTA/SD/11	6.87-fold	3.3-fold	3.82-fold	2.96-fold	1.53-fold
ABTA/SD/12	8.35-fold	3.18-fold	3.86-fold	2.18-fold	1.54-fold
ABTA/SD/13	7.35-fold	4.64-fold	3.06-fold	2.29-fold	1.48-fold

### 6.16. Effect on viscosity with change in pH and HPMC HME polymer concentration

Polymeric solution properties are influenced by conformational changes and environmental factors like concentration, temperature, and pH. Conformational changes occur in molecules when the pH is shifted to either acidic or basic levels. The effect of pH on the dispersion of HPMC HME (15 LV and 100 LV) is carried out at different concentrations (1.33 % and 2.66%) in the pH range 1.2-6.8 and in the Biorelevant media i.e., FaSSIF (pH 6.5) and FeSSIF (pH 5.0). It was observed in Figure 6.12 that at lower pH, viscosity was decreased because the HPMC coils more tightly as the ionic strength increases. At the lowest pH, HPMC macromolecules are more prevalent, and polymer-polymer interactions are less pronounced. In a basic pH environment, HPMC molecules are more extended, allowing them to interact with each other even at lower concentrations, resulting in increased polymer-polymer interactions (16). Thus, an increase in viscosity at a higher pH range is shown in Figure 6.12. In the case of FeSSIF media at pH 5.0, the viscosity of HPMC was higher compared to pH 6.8. This increase in viscosity is due to the higher amounts of bile salts and lecithin in FeSSIF, which contribute to its more viscous nature.

Moreover, the concentration of the HPMC HME (15LV and 100LV) affects the viscosity. In this study, it was observed that increasing the concentration (2.66 %) of the HPMC HME 15LV and 100 LV leads to increases in the viscosity but slower drug dissolution. The lower concentration (1.33 %) of the HPMC HME 15 LV and 100 LV tended to decrease in viscosity, but faster the drug dissolution (17). Table 6.7 shows the viscosity of the HPMC HME 15LV and 100 LV at



different concentrations in the pH range of 1.2-6.8. It was found that the viscosity of HPMC HME 15 LV and 100 LV is directly related to both the concentration of the polymer and the pH.

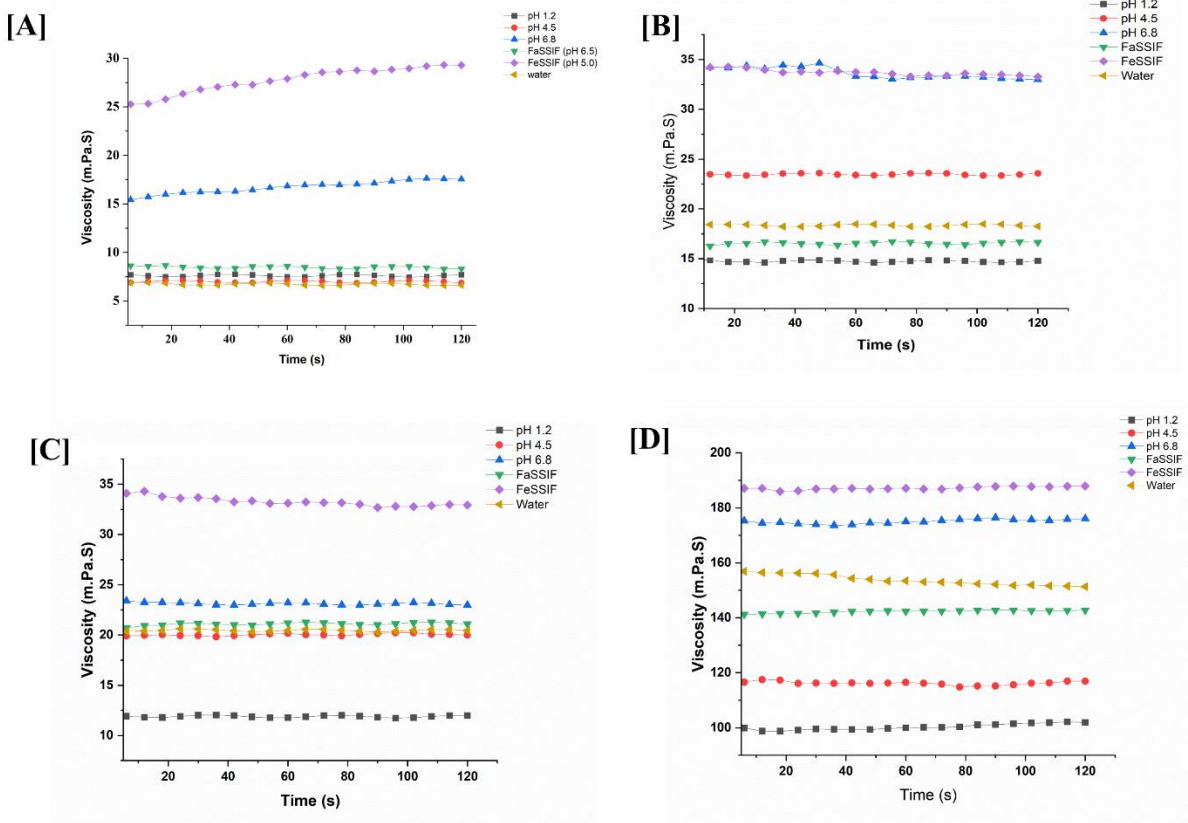


**Figure 6.12.** Viscosity of HPMC HME 15 LV and 100 LV in different pH media [A-B] illustrates the viscosity of HPMC HME 15 LV dispersion (1.33 % and 2.66%) in different pH media; [C-D] illustrates the HPMC HME 100 LV dispersion (1.33 % and 2.66%) in different pH media

**Table 6.7.** Viscosity of HPMC HME 15 LV and 100 LV in different pH media

Buffer	Viscosity (m.Pa.S)			
	HPMC HME 15 LV		HPMC HME 100 LV	
	1.33 %	2.66 %	1.33 %	2.66 %
pH 1.2	7.60	14.74	11.86	100.28
pH 4.5	6.99	23.48	20.02	116.21
FaSSiF (pH 6.5)	8.46	16.54	21.09	142.28
FeSSiF (pH 5.0)	27.74	33.73	33.26	187.23
pH 6.8	16.73	33.66	23.12	175.02
Water	6.75	18.35	20.45	153.72

6.17. In-vitro dissolution study

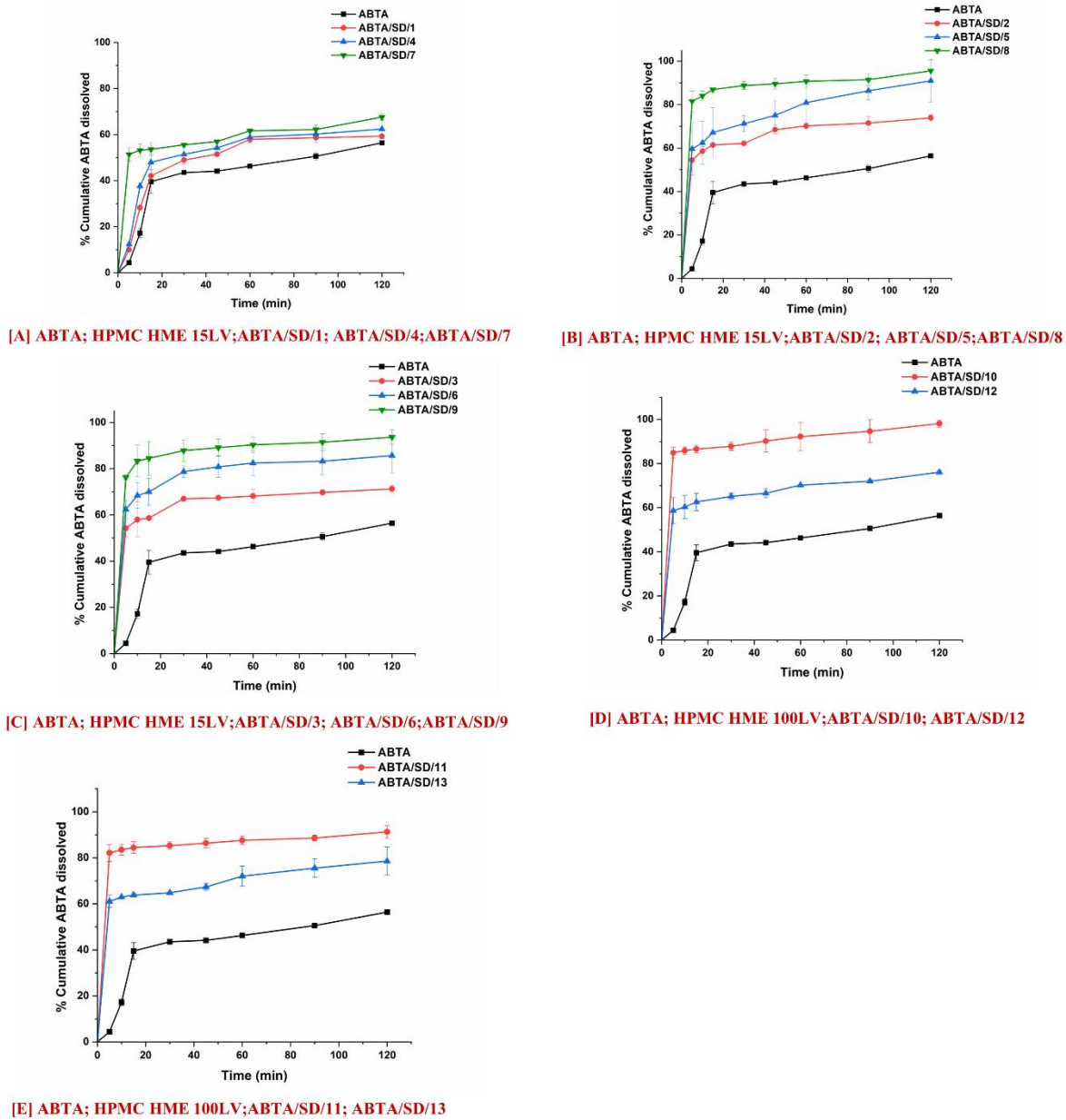
The in-vitro dissolution study of free ABTA and ABTA SD formulations was performed in dissolution media pH 1.2 as well as pH 4.5. The free ABTA dissolved approximately 56.41 % at pH 1.2 and 58.39 % at pH 4.5 after 120 min respectively. However, the SD formulations exhibited superior dissolution profiles, both rate and extent of dissolution, compared to the free ABTA. For SD formulations, dissolution was found to be increased and varied from 59.61% to 100.67% depending on the nature and concentration of the polymer and process and temperature used. The rate of dissolution was also found to be enhanced (Figure 6.13), as can be seen from the profiles. This difference is likely due to the amorphous nature of ABTA in the SD, which was also observed in the different characterization methods, resulting in enhanced solubility and dissolution rates. Moreover, it was observed that the extrusion temperature during the HME process (120°C, 140°C, and 160°C) and the concentration of HPMC HME polymer significantly impacted the dissolution behavior of the ABTA.

Figure 6.13 [A-C] shows the in-vitro dissolution profile of ABTA/SD/1 to ABT/SD/9 in pH 1.2 dissolution media. The ABTA/SD/7, ABTA/SD/8, and ABTA/SD/9 showed an increase in the dissolution rate compared to other ABTA SD formulations due to the higher concentration of HPMC HME 15LV at different extrusion temperatures (120°C, 140°C, and 160°C). The rate of dissolution of ABTA/SD/7, ABTA/SD/8, and ABTA/SD/9 was 67.59%, 95.54%, and 93.63% in 120 min at different extrusion temperatures, suggesting that dissolution was increased by 1.14-fold, 1.7-fold, and 1.66-fold compared to the free ABTA. It was observed that among the various extrusion temperatures used, 140 °C showed the highest dissolution of ABTA compared to 120°C and 160°C. Furthermore, the dissolution rate of ABTA increased with increasing concentrations of HPMC HME 15LV. Specifically, ABTA/SD/2, ABTA/SD/5, and ABTA/SD/8 prepared at 140°C extrusion temperature showed dissolution rates of 73.93%, 90.92%, and 95.54% in 120 min, respectively, representing increases of 1.31-fold for ABTA/SD/2, 1.61-fold for ABTA/SD/5, and 1.66-fold for ABTA/SD/8 compared to free ABTA.

In Figure 6.13 [D-E] the in-vitro dissolution profiles of ABTA/SD/10 to ABTA/SD/13 in pH 1.2 dissolution media are presented. The ABTA/SD/10 and ABTA/SD/12 showed an increase in the rate and extent of the dissolution process compared to the ABTA/SD/11 and ABTA/SD/13 when decreasing the HPMC HME 100 LV concentration. However, HPMC HME 100 LV polymer has a high molecular weight, swells faster, and forms a thicker viscous layer, which can delay or hinder

drug dissolution. Increasing the HPMC HME 100 LV concentration can increase the formulation's viscosity; this increased viscosity forms a barrier that slows the diffusion of the drug molecules, allowing more time to dissolve in media (6). The rate of dissolution of ABTA/SD/10 and ABTA/SD/12 was 98.12% and 91.28% in 120 min, suggesting the dissolution was increased by 1.74-fold and 1.66-fold compared to the free ABTA.

The extrusion temperature, and the concentration of the HPMC HME 15 LV and HPMC HME 100 LV significantly influenced the dissolution behavior in all ABTA SD formulations in pH 1.2 dissolution media. When comparing the dissolution profile based on extrusion temperature, at the lower extrusion temperature of 120°C, the dissolution rate was found to be lower compared to the 140°C and 160°C extrusion temperatures. This may be due to the improper or inadequate mixing of the drug and polymer at 120°C, which showed lower dissolution behavior, whereas at 140°C and 160°C extrusion temperature, better drug dispersion in the polymeric carrier, probably resulting from decreases in the melt viscosity and superior homogenization. At the 140°C and 160°C extrusion temperature, there is no significant difference in the dissolution behavior. Here, the dissolution of ABTA/SD/8 and ABTA/SD/9, rapid dissolution of the drug from the SD formulation occurred, reaching the plateau within 5 min; the maximum drug dissolution of 81.53 % and 76.23 % were obtained compared to the crystalline ABTA shown in Figure 6.13 [A-C]. When the dissolution of ABTA/SD/10 and ABTA/SD/12, rapid dissolution of the drug from the SD formulation occurred, reaching the plateau within 5 min; the maximum drug dissolved of 84.91 % and 82.14 % was obtained compared to the crystalline ABTA shown in Figure 6.13 [D-E].



**Figure 6.13.** In-vitro dissolution profile of ABTA SD formulations extruded at different extrusion temperatures 120°C, 140°C and 160°C and different concentrations of HPMC HME 15LV and 100LV in pH 1.2 dissolution media

Furthermore, the dissolution behavior pattern of ABTA SD was also investigated in the pH 4.5 dissolution media. Figure 6.14 [A-C] shows the in-vitro dissolution profile of ABTA/SD/1 to ABTA/SD/9 in pH 4.5 dissolution media. The ABTA/SD/1, ABTA/SD/2, and ABTA/SD/3 showed an increase in the dissolution rate compared to other ABTA SD when the HPMC HME 15

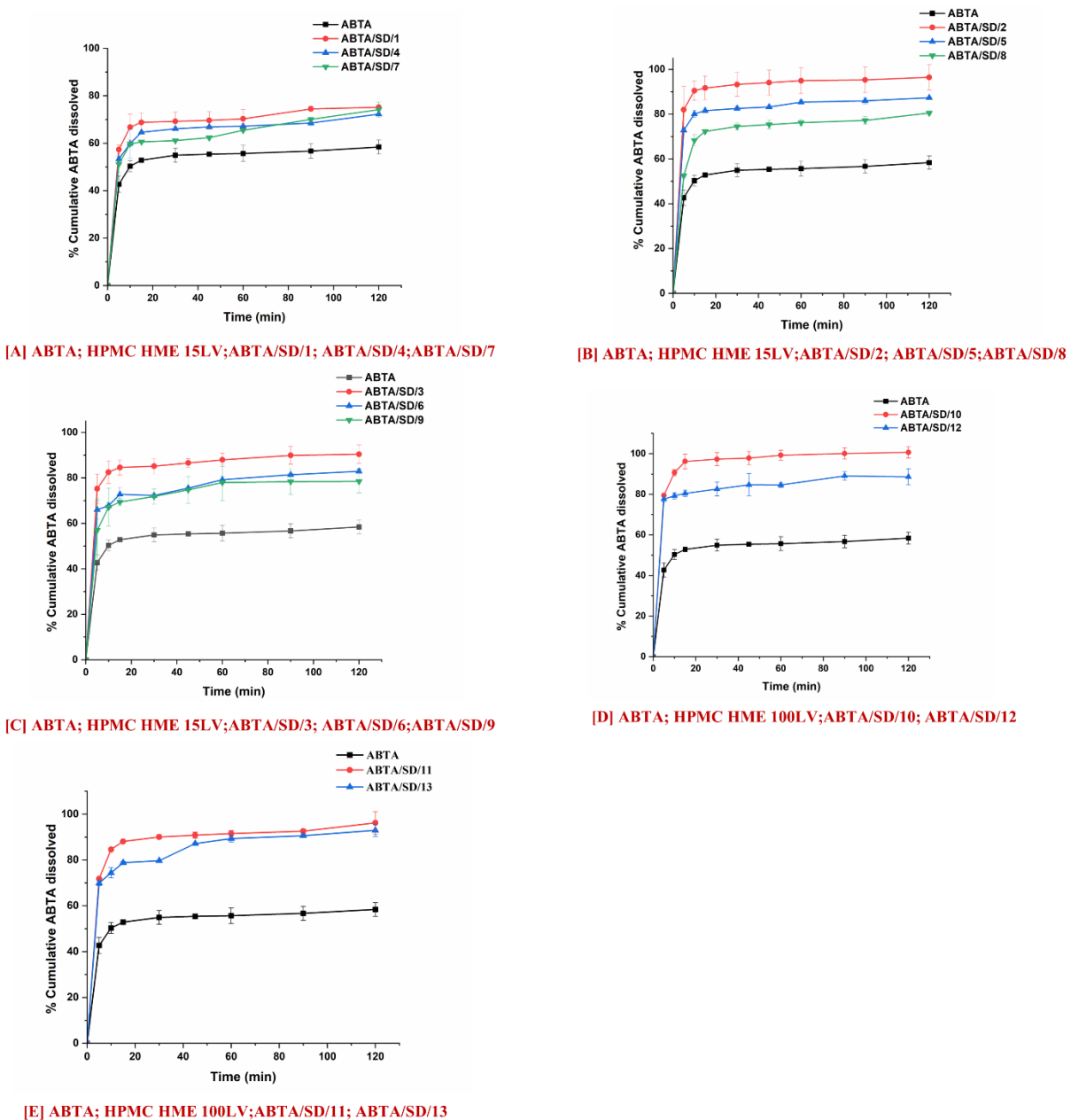
LV concentration was lower at different extrusion temperatures (120°C, 140°C and 160°C). However, the rate of dissolution of ABTA/SD/1, ABTA/SD/2, and ABTA/SD/3 was 72.25 %, 96.44 %, and 90.41 % in 120 min, suggesting that dissolution was increased by 1.24-fold, 1.65-fold, and 1.55-fold compared to the ABTA bulk powder. At 140 °C extrusion temperature, the dissolution rate in pH 4.5 was decreased with increases in the HPMC HME 15LV concentrations. Here, ABTA/SD/2, ABTA/SD/5, and ABTA/SD/8 showed dissolution rates of 96.44%, 87.34%, and 80.45%, respectively, representing increases of 1.65-fold, 1.50-fold, and 1.38-fold compared to the ABTA bulk powder.

Figure 6.14 [D-E] shows the in-vitro dissolution profiles of ABTA/SD/10 to ABTA/SD/13 in pH 4.5 dissolution media. ABTA/SD/10 and ABTA/SD/12 showed an increase in the dissolution rate compared to ABTA/SD/11 and ABTA/SD/13 when decreasing the HPMC HME 100 LV concentration. The rate of dissolution of ABTA/SD/10 and ABTA/SD/12 was 100 % and 96.20 % in 120 min, suggesting the dissolution was increased by 1.72-fold and 1.65-fold compared to the free ABTA.

The concentration of HPMC HME and pH of the dissolution media plays an essential role in the dissolution behavior of ABTA SD. When the concentration of HPMC HME 15 LV is increased, there is a notable enhancement in the dissolution rate of ABTA at pH 1.2, whereas, at pH 4.5, there is a decrease in the dissolution rate of ABTA. This disparity can be attributed to the distinct behavior of HPMC HME 15 LV in these environments. In the case of pH 1.2, HPMC HME 15 LV demonstrates a reduced propensity for forming a viscous layer. Consequently, its higher concentration facilitates enhanced dissolution of ABTA, likely by promoting the dissolution of the drug. Conversely, at pH 4.5, HPMC HME 15 LV exhibits the ability to hydrate and form a gel-like structure, forming a viscous solution or layer. As a result, the increased concentration of HPMC HME 15 LV impedes the dissolution rate of ABTA, possibly by forming a barrier that hinders the dissolution of the drug from the formulation. However, the concentration of the HPMC HME and pH directly affects the viscosity of the ABTA SD, as previously discussed in section 6.16.

Owing to this, in the case of HPMC HME 100 LV, the dissolution behavior was the same in both the dissolution media at pH 1.2 and pH 4.5; this is due to the higher molecular weight of HPMC

HME 100 LV, which rapidly swelled and formed a thicker viscous layer which can delay or hinder the drug dissolution. Increasing the HPMC HME 100 LV concentration can increase the formulation's viscosity; this increased viscosity forms a barrier that slows the diffusion of the drug molecules, allowing more time to dissolve in the media.



**Figure 6.14.** In-vitro dissolution profile of ABTA SD formulations extruded at different extrusion temperatures 120°C, 140°C and 160°C and different concentrations of HPMC HME 15LV and 100 LV in pH 4.5 dissolution media

### 6.18. Biorelevant dissolution studies

Biorelevant dissolution studies become particularly crucial when examining drugs susceptible to food effects, which pertain to alterations in a drug's absorption and pharmacokinetics following oral intake alongside food. Given ABTA susceptibility to food effects, it's essential to explore its dissolution under various food conditions. In this context, crystalline ABTA and ABTA SD formulations were subjected to biorelevant dissolution profiling in both FaSSIF (pH 6.5) and FeSSIF (pH 5.0), as illustrated in Figures 6.15 [A] and [B]. Notably, only 8.84 % and 32.20 % of the free ABTA dissolved after 120 min in FaSSIF and FeSSIF, respectively. In-vitro dissolution results indicated that ABTA/SD/2, ABTA/SD/5, ABTA/SD/8, and ABTA/SD/10, extruded at 140°C exhibited higher dissolution rates compared to other ABTA SD formulations in pH 1.2 and pH 4.5. However, only these above-mentioned ABTA SD formulations were used for conducted the biorelevant dissolution studies in FaSSIF (pH 6.5) and FeSSIF (pH 5.0).

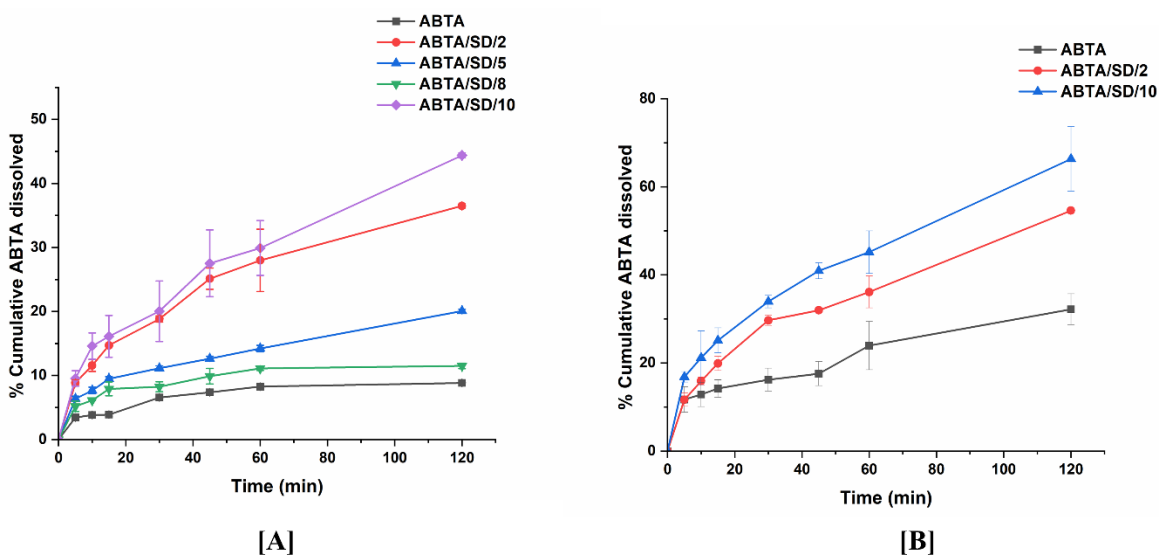


**Figure 6.15.** Biorelevant Dissolution of ABTA SD in [A] FaSSIF (pH 6.5); [B] FeSSIF (pH 5.0)

Figure 6.15 [A] shows the biorelevant dissolution of ABTA/SD/2, ABTA/SD/5, ABTA/SD/8, and ABTA/SD/10 in FaSSIF media. ABTA/SD/2 has an enhanced dissolution rate profile compared to the ABTA/SD/5 and ABTA/SD/8. However, when decreasing the concentration of HPMC HME 15 LV increases the dissolution rate of ABTA; this is due to the HPMC polymer having a higher tendency to form the viscous layer at higher concentrations and pH of dissolution media, which

retard the dissolution. The rate of dissolution of ABTA/SD/2, ABTA/SD/5, and ABTA/SD/8 at 140 °C extrusion temperature was 36.49 %, 16.05 %, and 11.50 % in 120 min, suggesting that dissolution was increased by 4.14-fold for ABTA/SD/2, 1.85-fold for ABTA/SD/5, and 1.30-fold for ABTA/SD/8 compared to the free ABTA. Furthermore, the rate of the dissolution of the HPMC HME 100 LV-based ABTA/SD/10 was 44.38 % in 120 min, suggesting that dissolution was increased by 5.02-fold compared to the free ABTA, which is shown in Figure 6.15. Based on the above result, ABTA/SD/2 and ABTA/SD/10 were selected for the biorelevant dissolution studies in FeSSIF dissolution media. The rate of the dissolution of the ABTA/SD/2 and ABTA/SD/10 was 54.60 % and 66.34 % in 120 min, suggesting that dissolution was increased by 1.70-fold and 2.06-fold compared to the ABTA bulk powder, which is shown in Figure 6.15 [B]. It concluded that ABTA/SD/10 showed a higher dissolution rate in FaSSIF and FeSSIF dissolution media, compared to other ABTA SD formulations and free ABTA

#### **6.19. Mathematical analysis of in-vitro and bio-relevant dissolution data**

The dissolution parameters, such as  $R^2$ -adjusted, DE, MDT, AIC, and MSC, were calculated using the Microsoft Excel add-in DDSolver for both ABTA and the optimized formulation ABTA/SD/2 and ABTA/SD/10 at 140 °C extrusion temperature across various dissolution media. The results are summarized in Table 6.8. It was observed that the dissolution models for the free ABTA and optimized formulation ABTA/SD/2 and ABTA/SD/10 at 140°C extrusion temperature demonstrated a better fit with the Korsmeyer Peppas and Higuchi models in pH 1.2, FaSSIF, and FeSSIF respectively as detailed in Table 6.8. In the case of pH 4.5 dissolution media, the First Order and Korsmeyer Peppas model was observed in ABTA/SD/2 and ABTA/SD/10 at 140 °C. Furthermore, in these dissolution media, the DE for the optimized ABTA/SD/2 and ABTA/SD/10 at 140 °C higher than the free ABTA, whereas the MDT for the optimized formulation of at 140 °C had a faster rate of dissolution than the free ABTA, as illustrated in Table 6.8. Moreover, the ABTA/SD/10 at 140 °C formulation showed good dissolution kinetics compared to the ABTA/SD/2 at 140 °C.



**Table 6.8.** Dissolution parameters of ABTA and ABTA SD in different dissolution media

Formulation	Model	R <sup>2</sup> - adjusted	AIC	MSC	MDT	DE	T50 (min)	T80 (min)
<b>pH 1.2</b>								
ABTA	Korsemeyer Peppas	0.8284	53.02	1.05	27	0.43	74.99	263.6
ABTA/SD/2	Korsemeyer Peppas	0.9971	22.15	3.83	11.96	0.66	<3	55.50
ABTA/SD/10	Korsemeyer Peppas	0.9973	23.52	3.59	10.01	0.89	<3	2.14
<b>pH 4.5</b>								
ABTA	Korsemeyer Peppas	0.9893	22.36	3.45	8.16	0.54	13.36	6080.9
ABTA/SD/2	Korsemeyer Peppas	0.9960	29.90	3.22	5.49	0.92	<3	16.41
ABTA/SD/10	First order	0.9949	31.85	3.18	5.94	0.96	<3	5.449
<b>FaSSIF</b>								
ABTA	Korsemeyer Peppas	0.9549	11.10	2.16	22.17	0.07	18307.9	76074.5
ABTA/SD/2	Korsemeyer Peppas	0.9950	15.23	4.54	36.34	0.25	1523.81	5341.79
ABTA/SD/10	Higuchi	0.9854	26.70	3.63	46.07	0.30	155.68	398.54
<b>FeSSIF</b>								
ABTA	Korsemeyer Peppas	0.8903	38.25	1.39	29.95	0.24	452.05	1579.1
ABTA/SD/2	Higuchi	0.9929	23.18	4.31	42.10	0.35	104.25	275.26
ABTA/SD/10	Korsemeyer Peppas	0.9959	22.38	4.73	40.90	0.44	67.99	189.69

## 6.20. Stability Studies

The optimized ABTA SD formulations (ABTA/SD/2 and ABTA/SD/10) were determined by in-vitro dissolution, DSC, and PXRD, after 90 days with results compared to initial results. The optimized formulation showed no change in the color of the ABTA SD formulation over 90 days compared to the initial results. An in-vitro dissolution study in pH 4.5 dissolution media was conducted to assess the stability of the optimized ABTA SD formulation. The T50 and T80 values showed no significant difference between the initial results and those after 90 days. The % assay of the optimized ABTA SD formulation remained within the range of  $96.67 \pm 1.24$  % to  $103 \pm 2.34$  % after 90 days of the stability study. The PXRD pattern and DSC thermogram of ABTA/SD/2 and ABTA/SD/10 at 0 days and 90 days are shown in Figure 6.16. In the stability

study, the PXRD pattern and DSC thermogram confirmed that the drug was not recrystallized, and ABTA/SD/2 and ABTA/SD/10 formulation was maintained in amorphous form for 90 days at accelerated temperature ( $40 \pm 2 \text{ }^\circ\text{C}/75 \pm 5 \%$  Relative humidity), illustrated in Figure 6.16.

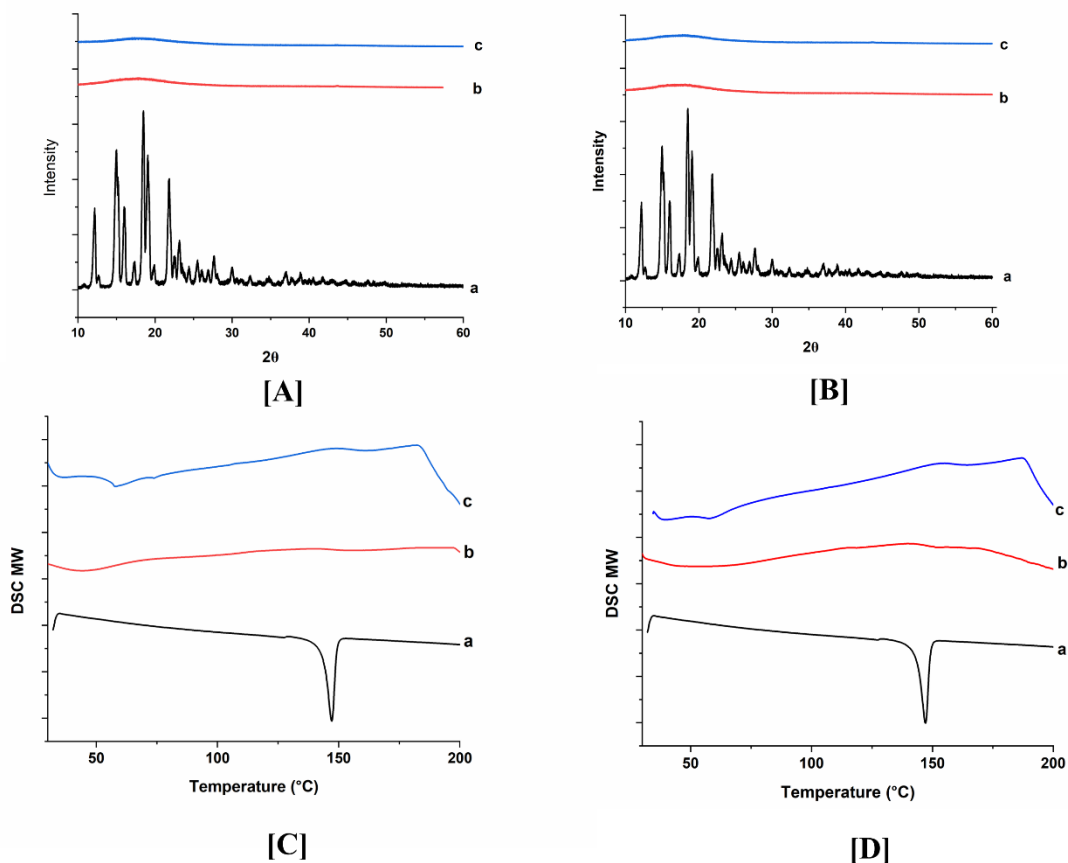


**Figure 6.16.** PXRD patterns [A] of (a) ABTA; (b) ABTA/SD/2 (0 days); (c) ABTA/SD/2 (90 days); [B] (a) ABTA; (b) ABTA/SD/10 (0 days); (c) ABTA/SD/10 (90 days); DSC patterns [C] of (a) ABTA; (b) ABTA/SD/2 (0 days); (c) ABTA/SD/2 (90 days); [D] (a) ABTA; (b) ABTA/SD/10 (0 days); (c) ABTA/SD/10 (90 days)

### 6.21. Conclusion

In this investigation, HPMC HME 15LV and HPMC HME 100 LV were chosen as appropriate polymers for the preparation of a new ABTA SD formulation via the HME technique. The theoretical Hansen solubility parameter indicated that the solubility parameter ( $\Delta\delta$ ) between ABTA and HPMC HME 15 LV and 100 LV was below  $7 \text{ MPa}^{1/2}$ , suggesting excellent miscibility. Both HPMC HME 15 LV and 100 LV exhibited the ability to prevent precipitation, thus

maintaining ABTA supersaturation, showcasing a spring and parachute effect. Solubility studies revealed that all ABTA SD formulations displayed higher solubility compared to free ABTA across all media. Notably, two ABTA SD formulations containing HPMC HME 15 LV (ABTA/SD/2) and HPMC HME 100 LV (ABTA/SD/10) demonstrated enhanced dissolution profiles compared to free ABTA. Among the various extrusion temperatures tested, 140 °C proved most suitable for preparing ABTA SD compared to 120 °C and 160 °C. Analysis via DSC and PXRD suggested that ABTA underwent conversion to the amorphous state within the formulations. ATR-FTIR results indicated decreased functional group intensity, suggesting potential physical interactions between ABTA and HPMC HME 15 LV/HPMC HME 100 LV. Stability assessments revealed that ABTA SD formulations remained amorphous without crystallization, likely due to the exceptional crystal inhibition properties of HPMC HME.

### References

1. Gala U, Miller D, Williams RO. Improved dissolution and pharmacokinetics of abiraterone through kinetisol® enabled amorphous solid dispersions. *Pharmaceutics*. 2020;12(4):1–24.
2. Schönfeld B V., Westedt U, Wagner KG. Compression of amorphous solid dispersions prepared by hot-melt extrusion, spray drying and vacuum drum drying. *International Journal of Pharmaceutics: X*. 2021;3:100102.
3. Zhang Q, Zhao Y, Zhao Y, Ding Z, Fan Z, Zhang H, et al. Effect of HPMCAS on recrystallization inhibition of nimodipine solid dispersions prepared by hot-melt extrusion and dissolution enhancement of nimodipine tablets. *Colloids and Surfaces B: Biointerfaces*. 2018;172:118–126.
4. Agrawal AM, Dudhedia MS, Zimny E. Hot Melt Extrusion: Development of an Amorphous Solid Dispersion for an Insoluble Drug from Mini-scale to Clinical Scale. *AAPS PharmSciTech*. 2016;17(1):133–147.
5. Zhao Y, Xie X, Zhao Y, Gao Y, Cai C, Zhang Q, et al. Effect of plasticizers on manufacturing ritonavir/copovidone solid dispersions via hot-melt extrusion: Preformulation, physicochemical characterization, and pharmacokinetics in rats. *European Journal of Pharmaceutical Sciences*. 2019;127:60–70.
6. Zarmpi P, Flanagan T, Meehan E, Mann J, Fotaki N. Biopharmaceutical Understanding of Excipient Variability on Drug Apparent Solubility Based on Drug Physicochemical

- Properties: Case Study—Hypromellose (HPMC). *AAPS Journal*. 2020;22(2):1–15.
7. Gupta SS, Meena A, Parikh T, Serajuddin ATM. Investigation of thermal and viscoelastic properties of polymers relevant to hot melt extrusion - I: Polyvinylpyrrolidone and related polymers. *Journal of Excipients and Food Chemicals*. 2014;5(1):32–45.
  8. Gupta SS, Solanki N, Serajuddin ATM. Investigation of Thermal and Viscoelastic Properties of Polymers Relevant to Hot Melt Extrusion, IV: Affinisol<sup>TM</sup> HPMC HME Polymers. *AAPS PharmSciTech*. 2016;17(1):148–157.
  9. Wu H, Liu Y, Ci T, Ke X. Application of HPMC HME polymer as hot melt extrusion carrier in carbamazepine solid dispersion. *Drug Development and Industrial Pharmacy*. 2020;46(12):1911–1918.
  10. Simões MF, Pereira A, Cardoso S, Cadonau S, Werner K, Pinto RMA, et al. Five-Stage Approach for a Systematic Screening and Development of Etravirine Amorphous Solid Dispersions by Hot-Melt Extrusion. *Molecular Pharmaceutics*. 2020;17(2):554–568.
  11. Greenhalgh DJ, Williams AC, Timmins P, York P. Solubility parameters as predictors of miscibility in solid dispersions. *Journal of Pharmaceutical Sciences*. 1999;88(11):1182–1190.
  12. Mukesh S, Joshi P, Bansal AK, Kashyap MC, Mandal SK, Sathe V, et al. Amorphous Salts Solid Dispersions of Celecoxib: Enhanced Biopharmaceutical Performance and Physical Stability. *Molecular Pharmaceutics*. 2021;18(6):2334–2348.
  13. Zhao Y, Inbar P, Chokshi HP, Malick AW, Choi DS. Prediction of the Thermal Phase Diagram of Amorphous Solid Dispersions by Flory–Huggins Theory. *Journal of Pharmaceutical Sciences*. 2011;100(8):3196–3207.
  14. Butreddy A, Sarabu S, Almutairi M, Ajjarapu S, Kolimi P, Bandari S, et al. Hot-melt extruded hydroxypropyl methylcellulose acetate succinate based amorphous solid dispersions: Impact of polymeric combinations on supersaturation kinetics and dissolution performance. *International Journal of Pharmaceutics*. 2022;615:121471.
  15. Tekade AR, Yadav JN. A review on solid dispersion and carriers used therein for solubility enhancement of poorly water soluble drugs. *Advanced Pharmaceutical Bulletin*. 2020;10(3):359–369.
  16. Punitha S, Uvarani R, Panneerselvam A. Effect of pH in aqueous (Hydroxy Propyl Methyl Cellulose) polymer solution. *Results in Materials*. 2020;7:100120.

17. Singhvi G, Shah A, Yadav N, Saha RN. Study the effect of formulation variables on drug release from hydrophilic matrix tablets of milnacipran and prediction of in-vivo plasma profile. *Pharmaceutical Development and Technology*. 2014;19(6):708–716.

# **Chapter 7: Pharmacokinetic studies**

## **7.0 Introduction**

Establishing the appropriate dosage regimen and evaluating the delivery system's potential to target the intended site and the therapeutic efficacy and safety are paramount considerations following the formulation development. Pharmacokinetics evaluation plays a pivotal role in drug development and novel delivery systems by providing crucial insights into how drugs are absorbed, distributed, metabolized, and eliminated within the body. Understanding these processes is essential for optimizing drug formulations and evaluation to ensure efficacy, safety, and patient compliance. Pharmacokinetic studies help to determine the appropriate dosage regimen, predict drug interactions, and assess bioavailability and selective distribution, enabling the development of more effective and efficient delivery systems. By comprehensively evaluating drug behavior *in-vivo*, pharmacokinetics contributes significantly to the design and refinement of pharmaceutical formulations, ultimately enhancing therapeutic outcomes and patient care. Preclinical animal studies serve to identify potential lead compounds, optimize formulations, establish appropriate dosing regimens, including route, frequency, and duration of exposure, and determine the starting dose for phase I clinical trials in humans (1).

In oral drug delivery, SD has been shown to enhance *in-vitro* performance as well as *in-vivo* bioavailability in animals and humans (2). SD can address the challenges associated with poorly water-soluble anticancer drugs and other drugs, such as gastro-intestinal solubility, improving oral bioavailability, minimizing pharmacokinetic variability (3,4), enhancing pharmacokinetic linearity (5,6), and reducing toxicity (7). Apart from the pharmacokinetic benefits, SD formulations of poorly water-insoluble drugs offer additional advantages, including dose reduction and decreased patient pill burden, thereby enhancing patient compliance (8).

In the present study, ABTA SD formulation was prepared through the solvent granulation method employing the different grades of the HPMCAS 716 and HPMCAS 912. The composition and preparation method of the ABTA SD formulations are outlined in Chapter 5. The outcomes revealed that the optimized F2 and F5 formulations exhibited higher solubility and dissolution rates than free ABTA. The transformation of ABTA into an amorphous state during SD formation was confirmed through DSC, PXRD, FTIR, and FE-SEM analyses. Subsequently, an ABTA SD formulation was formulated using the HME method, incorporating different concentrations of HPMC HME 15LV and HPMC HME 100 LV at varying extrusion temperatures. Chapter 6 briefly

details the compositions and preparation methods of the ABTA SD formulations. Solubility studies indicated that all ABTA SD formulations had higher solubility across all media than free ABTA. Notably, ABTA/SD/2 and ABTA/SD/10 formulations, containing HPMC HME 15 LV and HPMC HME 100 LV, respectively, demonstrated enhanced dissolution profiles compared to bulk ABTA powder. Analysis using DSC and PXRD suggested the conversion of ABTA into an amorphous state within the formulations.

On the basis of the solubility, dissolution, and amorphization characteristics, the F2, F5, ABTA/SD/2, and ABTA/SD/10 formulations were selected for pharmacokinetic studies in animal models. The current investigation of SD of ABTA has been developed with the objective of enhancing the absorption and oral bioavailability of ABTA. The pharmacokinetic studies were carried out on selected optimized ABTA SD formulations (F2, F5, ABTA/SD/2, and ABTA/SD/10), which were orally administered to the Wistar rats. The pharmacokinetic parameters such as maximum plasma concentration ( $C_{max}$ ), area under the curve ( $AUC_{0-t}$ , and  $AUC_{0-\infty}$ ),  $T_{max}$ , and MRT of the developed formulation were determined and compared to the free ABTA.

### 7.1. Experimental

#### 7.1.1 Materials and Equipment

The drug, formulation excipients, and chemicals were procured from the same suppliers previously referenced in Chapters 5 and 6. Prior to usage, all surgical instruments, such as scissors, forceps, and syringes, underwent sterilization procedures. For this study, selective optimized formulations (F2, F5, ABTA/SD/2, and ABTA/SD/10), discussed in Chapters 5 and 6 were utilized and compared against a suspension of free ABA administered orally.

#### 7.1.2. Animals

All experimental protocols were approved by the Institutional Animal Ethics Committee (IAEC) before start of the work ( Protocol No. IAEC/RES/32/01). Healthy Wistar rats were selected for pharmacokinetic studies for free ABTA and ABTA SD formulations. Rats with an average weight of 200-250 gm (6-8 weeks old) were issued from Central Animal Facility (CAF), BITS, Pilani, Pilani Campus, Rajasthan, India. Animals were kept in a standard plastic cage maintained under controlled conditions (  $23 \pm 2$  °C,  $60 \pm 5\%$  RH, and 12h dark-light cycle) and provided standard



laboratory pellet food with water ad libitum. Rats were acclimated to the study environment for at least five days before the study began. Throughout the study, all animals were monitored for general conditions, unusual signs, toxicity, and mortality.

### 7.1.3. In-vivo pharmacokinetic studies

Pharmacokinetic studies were carried out after a single oral administration of free ABTA and ABTA SD formulations administered orally in an equivalent dose. The concentration of ABT active metabolite of the ABTA was determined in the plasma, and the pharmacokinetic parameters of free ABTA and ABTA SD formulations are determined by using Phoenix WinNolin Certera™ (Pharsight, U.S.A; version:8.0). All the procedures are followed by the standard protocols.

Pharmacokinetic studies were performed on 5 groups (n=3) that received different oral formulations under fasting conditions. The rats were divided into five groups and given oral suspensions as follows: Group 1 was administered the free drug ABTA; Group 2 was administered ABTA with HPMCAS 716 (F2); Group 3 was administered ABTA with HPMCAS 912 (F5); Group 4 was administered ABTA with HPMC HME 15 LV (ABTA/SD/2); Group 5 was administered ABTA with HPMC HME 100 LV (ABTA/SD/10). Prior to the start of the experiments, animals were given free access to water and allowed to fast overnight for 12 h. The animals were marked, weighed, and dosed as per their body weight. The rats were administered orally with the suspension of ABTA, F2, F5, ABTA/SD/2, and ABTA/SD/10 by gavage as a single dose of 200 mg/kg of the drug. All the solutions and dispersion were prepared fresh and used immediately without any additional treatments.

Blood samples (0.5 mL) were collected from the retro-orbital venous plexus at specific time intervals (0.5h, 1h, 2h, 4h, 6h, 8h, and 12h) post-administration, respectively. Collected blood samples were transferred into a labeled microcentrifuge tube containing 20 µL of 10 % EDTA as an anticoagulant and mixed well. The plasma samples were separated by centrifugation at 8000 rpm for 10 min at 4°C. The supernatant was collected and stored at -20 °C till further analysis (9-11). The samples were analyzed using the bioanalytical procedure described in Chapter 3.

### 7.1.4. Pharmacokinetic Data Analysis

The obtained chromatographic peak was calculated for plasma drug concentration. To understand the plasma profile, plasma drug concentration vs. time was plotted. The maximum observed

plasma concentration ( $C_{\max}$ ) was recorded directly from the individual plasma concentration versus time profiles. Various pharmacokinetic parameters such as area under the curve ( $AUC_{0-t}$ , and  $AUC_{0-\infty}$ ),  $T_{\max}$ , and MRT were estimated using Phoenix WinNolin Certera™ (Pharsight, U.S.A; version:8.0). The relative bioavailability ( $F_{\text{rel}}$ ) of SD formulations were calculated using  $AUC_{0-\alpha}$  with respect to same for free ABTA suspension administered.

## 7.2. Result and discussions

The plasma concentration-time profile of ABT after a single-dose administration of free ABTA and an equivalent dose of ABTA SD formulations are illustrated in Figure 7.1. A comparison was made between the free ABTA and the optimized ABTA SD formulations (F2, F5, ABTA/SD/2, and ABTA/SD/10). The free ABTA fell below measurable levels within 6h, whereas the formulation remained detectable for a longer period of about 8 to 12h or more. Notably, the F2 and ABTA/SD/12 formulations were still detectable even after 12 h. The free ABTA showed a  $C_{\max}$  of  $243.27 \pm 24.40$  ng/mL with a  $T_{\max}$  of 3.33 h. Comparatively, the  $C_{\max}$  of ABTA SD of the F2 and F5 batches were  $466.76 \pm 14.75$  ng/mL and  $306.30 \pm 6.22$  ng/mL, respectively increased 1.92-fold and 1.26-fold when compared to the free ABTA.  $T_{\max}$  of F2 was found to be higher (6.67 h), but that of F5 was found to be lower (2.7h). The pharmacokinetics parameters of the free ABTA and all SD formulations are presented in Table 7.1. The  $AUC_{0-4h}$  of free ABTA was  $1102.8 \pm 47.6$  ng/mL, whereas the  $AUC_{0-12h}$  of F2 and  $AUC_{0-8h}$  of F5 batch were  $4299.1 \pm 66.7$  ng/mL.min and  $1910.4 \pm 12.97$  ng/mL. min, respectively, increased by 3.90-fold and 1.73-fold, respectively, when compared to the free ABTA.

The  $C_{\max}$  of ABTA SD of the ABTA/SD/2 and ABTA/SD/10 batches were  $1014.9 \pm 12.97$  ng/mL and  $1514.6 \pm 185.5$  ng/mL, respectively, increased by 4.17-fold and 6.22-fold when compared to the free ABTA, whereas the  $AUC_{0-8h}$  of ABTA/SD/2 and  $AUC_{0-12h}$  of ABTA/SD/10 batch were  $3243.1 \pm 517.7$  ng/mL.min and  $7342.7 \pm 1147$  ng/mL. min, increased by 2.95-fold and 6.66-fold increase when compared to the free ABTA. The  $T_{\max}$  of the F5, ABTA/SD/2, and ABTA/SD/10 formulations were found to be lower than that of free ABTA, indicating faster absorption. The pharmacokinetic profile of the ABTA/SD/2 formulation based on HPMC HME 15LV exhibited a  $T_{\max}$  of 0.66 h, whereas the ABTA/SD/10-based HPMC HME 100LV showed a  $T_{\max}$  of 2 h. This difference in  $T_{\max}$  can be attributed to the molecular weight variation of the HPMC HME. Briefly, the lower molecular weight HPMC HME 15LV facilitated quicker dissolution and absorption of

the drug, resulting in a reduced  $T_{max}$ . Conversely, the higher molecular weight HPMC HME 100LV led to faster swelling and the formation of a thicker viscous layer, acting as a barrier that slow the diffusion of drug molecules, thereby delaying absorption and prolonging the  $T_{max}$ . The pharmacokinetic profile of the ABTA/SD/10 formulation processed at 140°C demonstrated a higher  $C_{max}$  compared to ABTA/SD/2. This can be attributed to the higher concentration and molecular weight of HPMC HME 100 LV polymer in the formulation. Overall, the study clearly indicates that ABTA SD formulations, particularly ABTA/SD/10 processed at 140°C, exhibit superior ABTA absorption compared to free ABTA.

The mean residence time (MRT) for all the SD formulations was found to be higher compared to free ABTA, suggesting that more drugs were absorbed, and the drug remained in the body for a longer period. This extended residence time can improve therapeutic effectiveness and patient compliance and potentially reduce the frequency of dosing. The bioavailability of the developed formulation of F2, F5, ABTA/SD/2, and ABTA/SD/10 were 3.89-fold, 1.73-fold, 2.95-fold, and 6.66-fold enhanced compared to free ABTA.

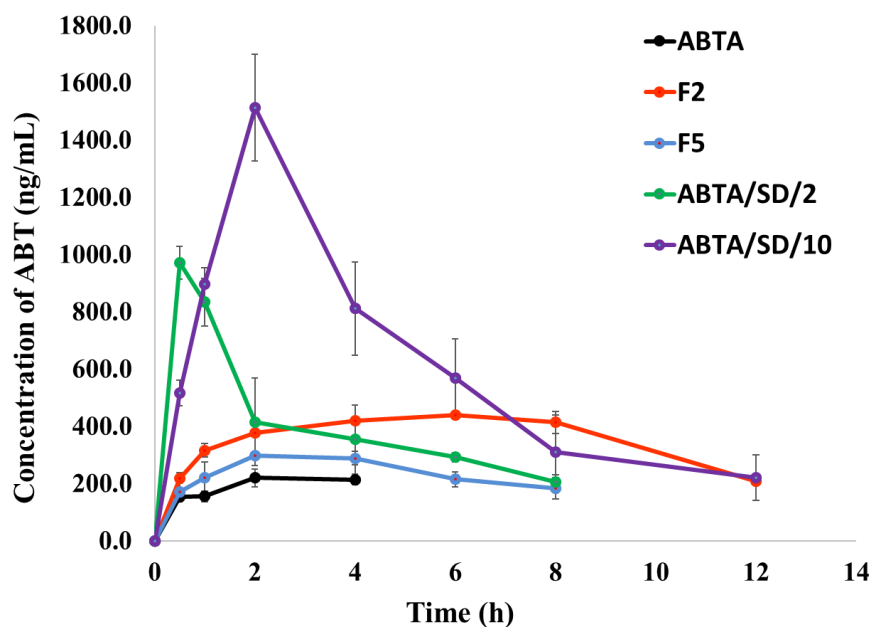


**Fig 7.1.** Plasma concentration-time profile of free ABTA and ABTA SD based on HPMCAS and HPMC HME after oral administration (Values represent mean + SEM)

**Table 7.1.** Pharmacokinetic parameters of free ABTA and ABTA SD after oral administration

Parameters	ABTA	F2	F5	ABTA/SD/2	ABTA/SD/10
<b>T<sub>max</sub> (h)</b>	3.33 ± 0.67	6.67 ± 0.67	2.7 ± 0.67	0.66 ± 0.16	2
<b>C<sub>max</sub> (ng/mL)</b>	243.27 ± 24.4	466.76 ± 14.75	306.3 ± 6.22	1014.9 ± 30.14	1514.6 ± 185.5
<b>AUC<sub>0-12</sub> (ng/mL.min)</b>	1102.8 ± 47.6	4299.1 ± 66.7	1910.4 ± 12.97	3243.1 ± 517.7	7342.7 ± 1147
<b>AUC<sub>0-∞</sub> (ng/mL.min)</b>	2622.22 ± 335	6508.17 ± 1140.9	3707.9 ± 547.65	4693.8 ± 344.2	8733.38 ± 1844.17
<b>t<sub>1/2</sub> (h)</b>	7.07 ± 1.6	6.20 ± 2.0	6.9 ± 1.18	4.64 ± 1.19	3.94 ± 0.3
<b>Vd (L/Kg)</b>	755.92 ± 100.5	264.41 ± 43.8	531.22 ± 17.25	289.50 ± 74.86	133.24 ± 7.60
<b>CL (L/h/Kg)</b>	79.18 ± 11.4	32.88 ± 5.29	56.75 ± 9.6	43.10 ± 3.38	24.72 ± 4.32
<b>Ke</b>	0.11 ± 0.074	0.14 ± 0.04	0.11 ± 0.06	0.18 ± 0.06	0.18
<b>MRT</b>	3.11 ± 0.1	5.82 ± 0.22	4.0 ± 0.11	3.13 ± 0.03	4.18 ± 0.39
<b>F<sub>rel</sub></b>	1	3.89	1.73	2.95	6.66

The free ABTA shows reduced exposure in the C<sub>max</sub>, AUC, and bioavailability attributed to the larger crystalline particles of the unformulated ABTA, which undergo slow dissolution and consequently exhibit limited absorption. But in the case of SD formulations, improved exposures demonstrate the desirable effect on the pharmacokinetic profile due to the micronized ABTA, the transformation of a crystalline state to an amorphous state, and the capability of HPMCAS to prevent precipitation, thereby maintaining the supersaturated state of ABTA. The pharmacokinetic profile of ABTA SD (F2) showed a delayed C<sub>max</sub> when compared to the free ABTA due to the pH-responsive nature of HPMCAS. Due to the tendency of API to release more when a pH shift is present, this HPMCAS may exhibit delayed dissolution or swelling under certain pH conditions, which in turn delays the release and absorption of the drug. Meanwhile, the cases of the ABTA/SD/2 and ABTA/SD/10 increased bioavailability by 2.95-fold and 6.66-fold compared to the free ABTA. These enhanced revelations observed the beneficial effect of reducing the particle size of ABTA; the formation of an amorphous state of the ABTA enhances solubility by disrupting the ordered crystalline structure; the intimate mixing of the drug and polymer promotes strong interactions, and the prevention of drug recrystallization maintains enhanced solubility over time.

The ABTA/SD/2 and ABTA//SD/10 formulations were prepared using the HME method using the HPMC HME 15LV and 100 LV, which showed a higher C<sub>max</sub> compared to the F2 and F5

formulations. The ABTA/SD/10 showed higher relative bioavailability compared to the ABTA/SD/2, F2 and F5 formulations. This is due to the hydrophilic properties and molecular weight of HPMC HME 100LV and the preparation method of this formulation. The pharmacokinetic parameters of HPMCAS and HPMC HME polymers are influenced by their respective nature and properties. HPMCAS, an amphiphilic and pH-dependent polymer with diverse acetate and succinate substitution patterns, and HPMC HME, a hydrophilic polymer with varied molecular weights, significantly impact dissolution and absorption processes. More importantly, the preparation methods, such as solvent granulation and the HME method, play crucial roles in enhancing the dissolution and absorption of ABTA. Consequently, the current study clearly demonstrates that ABTA SD absorption is higher with HPMC HME 100 LV polymer-based SD compared to HPMCAS.

### 7.3. Conclusion

A pharmacokinetic study of single-dose administration of pure drug and SD formulations in amounts equivalent to 200 mg/Kg of ABTA showed a significant increase in the  $C_{max}$  and area under the curve ( $AUC_{0-12h}$  and  $AUC_{0-\infty}$ ) compared to the free ABTA. The bioavailability of the developed formulations F2, F5, ABTA/SD/2, and ABTA/SD/10 was found to show 3.89-fold, 1.73-fold, 2.95-fold, and 6.66-fold, respectively enhanced compared to free ABTA.  $T_{max}$  for F5, ABTA/SD/2, and ABTA/SD/10 were found to decrease compared to FD to different degrees, indicating faster absorption of ABTA. The ABTA/SD/10 processed at 140°C demonstrated the highest bioavailability compared to all the ABTA SD formulations. The SD formulation showed enhanced pharmacokinetic parameters due to the transformation of a crystalline state to an amorphous state, the amphiphilic and hydrophilic nature of the polymer, the preparation method, and the capability of HPMCAS and HPMC HME to prevent precipitation, thereby maintaining the supersaturated state of ABTA. The present research clearly indicates that absorption of ABTA is improved for SD based on HPMC HME 100 LV polymer compared to the HPMCAS.

### References

1. P.M. Glassman, V.R. Muzykantov, Pharmacokinetic and pharmacodynamic properties of drug delivery systems, *The Journal of Pharmacology and Experimental Therapeutics*. 370 (2019) 570–580.
2. A. Schittny, J. Huwyler, M. Puchkov, Mechanisms of increased bioavailability through

- amorphous solid dispersions: a review, *Drug Delivery*. 27 (2020) 110–127.
3. Y. Gu, M. Xue, Q. Wang, X. Hong, X. Wang, F. Zhou, J. Sun, Y. Peng, G. Wang, Novel strategy of proxalutamide for the treatment of prostate cancer through coordinated blockade of lipogenesis and androgen receptor axis, *International Journal of Molecular Science* 2021(22) 1–14.
  4. S.D. Undevia, G. Gomez-Abuin, M.J. Ratain, Pharmacokinetic variability of anticancer agents, *Nature Review. Cancer* 200; 447–458.
  5. H. Chen, K. Shien, K. Suzawa, K. Tsukuda, S. Tomida, H. Sato, H. Torigoe, M. Watanabe, K. Namba, H. Yamamoto, J. Soh, H. Asano, S. Miyoshi, S. Toyooka, Elacridar, a third-generation ABCB1 inhibitor, overcomes resistance to docetaxel in non-small cell lung cancer, *Oncol. Lett.* 2017(14) 4349–4354.
  6. E. Sawicki, R.B. Verheijen, A.D.R. Huitema, O. van Tellingen, J.H.M. Schellens, B. Nuijen, J.H. Beijnen, N. Steeghs, Clinical pharmacokinetics of an amorphous solid dispersion tablet of elacridar, *Drug Delivery Translational Research*. 2017(7) 125–131.
  7. C. Shanholtz, Acute life-threatening toxicity of cancer treatment, *Critical Care Clinics*. 2001 (17) 483–502.
  8. U.H. Gala, D.A. Miller, R.O. Williams, Harnessing the therapeutic potential of anticancer drugs through amorphous solid dispersions, *BBA Reviews on Cancer* 1873 (202) 188319.
  9. S.V. Kumar, G. Rudresha, S. Gurav, M. Zainuddin, P. Dewang, R.R. Kethiri, S. Rajagopal, R. Mullangi, Validated RP-HPLC/UV method for the quantitation of abiraterone in rat plasma and its application to a pharmacokinetic study in rats, *Biomedical Chromatography* 2013 (20) 203–207.
  10. H.B. Schultz, A.D. Wignall, N. Thomas, C.A. Prestidge, Enhancement of abiraterone acetate oral bioavailability by supersaturated-silica lipid hybrids, *International Journal of Pharmaceutics*. 2020 (582) 119264.
  11. Y. Liu, Y. Li, P. Xu, Y. Shen, B. Tang, Q. Wang, Development of Abiraterone Acetate Nanocrystal Tablets to Enhance Oral Bioavailability: Formulation Optimization, Characterization, In Vitro Dissolution and Pharmacokinetic Evaluation, *Pharmaceutics* 14 (2022).

## **Chapter 8. Summary and Conclusion**

## **Summary and Conclusion**

Cancer stands as a primary contributor to mortality worldwide, highlighting the critical need for comprehensive strategies aimed at prevention and advanced treatments to reduce its impact on global health. The growing challenges of cancer treatment underscore the need not only for exploring and manufacturing novel anticancer drugs but also for improving the present anticancer drug. Prostate cancer is one of the most common cancers diagnosed in men worldwide. ADT is an effective treatment for controlling prostate cancer, especially during the phase when serum testosterone levels are suppressed. However, the disease eventually progresses to a phase known as mCRPC, where it continues to advance despite ongoing testosterone inhibition. The treatment landscape for mCRPC has greatly expanded with the introduction of several drugs, including enzalutamide, sipuleucel-T, docetaxel, cabazitaxel, radium-223, and ABTA. The approval of ABTA has significantly enhanced treatment options for prostate cancer, especially when combined with prednisone, demonstrating synergistic benefits and improved outcomes in mCRPC patients previously treated with docetaxel. Consequently, ABTA is considered a primary treatment option for prostate cancer, offering survival benefits, particularly for those with mCRPC. However, this available drug has its own limitations. It falls under the BCS class IV, characterized by extremely poor aqueous solubility ( $< 0.5\mu\text{g/mL}$ ) as well as low permeability, leading to poor oral bioavailability. Due to this, patients must consume a high daily dose of ABTA 1000 mg per day to achieve therapeutic efficacy, which can result in dose-related side effects such as hepatotoxicity, hypokalemia, and hypertension. Therefore, there is a need to develop new pharmaceutical formulations that enhance solubility through improved dissolution, thereby increasing the bioavailability of ABTA and leading to better therapeutic efficacy.

In this dissertation, we formulated the SD of ABTA by employing HPMCAS and HPMC HME polymers to address the challenges associated with ABTA. Initially, we developed and validated the UV visible and RP-HPLC analytical methods. The methods were simple, specific, accurate, precise, and robust. These methodologies were effectively utilized for preformulation investigations, % assay analysis, as well as in vitro and biorelevant dissolution examinations. Additionally, an accurate and precise simultaneous bioanalytical method for ABT and ABTA was developed and validated, facilitating the determination of their concentrations in rat plasma during pharmacokinetic studies. In the preformulation study, ABTA showed pH-dependent solubility,



slightly soluble in the pH range of 1-2, and practically insoluble in pH from 3-12. In the solution stability study, it was observed that ABTA is stable under acidic conditions, and the degradation rate increases (K) as the pH shifts from acidic to neutral.

In the present study, the SD of ABTA was prepared using the different grades of the HPMCAS 716 and 912 polymers using the solvent evaporation and solvent granulation method. The solubility parameter ( $\Delta\delta$ ) between the ABTA and HPMCAS was below  $7 \text{ MPa}^{1/2}$ , suggesting good miscibility amongst them according to the Hansen solubility parameter. The solubility studies of the optimized formulation of SD-based HPMCAS 716 (F2) and HPMCAS 912 (F5) in distilled water, pH 6.8, 0.1 N HCl (pH 1.2), FaSSIF (pH 6.5), and FeSSIF (pH 5.0) showed higher solubility compared to the free ABTA. It was observed that the F2 formulation-based HPMCAS 716 SD had higher solubility than the F5 formulation-based HPMCAS 912 SD, which indicated the substantial impact of acetate and succinate substitution. However, HPMCAS 716, a cellulose succinate derivative containing the 14-18% succinate and 5-9% acetate group, imparts hydrophilicity. While HPMCAS 912 polymer with 10-14% succinate group and 7-11% acetate group exhibits hydrophobicity, as an increase in the acetate group corresponds to hydrophobicity, while an increase in the succinate group correlates with hydrophilicity. The enhanced solubility of ABTA in HPMCAS 716 polymer is due to its hydrophilic properties compared to HPMCAS 912.

The precipitation inhibition study concluded that pre-dissolved HPMCAS 716 and 912 acted as a "Spring and Parachute" effect, stabilizing supersaturation and impeding crystal nucleation and growth. The amorphization of the ABTA during the SD formation was confirmed by the DSC, PXRD, and FTIR studies. In-vitro and bio-relevant dissolution behavior of ABTA was conducted in the various dissolution media, indicating the higher dissolution of ABTA SD (F2 and F5) compared to free ABTA. The stability assessment indicated that the ABTA SD maintained its amorphous state without undergoing crystallization, possibly due to the effective inhibition of crystal formation by HPMCAS. The pharmacokinetic parameter of the ABTA in the F2 and F5 batches of the SD exhibited higher  $C_{\text{max}}$ , which was enhanced by 1.92-fold and 1.26-fold, whereas  $\text{AUC}_{0-12}$  of F2 and  $\text{AUC}_{0-8\text{h}}$  of F5 batches enhanced by 3.90-fold and 1.73-fold compared to the free ABTA. These improved exposures demonstrate the advantageous effect of reducing the particle size of ABTA, the formation of an amorphous state of the ABTA by disrupting the ordered crystalline structure; the intimate mixing of the drug and polymer promotes strong interactions,

and the prevention of drug recrystallization maintains enhanced solubility over time.

Furthermore, in this investigation, HPMC HME 15LV and 100 LV were chosen as polymers for the preparation of an ABTA SD formulation via the HME technique. The theoretical Hansen solubility parameter indicated that the solubility parameter ( $\Delta\delta$ ) between ABTA and HPMC HME (15 LV and 100 LV) was below  $7 \text{ MPa}^{1/2}$ , suggesting excellent miscibility. Both HPMC HME (15 LV and 100 LV) exhibited the ability to prevent precipitation, thus maintaining ABTA supersaturation, showcasing a spring and parachute effect. Solubility studies revealed that ABTA SD formulation, at all the extrusion temperatures (120 °C, 140 °C, and 160 °C), displayed higher solubility compared to the free ABTA across the media. Moreover, it was observed that the extrusion temperature during the HME process (120 °C, 140 °C, and 160 °C) and the concentration of HPMC HME polymer significantly impacted the dissolution behavior of the ABTA SD formulations. Among the various extrusion temperatures tested, 140 °C proved most suitable for preparing ABTA SD compared to 120 °C and 160 °C. Notably, two ABTA SD formulations containing HPMC HME 15 LV (ABTA/SD/2) and HPMC HME 100 LV (ABTA/SD/10) demonstrated enhanced dissolution profiles compared to free ABTA bulk powder. The concentration of HPMC HME significantly influences the dissolution characteristics of ABTA SD in both pH 1.2 and pH 4.5 dissolution media. Analysis via DSC and PXRD suggested that ABTA underwent conversion to the amorphous state within the formulations. ATR-FTIR results indicated decreased functional group intensity, suggesting potential physical interactions between ABTA and HPMC HME 15 LV/HPMC HME 100 LV. Stability assessments revealed that ABTA SD formulations remained amorphous without crystallization, likely due to the exceptional crystal inhibition properties of HPMC HME. The pharmacokinetic parameter of the ABTA in the ABTA/SD/2 and ABTA/SD/10 batches of the SD exhibited higher  $C_{\text{max}}$ , which was enhanced by 4.17-fold and 6.22-fold, whereas  $\text{AUC}_{0-8\text{h}}$  of ABTA/SD/2 and  $\text{AUC}_{0-12\text{h}}$  of ABTA/SD/10 batches enhanced by 2.95-fold and 6.66-fold compared to the free ABTA.

All ABTA SD formulations i.e., F2 and F5 formulations prepared from HPMCAS (716 and 912), and ABTA/SD/2 and ABTA/SD/10 formulations prepared from the HPMC HME (15LV and 100LV) showed significant increases in the  $C_{\text{max}}$  and AUC compared to the free ABTA. The bioavailability of the developed formulation of F2, F5, ABTA/SD/2, and ABTA/SD/10 was 3.89-fold, 1.73-fold, 2.95-fold, and 6.66-fold enhanced compared to free ABTA.

The SD formulation of ABTA showed enhanced solubility and dissolution and improved pharmacokinetic parameters compared to the free ABTA. This is due to the conversion of a crystalline state to an amorphous state, the amphiphilic and hydrophilic nature of the polymer, the preparation method, and the ability of HPMCAS and HPMC HME to prevent precipitation, thereby maintaining the supersaturated state of ABTA. The current study clearly demonstrates that the absorption of ABTA is enhanced with the SD formulation using HPMC HME 100 LV polymer compared to HPMCAS. This research addresses significant challenges associated with the anticancer drug ABTA. The results strongly suggest that the formulated SD systems offer promising solutions to enhance ABTA solubility, dissolution rate, and bioavailability. These SD formulations have the potential to improve the therapeutic effectiveness of ABTA against prostate cancer. Moreover, the scalable and industrially feasible preparation methods underscore the prospect of advancing treatment strategies for prostate cancer.

# **APPENDICES**

### **Thesis related Publications**

**Choudhari M**, Donthi M, Damle S, et al (2022) Implementation of Quality by Design Approach for Optimization of RP-HPLC Method for Quantification of Abiraterone Acetate in Solid Dispersion in Forced Degradation Studies. *Current chromatography*, 09 <https://doi.org/10.2174/2213240609666221110090339>

**Choudhari M**, Damle S, Narayan R, et al (2023) Emerging Applications of Hydroxypropyl Methylcellulose Acetate Succinate: Different Aspects in Drug Delivery and Its Commercial Potential. *AAPS PharmSciTech* 1–26. <https://doi.org/10.1208/s12249-023-02645-1>

**Choudhari M**, Damle S, Narayan S, Dubey S, Singhvi G, Formulating Abiraterone Acetate-HPMCAS based Amorphous Solid Dispersion: Insight into In-Vitro and Biorelevant Dissolution Assessment and Pharmacokinetic Evaluation (under communication)

**Choudhari M**, Damle S, Narayan S, Dubey S, Singhvi G, Hot Melt Extruded-Abiraterone Acetate Solid Dispersion: An Industrial Feasible Approach for Enhancement of Solubility, Dissolution, and Bioavailability (under communication)

### **Other Publications**

Damle S, **Choudhari M**, Singhvi G, et al (2021) Development and Validation of Reverse-Phase High-Performance Liquid Chromatography Method for Estimation of Itraconazole through Hydroxypropyl Methylcellulose Acetate Succinate based Polymeric Films using Quality by Design principles. *Sep Sci Plus* 4:388–400. <https://doi.org/10.1002/sscp.202100037>

Singh G, Singh D, **Choudhari M**, et al (2021) Exemestane encapsulated copolymers L121/F127/GL44 based mixed micelles: solubility enhancement and in vitro cytotoxicity evaluation using MCF-7 breast cancer *J Pharm Investig* 51:701–714. <https://doi.org/10.1007/s40005-021-00540-0>

**Choudhari M**, Hejmady S, Narayan Saha R, et al (2021) Evolving new-age strategies to transport therapeutics across the blood-brain-barrier. *Int J Pharm* 599:120351. <https://doi.org/10.1016/j.ijpharm.2021.120351>

Priya S, **Choudhari M**, Tomar Y, et al (2024) Exploring polysaccharide-based bio-adhesive topical film as a potential platform for wound dressing application: A review. Carbohydrate Polymer 327:121655. <https://doi.org/10.1016/j.carbpol.2023.121655>

### **Book Chapters**

**Choudhari M**, Dey A, Singhvi G, Saha RN, Dubey SK. Approaches for administration of nanocosmetics. Nanocosmetics: Delivery Approaches, Applications and Regulatory Aspects. 2023 Sep 21;47-59.

**Choudhari M**, Dey A, Singhvi G, Saha RN, Dubey SK Fabrication of nanocosmetics. Nanocosmetics: Delivery Approaches, Applications, and Regulatory Aspects. 2023 Sep 21;61–92

### **Conference Presentation**

**Manisha Choudhari**, Ranendra Narayan Saha, Sunil Kumar Dubey, Gautam Singhvi “Solubility Enhancement of Abiraterone acetate: HPMCAS-stabilized Solid Dispersion Prepared by Solvent Evaporation Method” A scientific oral presentation competition for young pharmaceutical research across academia and industry, organized by SPDS in association with AAPS and APTI 2021.

**Manisha Choudhari**, Ranendra Narayan Saha, Sunil Kumar Dubey, Gautam Singhvi “Industrially Feasible and Scalable Approach in the Manufacture of HPMCAS-Stabilized Amorphous Solid Dispersion of Abiraterone Acetate” A scientific oral presentation competition for young pharmaceutical research across academia and industry, organized by SPDS in association with AAPS and APTI, Dissolution research presentation India (DRPI)-2022, 9-10th July 2022

**Manisha Choudhari**, Ranendra Narayan Saha, Sunil Kumar Dubey, Gautam Singhvi “Manufacturing of Abiraterone Acetate Amorphous Solid Dispersion Using HPMCAS: An Industrially Feasible and Scalable Approach” in 5<sup>th</sup> National Biomedical Research Competition dated 9-10<sup>th</sup> December 2023 (NBRCOM 2023, SYBS, India)

## Awards

Achieving **3rd position** in Central east south Zone in Dissolution Research\_Presentation India, 9<sup>th</sup> and 10<sup>th</sup> July 2022

Awarded '**Best Poster Award**' on Research Scholars' Day at BITS Pilani, Pilani Campus, 5th January 2024

## **Supervisor's Biography**

### **Prof. Gautam Singhvi**

Prof. Gautam Singhvi is an Associate Professor in the Department of Pharmacy, BITS, Pilani. He obtained his Ph.D. from BITS Pilani. He has 3 years of industrial research and 10 years of academic teaching and research experience. During his industrial tenure, he worked on solid oral, pellets, and complex pharmaceutical product development for the regular market. Currently, he is involved in industrially feasible nanocarrier-based formulation development and optimization for various therapeutic agents. His team extensively working on QbD-driven design of topical delivery systems for rheumatoid arthritis, psoriasis, and fungal infections. He has published several research/review articles and book chapters in reputed international peer-reviewed journals and international publishers. He has actively involved in sponsored research projects from government funding agencies and pharmaceutical industries. As an inventor, he has filed 10 formulation patents. He is also a peer reviewer of several international journals. Prof. Singhvi was listed in the "World Top 2% Scientist" in 2021 and 2022. He is very passionate about practicing the newer teaching pedagogy in his classroom teaching and motivating students to face the challenges of the new era.

### **Prof. Ranendra Narayan Saha**

Prof. Ranendra Narayan Saha is Senior Professor at Department of Pharmacy BITS-Pilani, Pilani campus, Rajasthan. He worked as acting Vice Chancellor of BITS-Pilani. Additionally, he served as Director of the Dubai Campus of BITS-Pilani for seven years. He has completed his Bachelor and Master of Pharmacy from Jadavpur University, Kolkata and was awarded Doctor of Philosophy from BITS-Pilani. He has over 35 years of experience in teaching, research and administration and has assisted several doctoral, graduate, and undergraduate students. He has an extensive background in research and is skilled in pharmacokinetics, novel drug delivery systems

and nanomedicine. He has published books, various book chapters, and over one hundred research papers in prestigious national and international journals. In addition, he has presented multiple invited lecture at seminars and conferences organized by various colleges, pharmaceutical companies, and institution in India and abroad. He is also a member of the advisory board and selection committees of several universities in India and overseas. Throughout the years, he has completed several governments-sponsored initiatives and worked closely with the pharmaceutical industry, earning several patents and commercial products. He has received ‘*Pharmacy Professional of the Year*’ an award given by Indian Association of Pharmaceutical Scientists and Technologists (IAPST). In , he has been awarded *Shri B.K. Birla and Shrimati Sarala Chair Professorship* at BITS Pilani for his contributions in teaching and research. He is also a recipient of ‘*The Best Pharmacy Teacher Award*’ for the year , awarded by Association of Pharmaceuticals Teachers of India (APTI), in recognition of his contribution in teaching and research in the field of Pharmacy.

### **Dr. Sunil Kumar Dubey**

Dr. Dubey is presently working as General Manager, Medical Research at Emami Ltd, Kolkata. He is involved in planning and ensuring the timely execution of several preclinical and clinical studies. His expertise involves validating the effectiveness of a vast range of healthcare products and providing business development-related insights. He is responsible for developing product concept notes, technical notes, monographs, and dossiers. His team is also involved in supporting medico-marketing, product licensing activities, and training personnel from marketing and sales teams. Collectively, his efforts are towards bridging the gap between the industry, consumers and the scientific community. He has completed various government and industry-funded projects related to new product development, alongside pharmacokinetic and pharmacodynamic investigations. All these concerted efforts have led to the grant of patents to his name as well. He has extensive research experience in the area of pharmacokinetic-pharmacodynamic modeling and simulations, the development of phytopharmaceuticals, and numerous nanotechnology-based drug delivery platforms. He is proficient in regulatory affairs, adeptly navigating guidelines established by various regulatory agencies. He has over 18 years of industrial, teaching, research, and administrative experience. He was also a visiting Assistant Research Professor in the Department of Chemical and Biomolecular Engineering at the University of Maryland, USA. He also serves



as a guest faculty at various leading institutes including NIPER Guwahati, NIPER Raebareli, Jamia Hamdard, and IIT Dhanbad. He has patents and has published over 200 articles, books, and book chapters in renowned high-impact journals and presented papers at conferences in India and abroad. He is included in the list of ‘World’s Top 2% Most-Cited Scientists’ as per the Elsevier-Stanford University report

### **Candidate Biography**

Manisha Vinayak Choudhari is currently a Ph.D. research scholar in the Department of Pharmacy, BITS-Pilani. She has obtained her Bachelor of Pharmacy degree from the Government College of Pharmacy, Aurangabad, and her Master of Pharmacy in Pharmaceutics from the National Institute of Pharmaceutical Education and Research (NIPER), Ahmedabad. She secured AIR-657 in GPAT 2017 and AIR-206 in NIPER 2017. During her Master’s degree, she worked on the “Colloidal carrier based topical delivery of ganciclovir for ocular administration.” She has worked as a JRF under the supervision of Prof.R.N.Saha and Prof. Gautam Singhvi on the project, “The impact of formulation variables and processing methods for solubility enhancement for poorly soluble drugs using Affinisol HPMCAS.” Funded by the Colorcon Asia Pvt, Ltd India. Since her admission to BITS-Pilani, she has been working on “Investigating the effect of suitable excipients to design better delivery system for the selected drug.” Her proficiency in the field of research is evident by her publication in the Scopus Indexed journals and books (4 review publications, 3 book chapters, 4 research publications). She was also achieving 3rd position in Central East South Zone in Dissolution Research Presentation India.